ADSORPTION DESALINATION:

THEORY & EXPERIMENTS

KYAW THU

NATIONAL UNIVERSITY OF SINGAPORE

2010

ADSORPTION DESALINATION:

THEORY & EXPERIMENTS

KYAW THU

(B.E. (YTU))

A THESIS SUBMITTED

FOR THE DEGREE OF DOCTOR OF PHILOSOPHY

DEPARTMENT OF MECHANICAL ENGINEERING

NATIONAL UNIVERSITY OF SINGAPORE

2010

ACKNOWLEDGEMENTS

The author is grateful to his supervisor, Professor Ng Kim Choon, for his guidance, encouragement, and motivation during the project.

The author would like to thank Dr. Yanagi Hideharu, Associate Professor Bidyut Baran Saha of Kyushu University, Associate Professor Anutosh of Nanyang Technological University and Dr. Ibrahim El Sharkawy for their support and advice for the design of the test facility.

The author would like to thank Mr. Sacadevan Raghavan and Ms. Hung Ang Yan Leng for their assistance in the project. The author would like to thank National University of Singapore for the financial support throughout the Ph.D. candidature period.

The author expresses his gratitude to his parents and teachers and would like to thank his wife, Ms. Naing Aye Theint, for her moral encouragement and support during his research.

List of publications

The Author is grateful to his supervisor Professor Ng Kim Choon to be co-author for the following publications.

Award:

"**INSTITUTIONS OF ENGINEERS SINGAPORE (IES) PRESTIGIOUS ENGINEERING ACHIEVEMENT AWARDS 2009**" with the project titled "**Adsorption Technology for Desalination and Cooling**"

Patents:

1. NG Kim Choon, **Kyaw THU**, Yanagi HIDEHARU, Bidyut Baran SAHA, Anutosh CHAKRABORTY, Tawfiq Y AL-GHASHAM, Apparatus and Method for Improved Desalination, PCT/SG2009/ 000223.
2. Bidyut Baran SAHA, NG Kim Choon, Anutosh CHAKRABORTY, **Kyaw THU**, Adsorption Cooling cum Desalination Unit Using Three Adsorption Beds and Two Evaporators Arrangement, file No. 61/226,783.

Journals Papers

1. Ibrahim I. El-Sharkawy1, **Kyaw Thu**, Kim Choon Ng, Bidyut B. Saha, Anutosh Chakraborty and Shigeru Koyama, *Performance Improvement of Adsorption Desalination Plant: Experimental Investigation*, International Review of Mechanical Engineering, January, 2007.

2. Anutosh Chakraborty, Bidyut B. Saha, Shigeru Koyama, Kim Choon Ng and **Kyaw Thu**, Adsorption sciences and Technologies for cooling and desalination: A review, Journal of Energy and Climate Change, Vol.2, No.2, (84-98), 2007.

3. **K. Thu**, K.C. Ng, B.B. Saha, A. Chakraborty and S. Koyama, "Operational strategy of adsorption desalination system", International Journal of Heat and Mass Transfer, Vol. 52, Nos. 7-8, pp. 1811-1816, 2009.

4. K.C. Ng, **K. Thu**, A. Chakraborty, B.B. Saha and W.G. Chun, "Solar-assisted dual-effect adsorption cycle for the production of cooling effect and potable water", International Journal of Low-Carbon Technologies, Vol. 4, (2009).

5. B.B Saha, K.C. Ng, A. Chakraborty, **K. Thu** (2009), Most Energy Efficient Approach of Desalination and Cooling, Cooling India, May-June, pp 72-78.

6. **Kyaw Thu**, Chakraborty A., Saha B.B., Won Gee Chun, Ng K.C, Life-Cycle Cost Analysis of Adsorption Cycles for Desalination, Desalination and Water Treatment, 2010 (Article in press).

7. **Kyaw Thu**, Bidyut Baran Saha, Anutosh Chakraborty and Kim Choon Ng, Study on an Advance Adsorption Desalination Cycle with Evaporator-Condenser Heat Recovery Circuit, International Journal of Heat and Mass Transfer, 2010 (Accepted).

Conference papers

1. **Kyaw Thu**, Kim Choon Ng , Ibrahim I. El-Sharkawy, and Bidyut B. Saha, *Experimental Testing of Adsorption Chiller with Heat and Mass Recovery Schemes*, International Congress of Refrigeration 2007, Beijing.

2. K. C. Ng, **K. Thu** and B.B. Saha, *A novel adsorption desalination method: A test programme for achieving the 1.5 kWh/m^3 benchmark*, International Water Week, 23-27 June, 2008, Singapore.

3. **Kyaw Thu**, Kim Choon Ng, Bidyut B. Saha, Anutosh Chakraborty, and Shigeru Koyama, and Chun WonGee, Solar assisted Dual-effect Adsorption cycle for the production of cooling effect and potable water, 7th International Conference on Sustainable Energy Technologies; Seoul, Korea, 2008.

4. Ng K.C., Charkarborty A and **Kyaw T**, Adsorption Technologies for Cooling and Desalination: A Review, The 1st International Meeting on Advances in Thermo-Fluid, August, 2008, Malaysia.

5. **Kyaw Thu**, Kim Choon Ng, Bidyut B. Saha, Anutosh Chakraborty, and Shigeru Koyama, Waste heat-driven Dual-purpose Adsorption Cycle for Cooling and Desalination, The 4th Asian Conference on Refrigeration and Air-Conditioning, May 21-22, 2009, Taipei.

6. Bidyut Baran Saha, **Kyaw Thu**, Anutosh Chakraborty and Kim Choon Ng, Experimental Investigation on a Waste Heat Driven Advanced Adsorption Desalination and Cooling Cycle with Internal Heat Recovery, HPC, 2 April, 2009.

7. **Kyaw Thu**, K.C. Ng, B.B. Saha and A. Chakraborty, Overall of heat transfer analyses of a heat-driven adsorption chiller at assorted regeneration temperatures, International Symposium on Next-generation Air Conditioning and Refrigeration Technology, Tokyo, 2010.

8. **Kyaw Thu**, Bidyut Baran Saha, Anutosh Chakraborty and Kim Choon Ng, Performance analysis of waste heat-driven cooling cum desalination cycle, IIR Gustav Lorentzen Conference, April 12-14, 2010,Sydney, Australia.

9. Kim Choon NG, **Kyaw THU**, Hideharu YANAGI, Anutosh Chakraborty, Bidyut B. Saha, Performance analysis of a low temperature waste heat-driven adsorption desalination prototype plant, The 5th Asian Conference on Refrigeration and Air-conditioning, June 7-9, 2010, Tokyo, JAPAN (Accepted)

Table of Content

Table of content

Table of content

Table of content

Summary

This thesis presents the theoretical and experimental studies of adsorption desalination (AD) cycles that utilize low temperature heat sources such as waste heat from industrial processes, exhaust of turbines or renewable solar thermal energy.

The theoretical study modelled the mass and energy balances of the AD cycle that operates in a batch manner, using the governing equations developed based on thermodynamic property fields of adsorbent-adsorbate systems such as the internal energy, the enthalpy, the specific heat capacity and the entropy as a function of pressure (P), temperature (T) and amount of adsorbate (q). Based on a lumped-parameter approach, the model is solved using the FORTRAN-based International Mathematics and Statistics Library (IMSL) Libraries.

The AD cycles studied here comprise the two-bed and the four-bed designs or operations. Extensive experiments have been conducted on these operations, for a wide range of hot and cooling water temperatures and cycle times. The performance results of the AD cycles are presented in terms of key parameters such as (i) the specific daily water production (SDWP), (ii) the performance ratio (PR) and the cycle time. Further tests are conducted which incorporate performance enhancement schemes such as water recirculation and pressure equalization between the desorber and the adsorber beds, and additional bed cooling by diverting the cooling effect of the evaporator.

Summary

In the two-bed cycle operation, the SDWP is measured to be 7.3 m^3 of potable water per tonne of adsorbent (silica gel) with a PR of 0.66. However, better SDWP, about 8.0 m^3 of potable water per tonne of silica gel, is observed for the four-bed operation mode at similar heating and cooling conditions. With the performance enhancement schemes, higher SDWP of 10 m^3 per tonne of silica gel per day can be achieved. Based on a broad range of data, the optimal cycle times for maximum water production have been evaluated.

Another useful effect achieved by the AD cycle, besides desalting, is the production of chilled water by the evaporator. This is known as the dual-effect of the AD plant. For a conventional two-bed AD cycle mode, the specific cooling capacity is measured to be about 47Rton per tonne of silica gel while producing SDWP of 7.2. Since two useful effects are obtained from single heat input, the overall conversion ratio, defined as useful effects to heat input, is about 1.4.

Further advanced cycles have been developed and investigated, for example, the incorporation of internal heat recovery scheme between the condenser and the evaporator in the AD plant. Using such a scheme and the same hot water inlet temperature, the water production of plant increases by two and a half times from 10 to 25 m^3 of water per tonne of silica gel per day. Owing to the increase in SDWP and savings in the pumping power requirements, the electrical energy consumption of the advanced AD cycle is found to be less than 1.5kWh/m^3.

A simple economic analysis of the AD cycle is performed with the consideration of interest rate and equipment lifespan as well as the production capacity of the plant. It

is found for a large AD plant (> 1000 m^3 per day), the asymptotic unit production cost water production is to be \$0.457/m^3 of water. This is well below the unit production cost of the other desalination methods reported in the literature. As waste heat is utilized for regeneration process in the AD plant, the corresponding annual CO_2 emission saving is 1172 tonne of CO_2/year.

Finally, the competitive advantages of the AD desalination cycles over the conventional methods are highlighted, namely, i) it has the lowest annualised unit production cost, ii) the low activation temperature of the adsorbent enables the AD cycle to utilize waste heat from industrial processes and exhausts of prime movers which is available in abundance, and iii) the AD cycle is environmental-friendly as almost no chemicals are used for cleaning of adsorbent. In short, these cited advantages of AD cycle offers great potential for a large scale implementation in the desalination industry.

Nomenclature

$\vec{v}$	linear momentum	
$\dot{m}$	mass flow rate	ms^{-1}
ψ	potential energy per unit mass	
ρ	the effective density	$kg\ m^{-3}$
$\mathbf{v}'$	the particle velocity vector at an infinitesimally time dt	
Φ	the source of momentum	
Π	tensor part of a pressure tensor	
A	area/flag which governs mode of operation	m^2
B	flag which governs mode of operation	
BPE	boiling point elevation	
COP	the Coefficient of Performance	
c_p	specific heat capacity	$J\ kg^{-1}\ K^{-1}$
D_{so}	a kinetic constant for the silica gel water system	$m^2\ s^{-1}$
e	the total energy per unit mass	$J\ kg^{-1}$
E_a	activation energy of surface diffusion	$Jmol^{-1}$
F	the external force	N
$\boldsymbol{F}_k$	tensor resulted from the external forces	
G	Gibbs free energy	$kJkg^{-1}$
h	enthalpy per unit mass	$J\ kg^{-1}\ K^{-1}$
H	the total enthalpy of the system	$J\ kg^{-1}$
h_{fg}	latent heat	$kJkg^{-1}$
J	heat flux	Wm^{-2}

Nomenclature

K	the thermal conductivity	W m^{-1} K^{-1}
K_o	pre-exponential coefficient	kPa^{-1}
L	length	m
m	mass	kg
MADS	master adsorber	
MDES	master desorber	
n	number of beds	
P	pressure	Pa
P_0	reference pressure	Pa
PR	performance ratio	
q	fraction of refrigerant adsorbed by the adsorbent	kg kg^{-1}
Q	the total heat or energy	W or J
q*	the adsorbed quantity of adsorbate by the adsorbent under equilibrium conditions	kg kg^{-1}
q_m	the monolayer capacity	kg kg^{-1}
Q_{st}	isosteric heat of adsorption	kJ kg^{-1}
r	the particle position vector	
R	Universal gas constant	J kg^{-1} K^{-1}
R_p	average radius of silica gel	m
s	entropy per unit mass	J kg^{-1} K^{-1}
S	total entropy	J kg^{-1} K^{-1}
SADS	slave adsorber	
SDES	slave desorber	
SDWP	specific daily water production	m^3/tonne-day

Nomenclature

SCP	specific cooling power	Rton/tone
	of silica gel	
T	temperature	K
t	time / $t/t_{h\text{-}cyde}$	s
T_0	reference temperature	K
u	internal energy per unit mass	$J\ kg^{-1}\ K^{-1}$
U	internal energy of the system /	$kJkg^{-1}$
	overall heat transfer coefficient	$W\ m^{-2}\ K^{-1}$
v	specific volume	$m^3\ kg^{-1}$
v	velocity	$m\ s^{-1}$
V	volume of the system	m^3
W	work done	J
α	Activity coefficient	
γ	flag which governs mode of operation	
δ	flag which governs mode of operation	
θ	flag which governs mode of operation	
λ	the thermal conductivity	$Wm^{-1}K^{-1}$
μ	the thermodynamic or chemical potential	
σ	the entropy source strength	
τ	the stress tensor	
φ	the fin efficiency	

Subscripts

a	adsorbate
abe	adsorbent

Nomenclature

ch	chilled water
cond	condenser
cw	cooling water
d	distillate
evap	evaporator
g	gas
hw	hot water
HX	heat exchanger
in	inlet
Mads	master adsorption
Mdes	master desorption
out	outlet
s	salt / adsorbent
Sads	slave adsorber
Sdes	slave desorber
sg	silica gel
th,R	theoretical minimum
w	pure water

List of Figures

List of Figures

List of Figures

List of Figures

List of Figures

List of Tables

Chapter 1 Introduction

Fresh water is an indispensible resource which is vital for human consumption as well as economic development of a country. According to the World Health Organization (WHO) standards, the total dissolved solids (TDS) of drinkable water is less than 500 mg/l or ppm. Of all the available water on Earth, 97% is salt water where the TDS of the sea water is more than 35000ppm (Parts per million) and unfit for consumption. Only 2 to 3% of the water resources are locked in lakes, ice caps and glaciers [1]. It is reported that at least one billion of the world's population is presently living in water-stressed regions and this number may further increase to 3.5 billion by the year 2025.

Although many countries have constructed ground reservoirs to store water when it becomes available during raining seasons, the problem of global water shortage is a pressing concern for many countries, particularly in the semi-arid and desert regions due to low rainfall. It is recognized that the water shortage is caused by two major factors, namely (1) the rapid increase in the world's population and (2) the relentless pursuit of economic development which leads to high water consumption of major sectors of industries. Therefore, the practical solution to solving the global water shortage is not only to develop a cost-effective technology for converting the sea or brackish water to potable water, the solution must also be environmental-friendly. One such solutions that can meet the mentioned objectives is adsorption desalination (AD), recently patented in 2006 [2], as it employs low temperature heat sources (typically less than 80o C) which can be tapped off from industrial waste heat,

exhaust of prime movers or from the renewable solar thermal energy. Thus, the motivation for this research is to investigate the potential of the adsorption cycle for desalination application and to quantify the energetic efficiency and the amount of CO_2 savings that could be achieved by the innovative sorption cycles.

1.1. Desalination

Desalination is the process by which fresh or potable water is produced from the sea or brackish water of high dissolved and suspended salts or solids. In general, desalination methods can be categorized into three major groups, namely: (1) thermally-activated systems which utilize thermal energy to split fresh water by evaporation and then condensing the vapor, (2) pressure-activated systems which split potable water from the salt water applying certain pressure higher than the osmotic pressure through semi-permeable membrane and (3) chemical-activated desalination which includes ion-exchange desalination, liquid-liquid extraction, and gas hydrate or other precipitation schemes [3]. The thermally-activated desalination systems include the well-known Multi-Stage Flash (MSF), the Multi-Effect Desalination (MED) and the solar distillation. These methods employ thermal energy to evaporate water vapour from salt solution. On the other hand, the membrane systems utilize semi-permeable membrane or nano-tubes to separate the water molecules from the salt solution and they comprise the reverse osmosis (RO) and the electro-dialysis. However, all existing desalination methods have shortcomings such as energy intensiveness and high maintenance arising from the cost of membrane replacement and corrosion. Other attempts to lower the unit cost of desalination have been reported such as hybrid desalination. In 2005, adsorption desalination is patented as a novel

desalination technology that is believed to have lowest specific energy input, typically less than 1.5 kWh/m^3, and the desalting process is environmental-friendly as only silica gel is regenerated with low temperature waste heat.

1.2. Adsorption Desalination

Adsorption processes are not new and they have been deployed in applications such as separation and air-conditioning. It employs physical uptake of water vapor on the surface of the adsorbent by van der Waal's or polar bonding forces such as silica gel, zeolite and activated carbon.

Adsorption desalination cycle mimics the processes found in ambient i.e., evaporation and condensation except that within the AD plant, these processes are performed in the single-component environment and at a faster pace. Ng et al. [2] has developed a waste heat driven adsorption desalination system utilizing the silica gel and water as adsorbent-adsorbate pair. A more complete literature review on the desalination and adsorption desalination system is discussed in Chapter 2.

The major components of typical adsorption desalination (AD) system are 1) the evaporator, 2) the condenser and 3) two or more adsorber beds in which the adsorbents are packed in tube-fin heat exchangers. The operation of the AD cycle can be sub-categorized into the evaporation-adsorption process and the desorption-condensation processes. Pre-treated sea water is evaporated by the suction effect from the adsorbent which takes place at a low pressure and temperature of the evaporating

unit. When the vapors are adsorbed on the adsorbent, the heat of adsorption is rejected into the cooling water circuit running across the adsorber bed. This adsorption process continues until the on-set of the switching cycle time. For regeneration of the adsorbent, low temperature waste heat is supplied to the bed at the on-set of the desorption mode. The desorber bed is now connected to the condenser where the water vapor migrates to the cooler tube surfaces of the condenser and the potable water is collected in the collection tank. The details of the AD system and its operation are discussed in Chapter 4.

As the AD cycle utilizes only low temperature waste heat or solar energy, it has the potential to be the most efficient method of converting the sea or brackish water to potable water as the only parasitic electric power needed are those used for powering the valves and water pumps. This thesis describes the experimental and theoretical modeling of the AD cycles for the production of potable water at assorted heat source and cooling water temperatures. To further enhance the product yield from the cycle, internal heat recovery between the condenser and the evaporator, as well as other methods of heat and mass recovery schemes are studied. The thesis also includes a brief section of theoretical modeling of the AD cycle which is powered from the low temperature heat sources such as solar energy.

1.3. Objectives

The objectives of the thesis are:

a) To conduct numerical investigation on the performance of a prototype adsorption desalination (AD) plant. The numerical simulations are applied to evaluate the AD cycle performances and to optimize the operation of both two-bed and four-bed configurations. The code is also a valuable tool to examine the suitability of any energy recovery schemes to be implemented in the AD cycle.

b) To investigate experimental tests on the performance of the AD plant for a wide range of heat source and coolant temperatures supplied to the AD cycle. For the experimentally determined optimal rating conditions, tests are also conducted to evaluate the efficacy of dual useful effects that could be derived from the AD cycle i.e., cooling and desalination.

c) To investigate the improvements that could be achieved by heat and mass recovery schemes that are proposed for the AD plant, namely (i) the master-slave operation, (ii) the re-circulation of the residual hot water in the master bed or desorber to pre-heat the slave bed, (iii) the pressure equalization (PE) scheme that is applied during the on-set of switching interval between the higher pressure desorber or bed to the lower pressure bed or adsorber and (iv) bed cooling scheme that utilizes the cooling effect from the evaporator to cool down the adsorber bed thus enhancing the water production rate. It has the effect of heat and mass recoveries that may lead to improvements in the water production rate of the AD cycle.

d) To map the optimal cycle time intervals for all regeneration temperatures ranging from 65^{o}C to 85^{o}C, and chilled water of evaporator from 12.5^{o}C to 30^{o} C. These optimal cycle times could be used as an operation strategy for part-load operation of the AD cycle.

e) To develop an advanced AD cycle for maximizing the yield in the production of water using the integrated evaporator-condenser concept - the direct recovery of

the condensation heat and rejecting it into the evaporator. The superior performance of the advanced AD cycle was first observed in the simulated investigation using the theoretical code.

f) To investigate the AD cycle as a dual-purpose cycle i.e., simultaneous production of cooling and potable water using low temperature hot water in the dynamic behaviour or temperature fluctuations of the hot water supply on the cycle. For experiments, the prototype test facility will be modified with electric heaters to emulate the low temperature hot water sources.

g) To investigate the maximum recovery ratio of seawater that the AD cycle could tolerate without crystallization of salts in the evaporator. The recovery ratio is a parameter needed for the determination of water production cost as well as to compare it with similar factors of the conventional desalination methods

h) To evaluate the economic analysis of the AD plant at both laboratory and large-scale plants. The specific water production cost of the AD plant is to be compared with the reported cost data found in the literature.

1.4. Scope

This thesis is presented in different sections and the arrangement of the Chapters is as follows:

- Chapter 1 gives general introduction, objective and scope of the thesis.
- Chapter 2 presents the literature review on the desalination and desalination methods.
- Chapter 3 describes the general theoretical description of Adsorption Desalination (AD) process. The minimum energy requirement for desalting is discussed in the first section followed by the formulation of mass, energy and entropy balance for

thermodynamic systems. The last section focuses on the thermodynamic of adsorption along with the formulation of thermodynamic surfaces.

- Chapter 4 discusses the performance analysis of a conventional adsorption desalination (AD) cycle which operates at low temperature waste heat. Both numerical and experimental investigation of the AD cycle is presented in this chapter.
- Chapter 5 describes the performance of dual-effect AD cycle. Extensive experimental investigation along with the mathematical formulization is presented. The results are analyzed using temperature-entropy map for a better understanding of the cycle.
- Chapter 6 explores the development of advanced AD cycles where heat of condensation is recovered to the evaporator. Two methods of recovery are discussed namely heat recovery using (i) evaporator-condenser device and (ii) evaporator-condenser heat recovery circuit.
- Chapter 7 gives the thermo-economic viability of the adsorption desalination (AD) process using a life-cycle approach.
- Chapter 8 summarizes the major findings of the thesis along with the recommendations.

Chapter 2 Literature Review

Introduction

This chapter presents the literature review on desalination along with different types of desalination methods and adsorption desalination. Water is the basic substance for all living creatures on earth and the lack of it may cause a bottle-neck of economic development of an economy; Adequate supplies of water are vital for agriculture, industry, recreation and human consumption [4]. Three-quarters of the earth is covered by water [5]. However, most of the water available to humans is unusable due to the high salinity- typically, salinity or total dissolved solids (TDS) higher than 35,000 mg/l. According to the World Health Organization's standards, water with TDS less than 500ppm is considered to be drinkable [6]. Over 97.5% of the earth's water represents oceans or sea whilst the remaining 2.5% is fresh water, and of which 80% of this amount frozen in the icecaps or combined as soil moisture. [7].

Global water distribution in the world is illustrated by Figure 2.1 where it can be seen that a large amount of available water is locked in the Ground and ice caps. The distribution of water has also created problems since the global water distribution is uneven and the availability of freshwater varies by geographical region, and with the seasons.

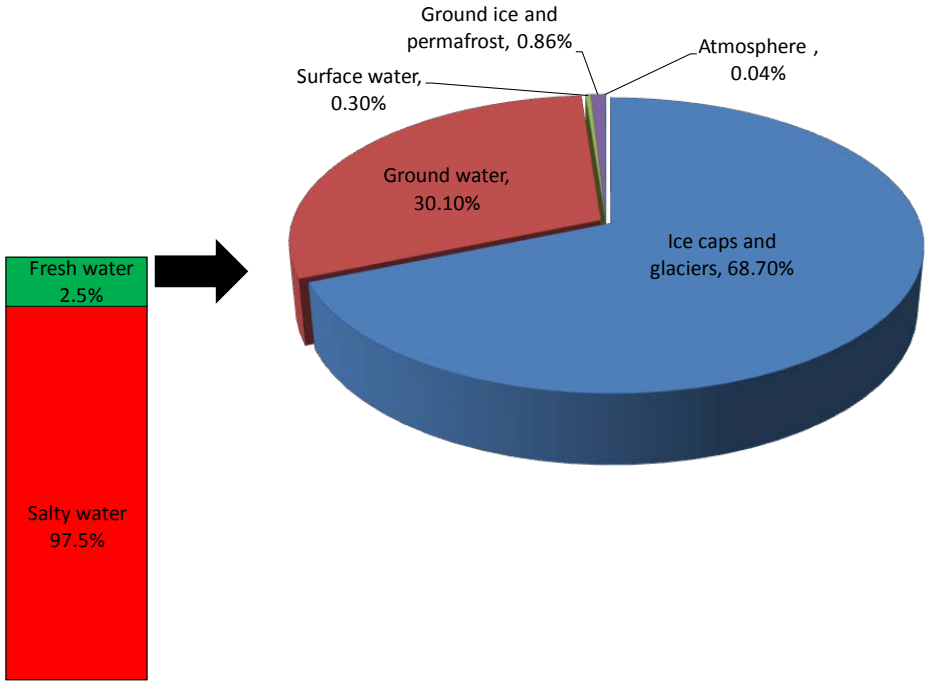

Figure 2.1 Global water source distribution

2.1. Overview on Global water shortage

Prior to the discussion of the water scarcity, it is important to distinguish type of water shortages faced by us – the humans. Generally, fresh water requirements can be grouped into drinking purposes and industrial usage. Global potable water demand has been increasing with economical and industrial growths: For instance, the yearly bottled water consumption of United States jumped from 14,362 m^3 in 1996 to 25,893 m^3 in 2004 while the daily water consumption per person is estimated at 575 litres [8]. Industrial applications of water include food processing, boiler make-up water, applications related to the electronic industry and pharmaceuticals, where the TDS is generally limited to a maximum TDS of 5ppm [9], chemical reactions, dairy and food, washing and cleaning.

With the increase in population, the fresh water demand for food production increases exponentially. For example, the production of a kilogram of grains under proper climatic and management conditions requires about 1-2m^3 of water whilst this amount can reach as much as 4m^3 in tropical dry climates [10-12]. Figure 2.2 gives the water usage by different sectors such as agriculture, industry and municipal [13]. The data shows the constant increase in water demand by all sectors especially agriculture. Two-thirds of all the water consumed in the world goes to farming, a share expected to shrink only slightly by 2025. The increase in water demand is attributed to the rapid population growth and the development of industrialization [14, 15].

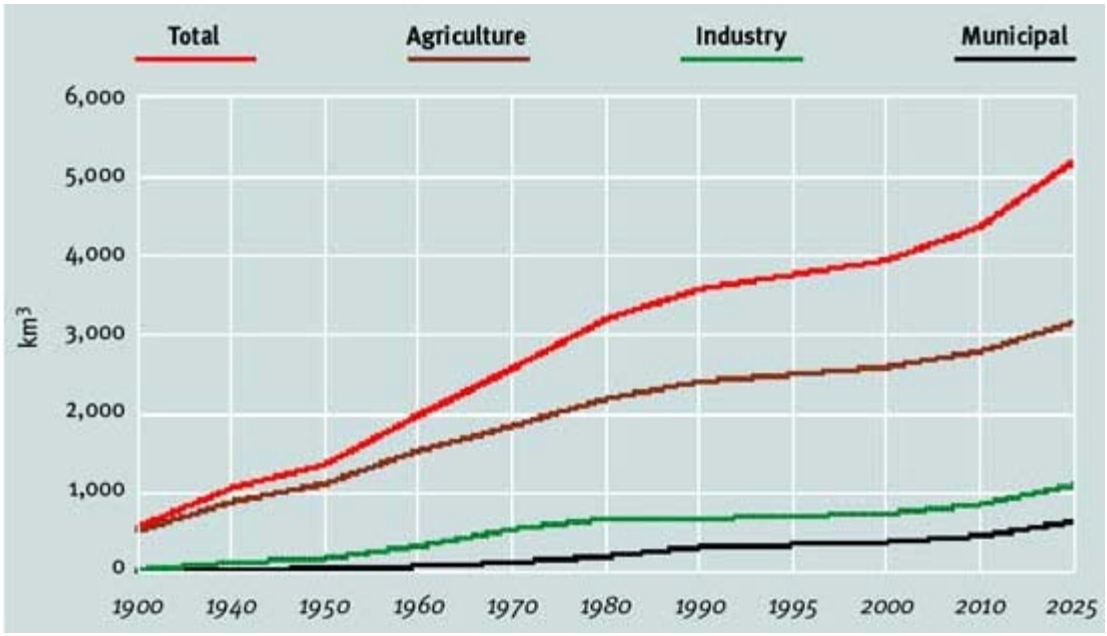

Figure 2.2 Global fresh water usages by different sectors

On the other hand, Global fresh water sources are diminishing with increasing environmental issues such as CO_2 emission, Global warming and climate change. Thus, Water cannot be considered now as a natural, self-renewable, low-cost

resource, easily accessible to all [16]. A World Health Organization (WHO) report states that at least one billion people do not have access to clean and fresh water, and about 41% of Earth's population live in the water-stressed areas, and this deprived population may climb to 3.5 billion by the year 2025 [17,18]. Concurrently, health issues related to water supplies call for urgent solutions. For examples, 1.8 million children die each year as a result of diarrhea and 443 million school days are lost each year from water-related illness [19].

Water shortage is severe in arid and semi-arid regions where much of the annual rainfall evaporates back. Especially, the Arabian Gulf countries have been struggling for many decades to meet fresh water demand with a considerable amount of desalination plants and several of these countries already have an acute potable water shortage, and that the problem will increase by the year 2020. [20-25].

Ultimately, it is a necessity to limit the effects of water shortages including improving the efficiency of water use, implementing technologies and policies to encourage water conservation and reuse, slowing population growth, and tapping non-traditional sources of freshwater such as seawater, fog water, atmospheric water vapor, and water "produced" in conjunction with fossil energy or other resource recovery operations. A number of attempts have been applied to improve fresh water supply such as construction of dams to collect rain and river water [26]. However, this solution is subjective to rainfall and climatic situations. The amount of water in the oceans, on the other hand, can provide as an inexhaustible and sustainable source for the planet's freshwater needs through desalination, process which converts high TDS water into low TDS or potable water. The conversion of the vastly available sea water

into potable water with minimum production cost might be the best solution for the global water shortage. The following section discusses the type of desalination methods along with the production cost and the market share.

2.2. Reviews on Desalination Processes

Desalination is a process by which the dissolved salts in the sea or brackish water are removed through a number of processes. Desalination has become a practical solution to the regions where the annual rainfall is significantly low and no fresh water is available within a reasonable distance and no access to the sea or ocean. Desalination is not a new technique. Since 1800 desalination was practiced on ship boards using single stage stills operated in the batch mode while energy is supplied from stoves or furnaces without recovering the heat of condensation [9]. Since then, desalination has been growing both technically and economically. Figure 2.3 shows the progressive amount of desalinated production capacity from 1990 to 2008 [27]. It can be seen that the amount of production of potable water by desalination drastically increases year by year highlighting the contribution to solve the global water shortage problem.

At the same time, a wide range of feed water from sea water to waste water has been used to produce potable water by desalination. Desalination capacity can also be accessed by type of source feed water and Figure 2.4 illustrates that about 62% of the desalination system uses sea water as feed water whilst 19% uses brackish water as feed source [28].

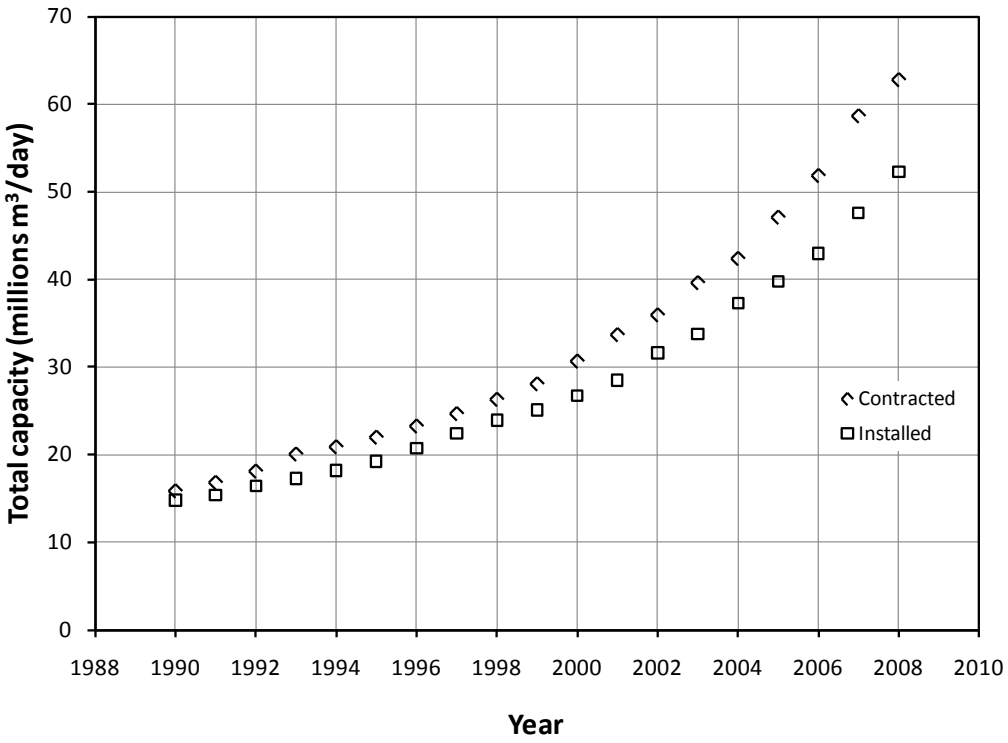

Figure 2.3 Cumulative desalination capacity growth from 1990 to 2008

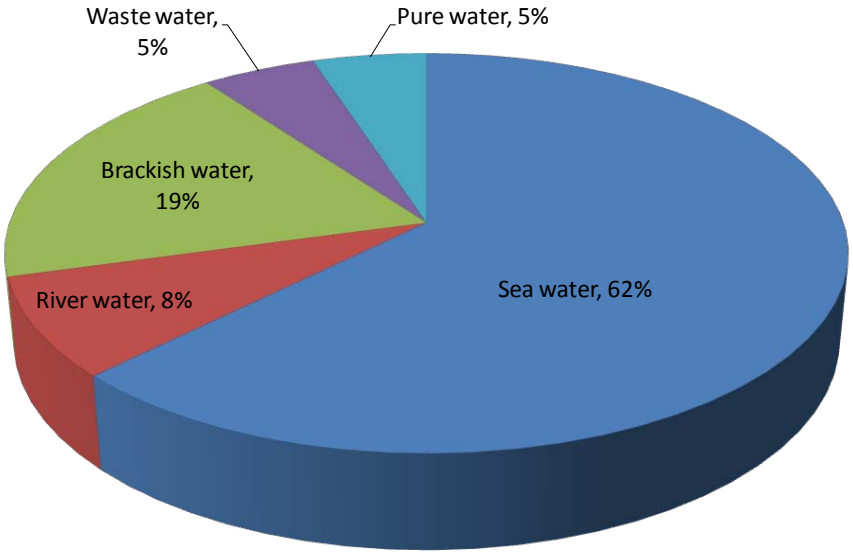

Figure 2.4 Desalination Capacity by Source feed Water

In general, desalination methods can be categorized into three major groups, namely: (1) thermally-activated systems which utilize thermal energy to split fresh water by evaporation and then condensing the vapor, (2) pressure-activated systems

which split potable water from the salt water applying certain pressure higher than the osmotic pressure through semi-permeable membrane and (3) chemical-activated desalination which includes ion-exchange desalination, liquid-liquid extraction, and gas hydrate or other precipitation schemes [29, 30].

Thermally-activated systems mimic the natural water cycle by producing water vapor that is then condensed into fresh water. They include multi-stage-flash (MSF) distillation, multi-effect distillation (MED) and mechanical vapor compression (MVC) which combines thermal and mechanical processes [31].

In 1957, the landmark of the four-stage flash distillation plant by Westinghouse was installed in Kuwait, however the plant did not have the standard MSF features [9]. R.S. Silver patented a MSF system which gives a major advancement over the Westinghouse configuration because of the much smaller specific heat transfer area for the condenser tubing reducing the capital cost since the high tubing cost in the Westinghouse system was replaced by inexpensive partitions in the MSF systems [32].

The invention of the MSF was a novel achievement and gave a new direction to desalination industries because, in MSF, evaporation “flashing” occurs from the bulk liquid, not on a heat-exchange surface, as is the case with other distillation processes and also the heat of condensation is utilized to pre-heat the incoming sea water through a number of stages and have high gained output ratio [33]. This approach minimizes scale and is a major reason MSF has been popular for several decades especially in the Persian Gulf region where large MSF units are often coupled

with steam or gas turbine power plants for better utilization of the fuel energy. The low to moderate temperature and pressure steam exiting the turbine is used to drive the desalination process [34, 35]. Fiorini et al. has proposed a new formulation for the non-equilibrium allowance in MSF processes [36] introducing stage efficiency similar to the polytropic efficiency, commonly adopted in gas in a turbine and compressor.

Thermal performance analyses of MSF systems have been conducted by N. H. Aly, A. and K. El-Fiqi [37]. A steady-state mathematical model was developed to analyze both the multi-stage and multi-effect desalination systems. The model accounts for the geometry of the stages, the mechanism of heat transfer, the variation of the physical properties of seawater with temperature and salinity and the role of fouling and its effect on the plant performance ratio defined as the ratio of tons of water produced per ton of initial steam. The results obtained by the model were compared with data from the Sidi-Krir plant in west Alexandria, which contains 17 recovery and three rejection stages and good agreement between the calculated results and the plant data were observed. However, the performance ratio of MSF plants are limited to 10 [38] and the efficiency is limited due to the conversion of the sensible heat into latent heat and thus, the market share of MSF technology is declining in recent years with the development of multi-effect distillation (MED) and reverse osmosis (RO).

The multi-effect distillation (MED) process is the oldest process in desalination [38]. It is a process thermally-activated desalination process where latent heat (condensation) is used to produce secondary latent heat (evaporation) in each section or effect. In MED systems, low or high temperature steam is used to boil the

sea water. The vapour is condensed in the next effect where the latent heat is given away to evaporate the feed water again at lower pressure. The process is repeated as many times as the design permits, between the upper possible temperature and the lower possible cooling temperature, which depends on seawater temperature. The condensate is accumulated stage-wise as the potable water. A vacuum pump takes the remaining vapor after the last condensation stage, to maintain the gradual pressure gradient inside the vessel. Normally, the number of effects in MED systems varies from eight to sixteen [38].

The MED process can have several different configurations according to the type of heat transfer surface (vertical tube falling film, vertical tube climbing film, horizontal tube falling film, plate heat exchanger) and the direction of the brine flow relative to the vapour flow (forward, backward, or parallel feed) [39].

El-Dessouky et al. have studied the thermal analysis of MED system with several operating configurations including the parallel flow (MED–P), the parallel/cross flow (MED–PC), and systems combined with thermal (TVC) or mechanical (MVC) vapor compression [40, 41]. The models take into account dependence of the stream physical properties on temperature and salinity, thermodynamic losses, temperature depression in the vapor stream caused by pressure losses and the presence of non-condensable gases, and presence of the flashing boxes. It was observed that the thermal performance ratio of the TVC and specific power consumption of the MVC are found to decrease at higher heating steam temperatures.

Simulation of the steady-state operation of a multi-effect stack seawater distillation plant was conducted by E1-Nashar et al [42]. The computer program based on the simulation models of the different plant components was applied to an MES distiller having the same design and operational characteristics as the distiller currently in operation at Abu Dhabi, UAE. Reasonably good agreement was observed for the heat transfer coefficients for the heater.

Initially, MED lost their market to MSF due to the serious fouling problems encountered in the evaporation units [38]. The development in the material science helped MED to utilize more anti-corrosive materials and subsequently over the fouling problems. MED processes have a great potential because they operate with higher thermal efficiency and thus the process has been stated as the most important large-scale evaporative process and offers significant potential for cost reduction.

However, both MSF and MED suffer from major drawbacks such as i) high energy intensive (high energy cost) ii) high corrosive and fouling to the evaporating units due to the higher evaporation temperatures and iii) high capital and operation cost iv) high maintenance cost and iv) low recovery ratio defined as the ratio of the produced potable water to feed water [43- 46].

The vapor compression distillation (VCD) process is another kind of thermally-activated desalination method where the heat for evaporating the water comes from the compression of vapor, rather than the direct exchange of heat from steam produced in a boiler. Vapor compression (VC) units have been built in a variety of configurations. Usually, a mechanical compressor is used to generate the heat for

evaporation. The VC units are generally small in capacity, and are often used at hotels, resorts and in industrial applications.

M.A. Darwish has conducted thermal analysis of vapor compression desalination system considering the effects of the operating parameters such as the evaporator temperature, pressure drop across the evaporator, feed temperature to the evaporator on the work done, compressor size, heat transfer areas of the evaporator and the multi-flow heat exchanger [47]. A new expression, the available energy consumption per unit amount of distillate, was proposed.

A comprehensive design model of the single effect mechanical vapor compression process was presented by Hisham Ettouney [48]. Several new design features such as the evaporator dimensions, demister dimensions, dimensions of the non-condensable gases venting orifice, and capacity of the vacuum system were considered in the model. Comparison of the design results against available field data showed good agreement for the predictions of specific power consumption and specific heat transfer area.

Pressure-activated systems include electro-dialysis reversal (EDR) process and reverse osmosis (RO) process.

The EDR process utilizes electricity to energize opposing electrodes to attract and separate out positive and negative ions of the dissolved salts from a saline water supply [49, 50]. The ions are attracted to the electrodes and travel through semi-permeable membranes screening the ions from the water stream. Thus, salt water

flowing through an EDR unit loses dissolved salts and the resulting stream is pure water. EDR systems may be used with water containing low amounts of TDS. However, when TDS levels exceed 3,000 mg/l, RO systems are typically the preferred choice for desalination.

An electrodialysis desalination plant has been set up and tested to treat brackish water while driven from an off-grid wind energy system by Veza et al. [51]. The tests were carried out in the framework of a wider scope project, located on Gran Canaria Island (Spain). Product flow rate between 3 and 8.5 m^3/h, power requirements between 4 and 19 kW, while product water conductivity ranged between 200 and 500 μS/cm were recorded. The desalination unit showed good flexibility, adapting smoothly to variations in wind power, even when sudden drops or rises occurred.

Reverse Osmosis (RO) process is the major candidate of the pressure-activated desalination system which split the water from salt through semi-permeable membrane by applying external pressure. The system was first demonstrated as a possible desalination process in the mid fifties. Salt is separated from the seawater using a semi-permeable membrane by applying a pressure greater than the osmotic pressure of the seawater. It is a breakthrough desalination technology because the desalination process is performed without changes in phase since no evaporation of the seawater is involved.

The RO membranes used are semi-permeable polymeric thin layers, which hold on to a thick support layer. Membranes are usually made of cellulose acetates, polyamides, polyamides, and polysulfones. They differ between symmetric,

asymmetric, and thin film composite membranes. The operating pressure for brackish water systems ranges from 10 - 15 bar and for seawater systems from 50 to 80 bar (the osmotic pressure of seawater with a salinity of 35 g/kg is about 25 bar) [52].

Since most of energy losses for RO result from releasing the pressure of the concentrated brine, large scale RO systems are now equipped with devices to recover the mechanical compression energy from the discharged concentrated brine stream with claimed efficiencies of up to 95%.

However, RO membranes are sensitive to pH, oxidizers, a wide range of organics, algae, bacteria, depositions of particulates and fouling. Therefore, pre-treatment of the feed water is an important process step and can have a significant impact on the cost and energy consumption of RO, especially since all the feed water, even the amount that will eventually be discharged, must be pre-treated before being passed to the membrane.

RO has become a relatively mature technology and is experiencing rapid growth [53, 54]. Some of the largest new desalination plants under construction and in operation now use RO membranes, including Ashkelon in Israel and the new plant at Tuas in Singapore. Ashkelon, the largest RO plant in the world, desalinates seawater for municipal purposes with a capacity of 100 million gallons per day (MGD) or 395,000 cubic meters per day (m^3/d).

Yosef Dreizin reviewed direct and indirect, fixed and variable costs, including several cost escalation scenarios anticipated due to the linkage of the

contracted water price to various indices (using an item by item and index by index cost sensitivity analysis) of the Ashkelon seawater desalination project [53].

RO plants are struggling with some significant drawbacks such as i) high electricity usage from the pressurizing the seawater through the membrane, ii) the low recovery ratio i.e., only 40% of the input seawater can be extracted as fresh water [54] iii) cost related to the replacement of the membrane (typically the membrane has to be replaced every 2-3 years and iv) cost related to the addition of anti-scalants and dispersants to inhibit the precipitation and growth of microbiological organisms and contaminants [55].

Other desalination systems comprise chemical-activated desalination methods which include ion-exchange desalination [56, 57], liquid-liquid extraction [58], and gas hydrate or other precipitation schemes, membrane distillation which combines thermal and membrane technology to produce potable water [58-61], and hybrid desalination such as RO-MSF or RO-MED. In hybrid cycle, the power generation cycle provides the electricity for the RO plant and the steam for the MSF or MED plant. Considerable savings are possible in terms of shared facilities. However, these systems also suffer from the combined drawbacks of the thermally activated systems and the pressure-activated systems.

2.3. Energy sources and cost of desalination

The theoretical minimum energy for desalination of seawater, with an incremental recovery of freshwater is about 0.706 kWh/m^3 as reported by K.S.

Spiegler [62] where detailed derivation is discussed in Chapter 3. In practice, desalination processes are not ideal with perfect efficiency. Table 2.1 gives the thermal and electrical energy consumption of some of the commercially available desalination methods. However, it should be noted that the energy consumption figures of desalination is dependant of several factors such as design configuration, site situation etc.

Table 2.1 Energy consumption of different desalination methods

Method of Desalination	Thermal energy consumed kWh/m^3	Electric energy kWh/m^3 consumed
Multi-stage Flash (MSF)	19.4	5.2
Multi-effect Distillation (MED)	16.4	3.8
Vapor compression (VC)	-	11.1
Reverse Osmosis (RO) – single pass	-	8.2
Reverse Osmosis (RO) – double pass	-	9.0

(All data is extracted from Seawater Desalination in California, California coastal commission Chapter 1-: Energy Use section, http://www.coastal.ca.gov/index.html [120].)

However, it is reasonable to say that MSF process consumes the most energy, despite its relative maturity (at least 50 years). MSF is followed by MED (or hybrid MED) systems and then vapor compression systems. The energy consumption of MSF, by far the most widely used thermal process (see below), is still at least 20-30 times the theoretical minimum. RO is a newer technology (30 years) that with recent improvements in energy recovery is remarkably efficient, consuming only 3 to 10 times the theoretical minimum. It is important to consider however that RO consumes energy in the form of electricity. On the other hand, MSF uses heat (or fuel)

more directly. The conversion of thermal energy to electrical energy is only about 35% efficient. Therefore, on a fuel basis, RO consumes 9-30 times the theoretical energy requirement.

A number of attempts have been applied to operate desalination process using renewable energy [63-69]. Renewable energies for use in desalination processes include wind, solar thermal, photovoltaic and geothermal. Reviews on the renewable energy driven desalination can be found in the literature.

Water production cost by different desalination has been summarized by Karagiannis et al [70] and M.A. Eltawil et al. [71] and table 2.2 summarizes the unit production cost of desalination methods.

Table 2.2 Unit production cost of different desalination methods

Method of Desalination	Unit product cost, $/m^3
Multi-stage Flash (MSF)	0.77-1.64
Multi-effect Distillation (MED)	0.87-1.95
Vapor compression (VC)	0.46-4.99
Reverse Osmosis (RO) – single pass	0.64
Reverse Osmosis (RO) – double pass	0.76

It is observed that unit production cost of desalination varies a very wide margin. Thus, J.E. Blank et al. has investigated the real cost of desalination and concluded that large thermal and membrane desalination plants may reach in the future the same level of specific water cost and that a water production cost of 1.6 $/m³, with energy cost of the year 2006 can be achieved with moderate R&D efforts [72].

Overall, it is reasonable to conclude that today's desalination cost are around $\$5/m^3$ and the energy consumption is at least five times that of the theoretical thermodynamic limit. Ng et al. [2] have proposed adsorption desalination process that mitigates the shortcomings such as high maintenance cost, high energy consumption etc., of the current desalination technologies are facing. Adsorption desalination is a novel desalination technology that has the potential of being the most energy efficient method to produce potable water typically less than the benchmark energy consumption of $1.5kWh/m^3$. The following section discusses the adsorption desalination process.

2.4. Overview of the Adsorption and adsorption desalination

The term adsorption is believed to have been first introduced by Kayser in 1881 to describe his observation of the condensation of gases on free surfaces [73]. Adsorption occurs whenever a solid surface is exposed to a gas or liquid: it is defined as the enrichment of material or increase in the density of the fluid in the vicinity of an interface [74]. Adsorption deals with the process in which molecules accumulate in the interfacial layer, but desorption denotes the converse process [75].

The earliest quantitative studies appear to have been made by Scheele in 1773 and independently by Priestley in 1775 and the Abbé Fontana in 1777. The decolorizing properties of charcoal were first investigated by the Russian chemist Lowitz in 1785 [74]. Readers interested in more details of the historical background are referred to 74.

Adsorption processes have been widely and successfully applied in separation industries decades ago using different kinds of adsorbents such as activated carbon, alumina, silica gel etc. Waste heat driven adsorption has been used in air-conditioning systems. For example adsorption refrigeration was commercialized in Japan more than a decade ago [76-80]. In these decades, much theoretical and experimental work about the adsorption refrigeration technology has been proposed and undertaken along with the development of new cycles, working pairs, system design and new research methods [81, 82].

The working pairs for the adsorption have also been developed improving the uptake of the refrigerant. The working pairs include activated carbon–methanol, silica gel-water, activated carbon–ammonia, zeolite-water and calcium chloride–ammonia [82-86].

However, the coefficient of performance of adsorption cycles has been low due to the huge thermal mass of the adsorbent material in the heat exchanger as well as the requirement for switching from exothermic adsorption process to endothermic desorption phenomenon and vice versa in the cycle. The number of reactor beds for the cycle varies from single to multi-bed while the enhancement scheme such as heat recovery and heat and mass recovery have also been incorporated to improve the performance of the adsorption chillers [87-92].

The earliest development on adsorption-based desalination was reported by Broughton [93], using an ion-retarded resin for the vapor uptake, where a process with a thermally-driven two-bed configuration is simulated. Similar theoretical studies

on the adsorption desalination plant were also proposed recently by Zejli et al. [94] and Al-kharabsheh and Goswami [95]. The solar heat source was studied as a heat source for the desalination plant, combined with an open-cycle adsorption heat pump using the zeolite as the adsorbent. Wang and Ng investigated the performance of the AD cycle using a four-bed regeneration scheme and reported the optimal specific daily water production (SDWP) of 4.7 kg/kg silica gel [96].

Ng et al. has patented adsorption based desalination process which utilizes low temperature heat from waste heat or solar energy. The first adsorption desalination experimental plant employed the multi-bed strategy and pressure equalization scheme to obtain higher performance. Adsorption desalination is a novel development for it mitigates the shortcomings of the existing desalination technologies. The advantages of the Adsorption Desalination (AD) process are i) the utilization of the low temperature waste heat ii) no moving parts rending low maintenance costs and iii) low fouling rate to the evaporating units due to lower evaporation temperature. The same authors concluded that the AD plant can produce specific daily water production of 4.7 kg of potable water per kg of silica gel using the chilled water temperature at 12.5^{o}C [96].

However, the following important detailed information on the Adsorption desalination has not been reported.

i) The performance of the AD plant at higher evaporating temperatures typically 30^{o}C.

ii) The performance of the AD plant running as a dual-effect plant, i.e., producing both cooling and potable water with the heat input.

iii) The evaluation of the optimal cycle time of the AD plant at different heat source temperatures.

iv) The performance of the AD plant with the implementation of the heat and mass recovery process.

v) The recovery ratio of the AD plant which is the percentage of the fresh water extraction from a specific amount of the feed sea water.

vi) Further development on the AD process which will improve the water production rate as well as reduce the production cost.

vii) The performance of the AD plant coupled with fluctuating heat sources such as solar energy.

The following chapter discusses the thermodynamic minimum energy requirement for desalting along with the general theoretical description of Adsorption Desalination (AD) process.

Chapter 3 General thermodynamic framework

Introduction

This chapter provides the general theoretical description of Adsorption Desalination (AD) process. The minimum energy requirement for desalting is discussed in the first section followed by the formulation of mass, energy and entropy balance for thermodynamic systems. The last section focuses on the thermodynamics of adsorption systems along with the formulation of thermodynamic surfaces of such systems. The following section describes the theoretical minimum energy required for desalination or thermodynamic limit of desalination.

3.1. Minimum Power for desalting sea water

Desalination is an energy intensive process and it requires an intrinsic minimum available energy [32, 62]. In general, desalination methods may be categorized into only two groups, namely, i) the thermally-activated methods and ii) the pressure-driven methods. For comparison purposes, the minimum energy or the thermodynamic limit of desalination should be evaluated with respect to the concentration and temperature of the solution.

3.1.1. Gibbs free energy approach

Using the Gibbs free energy, a simple expression for the separation of salt per unit amount of potable water can be expressed in terms of the chemical potential of the salt species [32, 62], that is;

$$\begin{aligned}\left(dG\right)_{P_0,T_0} &= \sum_i \mu_i dM_i \\ &= \left(\mu_w^0 dM_d\right)_{distillate\ stream} + \left(\mu_w dM_b + \sum_s \mu_s dM_s\right)_{brine\ stream}\end{aligned} \qquad 3.1$$

where G is the Gibbs free energy, μ_i is the chemical potential of species i and M_i is the mass of species i. μ_w^0 represents the pure water, M_d is the mass of distillate, μ_w is the water in the brine whereas μ_s refers to the salt species. Assuming the product is salt free and thus, from the mass balance, $dM_d = -dM_b$ and dM_s=0. Hence Equation 3.1 becomes,

$$\left(dG\right)_{P_0,T_0} = \left(\mu_w^0 - \mu_w\right) dM_d \qquad 3.2$$

For a dilute solution, $\left(\mu_w^0 - \mu_w\right) = -RT_0 \ln\left(X_w\right)$. For the case of large amount of X_w, $-\ln\left(X_w\right) = X_s$ where X_s is the mole fraction of the total salts in the feed and X_w is the mole fraction of water. Therefore, the theoretical minimum work per unit product for a limiting recovery rate is written as

$$W_{th,0} = \left(\frac{\partial G}{\partial M_w}\right)_{P_0,T_0,M_W \to 0} \Rightarrow R\,T_0\;X_s \qquad 3.3$$

Accounting for the ionic composition, the amplication factor φ, which has a value between 1 to 2, is introduced into Equation 3.3 and then the theoretical minimum work for desalination is given by

$$W_{th,0} = \left(\frac{\partial G}{\partial M_w} \right)_{P_0, T_0, M_W \to 0} = \varphi \, R \, T_0 \, X_s \qquad 3.4$$

Using the above Equation, the theoretical minimum energy for desalting at specific conditions such as temperature and initial salt concentration can be estimated. Equation 3.4 can be integrated from the initial feed concentration, X_s, to the final brine concentration, X_b as

$$W_{th,R} = \frac{1}{M_d} \int_{X_s}^{X_b} R \, T_0 \, X \, dM_d \qquad 3.5$$

Applying the concentration and mass balances, the Equation 3.5 integrated for desalination with a finite recovery (the detailed derivation is given in Appendix A).

$$W_{th,R} = R T_0 \frac{X_s X_b}{X_b - X_s} \ln \frac{X_b}{X_s} . \qquad 3.6$$

3.1.2. Minimum energy by the work done method

An alternative approach for evaluating the minimum energy of desalting the saline solution is the work done method in which the work against the reverse osmotic pressure is evaluated. Writing in terms of the chemical potential of water in a solution,

$$\mu = \mu_0 + P\bar{v} + RT\ln a \qquad 3.7$$

where μ_0 is the chemical potential of pure water at 1 atm pressure, P is the pressure in access of the 1 atm acting on the solution, $\bar{v}$ is the molar volume of water, R is the gas constant, T is solution temperature, and a is the activity of the water in the solution where a decreases with the increase in salt concentration. At the membrane interface, the water on both side of the membrane is in equilibrium and thus their chemical potentials are assumed equal:

$$\mu_0 = \mu_0 + P_{os}\bar{v} + RT\ln a \qquad 3.8$$

$$P_{os} = -\frac{RT}{\bar{v}}\ln a \qquad 3.9$$

To separate water from the salt solution, an elemental pressure which is higher than the osmotic pressure is assumed to produce a pure water volume of dv. The corresponding work done dW is given as

$$dW = P_{os}dv \qquad 3.10$$

Assuming T=298K, S=34.3% (or 34.3 ppt), the theoretical minimum free energy required for desalting at a limiting recovery rate is

$$W_{th,0} = \frac{ARTS}{\bar{v}} = 0.706kWh/m^3, \quad (v_1 - v_2) \to 0 \qquad 3.11$$

where A is coefficient for the calculation of vapor of the sea water at different salinities. For the initial and finite final volumes of the salt solution as v_1 and v_2, the total work per unit volume of fresh water produced can be evaluated by integrating from initial volume to final volume as

$$W = \frac{1}{v_1 - v_2}\int_{v_1}^{v_2} P_{os}\,dv = \frac{-RT}{(v_1 - v_2)\bar{v}}\int_{v_1}^{v_2} \ln a\,dv \qquad 3.12$$

where a is the activity coefficient which is defined as $a \equiv \frac{P}{P_0}$ where P_0 and P are the equilibrium water vapor pressures above pure water and the solution.

Using the vapor pressure of the sea water given by $P = P_0(1 - AS)$[97] where A=0.000537 and S is the salinity, the theoretical work for finite recovery becomes

$$W_{thR} = \frac{ART}{\bar{v}}\frac{v_1}{(v_1 - v_2)}\ln\frac{v_2}{v_1} \qquad 3.13$$

Table 3.1 summarizes the theoretical energy requirement for desalting by Gibbs approach and work done approach. The detailed comparison on the theoretical work by these two approaches is given in the Appendix B.

Table 3.1 Summary of the theoretical energy requirement for desalting

Theoretical minimum work (kWh/m^3)	Gibbs approach	Work done approach

$W_{th,0}$	$RT_0\ X_s$	$\frac{ARTS}{\bar{v}}$
$W_{th,R}$	$RT_0 \frac{X_s X_b}{X_b - X_s} \ln \frac{X_b}{X_s}$	$\frac{ART}{\bar{v}} \frac{v_1}{(v_1 - v_2)} \ln \frac{v_2}{v_1}$

3.2. General formulation of mass, energy and entropy balances

This section discusses the general formularization of the mass, energy and entropy of a system that involves the simultaneous transfer of mass, heat and momentum. The Reynolds Transport Theorem approach along with the combination of Gauss Divergence theorem and Leibniz integral rule are applied to formulate the balances. Consider an extensive property, *N*, (a scalar, vector or tensor) of the identifiable fixed mass (system) such as total mass, momentum, or energy, the corresponding intensive property will be designated as α, then if $(N)_S = \int_{mass} \alpha\, dm = \int_{volume} \alpha\, \rho\, dV$, where the Reynolds transport Theorem with the application of Leibniz integral rule states that

$$\underbrace{\frac{D}{Dt}(N)_s = \frac{D}{Dt}\left(\int_{volume} \alpha\, \rho\, dV\right)}_{Lagrangian} = \underbrace{\frac{\partial}{\partial t}\left(\int_{CV} \alpha\, \rho\, dV\right) + \int_{CS} \alpha\left(\rho \vec{v} \bullet d\vec{A}\right)}_{Eulerian} \quad . \qquad 3.14$$

Here, the $\frac{D}{Dt}(N)_s$ and $\frac{D}{Dt}\left(\int_{volume} \alpha\, \rho\, dV\right)$ are the total rate of change of any arbitrary extensive property of the system, $\frac{\partial}{\partial t}\left(\int_{CV} \alpha\, \rho\, dV\right)$ is the time rate of change of the arbitrary extensive property *N* within the control volume evaluated by an observer

fixed in the moving control volume, and $\alpha\left(\rho\vec{v}.d\vec{A}\right)$ is the net rate of efflux of the extensive property *N* through the control surface where $\vec{v}$ is the velocity measured relative to the control volume. The intensive property, α, corresponding to *N* can be expressed in terms of engineering applications such as described in Table 3.2.

Table 3.2 Coefficient α for different properties

Quantity	**α**
Mass	1
Linear momentum	$\vec{v}$
Angular momentum	$\vec{r}\times\vec{v}$
Energy	*e*
Entropy	*s*

3.2.1. Conservation of mass

When Equation 3.14 is applied in the fixed control volume with the total mass in the system, the conservation of mass states that rate of change of mass of a system sums to zero. The Reynolds' transport theorem stipulates that $\alpha = 1$, and hence the conservation of mass becomes;

$$\frac{D}{Dt}\left(\int_{Volume}\rho dV\right)=\frac{\partial}{\partial t}\left(\int_{CV}\rho\, dV\right)+\int_{CS}\left(\rho\vec{v}.d\vec{A}\right)=0 \qquad 3.15$$

Within a fixed control volume and a fixed coordinate system, the limits of integration simplifies to

$$\int_{CV} \frac{\partial \rho}{\partial t} dV + \int_{CS} \left(\rho \vec{v} . d\vec{A} \right) = 0 \qquad 3.16$$

Applying the Gauss divergence theorem and setting the integrand to zero, the conservation of mass becomes

$$\frac{\partial \rho}{\partial t} + \nabla . \left(\rho \vec{v} \right) = 0 \qquad 3.17$$

where ρ is the total density which is $\rho = \sum_{k=1}^{n} \rho_k$ and v is the bari-centric velocity, i.e., $v = \sum_{k=1}^{n} \frac{\rho k v k}{\rho}$.

3.2.2. Conservation of momentum:

Similarly, using the Reynolds transport theorem and Gauss divergence theorems, the conservation of momentum where $\alpha = \vec{v}$ can be written as

$$\frac{d\left(\rho \vec{v} \right)}{dt} = \frac{\partial \left(\rho \vec{v} \right)}{\partial t} + \nabla . \left(\rho \vec{v} \vec{v} \right) \qquad 3.18$$

In tensor notation, the Equation 3.18 can be written as

$$\frac{d \rho \vec{v}}{dt} = -\nabla . P + \sum_{k} \rho_k F_k \qquad 3.19$$

where P is the pressure tensor resulted from the short-range interactions between the particles of the system and $\boldsymbol{F}_k$ is the tensor resulted from the external forces and long-range interactions in the system. From Equations 3.18 and 3.19, the balance Equation of the momentum density becomes

$$\frac{\partial(\rho\vec{v})}{\partial t} = -\nabla.(\rho\vec{v}\vec{v} + P) + \sum_k \rho_k F_k \qquad 3.20$$

Here $\rho\vec{v}$ is momentum density, $\rho\vec{v}\vec{v} + P$ is momentum flow where $\rho\vec{v}\vec{v}$ is the convective part and $\sum_k \rho_k F_k$ is the source of momentum and $\vec{v}\vec{v}$ is dyadic product.

3.2.3. Conservation of energy

Applying the principle of conservation of energy, the total energy content within an arbitrary volume V of the system can only change due to the energy flows through the boundary and can be expressed as

$$\frac{d}{dt}\int_{CV} \rho e dV = \int_{CV} \frac{\partial(\rho e)}{\partial t} dV = -\int_{CS} \mathbf{J}_e dA \qquad 3.21$$

Defining $\mathbf{J}_e$ as the total energy flux, which is given as $\mathbf{J}_e = \rho e\vec{v} + P.\vec{v} + \sum_{k=1}^{n} \psi_k J_k + \mathbf{J}_q$ and the total energy, $e = \left(\frac{1}{2}\rho\vec{v}^2 + \psi + u\right)$, u is the internal energy. From the microscopic point of view, it represents the energy due to the short-range molecular interactions and of thermal agitation. In the total energy

flux, $\rho e\vec{v}$ is the convective term, $P.\vec{v}$ is the energy flux due to the mechanical worked applied to the system, $\sum_{k=1}^{n}\psi_k J_k$ is the potential energy flux due to the diffusion of the various components in the field of force, and $\mathbf{J}_q$ is the heat flow.

Using the Reynolds transport and Gauss divergence theorems, the conservation of energy can be written as

$$\frac{\partial(\rho e)}{\partial t} = -\nabla.\mathbf{J}_e \qquad 3.22$$

Equation 3.22 can be expanded to include the potential and kinetic terms, as well as the internal energy as

$$\frac{\partial\rho\left(\frac{1}{2}\vec{v}^2+\psi\right)}{\partial t}+\frac{\partial(\rho u)}{\partial t} = -\nabla.\left(\rho\, e\vec{v}+P.\vec{v}+\sum_{k=1}^{n}\psi_k J_k+\mathbf{J}_q\right) \qquad 3.23$$

Note the term $\frac{\partial\rho\left(\frac{1}{2}\vec{v}^2+\psi\right)}{\partial t}$ in Equation 3.23 can be eliminated by replacing the "e" term to "u" term on the right side. Detailed derivation is given in Appendix C.

$$\frac{\partial(\rho u)}{\partial t} = -\nabla.\left(\rho u\vec{v}+\mathbf{J}_q\right)-\mathbf{P}:\nabla.\vec{v}+\sum_{k=1}^{n}J_k F_k \qquad 3.24$$

Here, the $\rho u\vec{v} + \mathbf{J}_q$ is the energy flow due to convection and thermal energy transfer that gives rise to an internal energy change, while $-\mathbf{P}:\nabla.\vec{v} + \sum_{k=1}^{n} J_k F_k$ is an internal energy source term. Equation 3.24 can be further simplified as

$$\rho\frac{du}{dt} - \nabla\cdot\left(\rho u\vec{v}\right) = -\nabla\cdot\left(\rho u\vec{v} + \mathbf{J}_q\right) - \mathbf{P}:\nabla.\vec{v} + \sum_{k=1}^{n} J_k F_k \qquad 3.25$$

The third term of Equation 3.25 can be expanded into a scalar hydrostatic part p and a tensor Π as $\mathbf{P} = pU + \Pi$ where U is the unit matrix and thus Equation 3.25 becomes

$$\rho\frac{du}{dt} = -\nabla\cdot\mathbf{J}_q - p\nabla\cdot\vec{v} - \Pi:\nabla.\vec{v} + \sum_{k=1}^{n} J_k F_k \qquad 3.26$$

Noting that $\rho\frac{dq}{dt} = -\nabla.\mathbf{J}_q$ and $\rho\frac{d\nu}{dt} = \nabla\cdot\vec{v}$ and hence the energy balance Equation becomes

$$\frac{du}{dt} = \frac{dq}{dt} - p\frac{d\nu}{dt} - \nu\Pi:\nabla.\vec{v} + \nu\sum_{k=1}^{n} J_k F_k \qquad 3.27$$

The first term on the right hand side of Equation 3.27 represents the heat flux, the second and third term stand for the mechanical work and the last term states the externally induced forces such as electro-magnetic forces.

3.2.4. Entropy Balance

For any macroscopic thermodynamic system, the change of a state function such as the entropy, dS may be written as $dS = d_e S + d_i S$ where $d_e S$ is the entropy contributed by the surroundings and $d_i S$ is the entropy produced inside the system. The Second Law of Thermodynamics demands that the entropy generation inside the system $d_e S \geq 0$. Using the Reynolds transport theorem, the entropy functions can be written as

$$S = \int_{CV} \rho s dV \qquad 3.28$$

$$\frac{d_e S}{dt} = -\int_{CS} \mathbf{J}_{s,tot} d\vec{A} \qquad 3.29$$

$$\frac{d_i S}{dt} = -\int_{CV} \sigma dV \qquad 3.30$$

where $\mathbf{J}_{s,tot}$ is the total entropy flow per unit area and unit time and σ is the total entropy generation inside the unit control volume per unit time. Applying the Gauss theorem and setting the integrand to zero,

$$\frac{\partial \rho s}{\partial t} = -\nabla . \mathbf{J}_{s,tot} + \sigma \qquad where\ \sigma \geq 0 \qquad 3.31$$

Equations 3.30 and 3.31 are the mathematical forms of the second law of thermodynamics. Equation 3.31 can be also written as

$$\rho \frac{ds}{dt} = -\nabla.(\mathbf{J}_s) + \sigma \qquad 3.32$$

where $\mathbf{J}_s = \mathbf{J}_{s,tot} - \rho s v$ is the entropy flux. The entropy per unit mass is a function of the internal energy u, the specific volume v, and the mass fractions c_k which is $c_k = \frac{\rho_k}{\rho}, \left(\sum_{k=1}^{n} c_k = 1 \right)$. Applying the Gibbs relation, the total differential of the entropy at equilibrium is written as

$$Tds = du + pdv - \sum_{k=1}^{n} \mu_k dc_k \qquad 3.33$$

where p is the equilibrium pressure and μ_k is the chemical or thermodynamic potential of component *k*. Assuming local equilibrium exists within small mass elements, (even though the total system is not in equilibrium) Equation 3.33 now can be written as

$$T \frac{ds}{dt} = \frac{du}{dt} + p \frac{dv}{dt} - \sum_{k=1}^{n} \mu_k \frac{dc_k}{dt} \qquad 3.34$$

Inserting $\frac{du}{dt}$ and $p \frac{dv}{dt}$ from energy balance Equation,

$$\rho \frac{ds}{dt} = -\frac{\nabla \cdot \mathbf{J}_q}{T} - \frac{1}{T} \Pi : \nabla.\vec{v} + \frac{1}{T} \sum_{k=1}^{n} J_k F_k + \frac{1}{T} \sum_{k=1}^{n} \mu_k \nabla.\mathbf{J}_k - \frac{1}{T} \sum_{j=1}^{r} A_j J_j \qquad 3.35$$

where A_j is the chemical affinity of the reaction j and is defined by $Aj = \sum_{k=1}^{n} \nu_{kj} \mu_{kj}$.

Finally, the entropy balance Equation can be expressed as

$$\rho \frac{ds}{dt} = -\nabla . \left(\frac{\mathbf{J}_q - \sum_{k=1}^{n} \mu_k \mathbf{J}_k}{T} \right) - \frac{1}{T^2} \mathbf{J}_q . \nabla T - \frac{1}{T} \Pi : \nabla . \vec{v} - \frac{1}{T} \sum_{k=1}^{n} J_k . \left(T \nabla \frac{\mu_k}{T} - F_k \right) - \frac{1}{T} \sum_{j=1}^{r} A_j J_j \qquad 3.36$$

Comparing with Equation 3.32, the entropy flux and the entropy generation now become

$$\mathbf{J}_s = \frac{1}{T} \left(\mathbf{J}_q - \sum_{k=1}^{n} \mu_k \mathbf{J}_k \right) \qquad 3.37$$

$$\sigma = -\frac{1}{T^2} \mathbf{J}_q . \nabla T - \frac{1}{T} \Pi : \nabla . \vec{v} - \frac{1}{T} \sum_{k=1}^{n} J_k . \left(T \nabla . \frac{\mu_k}{T} - F_k \right) - \frac{1}{T} \sum_{j=1}^{r} A_j J_j \qquad 3.38$$

3.3. Thermodynamic frame work for adsorbent-adsorbate pair

The thermodynamic approach to the equilibrium study is general practice and it is applied to adsorption just as to other phase equilibrium processes. The general assumption for adsorption is that the adsorbed phase may be treated as a distinguishable phase in the thermodynamic sense. Adsorption of water vapors on the pores of the adsorbent is physisorption and the adsorbed phase is held near the pores by the existence of van deer Walls forces [98-101]. When adsorbate gas molecules

come into contact with the surface of the adsorbent, these molecules are captured by the field of force by the adsorbent surface (Van der Waals forces). By neglecting the unadsorbed molecules, the porous surface of the adsorbent would be covered by a layer of molecules which is considered to be monolayer and such process occurs over wide ranges of pressures and temperatures.

Thermodynamic properties such as internal energy, enthalpy and entropy of the system, the specific heat capacity, the adsorbed phase volume and the heat of adsorption are required to characterize the nature of adsorbent+adsorbate system. These thermodynamic properties to describe the adsorbent+adsorbate system are discussed in this section.

3.3.1. Enthalpy

Total differential entropy of the adsorbent+adsorbate system can be written as

$$dh = dh_s + dh_a \tag{3.39}$$

Here h_s and h_a stand for enthalpies of adsorbent and adsorbate. Using the Gibbs free energy and Maxwell relationship and Clapeyron relation, dh is written as,

$$dh = \left(C_{p,s} + C_{p,a}\right)dT + \left\{v_s - T\left(\frac{\partial v_s}{\partial T}\right)_P\right\}dP + \left\{v_a - T\left(\frac{\partial v_a}{\partial T}\right)_{P,x}\right\}dP + \left\{h_g - Q_{st}\right\}dx \tag{3.40}$$

Where $Q_{st}(P,T,x)$ is the isosteric heat of adsorption, $C_{p,s}$ and $C_{p,a}$ are the specific heat capacities of adsorbent and adsorbate phase, and v_s and v_s are the specific volumes of the adsorbent and adsorbate, respectively.

3.3.2. Internal Energy

The total internal energy of the adsorbent+adsorbate system is the summation of the internal energies of the solid phase and adsorbed phase and can be written as

$$du = (dh_a + dh_s) - (Pdv_s + v_s dP + Pdv_a + v_a dP) \qquad 3.41$$

Substituting dh in Equation 3.41, the internal energy becomes,

$$du = (C_{p,s} + C_{p,a})dT + \left\{ v_s - T\left(\frac{\partial v_s}{\partial T}\right)_P \right\} dP + \left\{ v_a - T\left(\frac{\partial v_a}{\partial T}\right)_{P,x} \right\} dP + \{h_g - Q_{st}\}dx - (Pdv_s + v_s dP + Pdv_a + v_a dP) \qquad 3.42$$

3.3.3. Entropy

The total differential of the entropy of the adsorbent+adsorbate system is the summation of the entropies of its solid and adsorbed phases which is given as $ds = ds_s + ds_a$. Using the Gibbs free energy and Maxwell relations, the entropy of the solid phase may be determined as

$$ds_s = \frac{c_{p,s}}{T} dT - \left(\frac{\partial v_s}{\partial T}\right)_P dP \qquad 3.43$$

In the same way, the total differential of entropy for adsorbed phase may be written as a function of T, P, x

$$ds_a = \left(\frac{\partial s_a}{\partial T}\right)_{P,x} dT + \left(\frac{\partial s_a}{\partial P}\right)_{T,x} dP + \left(\frac{\partial s_a}{\partial x}\right)_{T,P} dx \qquad 3.44$$

where $x = \frac{m_a}{M_s}$ and M_s is the mass of adsorbent. Assuming $\mu_a \cong \mu_g$ at equilibrium and constant adsorbate amount, ds_a becomes

$$ds_a = \frac{C_{p,a}}{T} dT - \left(\frac{\partial v_a}{\partial T}\right)_{P,x} dP + s_g - \left(v_g - v_a\right)\frac{dP}{dT} \qquad 3.45$$

Finally, the total differential entropy of the adsorbent+adsorbate system can be written as

$$ds = \left(\frac{C_{p,s}}{T} + \frac{C_{p,a}}{T}\right)dT - \left(\frac{\partial v_s}{\partial T}\right)_p dP - \left(\frac{\partial v_a}{\partial T}\right)_{P,x} dP + \left\{s_g - \left(v_g - v_a\right)\frac{dP}{dT}\right\}dx \qquad 3.46$$

3.3.4. Isosteric heat of adsorption

For adsorption applications, these thermodynamic variables are expressed with respect to the isosteric heat of adsorption of an adsorbent+adsorbate pair. The detailed derivation is given in the sections below. The isosteric heat of adsorption is defined as the differential change in energy δq that occurs when an infinitesimal amount of

adsorbate δx is transferred at constant pressure, temperature and the amount of adsorbent or the constant adsorbent surface ranging from bulk gas phase to the adsorbed phase

$$Q_{st} = \left(\frac{\partial q}{\partial x}\right)_{P,T,M_s} \qquad 3.47$$

The elemental heat rejected onto the adsorbent can be expressed by $-dq = Tds$ where s is the sum of the entropy of the adsorbent+adsorbate system i.e., $ds = ds_a + ds_s + ds_g$ and Equation 3.47 now becomes,

$$Q_{st} = -T\left[\left(\frac{\partial s_g}{\partial x}\right)_{P,T,M_s} + \left(\frac{\partial s_a}{\partial x}\right)_{P,T,M_s} + \left(\frac{\partial s_s}{\partial x}\right)_{P,T,M_s}\right] \qquad 3.48$$

However, as $\left(\frac{\partial s_s}{\partial x}\right)_{P,T,M_s}$ is negligibly small, the isosteric heat becomes,

$$Q_{st} = T\left[\left(v_g - v_a\right)\frac{dP}{dT}\right] \qquad 3.49$$

3.3.5. Specific volume of the adsorbed phase

The adsorbed phase volume, which is calculated by Equation 3.49 from the experimentally measured isosteric heat of adsorption data, is given as,

$$v_a = v_g - \left\{ Q_{st}^{\exp t} - T v_g \left(\frac{\partial P}{\partial T} \right)_g \right\} \Big/ T \left(\frac{\partial P}{\partial T} \right)_x \qquad 3.50$$

where v_g is the specific volume of the gaseous phase. The term $\left(\frac{\partial P}{\partial T} \right)_x$ is calculated from experimentally measured adsorption isotherm data or Equations.

3.3.6. Specific heat capacity of the adsorbed phase

The specific heat capacity of the adsorbed phase is defined as the temperature derivative of the adsorbed phase enthalpy at constant surface coverage, *x*, i.e., $C_{p,a} = \left(\frac{\partial h_a}{\partial T} \right)_x$. Using the determinants or Jacobians (Detailed derivation can be found in Appendix D) for the calculation of $\left(\frac{\partial h_a}{\partial T} \right)_x$, where h_a and x for *T* are the determinants, $C_{p,a}$ can be expressed as

$$C_{p,a} = \left(\frac{\partial h_a}{\partial T} \right)_x = \left(\frac{\partial h_a}{\partial T} \right)_P + \left(\frac{\partial h_a}{\partial P} \right)_T \left(\frac{\partial P}{\partial T} \right)_x \qquad 3.51$$

Using the Gibbs law and the Maxwell relations, the enthalpy changes with respect to pressure at constant temperature and uptake can be written as,

$$\left(\frac{\partial h_a}{\partial P} \right)_T = -T \left(\frac{\partial v_a}{\partial T} \right)_P + v_a + P \left(\frac{\partial v_a}{\partial P} \right)_T \qquad 3.52$$

where the first term indicates thermal expansion of the adsorbed phase and the last term defines the isothermal compressibility of the adsorbed phase on the adsorbents. Here v_a is the specific volume of the adsorbed phase. For simplicity,

$$\left(\frac{\partial h_a}{\partial P}\right)_T \approx -T\left(\frac{\partial v_g}{\partial T}\right)_P + v_g + P\left(\frac{\partial v_g}{\partial P}\right)_T \qquad 3.53$$

In terms of the measurable variables, $C_{p,a}$ can be expressed as,

$$c_{p,a} = c_{p,g} + \left\{\frac{1}{T} - \frac{1}{v_g}\left(\frac{\partial v_g}{\partial T}\right)_P\right\} Q_{st} - \left.\frac{\partial Q_{st}}{\partial T}\right|_P \qquad 3.54$$

3.4. Thermodynamic property surface

The extensive thermodynamic quantities such as entropy (s), internal energy (u), and enthalpy (h) of a single-component adsorbent+adsorbate system at a given mass of adsorbent, (M_s), are path independent, and their changes can be tracked by integrating in succession between the limits of initial pressure (P_o) and P, initial temperature (T_o) and T, and x_o (x= 0) and x with T, x; P, x; and P, T being held constant, respectively, for these integration processes. Neglecting the pressure and uptake dependence of solid phase thermodynamic properties with respect to pressure and temperature, the entropy of the adsorbent + adsorbate system becomes,

$$s(P,T,x) = s(P_o,T_o,x_o) + \int_{T_0}^{T}\left(\frac{\partial s_s}{\partial T}\right)_{P,x} dT + \int_{T_0}^{T}\left(\frac{\partial s_a}{\partial T}\right)_{P,x} dT + \int_{P_0}^{P}\left(\frac{\partial s_a}{\partial P}\right)_{T,x} dP + \int_{0}^{x}\left(\frac{\partial s_s}{\partial x}\right)_{T,P} dx \quad 3.55$$

$$s(P,T,x) = s(P_o,T_o,x_o) + \int_{T_o}^{T}\frac{c_{p,s}}{T}dT + \int_{T_o}^{T}\frac{c_{p,a}}{T}dT - \int_{P_o}^{P}\left(\frac{\partial v_a}{\partial T}\right)_{p,x} dP + \int_0^x\left\{s_g - (v_g - v_a)\frac{dP}{dT}\right\}dx \quad 3.56$$

$$s(P,T,x) = s(P_o,T_o,x_o) + \int_{T_o}^{T}\frac{c_{p,s}}{T}dT + \int_{T_o}^{T}\frac{1}{T}\left[c_{p,g} + Q_{st}\left\{\frac{1}{T} - \frac{1}{v_g}\left(\frac{\partial v_g}{\partial T}\right)_p\right\} - \frac{\partial Q_{st}}{\partial T}\right]dT - \int_{P_o}^{P}\left(\frac{\partial v_a}{\partial T}\right)_{p,x} dP + \int_0^x\left\{s_g - \frac{Qst}{T}\right\}dx \quad 3.57$$

For simplicity [103],

$$s(P,T,x) \approx s(P,T,x_o) + \int_{T_o}^{T}\frac{c_{p,s}}{T}dT + \int_{T_o}^{T}\frac{1}{T}\left[Q_{st}\left\{\frac{1}{T} - \frac{1}{v_g}\left(\frac{\partial v_g}{\partial T}\right)_p\right\} - \frac{\partial Q_{st}}{\partial T}\right]dT - \int_0^x\left\{s_g - \frac{Q_{st}}{T}\right\}dx \quad 3.58$$

Similarly, the enthalpy and the internal energy of the adsorbent+adsorbate can be written as follows.

$$h(P,T,x) = h(P_o,T_o,x_o) + \int_{T_o}^{T}(c_{p,s} + c_{p,a})dT + \int_{P_o}^{P}\left\{v_a - T\left(\frac{\partial v_a}{\partial T}\right)_{p,x}\right\}dP + \int_{x_o}^{x}(h_g - Q_{st})dx \quad 3.59$$

$$h(P,T,x) \approx h(P,T,x_o) + \int_{T_o}^{T} (c_{p,s} + c_{p,g}) dT + \int_{T_o}^{T} \left[Q_{st} \left\{ \frac{1}{T} - \frac{1}{v_g} \left(\frac{\partial v_g}{\partial T} \right)_p \right\} - \frac{\partial Q_{st}}{\partial T} \right] dT + \int_0^x \{h_g - Q_{st}\} dx \quad 3.60$$

$$u(P,T,x) \approx u(P,T,x_o) + \int_{T_o}^{T} (c_{p,s} + c_{p,g}) dT + \int_{T_o}^{T} \left[Q_{st} \left\{ \frac{1}{T} - \frac{1}{v_g} \left(\frac{\partial v_g}{\partial T} \right)_p \right\} - \frac{\partial Q_{st}}{\partial T} \right] dT + \int_{x_o}^{x} \{h_g - Q_{st}\} dx - \int_0^{v_a} P dv_a - \int_{P_o}^{P} v_a dP \quad 3.61$$

3.5. Summary of Chapter 3

Minimum energy requirement for desalting regardless of the method has been derived from the Gibbs free energy as well as the work done approaches. The general balances for mass, energy and entropy have also been discussed. Table 3.3 summarizes the thermodynamic properties for the adsorbent-adsorbate system which will be used for the modeling for the adsorption desalination cycle in the following Chapters.

Table 3.3 summarizes the thermodynamic properties for the adsorbent-adsorbate system

Property	Equation
Enthalpy (h)	$dh = (C_{p,s} + C_{p,a}) dT + \left\{ v_s - T \left(\frac{\partial v_s}{\partial T} \right)_P \right\} dP + \left\{ v_a - T \left(\frac{\partial v_a}{\partial T} \right)_{P,x} \right\} dP + \{h_g - Q_{st}\} dx$

Internal energy (u)	$du = \left(C_{p,s} + C_{p,a}\right)dT + \left\{v_s - T\left(\frac{\partial v_s}{\partial T}\right)_P\right\}dP + \left\{v_a - T\left(\frac{\partial v_a}{\partial T}\right)_{P,x}\right\}dP + \left\{h_g - Q_{st}\right\}dx - \left(Pdv_s + v_s dP + Pdv_a + v_a dP\right)$
Entropy (s)	$ds = \left(\frac{C_{p,s}}{T} + \frac{C_{p,a}}{T}\right)dT - \left(\frac{\partial v_s}{\partial T}\right)_p dP - \left(\frac{\partial v_a}{\partial T}\right)_{P,x} dP + \left\{s_g - \left(v_g - v_a\right)\frac{dP}{dT}\right\}dx$
Isosteric heat of adsorption (Q_{st})	$Q_{st} = T\left[\left(v_g - v_a\right)\frac{dP}{dT}\right]$
Specific volume of adsorbed phase (v_a)	$v_a = v_g - \left\{Q_{st}^{\exp t} - Tv_g\left(\frac{\partial P}{\partial T}\right)_g\right\} \Big/ T\left(\frac{\partial P}{\partial T}\right)_x$
Specific heat capacity of adsorbed phase ($c_{p,a}$)	$c_{p,a} = c_{p,g} + \left\{\frac{1}{T} - \frac{1}{v_g}\left(\frac{\partial v_g}{\partial T}\right)_P\right\}Q_{st} - \left.\frac{\partial Q_{st}}{\partial T}\right\|_P$

Chapter 4 Thermodynamic modeling and performance analysis of an adsorption desalination cycle

Introduction

This chapter discusses the performance analysis of a conventional adsorption desalination (AD) cycle which operates at low temperature waste heat. The thermodynamic formulation, described in Chapter 3, is applied to construct a thermodynamic model and the predicted performance results of the AD cycles i.e., both 2-bed and 4-bed operation modes, are verified with experimental data. Prior to the thermodynamic formulization, it is important to select a suitable adsorbent for the AD cycle. Considerations include the physical characteristics of the adsorbent such as surface area, pore size distribution, pore volume and isotherm. The characteristics of the adsorbent employed in the AD cycle are discussed in the following section.

4.1. Characteristics of silica gel and Isotherms of silica gel + water system

The efficacy of an adsorption desalination (AD) cycle depends on the sorption characteristics of adsorbent (silica gel) and adsorbate (water vapor) for the production of potable water. Water vapor uptake by the adsorbent is a direct function of cycle performance. Thus, the adsorbent to be used in the cycle should possess good uptake of the adsorbate (water vapor) as well as the ability to regenerate at reasonably low temperature. Usually, the adsorbent material is a hydrophilic porous material having a higher surface area with transient bonding to water molecules via the

hydrogen bonds. A suitable adsorbent is based on the regeneration temperature and Table 4.1 shows types of hydrophilic adsorbents and their respective regeneration temperatures.

Table 4.1 Types of adsorbent and their regeneration temperatures

Type of adsorbent	Regeneration temperature (°C)
Silica gel	55-140
Activated Alumina	120-260
Zeolite molecular sieve	175-370

Silica gel has been selected as it is able to perform regeneration at the lowest temperature since the AD cycle is designed to recover low temperature waste heat which is essentially "free" and hence, a lower cost to desalt seawater or brackish water. This section discusses i) the measurement of the surface characteristics, such as surface areas, pore size distributions and pore volume, of silica gels through the sorption of nitrogen gas at liquid nitrogen temperature (77 K), and ii) the isotherm characteristics of water vapor for many types of silica gel ($SiO_2.nH_2O$), which is a partially dehydrated form of polymeric colloidal silicic acid [102].

The properties of silica gel are analysed using an AutoSorp-1 analyser. This instrument measures the amount of gas adsorbed or desorbed from a porous surface at a predetermined equilibrium (vapour) pressure by the static volumetric method with liquid Nitrogen at 77K as the filling fluid. [Detailed description of AutoSorp-1 analyser is given in Appendix D]. The adsorption and desorption of N_2 by different types of silica gels are given in Figure 4.1 and it is observed that MYCOM-manufactured silica gel has the highest uptake.

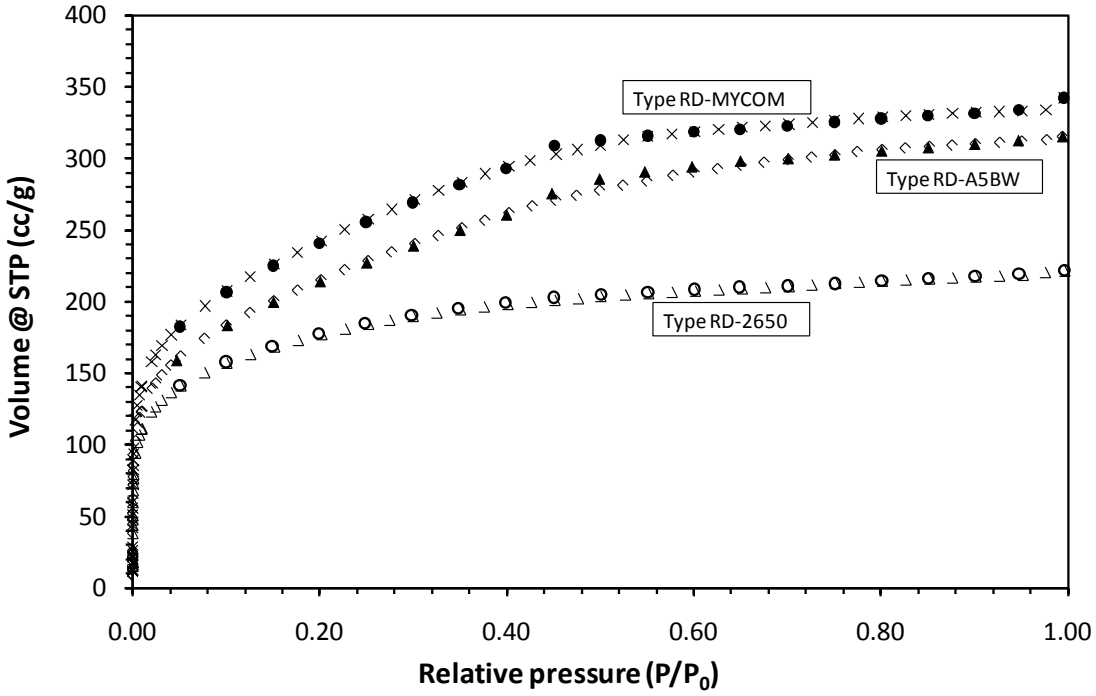

Figure 4.1 Nitrogen (N2) uptakes of different types of silica gels

The surface area of the adsorbent (silica gel), as determined by using the Brunauer-Emmett-Teller (BET) method and the BET Equation, is given as

$$\frac{1}{W\left(\frac{P_0}{P}-1\right)}=\frac{1}{W_m C}+\frac{C-1}{W_m C}\left(\frac{P}{P_0}\right) \qquad 4.1$$

where W is the weight of the gas adsorbed at a relative pressure $\frac{P}{P_0}$ and W_m is the weight of adsorbate at a monolayer coverage and C is the BET constant. This is related to the adsorption energy of the first adsorbed layer, indicating the magnitude of the adsorbent/adsorbate interactions. Three types of silica gels from different manufacturers namely: i) Type RD-MYCOM, (ii) type RD-2650, and (ii) Type-A5 BW were investigated. Figure 4.2 gives the BET plot for these silica gels. The BET results show that Type RD-MYCOM silica gel has the highest surface area which is

about 746.2 m^2/g while the summary of the surface area analysis BET method is given in Table 4.2.

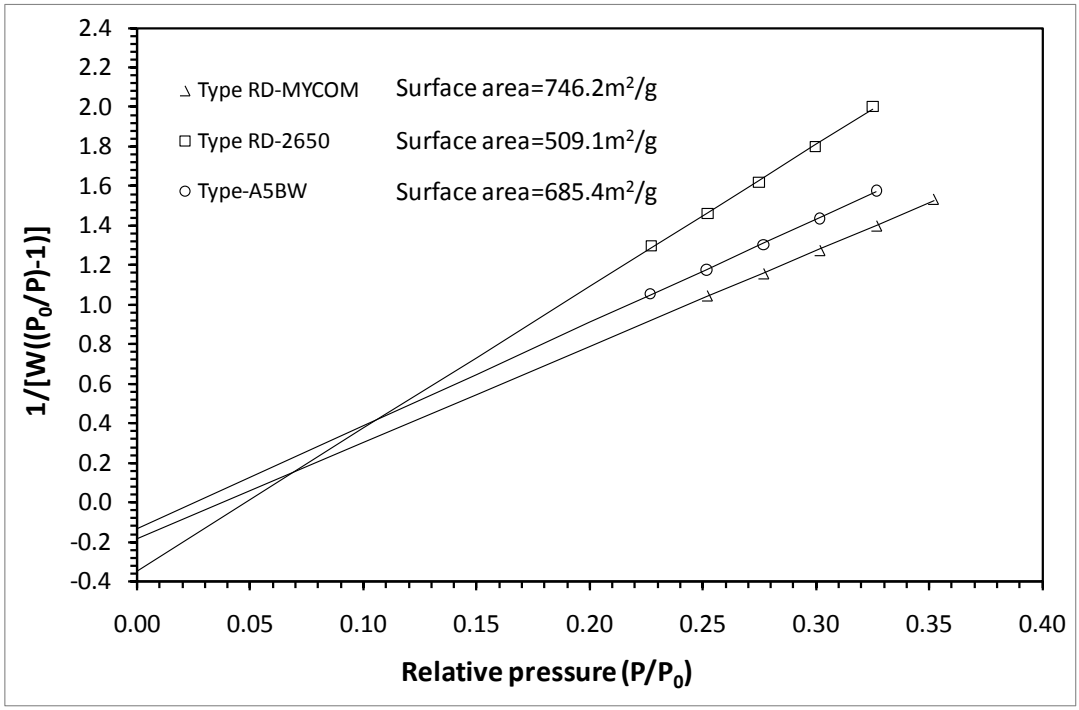

Figure 4.2 BET plot of different types of silica gels

Table 4.2 Summary of the BET analysis

	Type RD-Mycom	Type RD-2650	Type A5-BW
Slope	4.849	7.186	5.215
BET constant, C	-25.667	-19.81	-37.953
Y-intercept, i	-0.1818	-0.3453	-0.1339
Correlation coefficient, r	0.999373	0.999248	0.999622
Surface area (m^2/g)	746.17	509.07	685.38

The pore-size distribution analysis of the above mentioned silica gels are conducted using the density functional theory (DFT) method with the application of the provided software package of the AutoSorb and it is given in Figure 4.3. The

results showed that all three parent silica gels have a two-maximum distribution or bimodal type and their pore diameter ranges are between 12Å and 17Å.

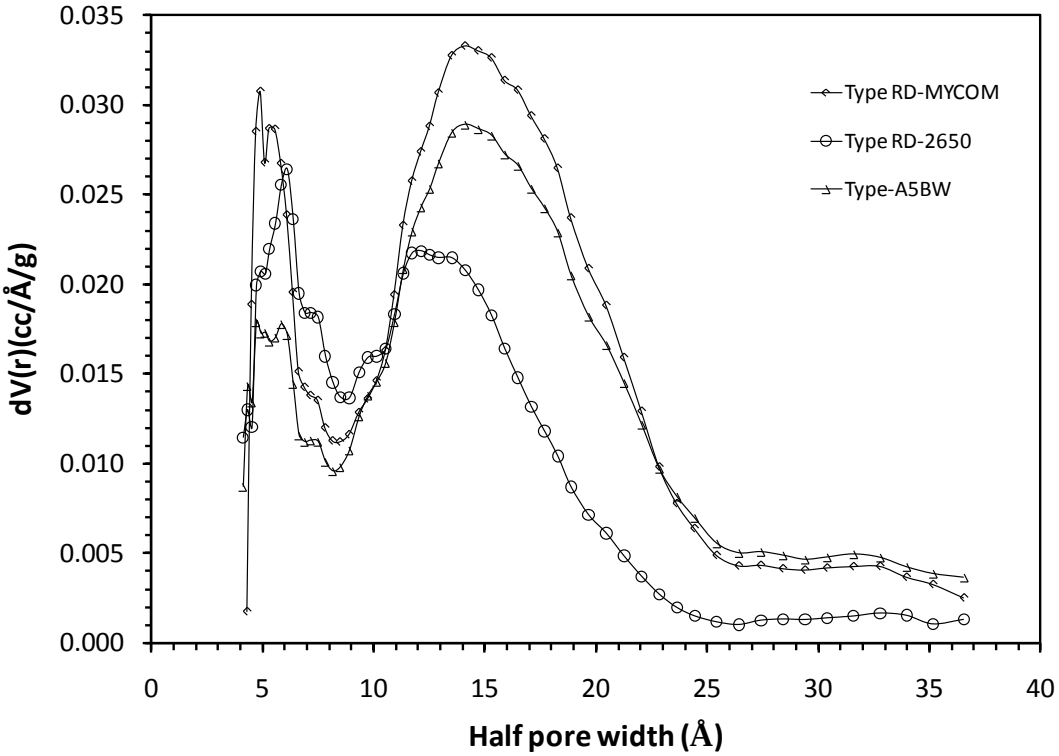

Figure 4.3 Pore size distribution of three different parent silica gels.

In an AD cycle, the adsorbate is water vapour which is an important factor in the selection of silica gel. Such an analysis can be performed using the HydroSorb 1000, while the detailed description of this analyser is found in Appendix E. Figure 4.4 compares the water vapor uptake of the silica gel at 25^{o}C which keeps the adsorbent at isothermal condition. The results indicated that the MYCOM type silica gel possesses the highest equilibrium uptakes of 537cc/g. The insert diagram in Figure 4.4 shows the adsorption and desorption of the water vapor by MYCOM type silica gel.

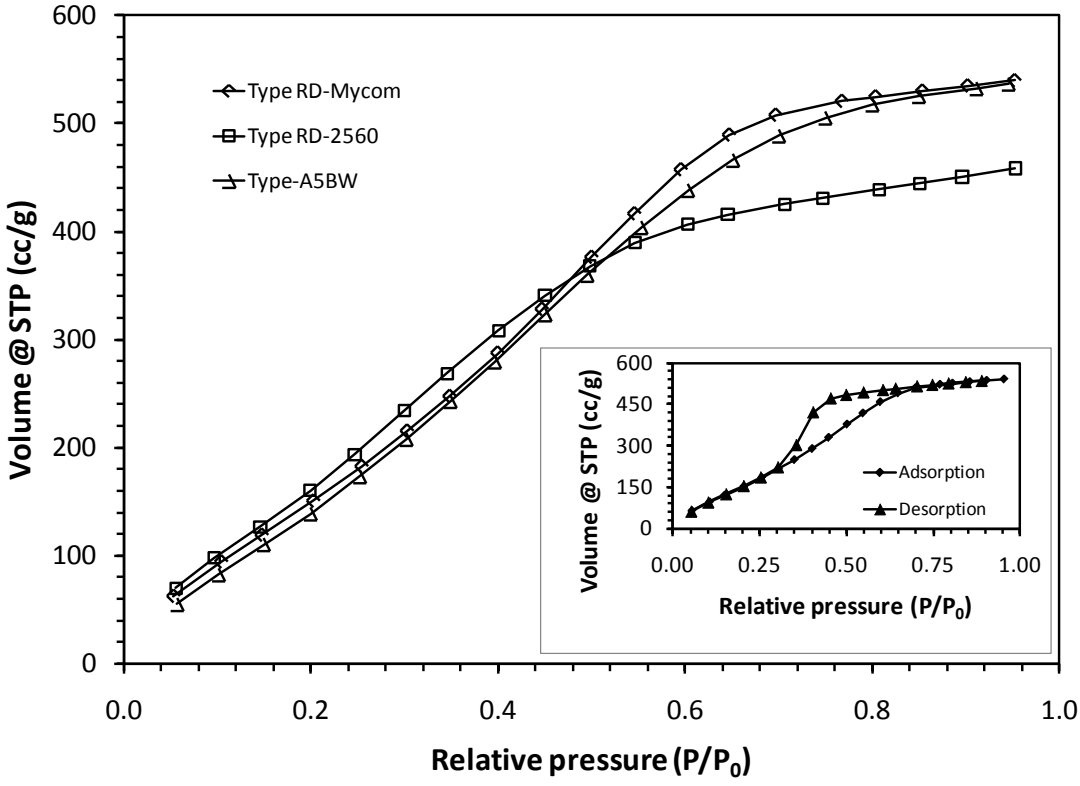

Figure 4.4 Water vapor uptakes of different types of silica gels

4.2. Performance investigation of an Adsorption desalination cycle

The performance of an adsorption desalination cycle with an adsorption-triggered-evaporation of seawater at low heat-activated desorption process is discussed. The numerical simulation of two types of cycles, namely, the two-bed and four-bed adsorption cycles, are simulated and compared with the experiments. This section has four sub-sections; (i) Section one describes the working principles of the adsorption desalination cycle, (ii) Section two discusses numerical simulation of the AD cycle, (iii) Section three describes the validation of the model with experiments and (iv) Section four describes the experimental investigation of the AD cycle with a wide range of input parameters such as heat source temperature, cycle time and flow rate of the heat transfer fluids.

4.2.1. Description of adsorption desalination cycle

Adsorption desalination (AD) cycle is a novel desalination method to produce potable water from sea or brackish water, utilizing only low-temperature hot water from renewable energy such as process exhaust and solar energy. The AD cycle is based on the recently patented cycle of Ng et al. [2] that produces both the desalted water and cooling by using low temperature waste heat. A typical AD plant comprises of three major components namely (1) the evaporator, (2) single to multi-reactor beds where the adsorbent is placed and (3) the condenser. The schematic diagram of adsorption desalination (AD) cycle is given in Figure 4.5 showing the major components. The sub-systems involved in AD cycle are:

1) Pre-treatment system: Sea water is first pre-treated where unwanted physical particles such as debris in the sea water are screened using a conventional filter (mesh size between 20 to 30) and the dissolved air in the sea water is removed by de-aeration.

2) Adsorption-initiated-evaporation system: The de-aerated sea water is pumped intermittently into the evaporator where the evaporation is achieved by the water vapor uptake by the adsorbent (type RD silica gel). The evaporation process is enhanced by a spray system using the full-cone type nozzles. The evaporation process is maintained by an external water circuit that provides the heating capacity to sustain the evaporation. The energy required for the evaporation is supplied either from the ambient or recovered internally within the condenser or adsorption process. The concentrated brine is discharged occasionally from the evaporator.

Water vapor from the evaporator is adsorbed by the unsaturated silica gel which is packed into a tube-fin heat exchanger housed inside a reactor bed. When the vapor valve is opened, a continuous vapor uptake is achieved. Owing to the exothermic nature of the adsorption process, heat is released during the vapor uptake and the adsorption process would continue at a preset cycle time. In general, process cycle time is one of the input parameters to control the adsorption desalination process and its time interval of operation is a direct function of hot water inlet temperatures.

3) Heat-activated desorption-condensation system: The saturated silica gel (from adsorption of previous half cycle) can be regenerated by introducing a low temperature hot water (typically less then 85^{o}C) and this is known as the desorption process. With the connecting vapor valves set to open position, the regenerated water vapor flows to the external surfaces of the water-cooled tubes and it condenses to give the distilled water. The condensation process is accompanied by the rejection of the latent heat of condensation into the cooling water passing through the condenser and the condensate is collected as potable water.

4) Potable water collection system: The condensate inside the condenser is taken out using by a fresh water pump or using a 10 m U-tube arrangement to overcome the differential pressure.

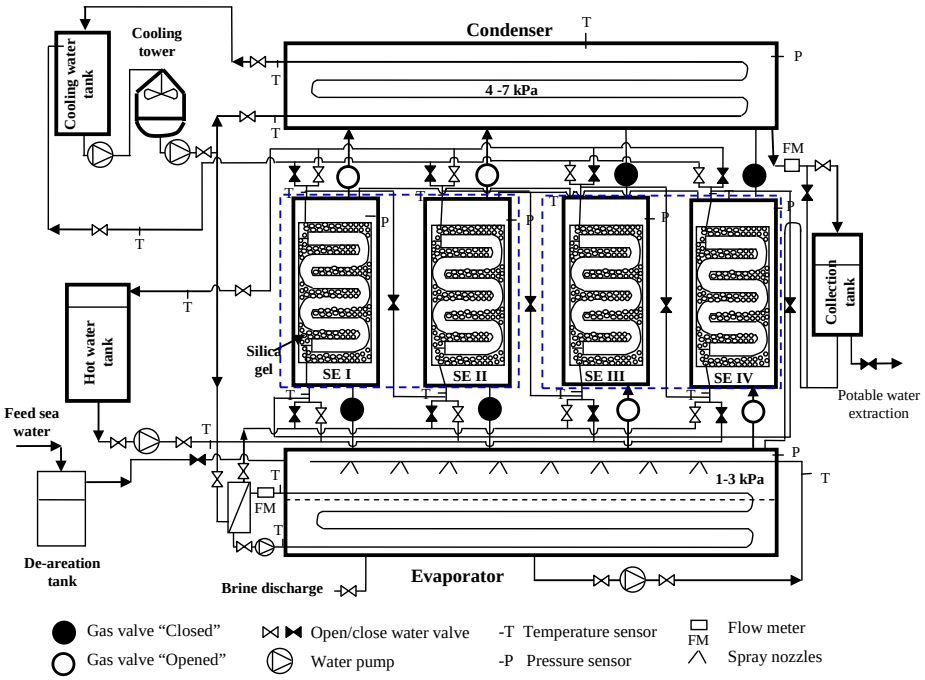

Figure 4.5 Schematic diagram of an adsorption desalination cycle

An adsorption desalination cycle operates in a batch-type process to achieve the useful effects using two or more adsorbers or rector beds, cycling one or a group of beds as adsorption mode whilst the others are in desorption mode during the first half-cycle period. The roles of the reactor beds are reversed in the next half cycle. Prior to switching their roles, the desorber beds need to be cooled down and the adsorber beds are pre-heated for a short period which is known as switching process. Other performance enhancement schemes have been incorporated, such as the heat and mass recovery that recovers the residual energy in a short time. In the AD plant, the following heat recovery schemes have been implemented;

a. **The Master-Slave configuration:** The extraction of input energy source can be increased in the AD cycle by first introducing the higher temperature heat source to a "master" bed containing the saturated silica gel. Rather than purging the heat source, the exit stream of the master bed is passed onto a "slave" bed for further sorption processes on the saturated silica gel, as shown

in Figure 4.6-(a). Similarly, the same flow arrangement is applied to the cooling water, i.e., in a master-slave manner for the adsorption processes in these beds. In a master-slave flow design, the adsorbent resources are distributed equally to the master and slave beds and the time interval for the arrangement is half of the conventional two-bed configuration. The performance of the AD cycle could be enhanced due to the further extraction of the energy in the slave desorber.

b. **Heat recovery by water re-circulation:** During the start of a switching operation, the desorber beds are hot (typically 65 to 80^{o}C) whilst the adsorber beds are cold (typically 33 to 37^{o}C). Owing to the higher thermal masses in these beds, they contain substantial amount of thermal or residual energy. The implementation of heat recovery schemes at these beds can be effected by channeling the residual hot water in the desorber bed and passing the hot water to pre-heat the adsorber beds by a pump, as shown in Figure 4.6-(c). The re-circulating pump operates only during the switching period and hence, it will not affect the overall operating half cycle interval.

c. **Heat recovery by water valve delay:** Figure 4.6-(b) describes the heat recovery by delaying the opening of the water valves during switching period. The residual hot water in the pre-cooler which was in desorber mode in the previous cycle is sent to the hot water tank by delaying the opening of the respective valves until the cold front of the cooling water is detected by the bed outlet temperature sensor. This arrangement not only recovers the residual thermal energy as well as reduces the load to the cooling tower which

otherwise has to reject this amount of heat. Concurrently, the residual cooling water in the pre-heating bed was sent to the cooling water tank instead of being sent to the hot water tank thus reduces the temperature fluctuation in the hot water storage system.

(a) Master-slave configuration

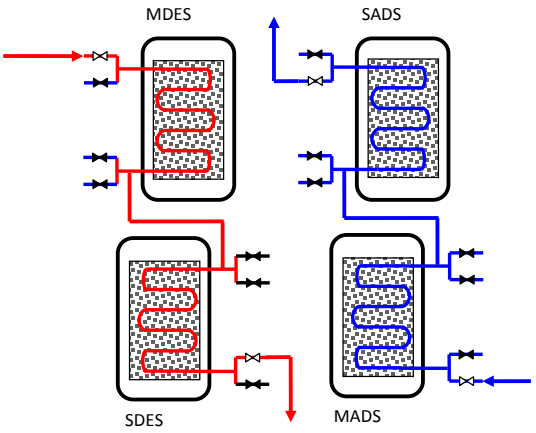

MDES-master desorber SDES-Slave desorber

MADS-Master adsorber SADS-Slave adsorber

(b) Water recirculation

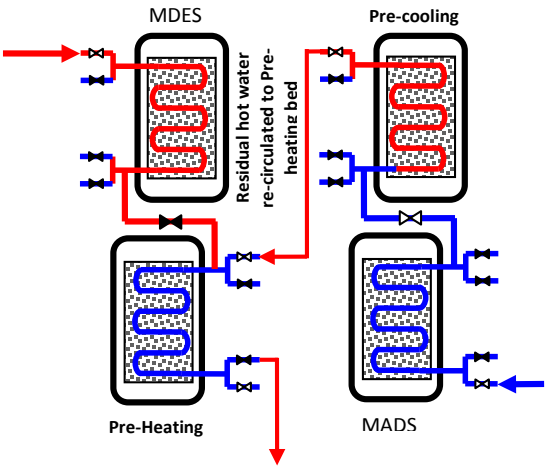

(c) Water valve delay

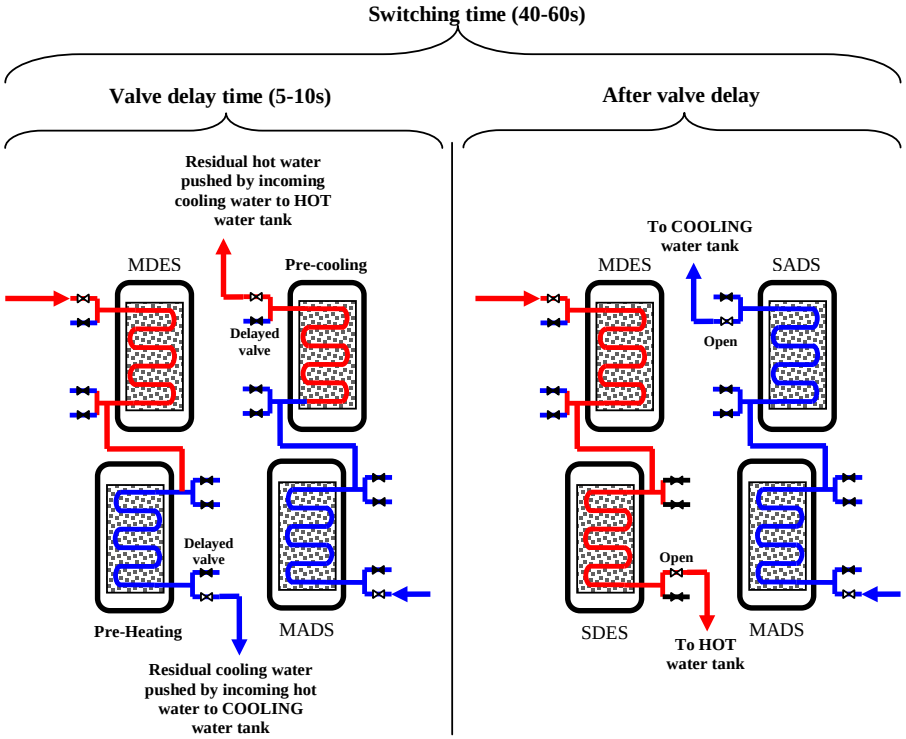

(d) Pressure equalization

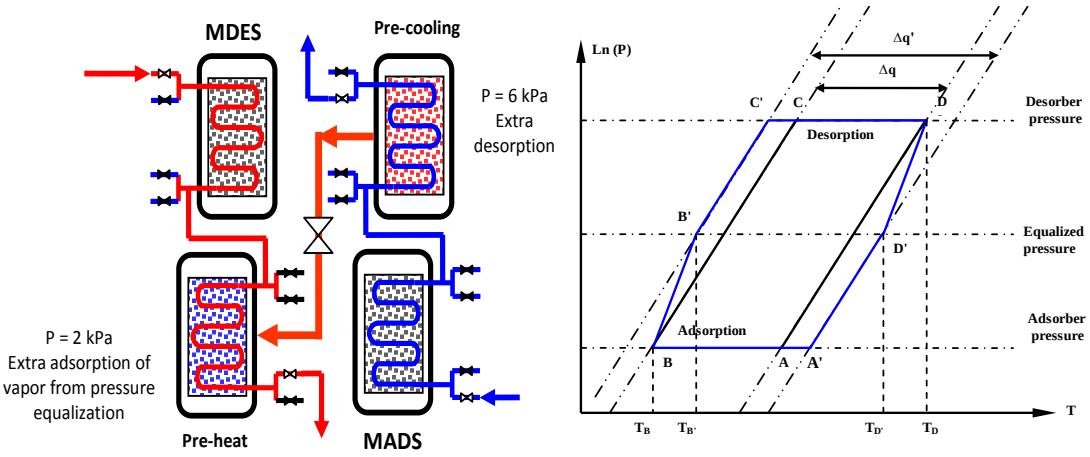

(e) Bed cooling

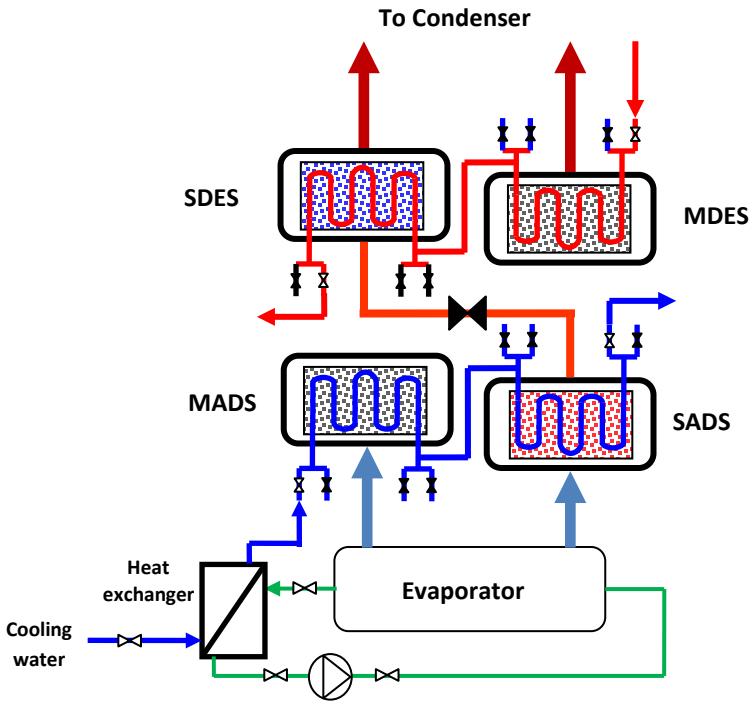

Figure 4.6 Heat and mass recovery schemes applied to AD cycle

d. **Pressure equalization:** Figure 4.6-(d) illustrates the pressure equalization procedures in an AD cycle that enables heat and mass recovery across two beds (a desorber with an adsorber) to occur simultaneously. Such a recovery is achieved by opening the valve connecting the adsorber and desorber at the start of a switching interval. The instantaneous equalization of the pressures makes the adsorbate in the desorber to further be removed from the pores as well as enables the pores in the adsorbent of adsorber to take in more water vapor. This phenomenon is best explained using Durhing diagram where $(\Delta q' - \Delta q)$ indicates the net mass recovery. Pre-cooling is resulted by the exothermic process of the desorption and pre-heating of the adsorber bed is achieved from the adsorption of the water vapors. The pressure equalization scheme is simple and can be easily implemented by the changes in the PLC codes.

e. **Bed cooling scheme:** Figure 4.6-(e) shows the bed cooling scheme applied in the AD cycle where the energy for the evaporation of the sea water is recovered from the cooling water and concurrently utilizes the chilling effect from the evaporation to cool down the adsorber temperature and thus enhances the adsorption capacity.

The drawbacks of conventional desalination methods are high primary energy consumption, high maintenance either resulted from the fouling and corrosion to the evaporation units or the blockage of membranes of RO systems. When compared with the conventional methods, the main advantages of the AD method are (i) the utilization of renewable or waste heat sources at temperatures below 80ºC, (ii) low corrosion and fouling rates on the evaporator tube materials due to the evaporation of saline water at low temperatures (typically below the ambient temperature), (iii) no major moving parts, which renders low maintenance cost, (iv) the usage of environmentally friendly adsorbent-adsorbate pair i.e., silica-gel and water, and (iv) low electricity usage other than the pumping power.

A mathematical model was developed based on the mass, energy balance and thermodynamic properties that were discussed in Chapter 3, along with the isotherm characteristics of the silica gel-water pair. The following section gives the detailed mathematical modeling and the numerical simulation of the adsorption desalination cycles.

4.2.2. Mathematical modeling

This section describes the development of the mathematical models of the AD cycles for both the two-bed and the four-bed modes and the latter is coupled with the master-slave heat recovery. It is based on the adsorption isotherms, kinetics and energy balances between the sorption elements, the evaporator and the condenser and the type-RD silica gel is employed as the adsorbent. To simplify the models, the following lumped parameter assumptions are made: (i) the temperature is uniform across the adsorbent (silica gel) layer; (ii) the adsorption of the water vapor by the silica gel inside the adsorber bed is uniform; and, (3) both the adsorbent (silica gel) and the adsorbate gas phases are in equilibrium condition.

The uptake of water vapor by the silica gel at temperature (T) and pressure (P) can be estimated using Dubinin–Astakhov (D-A) Equation as

$$q^* = q_0 \exp\left[-\left(-\frac{RT}{E} \ln\left(\frac{P}{P_0} \right) \right)^n \right] \qquad 4.2$$

where q_0 is the maximum adsorbed amount, E is the characteristic energy and n is the non-integer value, R is gas constant, P is the adsorption pressure and P_0 is the equilibrium pressure. E is the activation energy and the index n is the heterogeneity parameter and their values are determined by water vapor uptake analysis using the Hydro-Sorp analyzer. For silica gel+water pair, they are found to be 2.993kJ/mol and n=1, respectively.

The transient uptake of water vapor at specific temperature, pressure and adsorbate i.e., the kinetic of adsorption or desorption, is calculated by the linear driving force Equation [82, 102] and this is given by,

$$\frac{dq(t)}{dt} = K\left(q^{*} - q(t)\right) \qquad 4.3$$

where K is the mass-transfer coefficient. For a small range pressure regime (2 to 10 kPa), K is expressed in terms of key parameters R_p and D_{so} as [103],

$$K = \frac{15 D_{so} e^{-\frac{E_a}{RT}}}{R_p^2} \qquad 4.4$$

where R_p denotes the average radius of a silica gel particle, E_a is the activation energy of surface diffusion, and D_{so} is the kinetic constant for the silica gel water system.

The inventory of the amount of sea water is fed into the evaporator and potable water is extracted from the condenser of the AD cycle and the mass balance of the cycle is thus given by

$$\frac{dM_{s,evap}}{dt} = \dot{m}_{s,in} - \dot{m}_{d,cond} - \dot{m}_b \qquad 4.5$$

Here, $M_{s,evap}$ is the amount of sea water in the evaporator, $\dot{m}_{s,in}$ is the rate of feed sea water, $\dot{m}_{d,cond}$ is the mass of potable water extracted from the condenser and $\dot{m}_b$ is the

mass of concentrated brine rejected from the evaporator. The feed sea water is intermittently pumped into the evaporator depending on the amount and level of sea water whilst brine is discharged once the concentration reaches to the predetermined limit.

The mass and salt balance for the evaporator of the AD cycle is given as

$$\frac{dM_{s,evap}}{dt} = \overbrace{\theta \dot{m}_{s,in}}^{Feed} - \overbrace{\gamma \dot{m}_{brine}}^{Brine\ discharge} - \overbrace{n \times \left[A\left(\frac{dq_{Mads}}{dt} \right) + B\left(\frac{dq_{Sads}}{dt} \right) \right] M_{sg}}^{Vapor\ uptake\ by\ adsorption\ processes} \tag{4.6}$$

$$M_{s,evap} \frac{dX_{s,evap}}{dt} = \theta X_{s,in} \dot{m}_{s,in} - \gamma X_{s,evap} \dot{m}_{brine} - n \times X_D \left[A\left(\frac{dq_{Mads}}{dt} \right) + B\left(\frac{dq_{Sads}}{dt} \right) \right] M_{sg} \tag{4.7}$$

where $X_{s,in}$ and $X_{s,evap}$ are the concentration of the feed and sea water in the evaporator X_D is the concentration of the vapor.

The AD plant comprises of two or more reactor beds where the adsorbent is packed around the fins and tube of the heat exchanger. Based on the theoretical framework developed in Chapter 3, the energy balance of the evaporator in communication with adsorber bed undergoing the adsorption process is written as,

$$\left[M_{s,evap}c_{p,s}\left(T_{evap},X_{s,evap}\right)+M_{HX,Evap}\ c_{p,HX}\right]\frac{dT_{evap}}{dt}=\theta\times h_f\left(T_{evap},X_{s,evap}\right)\dot{m}_{s,in}$$
$$-n\times h_{fg}\left(T_{evap}\right)\left[A\left(\frac{dq_{Mads}}{dt}\right)+B\left(\frac{dq_{Sads}}{dt}\right)\right]M_{sg}+ \qquad 4.8$$
$$\dot{m}_{chilled}\ c_p\left(T_{evap}\right)\left(T_{chilled,in}-T_{chilled,out}\right)-\gamma\times h_f\left(T_{evap},X_{s,evap}\right)\dot{m}_{brine}$$

where $M_{HX,Evap}$ is the total mass of the evaporator, M_{sg} is the mass of silica gel, $\dot{m}_{brine}$ is the mass flow rate of brine discharge, q_{Mads} and q_{Sads} denote water vapor uptake by the master adsorption and slave adsorption processes. The first term in the right hand side of Equation 4.8 represents the sensible heat by the supplied feed seawater, the second term stands for the heat removal by the uptake of adsorbent, the third and fourth terms denote the energy supplied by the chilled water and the sensible heat by the brine discharge. The specific heat $(c_{p,s})$ and enthalpy (h_f) of sea water are calculated as functions of temperature and pressure. The vapor pressure depression due to the concentrated salt water is taken into consideration in terms of boiling point elevation (*BPE*). Properties of sea water and the formulation for the *BPE* are given in Appendix F. The vapor pressure depression affects the uptake of water vapor by the adsorbent which varies with temperature and the pressure.

The energy balance of the condenser which is in communication with the desorber bed is given by;

$$\left[M_{cond}c_p\left(T_{cond}\right)+M_{HX,cond}\ c_{p,HX}\right]\frac{dT_{cond}}{dt}$$
$$=-h_f\left(T_{cond}\right)\frac{dM_d}{dt}+n\times h_{fg}\left(T_{cond}\right)\left[A\left(\frac{dq_{Mdes}}{dt}\right)+B\left(\frac{dq_{Sdes}}{dt}\right)\right]M_{sg} \qquad 4.9$$
$$+\dot{m}_{cond}\ c_p\left(T_{cond}\right)\left(T_{cond,in}-T_{cond,out}\right)$$

where $M_{HX,cond}$ is the total mass of the condenser and M_d is the mass of distillate extracted from the condenser.

The energy balance Equation of the master adsorber bed connected with the evaporator as well as that for the master desorber bed commuting with the condenser are given by

$$\begin{aligned}&\left[M_{sg}c_{p,sg}+M_{HX}c_{p,HX}+M_{abe}c_{p,a}(T,P)\right]\frac{dT_{Mads/Mdes}}{dt}=\\&\pm n\times AQ_{st}\left(T_{Mads/Mdes},P_{evap/cond}\right)M_{sg}\frac{dq_{Mads/Mdes}}{dt}\pm\\&\dot{m}_{cw/hw}\,c_p\left(T_{Mads/Mdes}\right)\left(T_{cw/hw,in}-T''_{cw/hw,out}\right)\end{aligned} \qquad 4.10$$

The energy balance for the slave adsorber/desorber bed is written as:

$$\begin{aligned}&\left[M_{sg}c_{p,sg}+M_{HX}c_{p,HX}+M_{abe}c_{p,a}(T,P)\right]\frac{dT_{Sads/Sdes}}{dt}=\\&\pm n\times BQ_{st}\left(T_{Sads/Sdes},P_{evap/cond}\right)\frac{dq_{Sads/Sdes}}{dt}M_{sg}\\&\pm\dot{m}_{cw/hw}\,c_p\left(T_{Sads/Sdes}\right)\left(T''_{cw/hw,out}-T_{cw/hw,out}\right)\end{aligned} \qquad 4.11$$

where $T''_{cw/hw,out}$ is the outlet water temperature of the master adsorber/desorber bed, Q_{st} and $c_{p,a}$ are the isosteric heat of adsorption and the specific heat of the adsorbed phase are is calculated using the expression derived in Chapter 3 as,

$$Q_{st} = h_{fg} + E\left\{-\ln\left(\frac{x}{x_m}\right)\right\}^{1/n} + Tv_g\left(\frac{\partial P}{\partial T}\right)_g \qquad 4.12$$

$$c_{p,a} = c_{p,g} + \left\{\frac{1}{T} - \frac{1}{v_g}\left(\frac{\partial v_g}{\partial T}\right)_P\right\}Q_{st} - \left.\frac{\partial Q_{st}}{\partial T}\right|_P \qquad 4.13$$

where v_g is the volume of the gaseous phase, h_{fg} is the latent heat, $c_{p,g}$ is the specific heat of gaseous phase.

Using the heat transfer Equation, the outlet temperature of the water from each heat exchanger is estimated using log mean temperature difference method and it is given by,

$$T_{out} = T_0 + (T_{in} - T_0)\exp\left(\frac{-UA}{\dot{m}c_p(T_0)}\right) \qquad 4.14$$

where T_0 is the temperature of the heat exchanger. The energy required to remove water vapors from the silica gels, here master adsorption or desorption, $(Q_{Mdes/Sdes})$, can be calculated using the inlet and outlet temperatures supplied to the reactors, and this is given by

$$Q_{Mads/Mdes} = \dot{m}_{cw/hw}c_p(T_{Mads/Mdes})(T_{cw/hw,in} - T''_{cw/hw,out}) \qquad 4.15$$

The energy rejected in an AD cycle to the cooling water by the slave adsorption or desorption process is estimated to be

$$Q_{Sads/Sdes} = \dot{m}_{cw/hw} c_p \left(T_{Sads/Sdes}\right)\left(T''_{cw/hw,out} - T_{cw/hw,out}\right) \quad 4.16$$

The heat of evaporation $\left(Q_{evap}\right)$, and the condensation energy $\left(Q_{cond}\right)$ rejected at the condenser are given by

$$Q_{evap} = \dot{m}_{chilled}\, c_p \left(T_{chilled}\right)\left(T_{chilled,in} - T_{chilled,out}\right) \quad 4.17$$

$$Q_{cond} = \dot{m}_{cond}\, c_p \left(T_{cond}\right)\left(T_{cond,out} - T_{cond,in}\right) \quad 4.18$$

Finally, the performance of the AD cycle is assessed in terms of specific daily water production (SDWP), and the performance ratio (PR) which can be calculated as,

$$SDWP = \int_0^{t_{cycle}} \frac{Q_{cond}\,\tau}{h_{fg}\left(T_{cond}\right) M_{sg}} dt \quad 4.19$$

$$PR = \int_0^{t_{cycle}} \frac{\dot{m}_d h_{fg}\left(T_{cond}\right)\tau}{Q_{Mdes} + Q_{Sdes}} dt \quad 4.20$$

The above model predicts the performance of different operation modes of the AD cycle such as the 2-bed, 4-bed with and without heat and mass recovery schemes by changing the coefficients $\theta, \varepsilon, A, B, and\ \gamma$ of which values for different operation modes are given in Table 4.3.

Table 4.3 Values of the indicators for changing the operation mode of the AD cycle

Mode	Parameter	2-bed mode	4-bed mode with master-slave
Operation	n	2	1
	θ	1 (charging sea water)	1 (charging sea water)
	A	1	1
	B	0	1
	γ	1 (brine discharge)	1 (brine discharge)
Switching	n	2	1
	θ	1 (charging sea water)	1 (charging sea water)
	A	0	1
	B	0	0
	γ	1 (brine discharge)	1 (brine discharge)

The mathematical modeling equations of the AD cycle are solved using the Gear's Backward Differentiation Formula method from the IMSL library linked by the simulation code written in FORTRAN PowerStation, and the solver employs a double precision with tolerance value of $1x10^{-6}$ using the input parameters summarized in Table 4.4.

Table 4.4 Parameters used in the simulation

Parameters or material properties	Values	Unit	Reference
Sorption thermodynamic properties			
Kinetic constant	2.54×10^{-4}	m^2/s	[103]
Activation Energy	4.2×10^{-4}	J/mole	[103]
Average radius of silica gel particle	1.7×10^{-4}	m	manufacturer
Specific heat of silica gel	921	J/kg K	[103]
Adsorber bed			

Mass of silica gel per bed	36	kg	
Adsorber/desorber bed heat transfer area (A_{bed})	41.7	m^2	
Tube length	0.576	m	
Number of tubes/cake	15	-	
Number of pass/distribution	30	-	
Thermal mass of adsorber bed including fins and support	284.6	kJ/K	
Overall heat transfer coefficient of adsorber	250	W/m^2K	Author's experimental data
Overall heat transfer coefficient of desorber	180-330	W/m^2K	
Condenser			
Condenser heat transfer area (A_{cond})	5.08	m^2	
Thermal mass of condenser including fins and support	18.61	kJ/K	Author's experimental data
Condenser heat transfer coefficient	2657.5	W/m^2K	
Mass of condensate in the condenser	10	kg	
Evaporator			
Evaporator heat transfer area (A_{evap})	3.5	m^2	
Evaporator heat transfer coefficient	1715.2	W/m^2K	
Thermal mass of evaporator including fins and support	25.44	kJ/K	
Mass of refrigerant in the evaporator	250	kg	

Concentration of the feed	35,000	ppm	
Concentration limit to discharge brine	110,000	ppm	

4.2.3. Simulation results

The predicted performances of the AD cycle for 2-bed and 4-bed operation modes are discussed in this section. The transient temperature profiles of the major components such as adsorber, desorber, evaporator and condenser of the AD cycle operating as a 2-bed mode are given in Figure 4.7. In the four-reactor mode, two of the beds served as adsorbers and the rest are the desobers. The predictions show that cyclic steady state is achieved after three half-cycles. The corresponding pressure profiles in the predictions are shown in Figure 4.8 and it is found that pressure drop is insignificant and can be neglected. The transient water production rates of the cycle are captured in Figure 4.9: The equivalent specific daily water production (SDWP) is estimated to be about 7.4 m^3/tonne of silica gel per day whilst the production ratio, defined here as the ratio of the latent energy of condensate to the heat input to produce the condensate or PR is about 0.64.

Similarly, the temperature and pressure profiles of the AD cycle operating in four-bed mode with master-slave configuration are shown in Figures 4.10 and 4.11. It is noted that the fluctuations in the temperature and pressure of the evaporator is lower than those of the 2-bed mode. A lower surge in pressure is also observed in the 4-bed mode. These are resulted from the operation nature of the 4-bed mode where the evaporator and the condenser are in communication with at least one adsorber and desorber bed, respectively, due to the master-slave arrangement.

Figure 4.12 illustrates the water production rates of the 4-bed mode and it gives a more continuous water production rates because of the master-slave arrangement. The minimum water production rate at switching period is about 0.7 litres/minute.

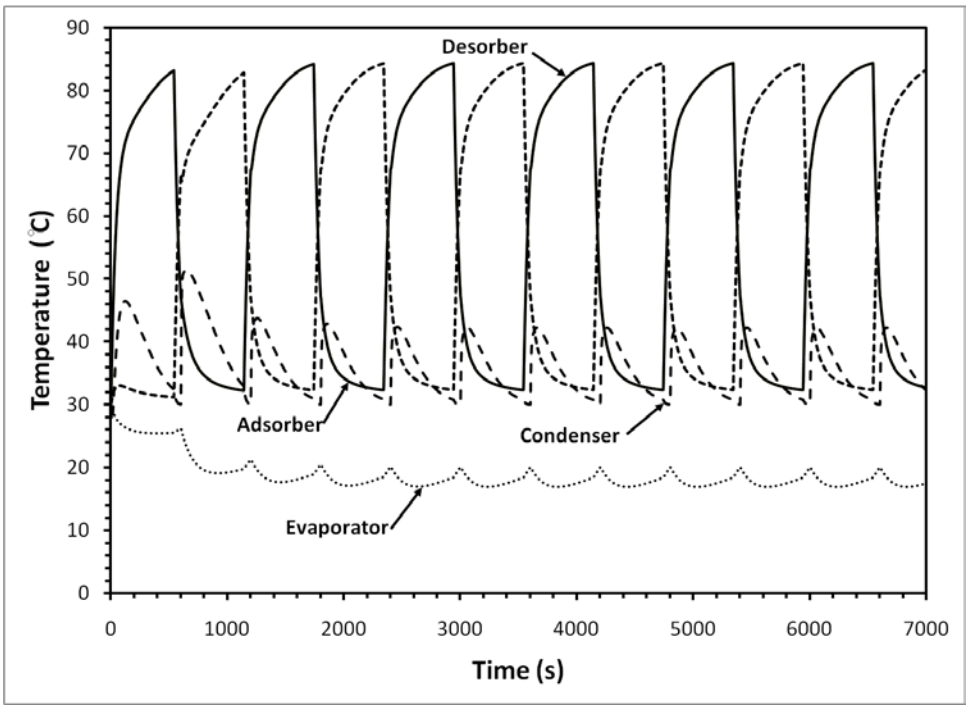

Figure 4.7 The temperature profiles of the major component of the AD cycle operating in 2-bed mode: T_{hw}=85°C, T_{cw}=29.8°C, $T_{chilled}$=30°C, $F_{hw/cw}$=0.8 kg/s, $F_{chilled}$=0.8 kg/s, $t_{half-cycle}$=600s, $t_{switching}$=40s

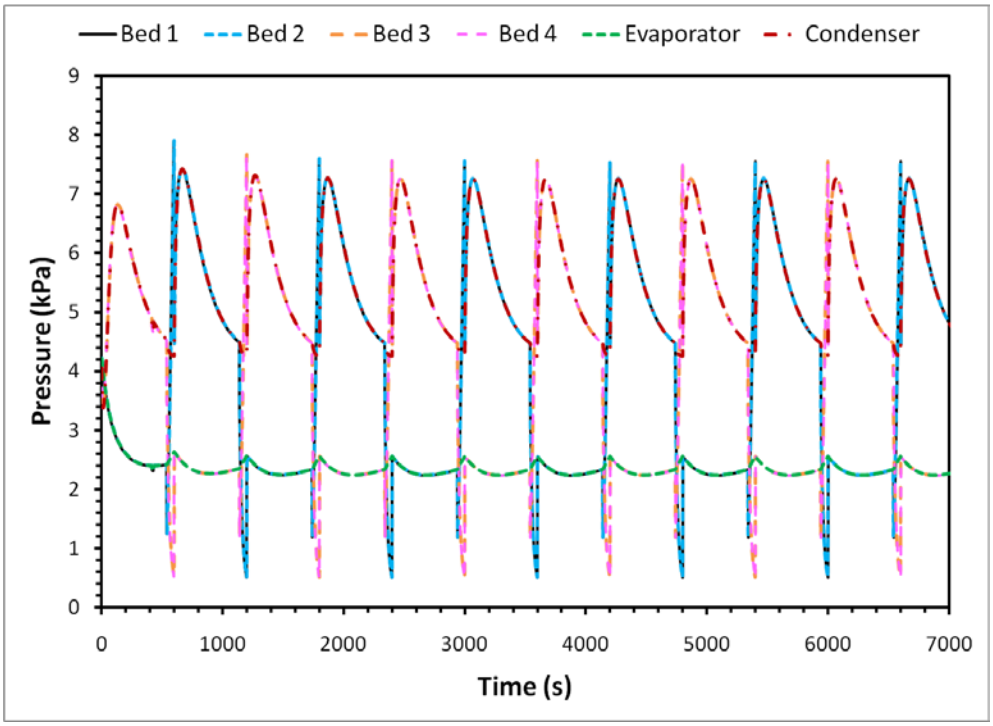

Figure 4.8 The pressure profiles of the AD cycle operating in 2-bed mode: T_{hw}=85 ℃, T_{cw}=29.8 ℃, $T_{chilled}$=30 ℃, $F_{hw/cw}$=0.8 kg/s, $F_{chilled}$=0.8 kg/s, $t_{half\text{-}cycle}$=600s, $t_{switching}$=40s

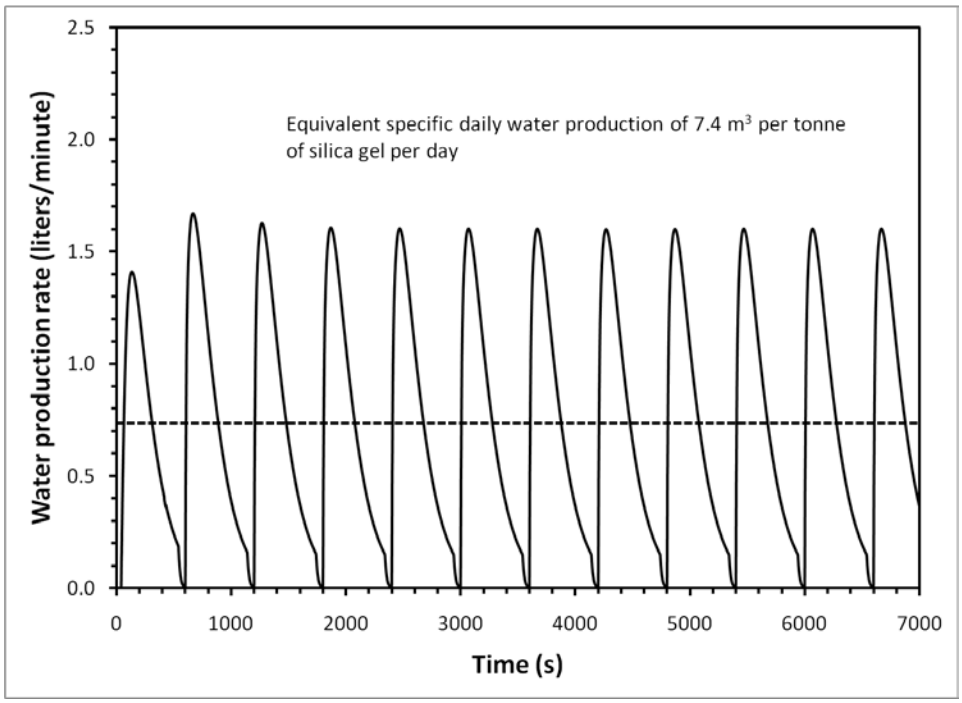

Figure 4.9 Water production rate of a 2-bed AD cycle

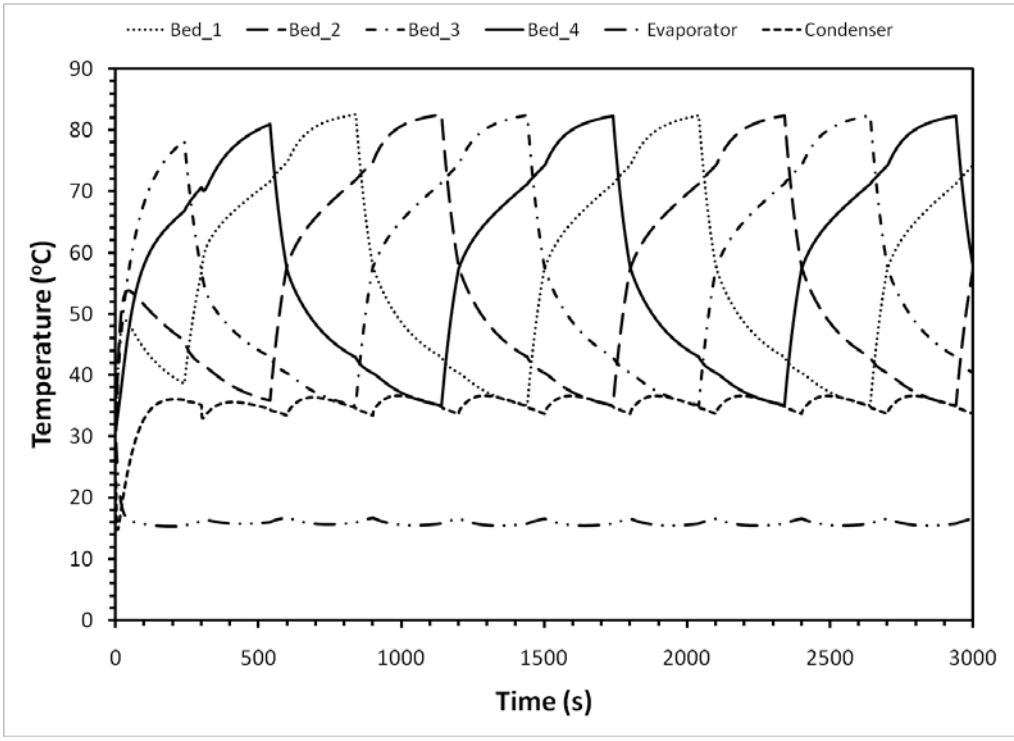

Figure 4.10 Temperature profiles of the major components of the 4-bed adsorption desalination cycle with master-slave configuration, T_{hw}=85℃, T_{cw}=29.8℃, $T_{chilled}$=30℃, $F_{hw/cw}$=0.8 kg/s, $F_{chilled}$=0.8 kg/s, $t_{quater\text{-}cycle}$=240s, $t_{switching}$=40s

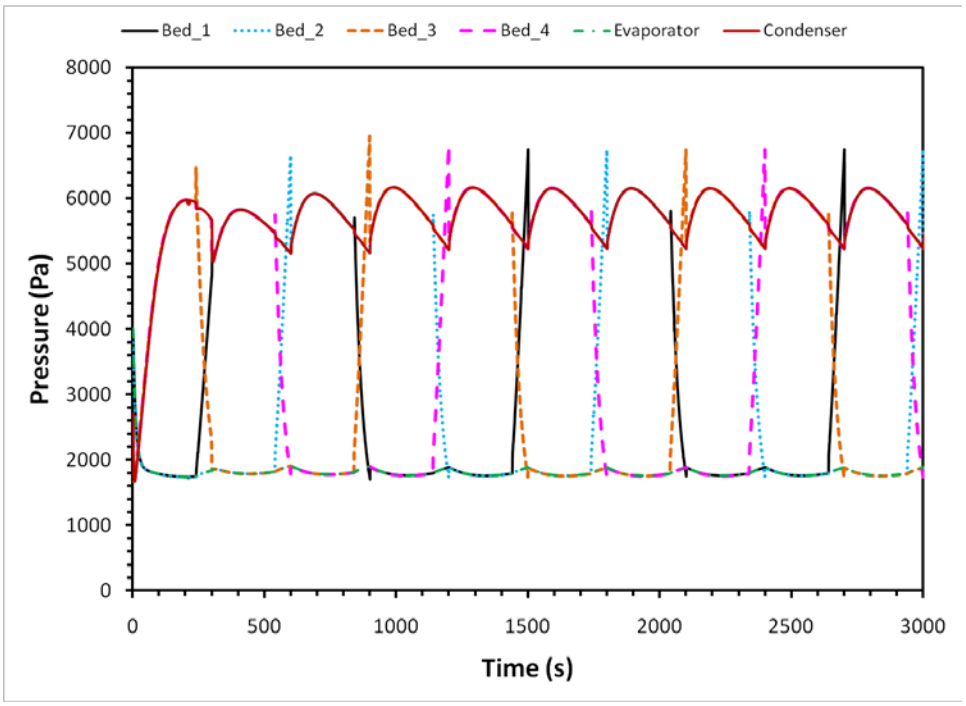

Figure 4.11 Pressure profiles of the 4-bed adsorption desalination cycle with maser-slave configuration, T_{hw}=85℃, T_{cw}=29.8℃, $T_{chilled}$=30℃, $F_{hw/cw}$=0.8 kg/s, $F_{chilled}$=0.8 kg/s, $t_{quater\text{-}cycle}$=240s, $t_{switching}$=40s

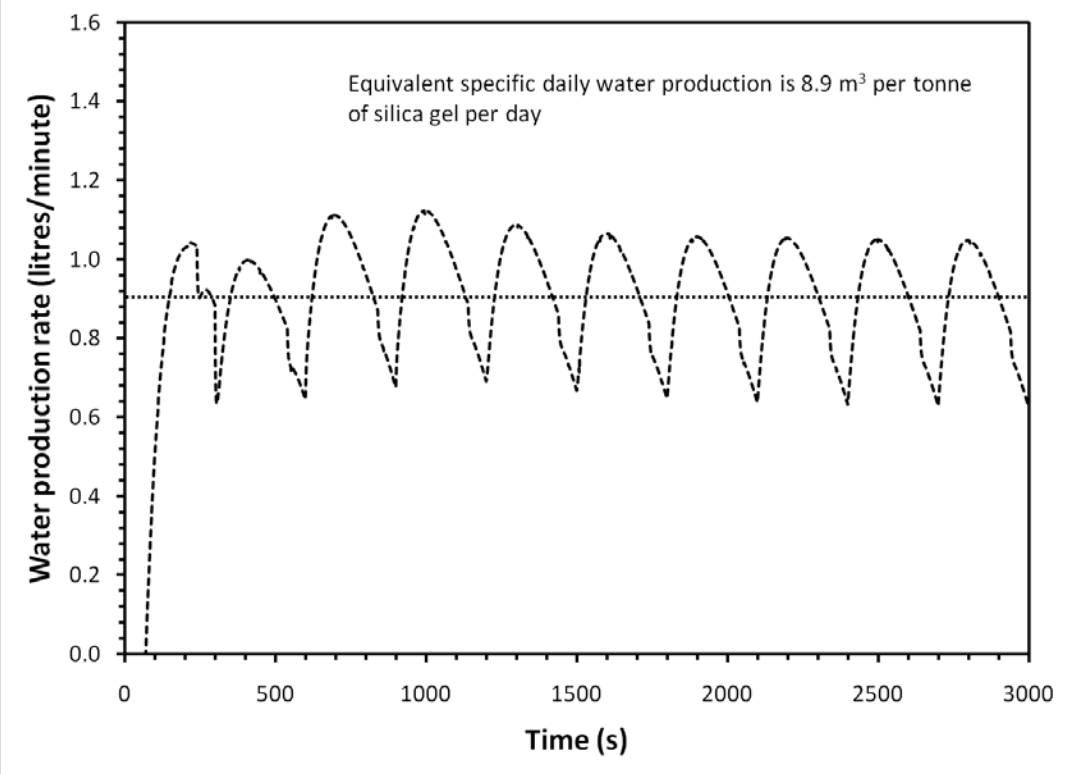

Figure 4.12 Water production rate of a 4-bed AD cycle

4.2.4. Validation of the simulation and experimental results

The numerical simulations are validated using the experimentally measured cycle's performance. The comparison is performed on both the 2-bed and 4-bed AD cycles operating over a half-cycle period. For example, Figure 4.13 shows the comparison between the simulated and the experimentally-measured temperatures of the major components of the 2-bed AD cycle. In the case of a 4-bed AD cycle with master and slave configuration, the comparisons are illustrated in Figure 4.14. It is observed that both models (2-bed and 4-bed) of the AD cycles agree well with the experimental performance except that the temperatures of the master desorber bed by experimental is slightly higher than that of the simulated cycle.

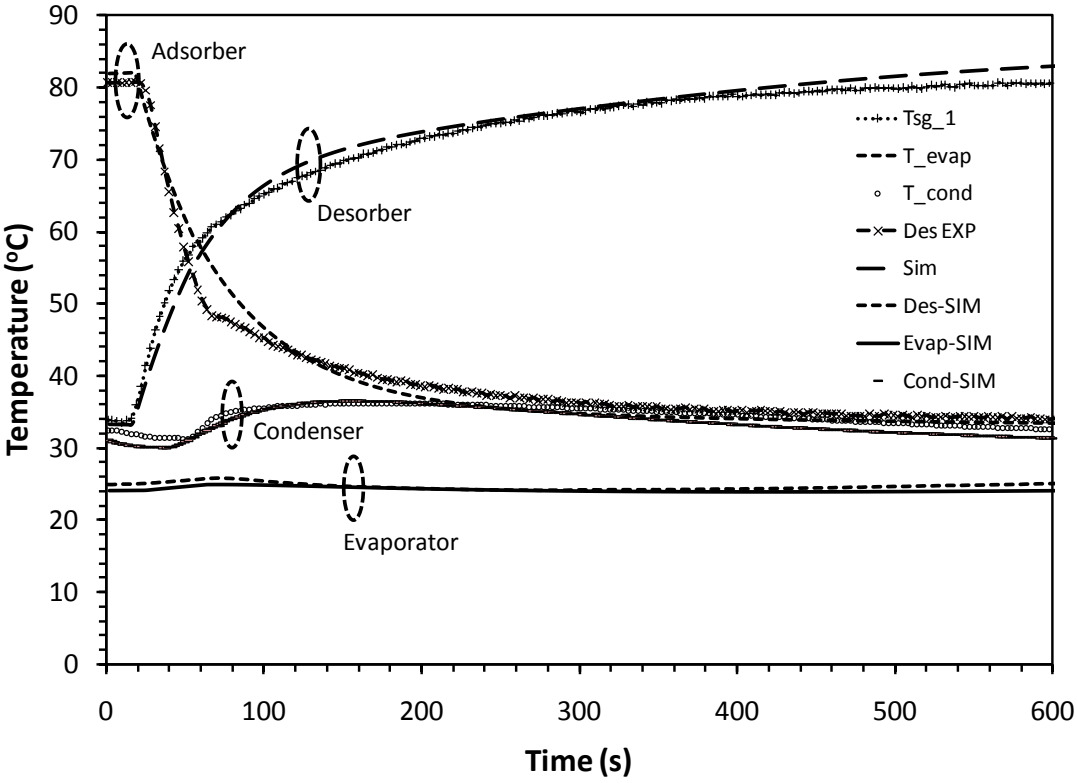

Figure 4.13 Validation of the 2-bed simulation AD cycle with experimental results

In terms of specific daily water production (SDWP), the comparisons are made at assorted hot water inlet temperatures, as summarized in Table 4.5. The current model predicts well to within the experimental margin of errors. Extensive experiments were conducted to investigate the performance of the AD cycle and the forthcoming sections present the performance results.

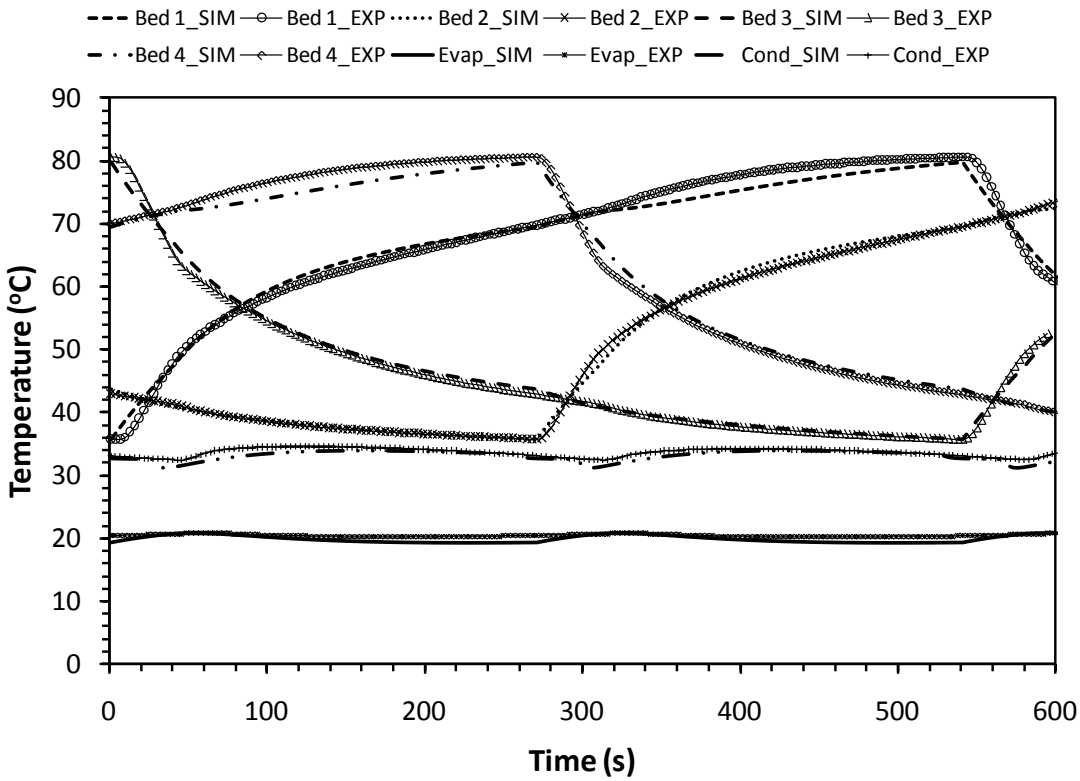

Figure 4.14 Validation of the simulated 4-bed AD cycle with experimental results configured with master and slave arrangement

Table 4.5 Comparison of SDWP of the AD cycle between simulation and experiment

	SDWP (2-bed)			SDWP (4-bed)		
T_{hot} (°C)	Simulation	Experiment	% Error	Simulation	Experiment	% Error
85	8.7533	8.5909	1.86	10.0023	10.3025	-3.00
80	8.2462	8.0894	1.90	9.0827	9.3434	-2.87
75	7.4869	7.3153	2.29	7.4577	7.6187	-2.16
70	6.3004	6.1997	1.60	6.4617	6.6470	-2.87
65	5.7041	5.6460	1.02	5.8204	5.7955	0.43

4.2.5. Experiments

This section describes the experimental investigation of the AD cycles of 2-bed and 4-bed cycle without and with heat and mass recovery schemes, as discussed

in previous sections. Figure 4.15 shows the pictorial view of the adsorption desalination plant constructed in the Air-conditioning laboratory of the National University of Singapore. It is designed with a conditioning facility for the heat source, cooling and chilled water temperatures so that it can be operated under different operation modes such as 2-bed and 4-bed and with or without heat and mass recovery schemes. Temperature measurements are achieved using 5 kΩ thermistors with a 3 s time constant (±0.2 ^{o}C, YSI). The flow rates of the heat transfer fluids are monitored using electromagnetic flow meters (±0.5% of reading). The absolute pressure sensors that are used have an accuracy ±0.125 kPa (Yokogawa). It is estimated that the accuracy of cycle averaged cooling capacity measurements is ±3.5%, COP measurements is ±3.8%, and heat input measurements is ±1.7%. A low-fin tube bundle with internal corrugation is used for the evaporator whilst the load-water flow rate is 0.8 kg/s. The condenser cooling water flow rate is set at 2.0 kg/s. The plate-type heat exchanger manufactured by Mayekawa manufacturing Co. Ltd is employed for the reactor bed where 36 kg of silica gel are packed in-between the fins. Cooling and hot water with rated flow rate of 0.8 kg/s are used during adsorption and desorption processes. Four temperature sensors of the same type are inserted in the reactor bed to measure the adsorbent temperature.

The cycle time is set at 600 s while the switching period for both modes of operation is fixed at 40 s. The electrically fired rating facility is able to supply heat source water, cooling water and hot water at a practically constant flow rate and a temperature process control accuracy of ±0.3 8 ^{o}C during cyclic steady state with an occasional drift to ±0.5 ^{o}C.

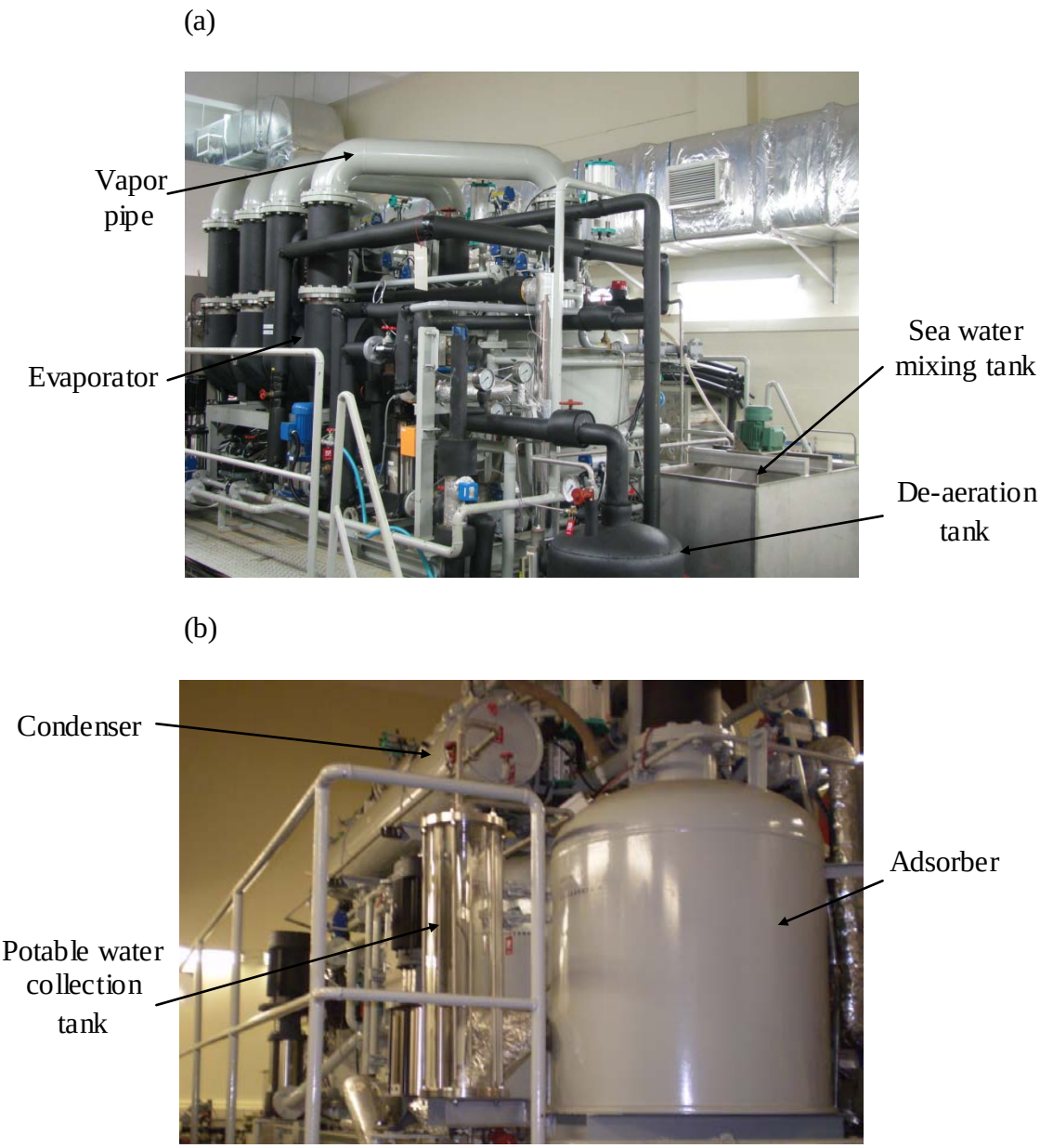

Figure 4.15 Pictorial views of the AD chiller (a) showing the feed water tank, evaporator (b) showing the bed, condenser and the potable water collection tank

4.2.5.1. Recovery ratio

The recovery ratio, defined as the ratio of potable water extraction to the feed sea water input, is an important parameter in determining the efficiency of a desalination method. It is a direct function of the unit production cost of water. For instance, the optimal recovery ratio of a reverse osmosis (RO) method is about 40%. Should the recovery ratio is increased, the membrane life-span would reduce

drastically [53]. The recovery ratio of the AD cycle is determined at various concentrations of saline water whilst the experimental parameters, such as the hot water inlet temperature (T_{hot}= 85^{o}C), chilled water inlet temperature ($T_{chilled}$ = 30^{o}C), the cycle time (t_{cycle}=10 mins) and the switching time ($t_{switching}$ = 40 s), are not changed throughout the experiments. From these experiments, it is found that at 67 ppt of sea water, the recovery ratio is 48% and at a concentration of 110 ppt the recovery ratio increases to 70%.

The quality of product water of the AD cycle was also measured and Table 4.6 gives the range of water qualities for different concentrated feed waters. It is found that the product water from the AD cycle has high purity (TDS < 15 ppm) even with highly concentrated feed water (recovery rate 70%). The TDS and conductivity of product water tends to increase slightly with the salinity of seawater feed whilst the pH remains constant.

Table 4.6 Potable water quality at different concentrated feed waters

Feed quality	% recovery	TDS (ppm)	Conductivity (μS)	pH
10 ppt	-	7.12	13.1	8.35
35 ppt	-	7.54	13.5	8.41
67 ppt	48	10.5	13.63	8.42
110 ppt	70	12.7	13.88	8.37

Figure 4.16 shows the specific daily water production (SDWP) of the AD cycle while the inserts in the figure show the SDWP and the PR at different saline feed water concentrations. It is noted that the performance of the AD cycle is not significantly affected by the concentration of the feed water. The AD plant is still

capable of producing 6.7 m^3 of potable water per tonne of silica gel per day at 110 ppt of the feed water which is equivalent to 70% recovery while the cycle's performance ratio remains unchanged. This is because the evaporation of the feed water in the evaporator of the AD plant is initiated by the affinity of the adsorbent (silica gel) to the adsorbate (water vapors) in contrast to the existing desalination technologies such as RO, MSF and MED where the evaporation or separation is achieved by an external energy input such as thermal energy or pressure input. In fact, the potable water production in the AD plant is essentially governed by the nature of the isotherm properties of the adsorbent+adsorbate pair, which is dependent only on the temperature and pressure of the adsorption and desorption conditions.

This robustness of the AD plant to different saline water concentration is further confirmed by the analysis of the overall heat transfer coefficient of the evaporation at feed water with different salinities. Figure 4.17 gives the overall heat transfer coefficient profiles of the evaporation of the AD cycle at different feed concentration levels. Generally, the overall heat transfer coefficient of evaporation translates the evaporation condition in a typical desalination unit. It is remarkable that there is no significant degradation in the overall heat transfer coefficient of the AD cycle as the salinity of the feed water increases. The results also show that the performance ratio (PR) of the AD plant is not affected by the high salinity of the feed water.

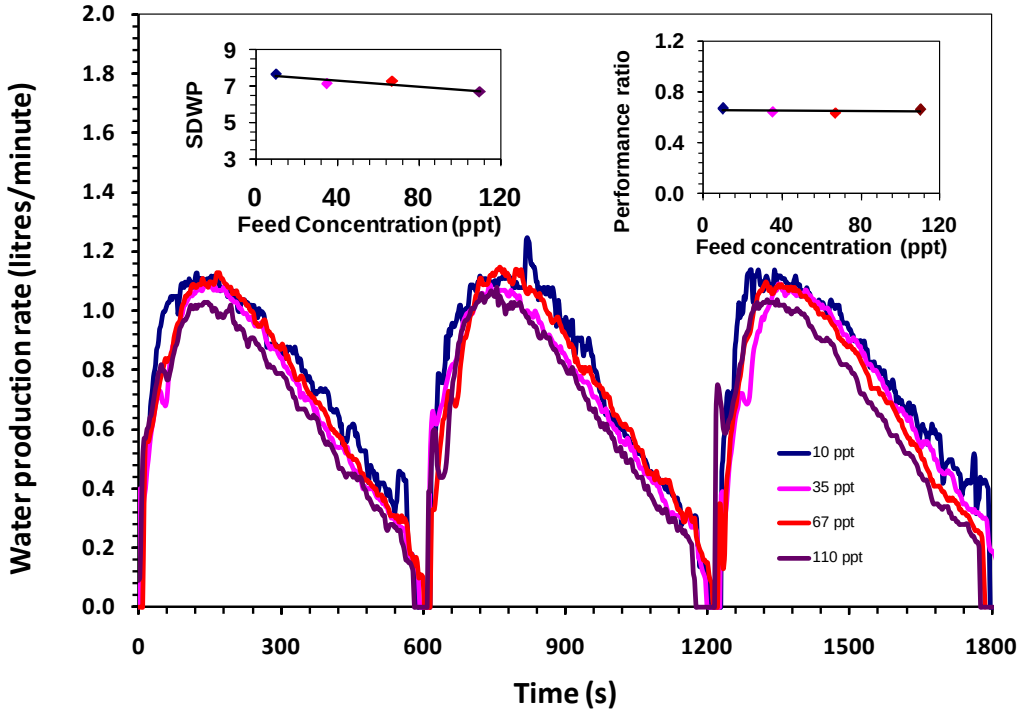

Figure 4.16 SDWP of the AD plant at different concentrations of saline feed water.

The SDWP of the AD plant slightly decreases at 70% extraction which is at 110 ppt feed water (Figure 4.16). This phenomenon is attributed to the boiling point elevation (BPE) of the feed water at higher salt concentration. As the concentration of feed water increases, the BPE increases proportionally, resulting in the drop of the vapor pressure inside the evaporator. Consequently, the pressure of the adsorber bed which sees the evaporator also decreases. According to the isotherm properties of the silica gel-water pair, the decrease in adsorption pressure results in the decrease in the vapor uptake. Hence, there is a slight degradation in the SDWP of the AD plant at higher % of potable water. However, it is experimentally confirmed that the potable water extraction of the AD plant can be obtained as high as 70% without major increment in the power consumption of the plant. It is also remarkable that the recovery rate of the AD cycle is much higher as compared to that of the RO plant whose maximum recovery rate is 40% [34]. The high recovery rate the AD plant may

translate to the decrease in the operation cost of the plant and the improvement in the reliability of the plant.

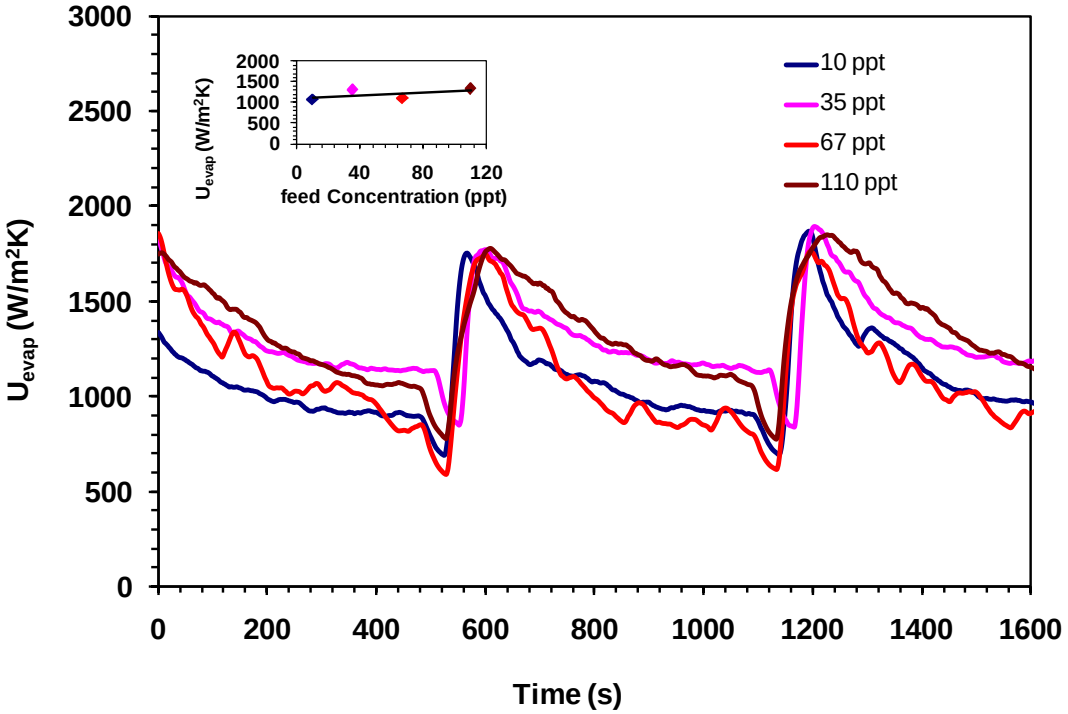

Figure 4.17 Overall heat transfer coefficient of evaporation-time history of the AD plant at different saline feed waters

4.2.5.2. Optimum cycle time

In this section, the investigations on the optimum operation cycle time of the AD cycles (2-bed and 4-bed modes) are discussed. In practice, it is obvious that the temperature of the available hot water to operate the AD cycle might not be constant, but it will fluctuate depending on the process from which the waste heat is extracted. On the other hand, desorption rate is faster for higher temperatures and thus a shorter cycle time may be required to regenerate the water vapor.

The AD cycle was experimented using different hot water temperatures ranging from 65 to 85 ^{o}C to evaluate the optimal cycle time at which the cycle gives the highest water production rate. Figures 4.18 and 4.19 show the SDWP against cycle times for two-bed and four-bed operation modes of the AD cycle at different hot water inlet temperatures. These results denote the existence of optimal cycle times at the specific hot water inlet temperature as the SDWP varies with cycle time. Lower SDWP is obtained at relatively shorter cycle times, and this is due to the fact that the regeneration process during desorption is not completed and the water vapors from silica gels are not fully emitted for condensation and producing water in the condenser. This means that the affinity of the adsorbent (silica gel) for the uptake of water vapor in the next cycle will be damped due to the incomplete regeneration. On the other hand, the lower SDWP at longer cycle time is due to the waste of thermal energy resulting from the excessively longer supply of the hot water to the sorption elements during desorption process. As a result, the additional energy supplied by the hot water has no effect for desorption but just heating the adsorbents and the heat exchanging components. In addition, the total numbers of operation cycles per day is also significantly reduced.

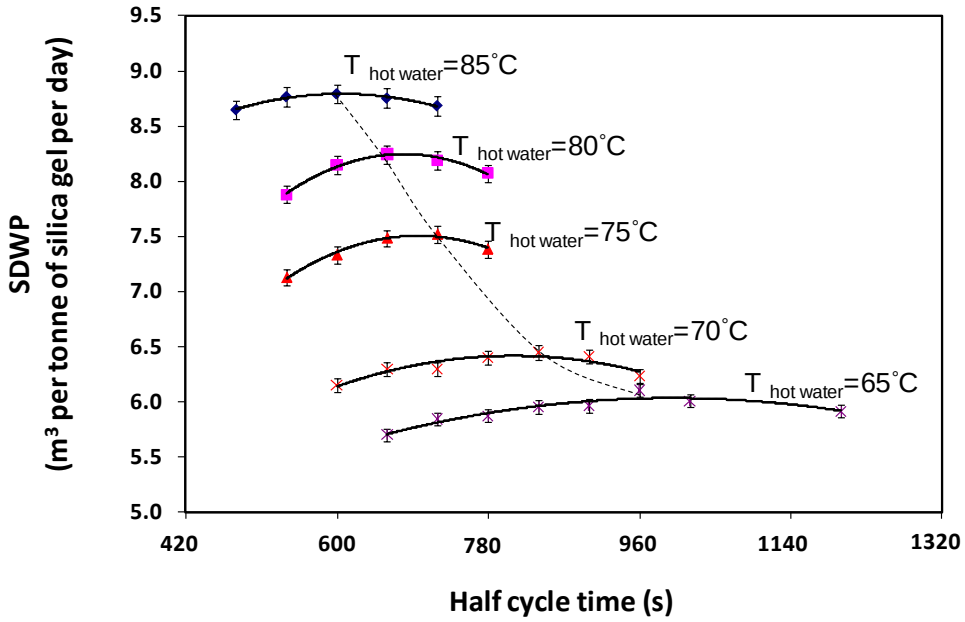

Figure 4.18 SDWP at different cycle times for 2-bed mode showing the optimum cycle times

Table 4.7 summarizes the SDWP and PR at optimal cycle times for different hot water inlet temperatures. On the basis of optimal conditions (the hot water temperature of 85ºC, operating cycle time 1080s, and the cooling water temperature of 30ºC), the maximum SDWP and PR are obtained as 10m^3 per tonne of silica gel and 0.61, respectively. It should be noted that the AD cycle is performed under heat and mass recovery schemes namely; bed cooling and pressure equalization.

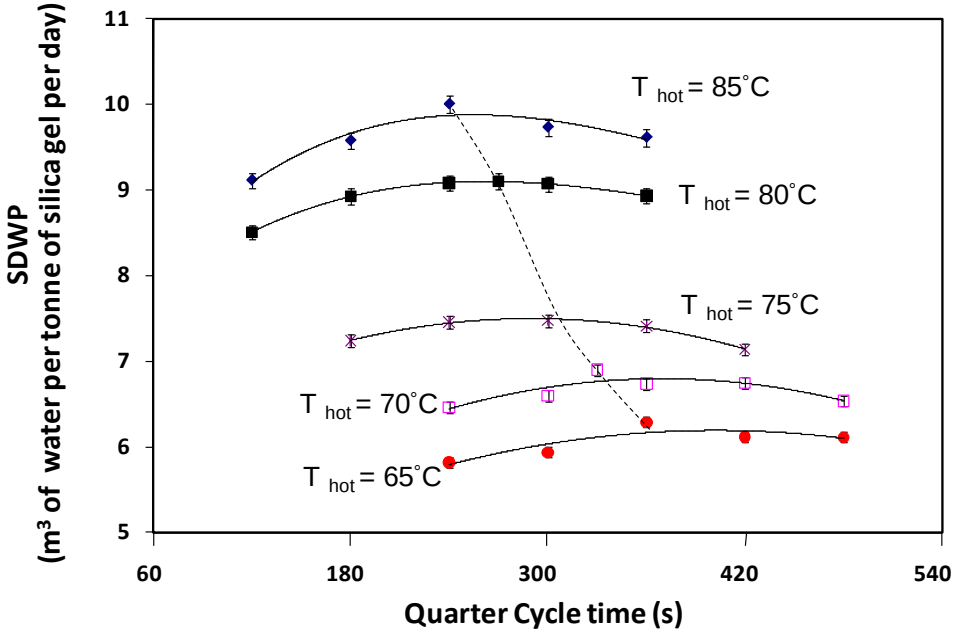

Figure 4.19 SDWP at different cycle times for 4-bed mode showing the optimum cycle times

Table 4.7 Specific daily water production and optimal cycle times at different regeneration temperatures

$T_{hot\ water}$ (°C)	Four-bed mode			Two-bed mode		
	t_{cycle} (s)	SDWP	PR	t_{cycle} (s)	SDWP	PR
85	1080	10.0023	0.6065	1240	8.7932	0.5731
80	1200	9.1036	0.6195	1360	8.2462	0.5997
75	1320	8.5218	0.6409	1480	7.5213	0.6231
70	1440	6.9012	0.6441	1720	6.4510	0.6380
65	1560	6.2895	0.6795	1960	6.1076	0.6830

Figure 4.20 shows the effects of cycle time on heating fluid inlet temperature, and it is found that the optimum cycle time varies linearly with the hot water inlet temperature in both operation modes. The longer cycle time is observed at

lower hot water inlet temperatures as a result of slower regeneration process in the desorption bed(s).

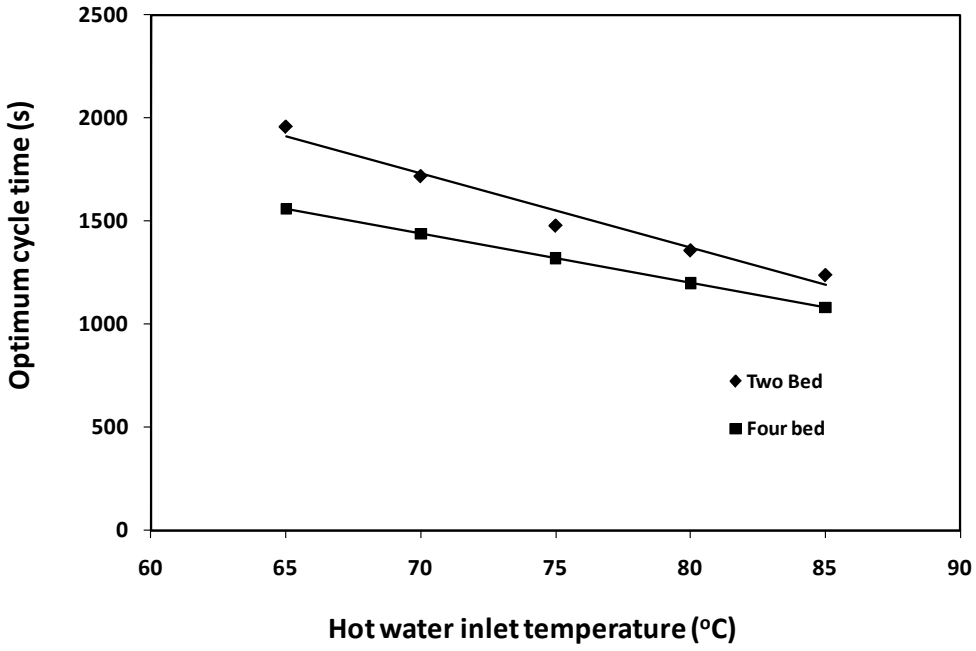

Figure 4.20 Optimum cycle time at different hot water inlet temperatures

Figure 4.21 shows the comparison of the specific daily water production and performance ratio of AD cycles operating with four-bed and two-bed operation modes at respective optimal cycle times with assorted hot water inlet temperatures. It is noticed that the AD cycle in four-bed operation mode produces higher SDWP compared with two-bed operation mode and the significant improvement can be realized at higher hot water inlet temperatures typically above 70 °C. This is because of the "master-slave" configuration in the four-bed mode which results in the better energy utilization of the hot water. For the lower hot water inlet temperatures, the "master-slave" configuration becomes less effective because the outlet hot water temperature from the master bed is not high enough to perform further desorption in the slave desorber. Thus, the advantage of four-bed operation mode diminishes at

lower heat source temperatures. The PR of the AD cycle for both modes is decreased with the increase of hot water inlet temperature.

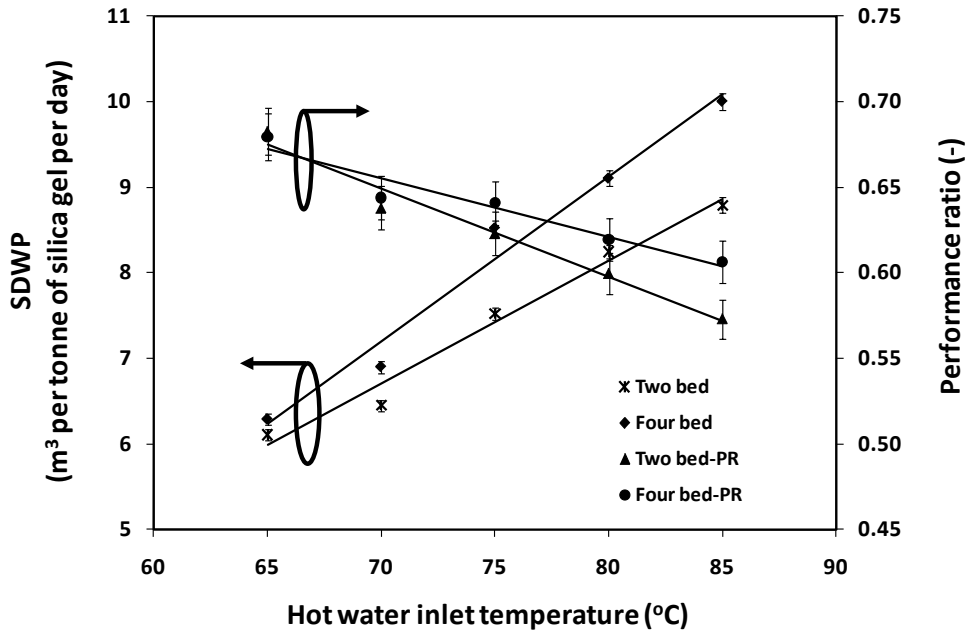

Figure 4.21 SDWP at different hot water temperatures for two-bed and four-bed modes

4.2.5.3. Sensitivity of water flow rates

The flow rates of the heat source supplied to the evaporator of the AD cycle might affect on the performance of the cycle due to the changes in the heat transfer coefficient. Experiments were conducted to investigate the load water flow rate effect on the SDWP of the AD cycle. The selected chilled water flow rates are 50, 75, 100, 125 litres/minute whilst the cooling water temperature is maintained at 29.5°C at optimum half-cycle times discussed in the previous section. Figures 4.22 and 4.23 depict SDWP of both 2-bed and 4-bed AD cycle for different load water flow rates at assorted hot water inlet temperatures.

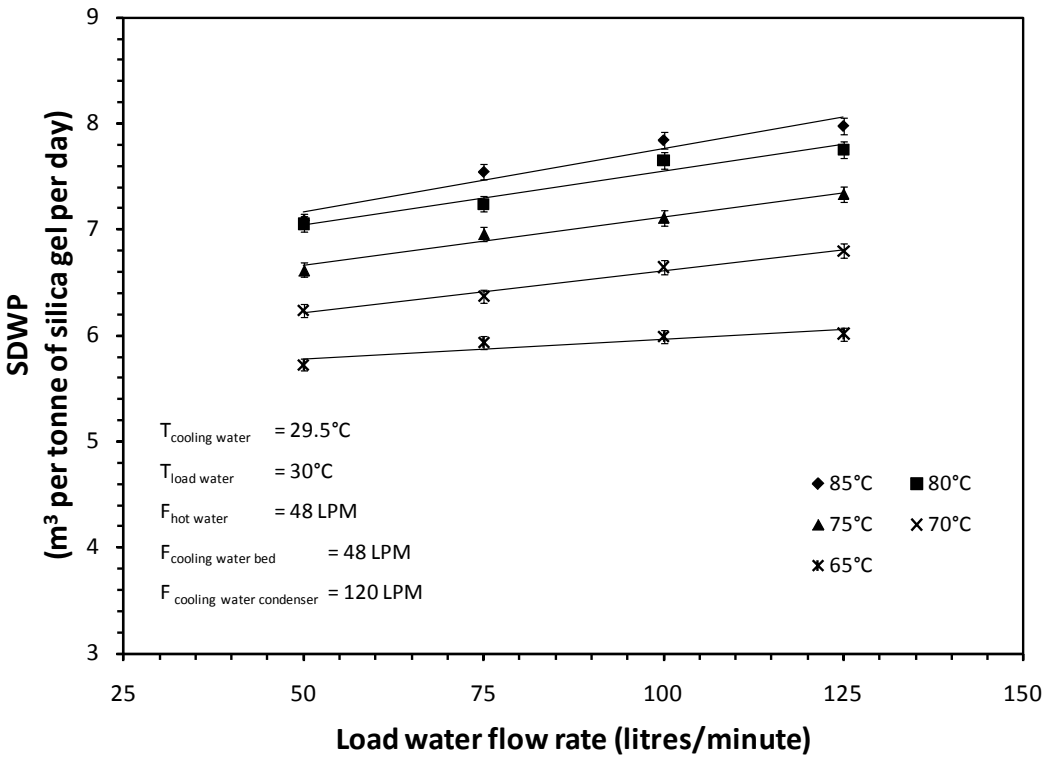

Figure 4.22 SDWP of a 2-bed AD cycle for assorted hot water inlet temperatures showing the effect of the chilled water flow rates on the cycle

The results show that the SDWP varies linearly with the load water flow rate. It is found that AD cycle gives SDWP of 8.0 and 8.5 m^3 of potable water per tonne of silica gel per day for 2-bed and 4-bed operation modes, respectively, at 85°C hot water inlet temperature.

The performance ratio (PR) of the AD cycle for different load water flow rates are presented in Figures 4.24 and 4.25. The results showed that the performance ratio also linearly varies with the load water flow rates. The better performance at higher load water flow rate is due to the improvement in the heat transfer coefficient at higher flow rates. However, it should be noted that the operation cost may increase through higher electrical energy consumption for higher flow rates.

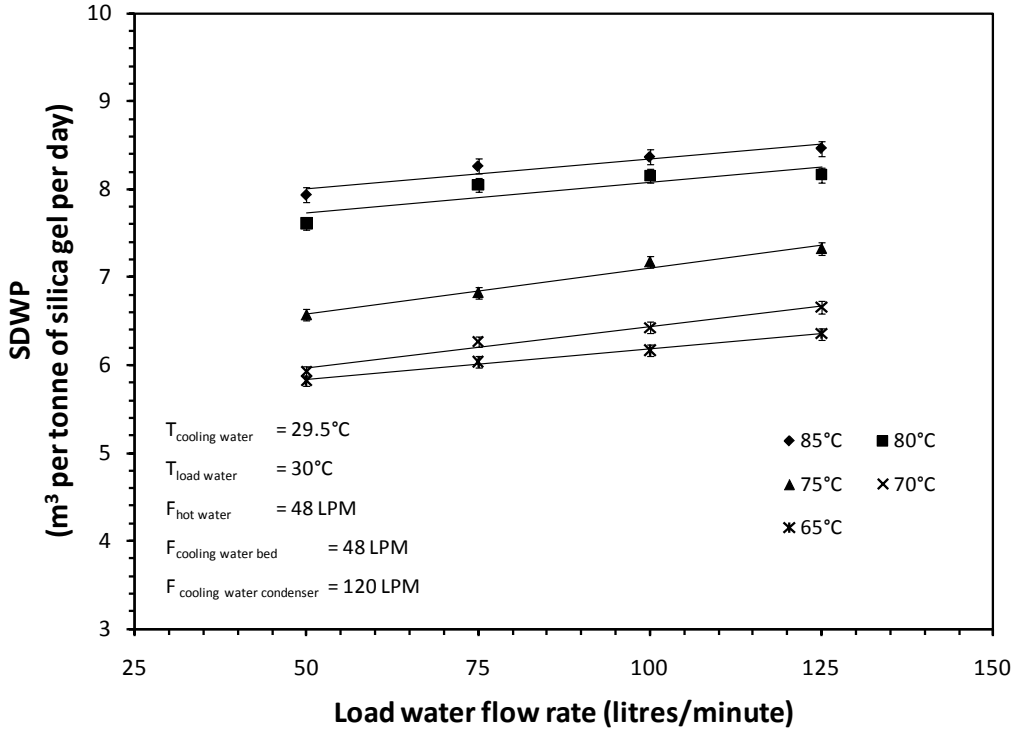

Figure 4.23 SDWP of a 2-bed AD cycle for assorted hot water inlet temperatures showing the effect of the chilled water flow rates on the cycle

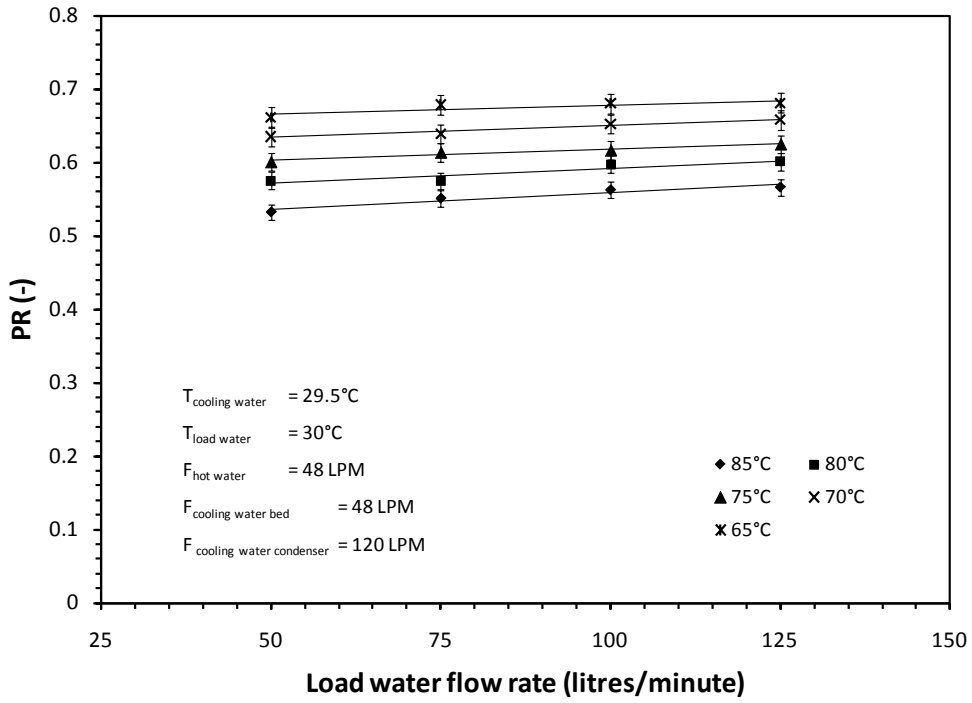

Figure 4.24 Performance ratio of the 2-bed AD cycle for assorted load water flow rates

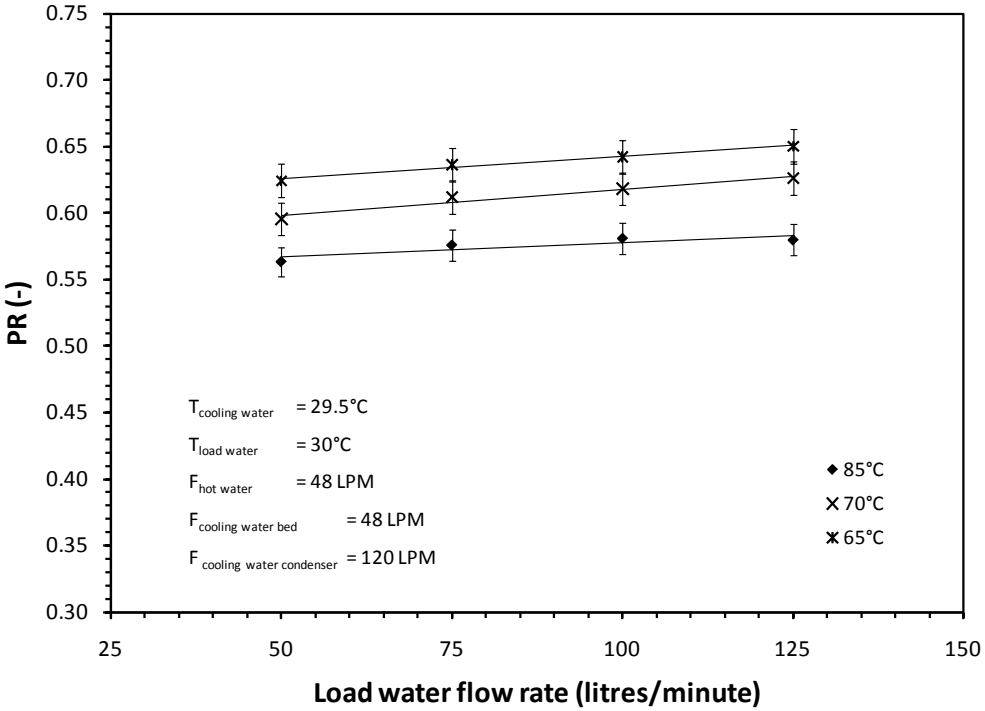

Figure 4.25 Performance ratio of the 2-bed AD cycle for assorted load water flow rates

4.2.5.4. Optimal pressure equalization time

The principle of heat and mass recovery by pressure equalization scheme has been discussed and explained how the scheme can improve the performance of the AD cycle. This section discusses the experimentally investigated performance of the AD cycle with the application of different pressure equalization times.

Figure 4.26 shows the SDWP of the AD cycle with assorted pressure equalization times namely; 0, 10, 20, 30s for different hot water inlet temperatures. The experimental result showed that the pressure equalization schemed improves SDWP and PR by 12% and 21%, respectively. It is observed that the optimal pressure equalization time is to be 10s for every hot water inlet temperature. The decrease in the SDWP of the AD cycle for longer pressure equalization times is due to the reverse adsorption and desorption phenomenon where the pre-heating bed starts regenerating and the pre-cooling bed adsorbs the vapors from the pre-heater instead of adsorbing from the evaporator thus reduces net adsorption and desorption capacity.

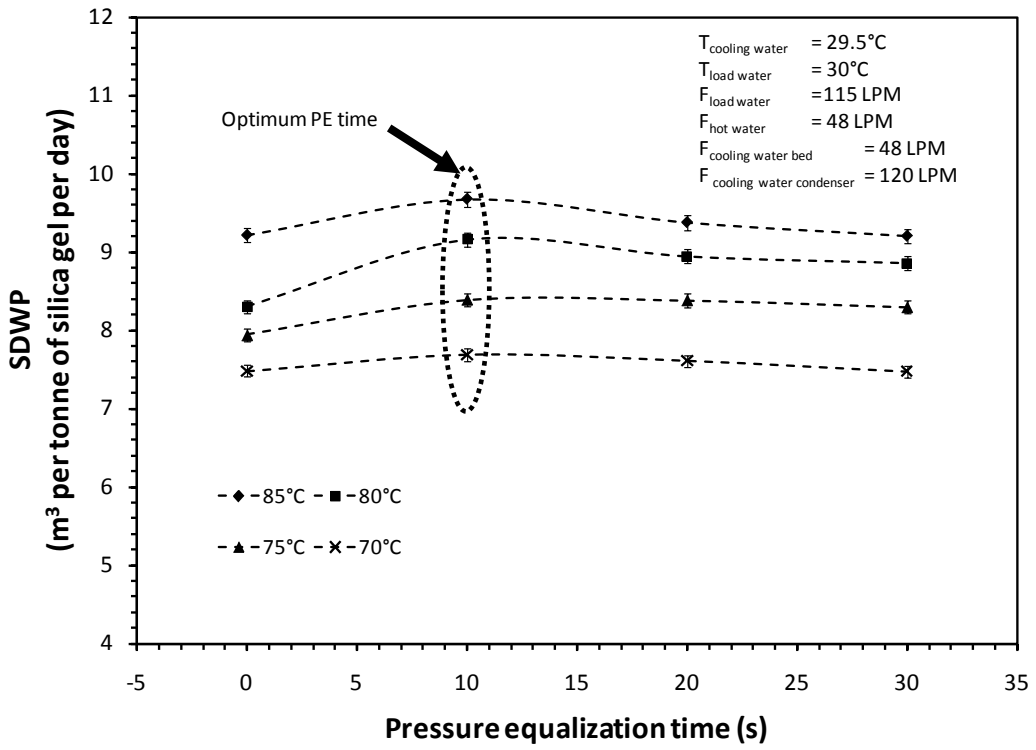

Figure 4.26 Pressure equalization time for the 4-bed AD cycle

4.2.5.5. Bed cooling scheme

The energy for the evaporation of the saline water can be recovered from the ambient or internally. In the bed cooling scheme, the ambient energy is extracted for evaporation while simultaneously cooling the adsorber bed with a boost the performance of the cycle. Figures 4.27 and 4.28 depict the comparison on the SDWP of 2-bed and 4-bed AD cycle without and with bed cooling scheme for assorted hot water inlet temperatures.

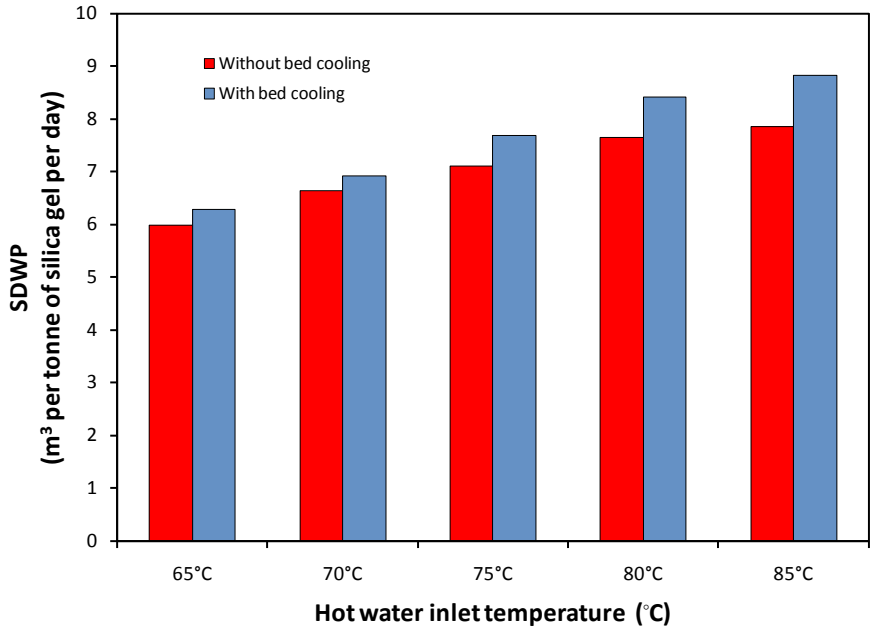

Figure 4.27 Comparison on the SDWP of a 2-bed AD cycle without and with bed cooling scheme

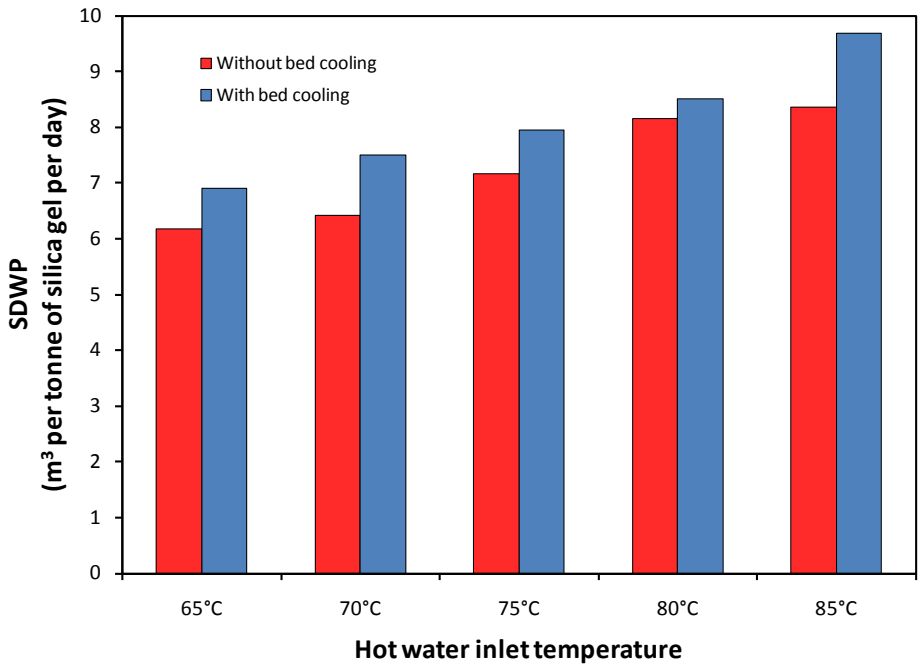

Figure 4.28 Comparison on the SDWP of a 4-bed AD cycle without and with bed cooling scheme

It is found that SDWP of the AD cycle is 8.8 for 2-bed mode and 9.7 for 4-bed mode whilst the percentage increment in SDWP is 12.5% and 16.0% for 2-bed

and 4-bed operate mode, respectively. More experimental results on the AD cycle with the bed cooling scheme can be found in Appendix G.

4.3. Summary of Chapter 4

The performances of the AD cycles have been investigated both numerically and experimentally. The performance of the cycle is evaluated for different operating conditions such as hot water inlet temperatures, cycle times and load water temperature and flow rates. It is observed that the recovery ratio of the AD cycle is as high as 70% with insignificant degradation in the performance. The evaluation of the optimal cycle time for different hot water inlet temperatures showed that the longer cycle time is required for lower hot water temperatures. The effects of heat and mass recovery schemes such as water recirculation, pressure equalization and bed cooling schemes are also investigated experimentally and the results showed that the optimum PE time is 10s enhancing SDWP and PR of the cycle by 12% and 21%, respectively. Similarly, the bed cooling scheme improves the SDWP by 16%. It should be noted that the energy for the evaporation for the saline water in AD cycle is recovered either from ambient or internally within the cycle such as from heat or adsorption. However, it observed that the AD cycle can produce cooling power from the evaporator for cooling purposes (outlet chilled water can be varied from 7°C to 20°C for space and process cooling) whilst producing potable water, simultaneously. The analysis of the AD cycle operating as a dual effect will be presented in Chapter 5.

Chapter 5 Performance investigation of a low temperature heat-driven adsorption cooling cum desalination cycle

This chapter describes the adsorption (AD) cycle that produces two useful effects namely: cooling from the evaporator and potable water from the condenser by utilizing only one heat source at low hot water temperature, either by extracting heat from an industrial waste heat source or the collection of solar energy with suitable collectors. The AD cycle can be operated in both the two-bed and the four-bed modes. A mathematical model is developed to predict the performances of the AD cycle and for accuracy, some experimental data are used to calibrate the simulation code, giving the much needed validation prior to conducting comprehensive comparison with the experiments. A theoretical framework of, a temperature-entropy (T-s) diagram has been constructed to represent the processes of the AD cycles for a better understanding of how the input energy is consumed within the cycle.

Introduction

Cooling and desalination are processes that permeate human's daily lives but these processes require substantial energy input, either from electricity or via thermal input. With greater awareness in environment friendly and climate change, utilization of solar thermal energy appears to be most logical and practical. Firstly, solar energy is inexhaustible. Secondly, the solar collectors are widely available and they are both cost effective (typically less than US\$300/m^2) and relatively high efficient (in excess of 45 % at application temperature of 80^o C or lower). The map of solar availability of the world is shown in Figure 5.1, where the desert regions have a daily solar incident

radiation in excess of 25 MJ/m^2.day whilst places in the equatorial regions such as Singapore have lower insolation of 16 to 17 MJ/m^2.day. In addition to efficient collectors, there is a necessity to develop thermally-activated technologies that could convert the low temperature waste heat, which is available in abundance, into useful effects such as cooling and desalination.

A novel cycle has been developed using adsorption process that employs the silica gel and water as the adsorbent-adsorbate pair. The following section describes the key processes in the thermally-activated adsorption cycle that produces two useful effects namely; cooling and desalination.

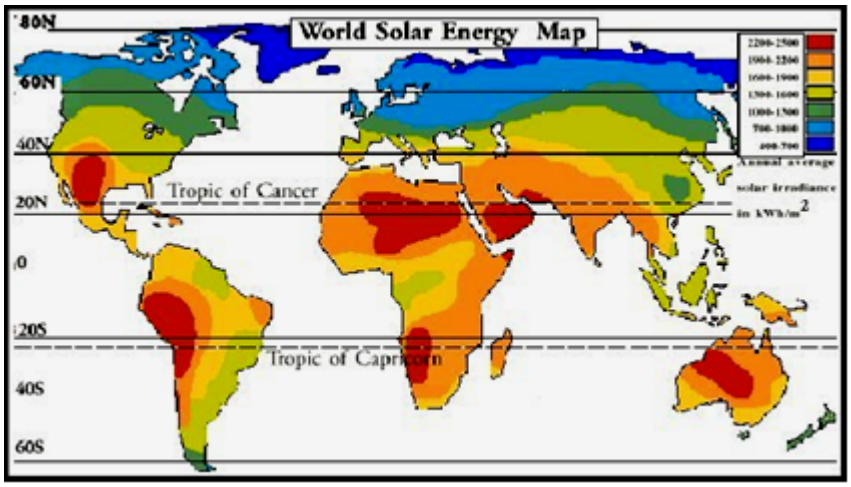

Figure 5.1 the map of solar availability of the world [104]

5.1. Description of a Dual-effect AD Cycle

The schematic diagram of a waste heat or solar driven adsorption cooling cum desalination plant is given in Figure 5.2. It comprises the following components: i) the externally-heated evaporator unit, ii) the cooling tower water-cooled condenser unit and iii) the thermally-activated adsorber/desorber beds. Sea or brackish water is

pretreated in a pretreatment system prior being introduced into the evaporator of the AD plant and these processes include the filtration to remove the unwanted suspended particles and the de-aeration. The evaporator of the AD plant performs two important functions: Firstly, it desalts the seawater by an evaporation process as seawater is sprayed over the external tube surfaces. This evaporation occurs at partial vacuum pressures, typically at 0.75 to 2 kPa. The evaporation of seawater at low pressures cools the re-circulation chilled water that flows through the internal tube passages, thereby supplying the cooling effect to an external application. Typically, the cyclic-steady state of water from the evaporator is at $12^{o}C\pm2$ with a temperature drop of 5°C.

The vapour pressure in the evaporator is maintained constant by the continuous vapor uptake of the silica gel. The evaporator and adsorbers are in heat and mass communication when the valves are set to open during a half-cycle time where vapour uptake occurs until the silica gel is almost saturated: Such duration varies typically from 3 to 10 minutes. Concomitantly, a low temperature heat source, typically varying from 65°C to 85°C, is employed to regenerate the previously saturated silica gel in the designated desorber beds. With heating supplied to the beds, the water vapor leaves the pores of silica gel due to higher kinetic energy, breaking away from the attraction forces of Van der Waals effect. Simultaneously, the vapor valves linking the desorber beds and the condenser are opened and the water vapor migrates quickly to the external surfaces of the tubes which they are cooled by water from the cooling tower. The condensate collected from the shell of condenser forms the high grade potable water (TDS<10ppm) which can either be collected in a tank and pumped out by a pump or simply be removed by gravity via a 10m high U-tube.

From the above description, the processes in the AD cycle are conducted in a batch manner where the roles of the beds are intermittently switched from absorber to the desorber and vice versa, and a pre-set switching interval demarcates these processes. During the switching, additional heat recovery features in the coolant circuits can be incorporated such as the pressure equalization interval, the coolant valve delay scheme, etc. These schemes enhance the performance of the AD cycle, in terms of the cooling and water production. Other than the water pumps and valves (vapor and liquid types), all major components of the AD plant such as the beds, evaporator, condenser, etc., are stationary. The stationary components used in the plant implied that a low specific energy consumption is deemed for the AD cycle: It is expected that the specific energy consumption is not higher than twice that of the thermodynamic limit for seawater desalination.

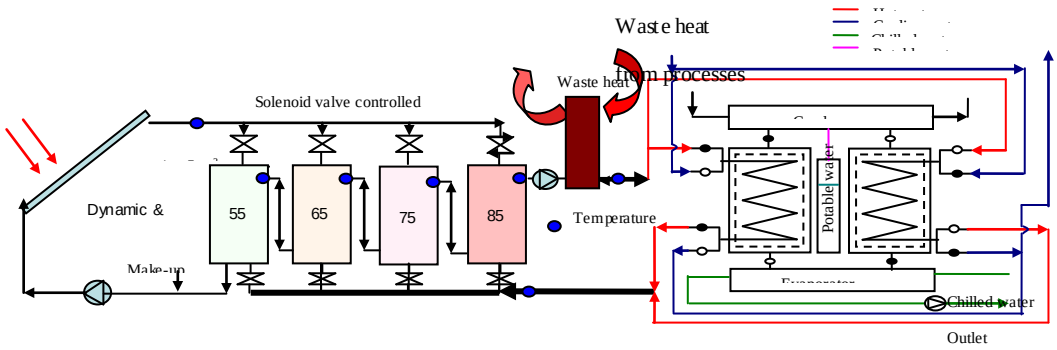

Figure 5.2 Schematic of solar driven dual-effect AD plant

5.2. Mathematical modeling and numerical simulation

Using the theoretical model, as developed in the Chapter 4, the performance of the dual-effect adsorption cooling cum desalination cycle is presented here. The cooling capacity and coefficient of performance of the cycle are estimated as,

$$Q_{cooling} = \dot{m}_{chilled} c_{p,chilled} \left(T_{chilled,in} - T_{chilled,out} \right) \quad 5.3$$

$$COP = \frac{Q_{cooling}}{Q_{heating}} \quad 5.4$$

where the useful effect refers to the cooling load and the heat input is the desorption heat that is supplied to the AD cycle. Another efficiency parameter, called the overall conversion ratio (OCR), accounts for the total useful effects by the cycle to the total heat input which is defined here as ,

$$OCR = \frac{Q_{cooling} + h_{fg} \dot{m}_{potable}}{Q_{heating}} \quad 5.5$$

where h_{fg} is the latent heat of condensation and $\dot{m}_{potable}$ is the potable water production rate. In the adsorption cooling cum desalination cycle, the useful effects produced are the cooling power either for residential or district cooling and desalination (potable water) and these useful effects are derived from single heat input at low water temperature.

The governing equations for the components of the plant have been presented in Chapter 4 and shall not be repeated here. The solving routines used here are the Gear's BDF method from the IMSL routines of the FORTRAN PowerStation, and the solver employs a double precision with tolerance value of 1×10^{-6}. The same parameters provided in Chapter 4 are used in the simulation.

5.2.1. Simulation results

Figure 5.3 shows the simulated temperature profiles of the two-bed mode adsorption desalination cum cooling cycle at standard rating conditions, namely, 85°C

regeneration or inlet hot water temperature and 12.5°C chilled water inlet temperature. The AD cycle starts from room temperature and the cyclic-steady-state can be obtained within four half-cycle operations. It is observed that the outlet chilled water temperature from the plant is around 7.5 ˚C which is suitable for space cooling. The corresponding energy utilization of the processes of the AD cycle i.e., adsorption, desorption, evaporation and condensation process, are shown in Figure 5.4. Positive energy quantities refer to heat input to the cycle and negative quantities are heat rejected by the plant and the net energy balance in the cyclic steady state is computed to be less than 0.5%.

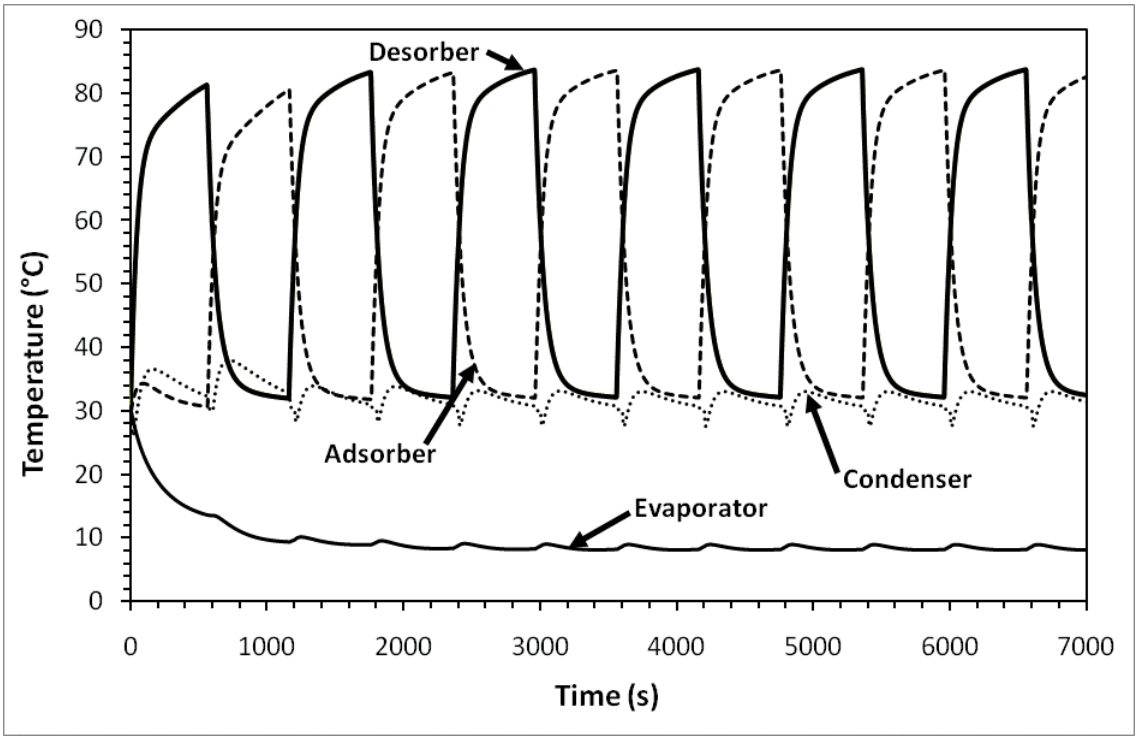

Figure 5.3 Temporal temperature profiles of the adsorption cooling cum desalination cycle at 85°C hot water inlet and 12.5°C chilled water inlet temperatures

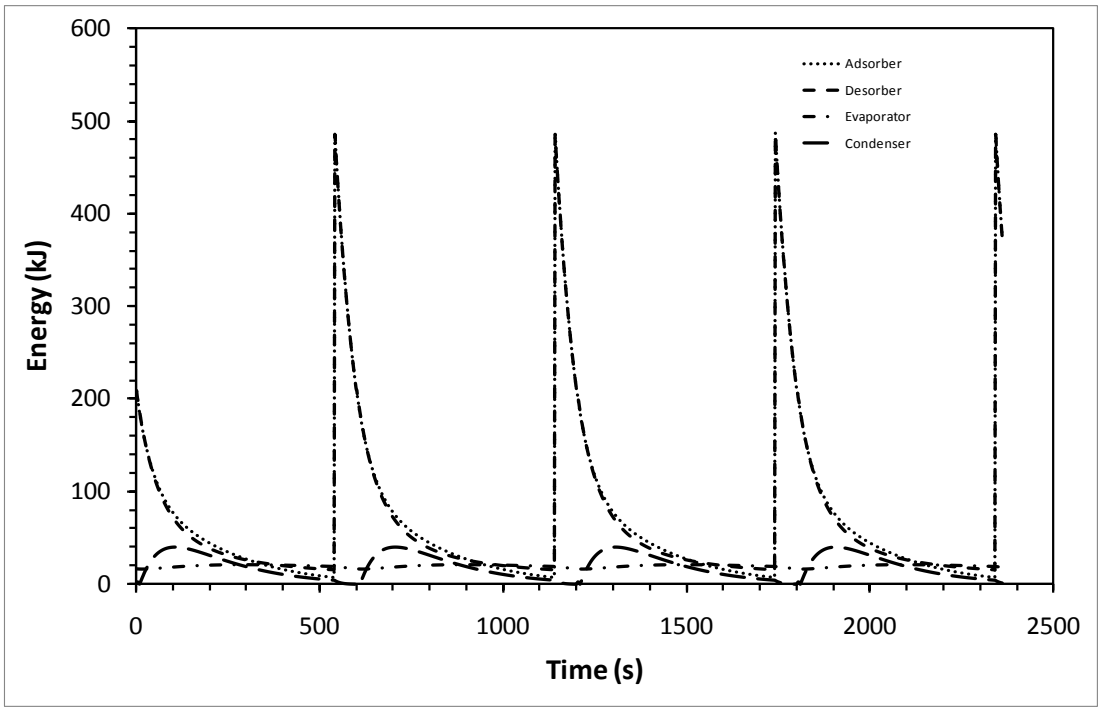

Figure 5.4 Analysis on the energy utilization of the adsorption, desorption, evaporation and condensation of the adsorption cooling cum desalination cycle

For better understanding of the AD cycle, a wide range of the heat source inlet and cooling water temperatures have been investigated. Figure 5.5 shows the performance of the AD cycle in terms of SDWP and specific cooling power (SCP) at assorted chilled water inlet temperatures ranging from 10°C to 30°C. The hot water and cooling water inlet temperatures are maintained at the rating conditions, namely at 85°C and 30°C respectively and the half-cycle for adsorption or desorption is 600s with the switching interval set at 30 seconds.

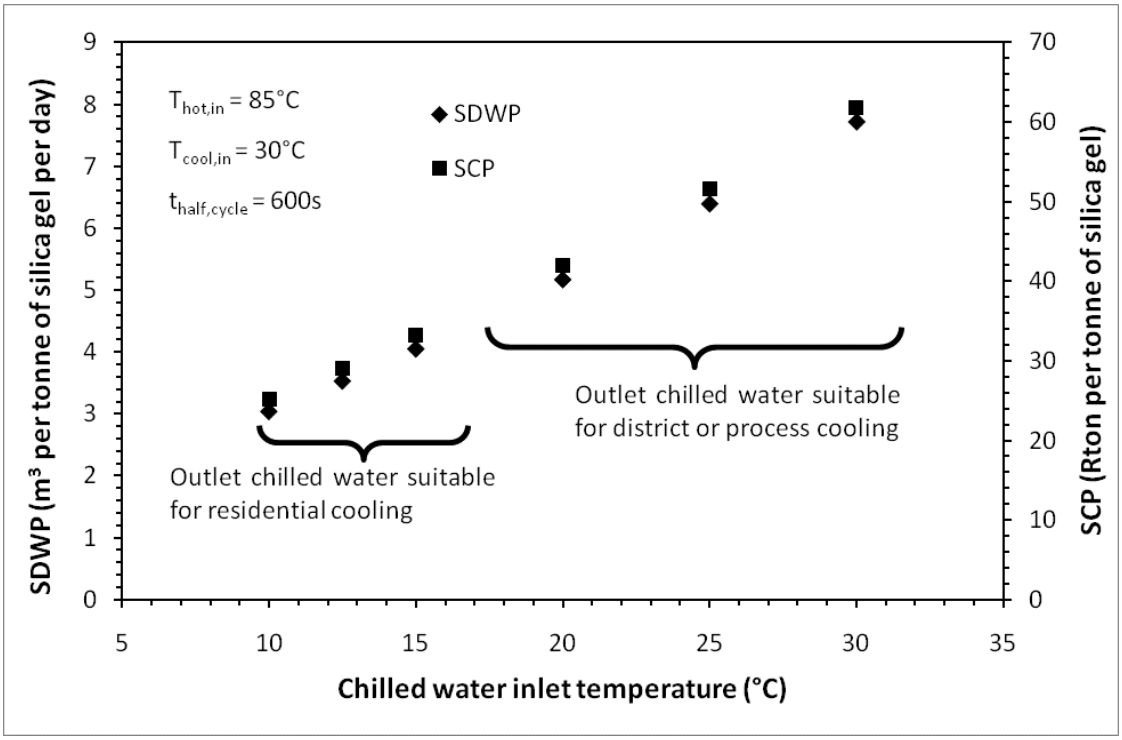

Figure 5.5 SDWP and SCP of the AD cycle with assorted chilled water inlet temperatures suitable for residential cooling and process cooling applications.

The results show that both SDWP and SCP have a linear relationship with the chilled water inlet temperatures, increasing performance at higher chilled water inlet temperature for the same regeneration temperature and cycle time. This is attributed to two factors: Firstly, an improvement in the boiling process at the evaporator and secondly, the increase in the pressurization effect of adsorbate onto the adsorbent caused by the higher evaporation temperature (hence P_{sat}).

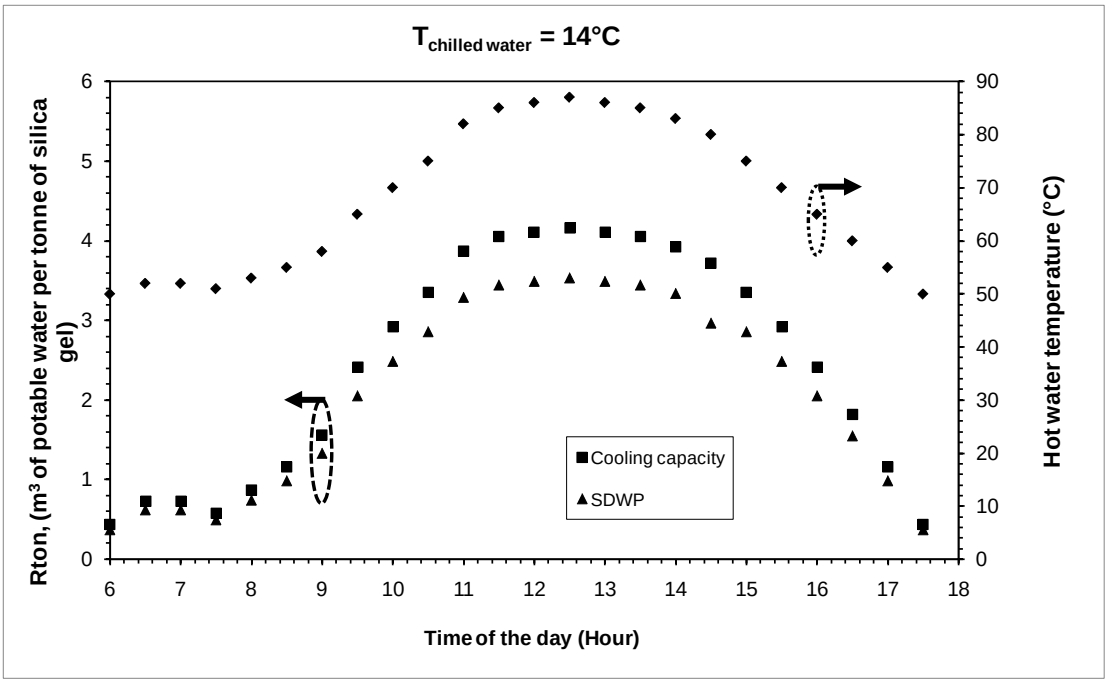

Figure 5.6 Simulated results of the cooling capacity and the SDWP of the AD plant with hourly varying hot water temperature at chilled water inlet 14°C

For transient heat source temperatures such as solar energy source, Figures 5.6 and Figure 5.7 depict the performance of the cycle for two different levels of chilled water temperature i.e., 14°C and 30°C with varying hot water inlet temperature. For 30°C chilled water inlet temperature, optimized for potable water production, the daily average values of the SDWP and SCP are found to be 5.62m^3 and 45Rton per tonne of silica gel per day, respectively. On the other hand, the SDWP is 2.1m^3 and SCP is 16.9 Rton per tonne of silica gel per day for the chilled water inlet temperature 14°C where the cycle is optimized for process cooling. The results showed that the adsorption cooling cum desalination cycle provides a perfect match for varying heat sources such as solar hot water system producing the two useful effects, i.e., cooling and potable water.

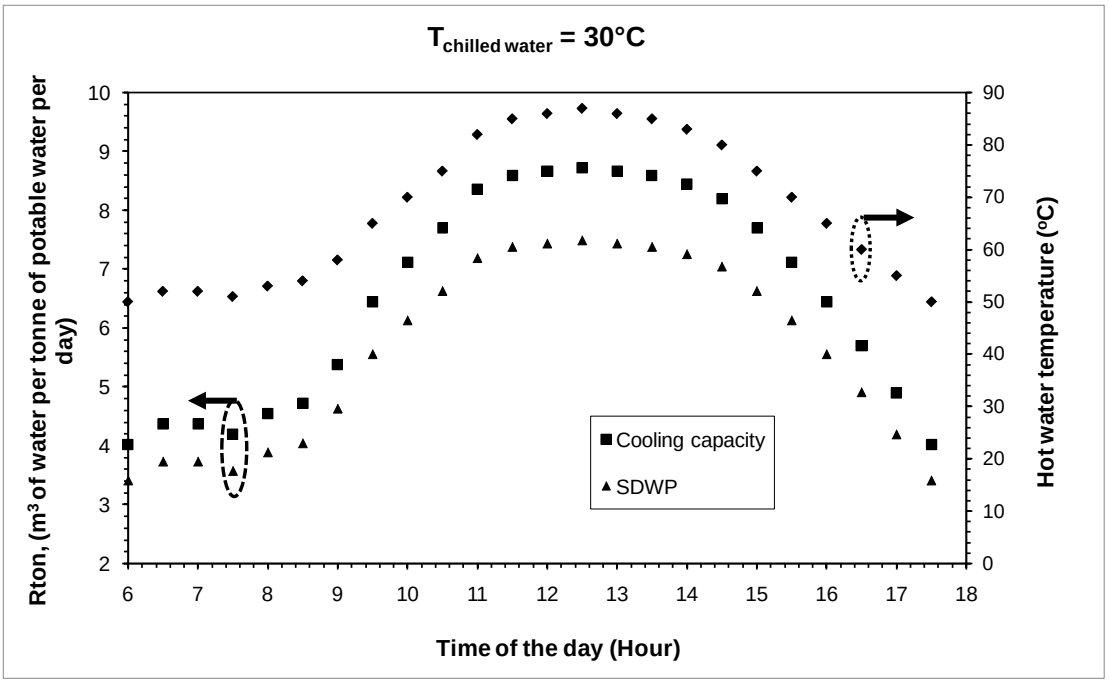

Figure 5.7 Simulated results of the cooling capacity and the SDWP of the AD plant with hourly varying hot water temperature at chilled water inlet 30°C

The key advantage of the AD cycle is the flexibility of operation over a wide range of heat source temperatures whilst the performances could improve with a lower coolant temperature supplied to the condenser. Being robust in the operational conditions, the cycle can be tailored to meet the requirements between the amount of cooling and the amount of desalted water needed by simply changing the temperature of evaporator. Should the AD operation is designed for more residential cooling, the predictions show that the cycle could produce a SCP of 32Rton and a SDWP of 4m^3 per day per tonne of silica gel when the outlet chilled water temperature spans from 7°C to 10°C. If more desalted water is desired from the condenser, the AD cycle operation could be adjusted to produce a SDWP and a SCP of 7.7 Rton and 60 m^3 per day per tonne of silica gel, respectively. For the latter operation, the cooling water from the evaporator would have to be raised higher, typically at 18 to 25°C, a temperature range that is suited for process or district cooling.

The numerically-simulated results showed that the AD cycle is indeed robust and it has great potential for meeting the needs of supplying cooling and high grade water at various proportions. The simulation results can be further validated with experiment which is discussed in the section below.

5.2.2. Experimental investigation

For validation of predictions, an elaborate experimental programme was mounted using the adsorption desalination pilot plant discussed in Chapter 4. Prior to each set of experiment, the adsorbent in the AD plant was regenerated using 85°C hot water so as to remove any unwanted gaseous residual still adsorbed in the silica gel, and thus reduces the experimental errors in the tests. The seawater feed is prepared by using the sea salt with the tap water, resembling to natural sea water to achieve a total dissolved solids (TDS) of 35000ppm. The seawater is pretreated by a de-aeration process to remove any non-condensable before it is fed into the evaporator of the AD plant.

The AD cycle produces both the cooling and desalted water from the evaporator and the condenser. The operational parameters of the plant are summarized in Table 5.1.

Table 5.1 The experimental parameter for the Dual-effect Adsorption plant

	Temperature (°C)	Flow rate (LPM)
Hot water inlet (desorber)	65-85	48
Cooling water inlet (adsorber)	29.5	48
Cooling water inlet (condenser)	30	120

Chilled water inlet (evaporator)	12.5-30	48
Pressure equalization time (s)	10	
Mass of silica gel per bed (kg)	36	
Switching time (s)	40	

In terms of water temperatures supplied to the heat source, cooling and chilled water circuits, the hot water inlet temperature range is from 65°C to 85°C, the chilled water inlet temperature ranges from 10° to 30°C. For the experiments, only one cooling tower with an inlet temperature of 30^{o} C is compared. The useful effects monitored in the experiments are the cooling capacity and the amount of desalted water in various proportions.

5.2.2.1. Results and Discussion

From the isotherms, the adsorption capacity of silica gel-water pair increases with the increase of adsorption pressure and hence, the SDWP would increase with increasing temperature of evaporator. Evaporator pressure is raised with the chilled water inlet temperature. For a given half-cycle time, the SDWP or water production can be increased by heat recovery methods: The cooling of the coolant supplied to the adsorption process with a plate heat exchanger. Alternately, the heat can be injected to the evaporator by tapping-off the free energy from cooling tower circuit. In the former method, the vapor uptake of silica gel is enhanced during the adsorption process as the adsorption temperature is lowered to a temperature below that of the ambient and hence it benefits both processes in the adsorber and condenser.

As mentioned previously, the performance parameters of the AD system are the specific daily water production (SDWP), the specific cooling capacity (SCC) and the performance ratio (PR), COP and the overall conversion ratio (OCR). These parameters are presented as a function of cycle time, the chilled water inlet temperature and the driving heat source temperature (hot water), from the experimental data in steady state conditions.

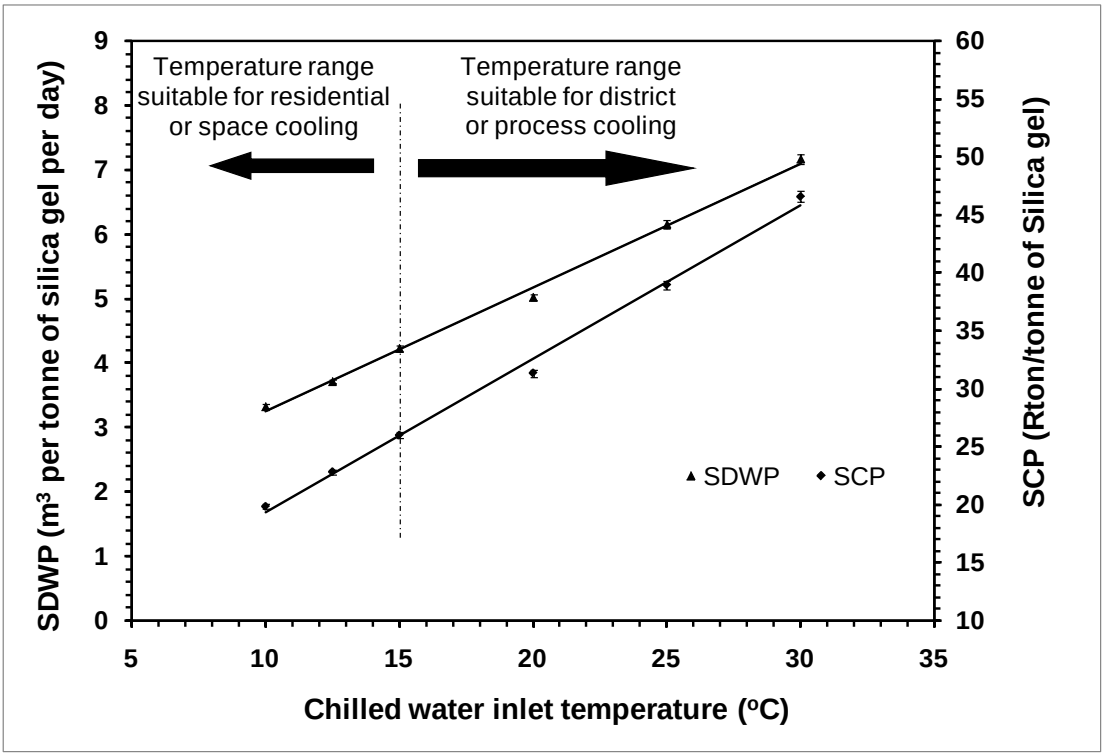

Figure 5.8 SDWP and the SCP of a two-bed AD cycle

Figure 5.8 shows specific daily water production (SDWP) and the specific cooling power (SCP) of the adsorption cycle at different chilled water inlet temperatures. The regeneration temperature and the half-cycle time are 85°C and 600s, respectively. For air-conditioning application with a chilled water inlet of 12.5^{o}C, the measured specific power (SCP) is 25 Rton, but the corresponding SDWP is merely 3 m^{3} per tonne of silica gel per day. Should the chilled water inlet

temperature be raised higher, say at 20°C to 30°C (optimized for the desalination process), the measured SDWP and SCP are 7.5 Rtons and 50 m^3 per tonne of silica gel per day, respectively. The higher cooling capacity is suitable for the process or district cooling application in oil refineries, etc. The main advantage is that there is a significant increase in the water production yield as some heat is recovered from the ambient. Hence, the overall conversion ratio of the AD cycle is expected to increase significantly.

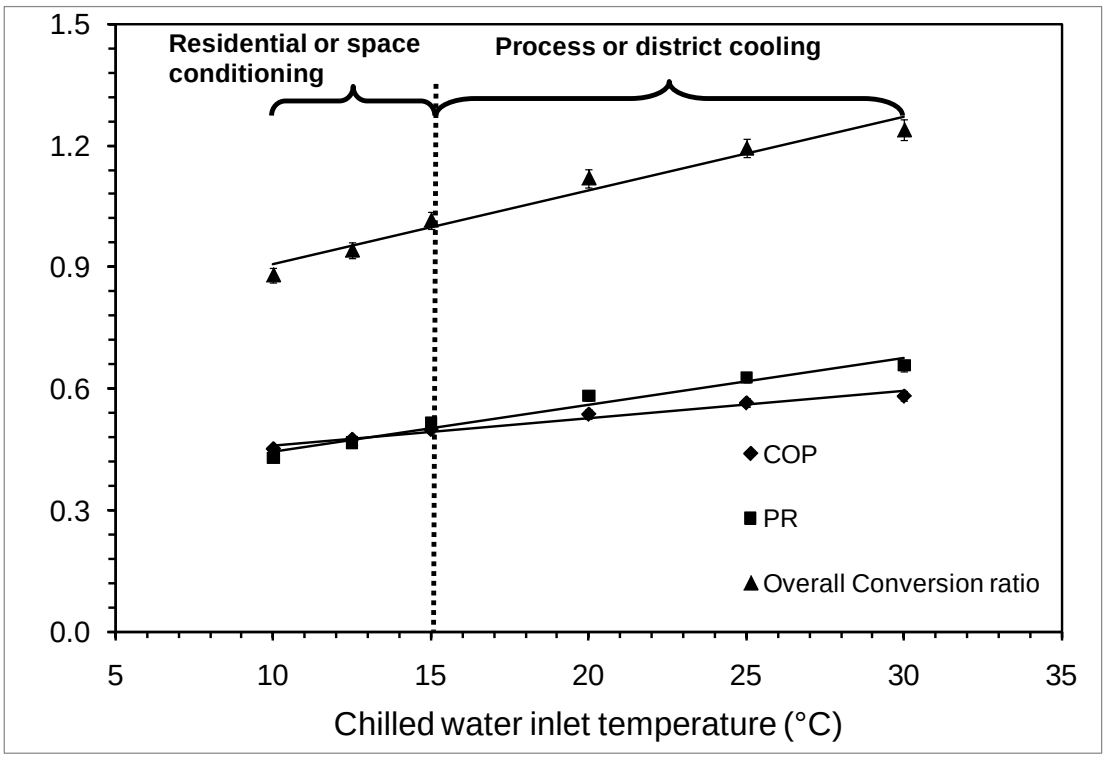

Figure 5.9 Performance of the adsorption cooling cum desalination cycle showing the COP, PR and OCR

The overall conversion ratio of the adsorption cycle, defined here as the ratio of total useful effects to the energy input, is shown in Figure 5.9. For a 30° C inlet to evaporator, an overall conversion ratio (OCR) is 1.2 at the rating conditions of $T_{heat\ inlet}$ = 85°C and T_{cool}=30°C. On the other hand, the OCR drops to 0.9 for lower chilled water inlet temperatures of 12.5 °C. The high value of OCR in the AD cycle is

attributed to the production of two useful effects i.e., cooling and potable water, from a single heat input. The flexibility in allocation of the cooling capacity and water production yields of the AD cycle makes the machine suited for demand-oriented applications. For example, the seasonal changes in the climate of a semi-arid or desert environment would require fluctuation in the production of cooling and water. The AD operation could be tuned to produce more water and less cooling during winter and vice versa for the summer operation.

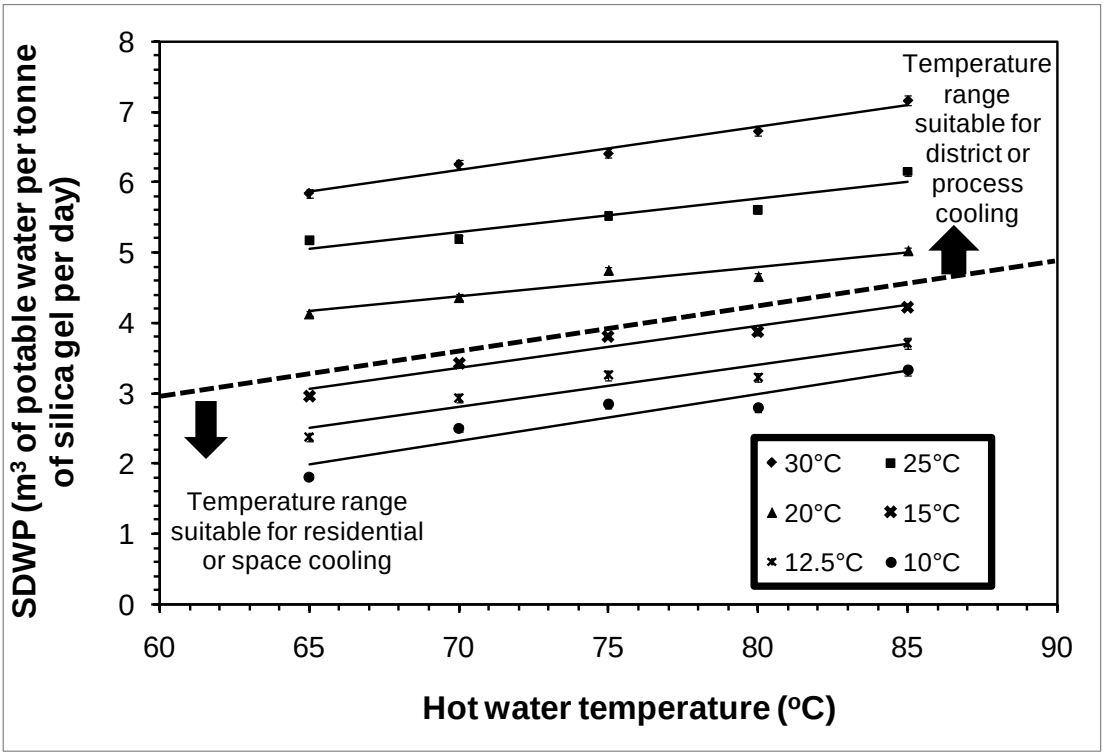

Figure 5.10 SDWP of the adsorption cooling cum desalination cycle for different chilled water temperatures with assorted hot water inlet temperature

For a solar-driven adsorption cycle, the hot water temperatures from collectors are a function of daily insolation where the hot water temperature is expected to vary from 65°C to 85°C. The simulated results are given in Figure 5.10 and Figure 5.11. It can be seen that the SDWP and the SCC of the adsorption cycle linearly increase with higher heat source temperature for every set of chilled water

inlet temperature. It is also observed that both the SDWP and SCC of the adsorption cycle improve at higher chilled water temperatures with higher heat source temperatures.

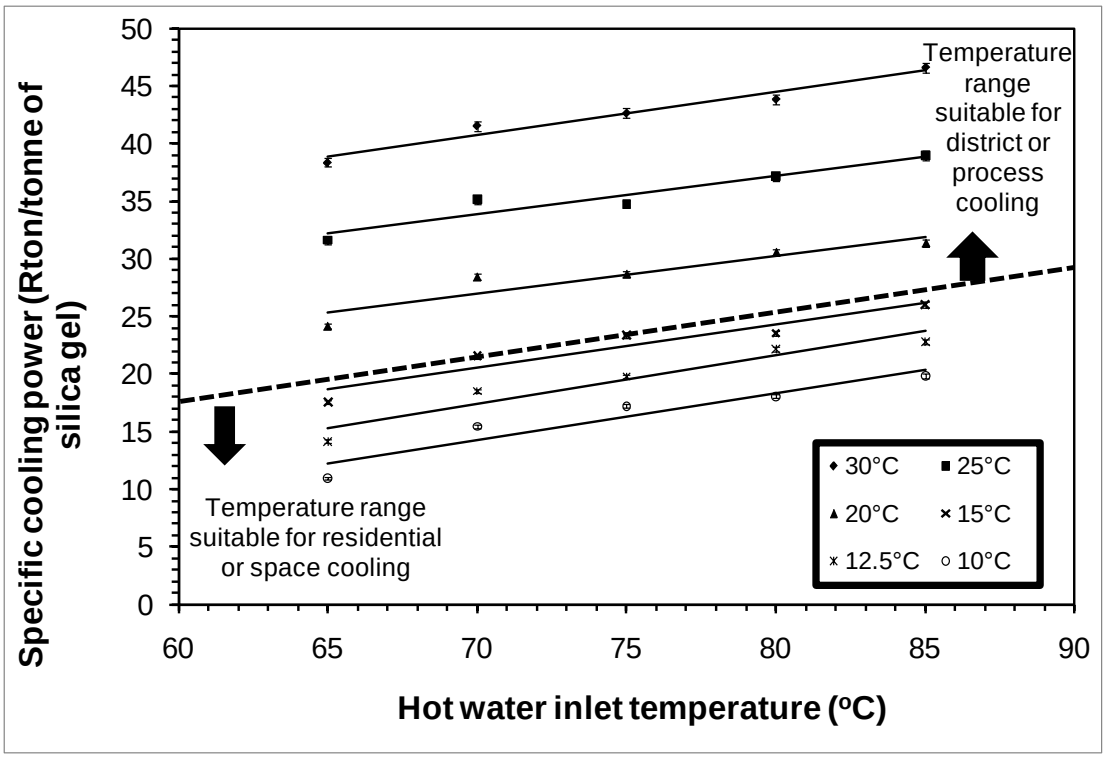

Figure 5.11 SCP of the adsorption cooling cum desalination cycle for different chilled water temperatures with assorted hot water inlet temperature

Figure 5.12 describes the overall conversion ratio of the two-bed adsorption cycle for both air-conditioning and desalting applications at assorted hot water inlet and chilled water inlet temperatures. The results show that overall conversion of the Adsorption cycle decreases with increasing hot water temperature. The overall conversion ratio of the Adsorption cycle can be as high as 1.5 at 65^{o}C regeneration temperature. The results also show that the adsorption cycles can operate efficiently using solar energy.

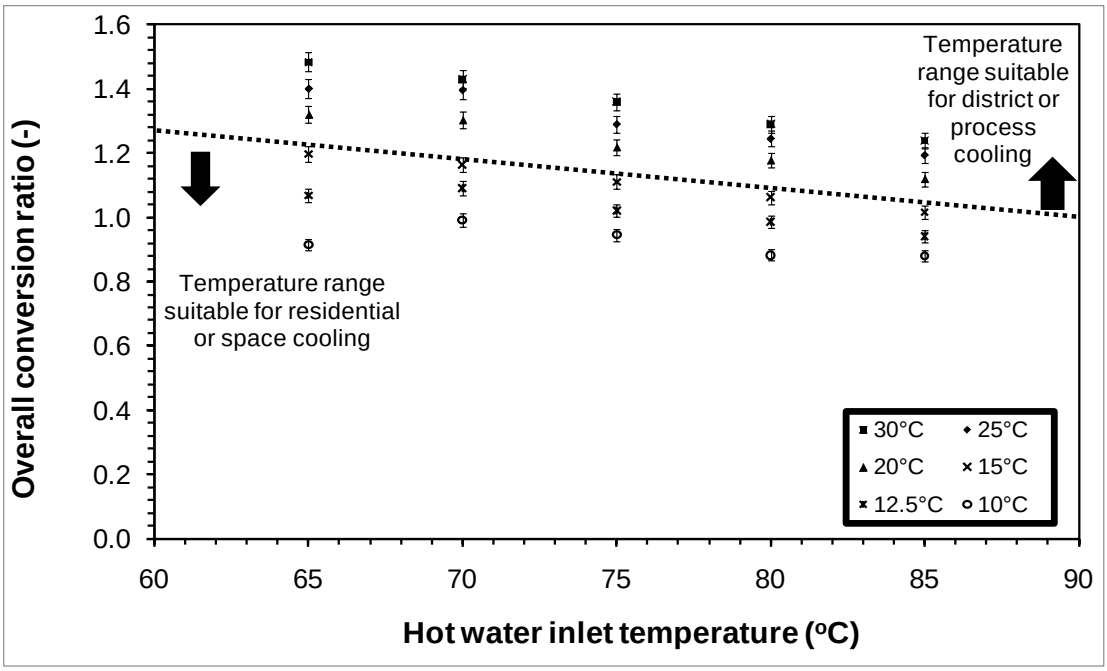

Figure 5.12 Overall conversion ratio of the two-bed adsorption cycle for cooling and desalination

The performance of the four-bed mode AD cooling cum desalination cycle is experimentally analyzed. Figures 5.13 and 5.14 show the SDWP and the SCP of the four-bed AD cycle operating at 30°C and 25°C chilled water and optimized for potable water production. The outlet chilled water which temperature ranges from 25°C to 20°C is suitable for district or process cooling. It is found that the SDWP and the SCP of the AD cycle is about 8 m^3 and 51.6 Rton per tonne of silica gel per day.

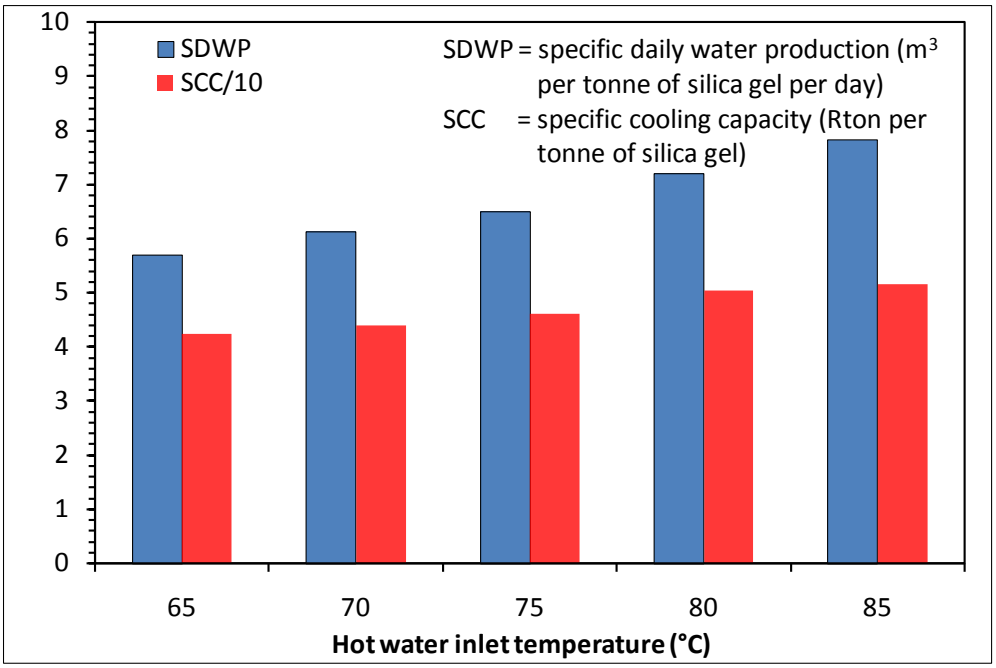

Figure 5.13 SDWP and SCP of the four-bed mode adsorption cooling cum desalination cycle at 30°C chilled water inlet temperature for assorted hot water inlet temperature

For the four-bed mode AD cycle, the plant can be operated to produce lower chilled water temperatures that are suitable for residential or space cooling, as shown in the Figures 5.15 and 5.16. The produced chilled water in this operation condition is 10°C and 15°C respectively. It is noted that the cycle produces SDWP of 3.6 m^3 and SCP of 23 Rton per tonne of silica gel while the chilled water outlet temperature is about 10°C and the hot water inlet temperature is 85°C. It is also found that both SDWP and SCP linearly vary with the regeneration temperature.

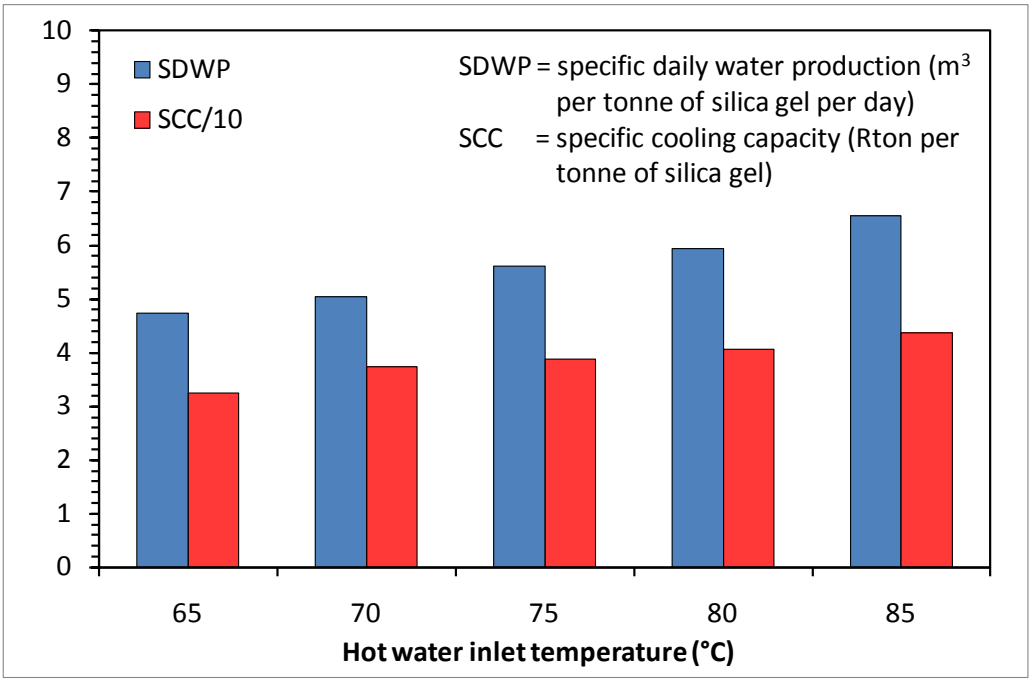

Figure 5.14 SDWP and SCP of the four-bed mode adsorption cooling cum desalination cycle at 25°C chilled water inlet temperature for assorted hot water inlet temperature

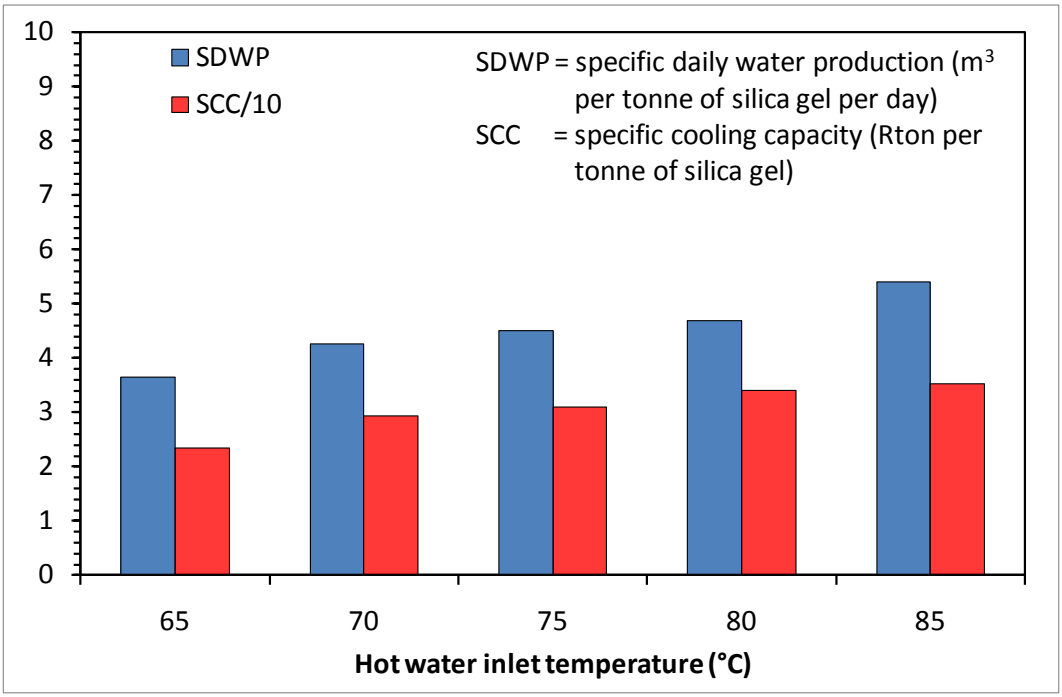

Figure 5.15 SDWP and SCP of the four-bed mode adsorption cooling cum desalination cycle at 20°C chilled water inlet temperature for assorted hot water inlet temperature

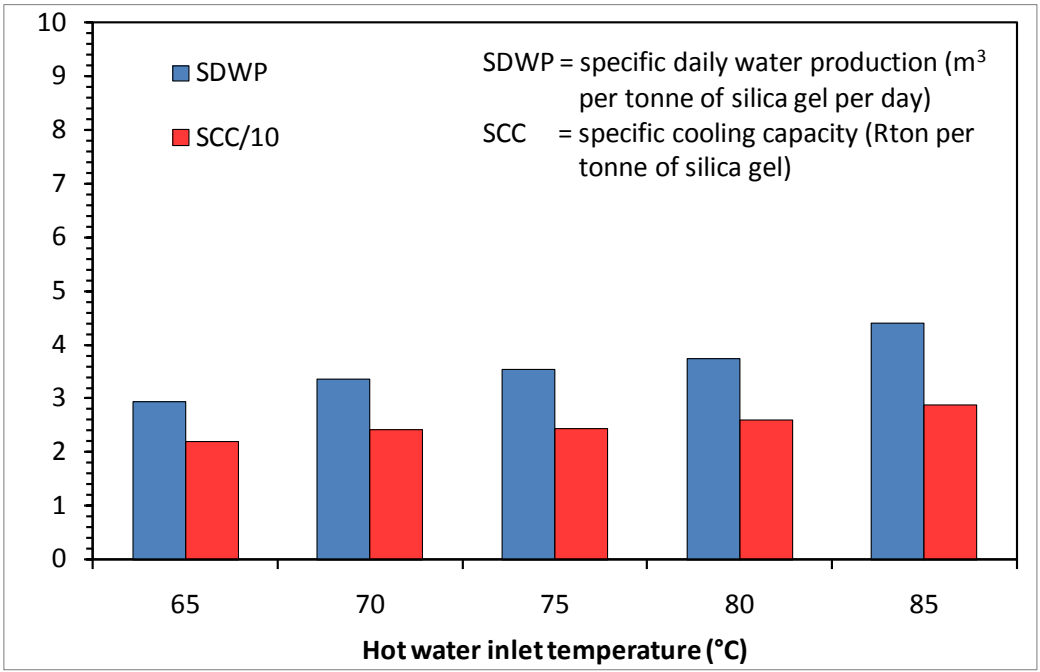

Figure 5.16 SDWP and SCP of the four-bed mode adsorption cooling cum desalination cycle at 15°C chilled water inlet temperature for assorted hot water inlet temperature

5.2.3. Validation of the simulation and experimental results

Experimental data from the prototype AD plant is used for validation of the mathematical model. The comparison is performed on a 2-bed adsorption cooling cum desalination cycle operating over a half-cycle period. Figure 5.17 shows the comparison between the simulated and the experimentally-measured temperatures of the major components of the adsorption cooling cum desalination cycle.

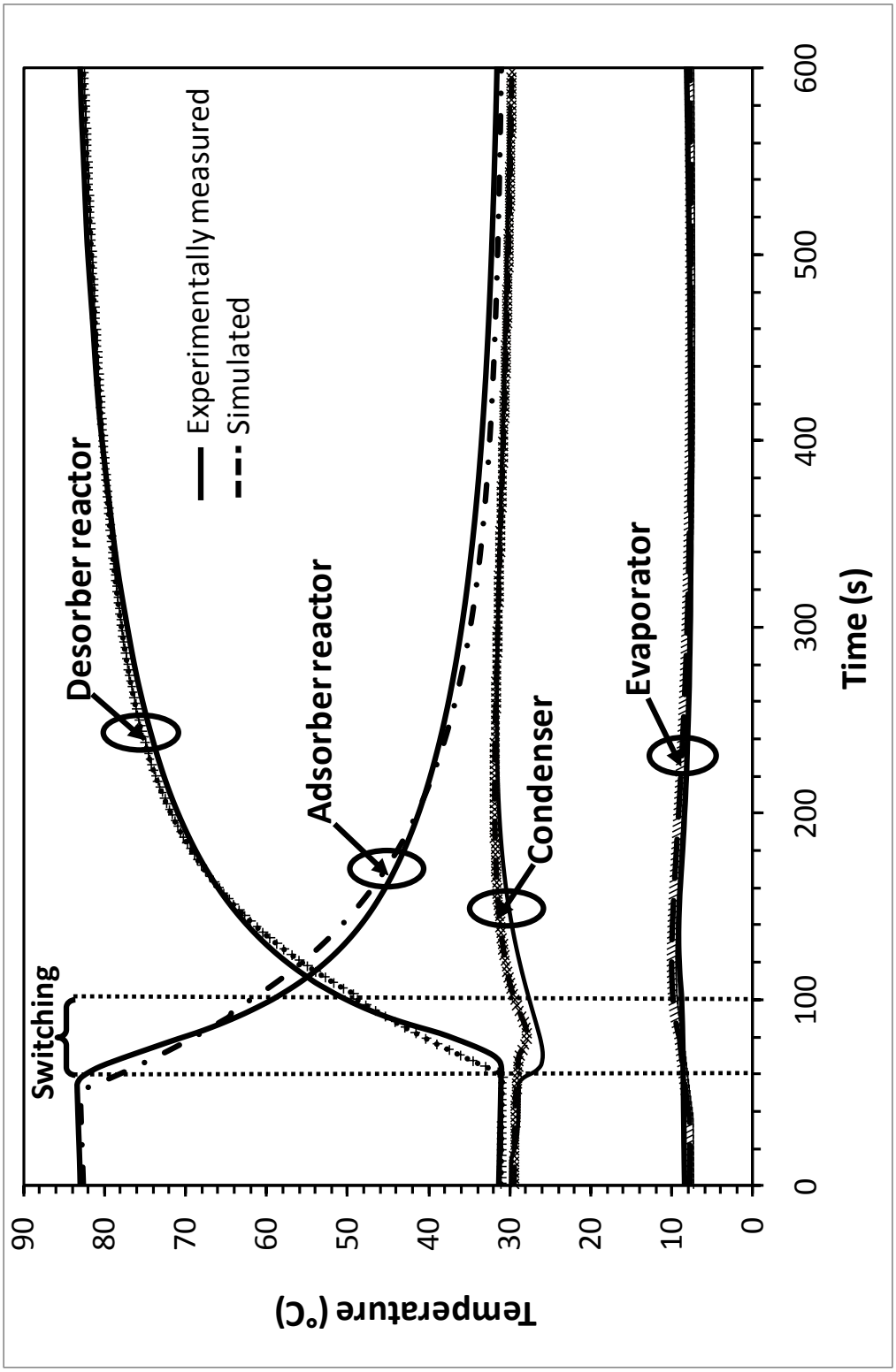

Figure 5.17 Temperature profiles of the major components of a 2-bed Adsorption cooling cum desalination cycle comparing the experimentally-measured and simulated values

The thermodynamics properties of the adsorbent-adsorbate pair used in the model have been described in Chapter 4. Both temperature traces of the adsorber and desorber displays first-order exponential-type behavior, increasing or decreasing asymptotically with time. The condenser and evaporator water temperatures rise of 5K or so over the half cycle. When compared with the experimentally measured results, the predicted performances of the cycle agree well Table 5.2 gives the comparison on the specific daily water production (SDWP), specific cooling power (SCP) of the AD cycle by simulation and experiments.

Table 5.2 SDWP and SCP of a two-bed AD cycle comparing by simulation and experiments

T_{hot} (°C)	Simulation		Experiment	
	SDWP	SCP	SDWP	SCP
85	7.16	56.85	7.16	46.57
80	6.83	54.03	6.73	43.83
75	6.42	50.63	6.41	42.63
70	6.13	48.39	6.26	41.55
65	5.80	45.74	5.84	38.36

It is found that the SDWPs of the plant by simulation agree well with the experiments while SCP by simulation is slightly higher than the experimental results. The lower SCP of experiments can be attributed to the fouling to the evaporating surface of the experimental AD plant.

5.3. Temperature-entropy map of the adsorption cooling and desalination cycle

Based on the thermodynamic property fields adsorbent/adsorbate system, as discussed in Chapter 3, a temperature-entropy (T-s) map for the AD cycles is plotted for both the simulation and the experiments. As shown in Figure 5.18, the area under the T-s diagram hives a measure of the energetic performance of the AD cycle in terms of entropy flow. For example, thermal compression by the adsorption-desorption process of the adsorbent (silica gel) is described by the path A-B-C-D indicated on the thermodynamic entropy surfaces. Points H to E are the path denoting the evaporation process of sea water within the evaporator. The vapors are adsorbed by the adsorbent at evaporator pressure over the preset half-cycle time. Pre-heating of the adsorbent occurs before the commencement of desorption process and it can be described by the path D-A-B. Regeneration of the adsorbent is performed by supplying a hot water heat source at condenser pressure, as represented by the process B-C. The regeneration process continues until another half-cycle and the adsorbent is pre-cooled (C-D) and the cycle completes. The changes of the entropy in the AD cycle can be tracked accordingly. The area under the T-s diagram of a process denotes the energy transfer needed for the process. In addition, the isotere (amount of adsorbate) can also be super-imposed onto the proposed T-s diagram. For example, the uptake by adsorbent during the evaporation-adsorption process (x_{ads}) is about 15-17% whilst desorption process can remove vapors up to 0.06 % (x_{des}) of the dry mass from the adsorbent. Most importantly, the area of the cycle, as bounded by the processes of the plant, signifies the amount of energy needed to execute the cycle and thus, it permits a comparison of the performance of one type of the AD cycle with another when additional features are incorporated, namely, heat recovery, etc.

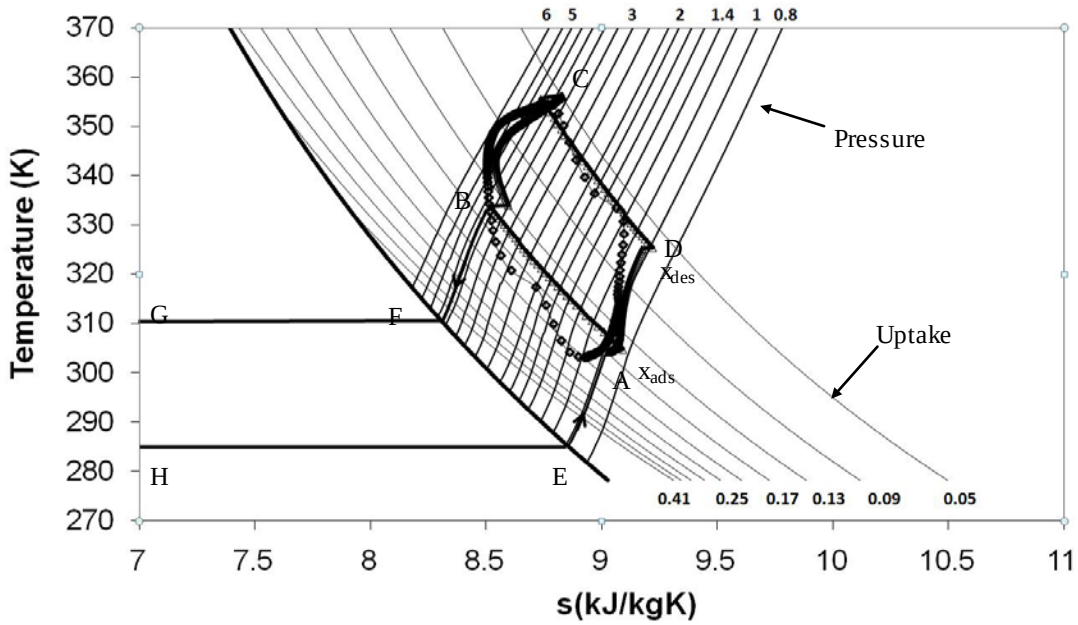

Figure 5.18 Temperature-entropy (T-s) maps of the adsorption cooling and desalination cycle

The desorbed water vapors are condensed in the condenser, the process F-G. Cooling energy is extracted from the evaporation process (H-E) and potable water is obtained from the process (F-G).

5.4. Summary of Chapter 5

The performance of an adsorption cooling cum desalination cycle has been investigated numerically and validated by experiments. The useful effects of the cycle i.e., cooling and potable water can be estimated accurately when a single heat input at low temperature is supplied to the cycle. Such a heat source can be derived from waste heat extraction from the industrial exhaust or from the solar thermal collection.

The simulated results showed that the AD cycle has an overall conversion ratio (OCR) of more than 1 since it produces two useful effects, namely, the cooling and potable water. The simulation code permits the detailed analyses of both 2-bed and 4-bed operation in the AD cycle.

The simulated results have been analyzed using a thermodynamic approach, i.e., the T-s diagram where the paths of the processes in the cycle have been accurately traced and the energy transactions as well as the amount of adsorbate (vapor) of each process can be computed.

Chapter 6 Performance Investigation of Advanced Adsorption Desalination Cycles with Internal Heat Recovery

Introduction

In Chapter 5, the conventional adsorption cooling cum desalination cycle with 2 and 4 –beds operation has been presented. However, from the thermodynamic point of view, AD cycle performances can be enhanced with internal heat recovery within the batch operation of cycle. In this chapter, an advanced adsorption desalination cycle is investigated using the heat of condensation process in condenser to affect the desalting and cooling processes in the evaporator. The details of the advance cycle is discussed in this chapter along with the performance analyses of the cycle

6.1. Advanced Adsorption Desalination cycle

Using the principles of internal heat recovery, it is proposed that the latent heat of condensation of water vapor, which is rejected during condensation at vapor pressures of 5 to 7 kPa, is recovered to the evaporative process of evaporator where the latter system pressure is much lower at 2 to 3 kPa. Such a heat recovery can be achieved by two methods of equipment layout: Firstly, an integrated condenser-evaporator design within a single housing for direct heat and mass transfer and secondly, a re-circulating coolant medium that flows between the evaporator and the condenser, transferring the latent heat from the condenser to the evaporator. The latter method is suitable for retrofitting an existing AD cycle and it will be discussed in

Section 6.2. Figure 6.1 shows the schematic diagram of an advanced adsorption desalination (AD) cycle where it comprises three major components, namely (i) the adsorber bed, (ii) the desorber bed, (iii) the evaporator-condenser device. Both methods of heat recovery, as outlined in the above, are simulated herewith in this chapter.

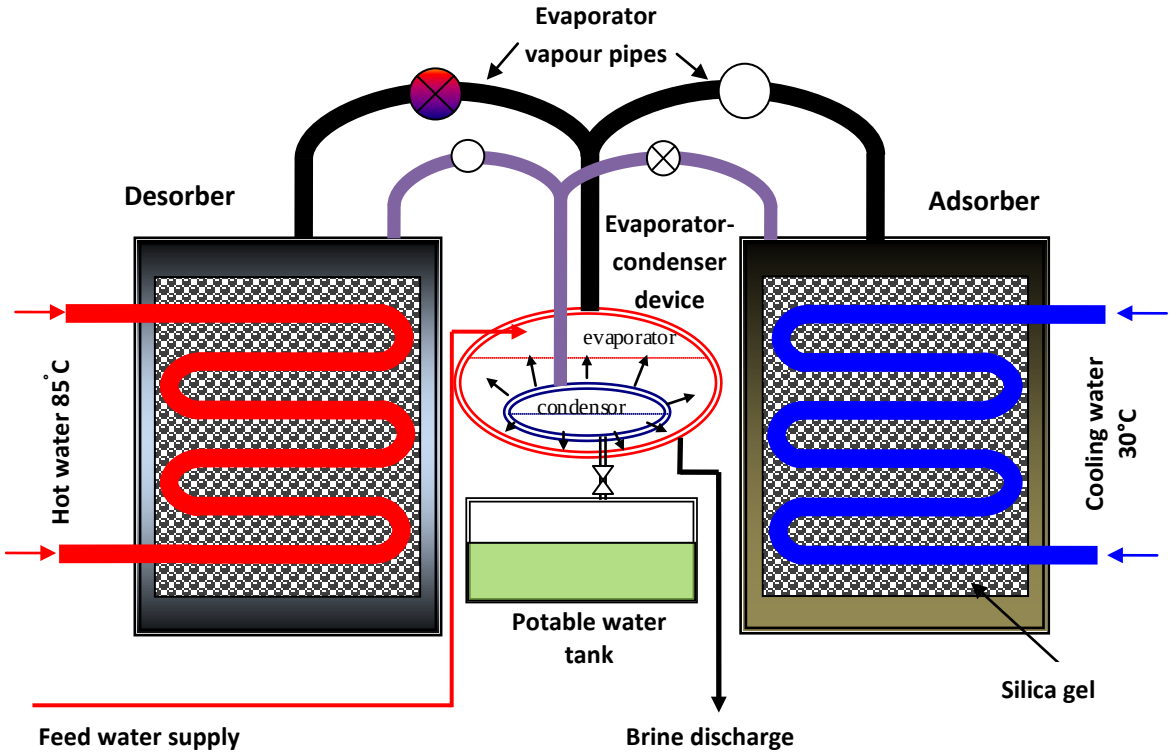

Figure 6.1 The advanced Adsorption Desalination (AD) cycle with integrated evaporator-condenser device.

It is noted that by integrating the condenser-evaporator, both the condenser and the evaporator water circuits of the conventional cycle are eliminated and hence, a significant saving in the pumping cost. The heat is transferred directly across the walls of the condenser tubes which are placed within the evaporator shell. This arrangement reduces the heat transfer resistances, leading to an improvement in the evaporation rates of water vapor from the seawater solution. Another consequence of integrating

the condenser and evaporator units is the higher vapor pressure in the evaporator, and this has a direct effect of increasing the vapor uptake by the silica gel during the adsorption process. Thus, the advantages of the advanced AD cycle (with integrated condenser-evaporator) are summarized as follows:

i) a reduction in the parasitic electrical power owing to the elimination of pumps for the chilled and cooling water circuits,

ii) an improvement in the adsorption capacity of silica gel due to the pressurization effect,

iii) a lowering of the effective condensation temperature in condenser and this tends to desorb more vapor during the desorption process, and

iv) the ability to operate low temperature of heat source at 50°C or higher.

For performance verification, a mathematical model has been developed based on the mass, energy balances and the thermodynamic properties (isotherms and kinetics) of the adsorbent/adsorbate system. The following sections describe the development of the numerical model to predict the performance of the advanced AD cycle.

6.1.1. Mathematical Modeling

A mathematical model for an advanced AD cycle that employs an integrated evaporator-condenser design for the internal heat recovery process was developed. Thermodynamic properties of the adsorbent/adsorbate system developed in the previous chapter, that is, the mass and energy balance equations are used to evaluate

the model. In the advanced cycle, the type RD-Mycom silica gel was employed as the adsorbent and Table 6.1 shows the physical properties of the silica gel used.

Table 6.1 Physical properties of type-RD silica gel

Property	**Value**
Pore size(nm)	0.8-7.5
Porous volume($cm^3.g^{-1}$)	0.37
Surface area($m^2.g^{-1}$)	720
Average pore diameter (nm)	2.2
Apparent density ($kg.m^{-3}$)	700
pH	4.0
Specific heat capacity ($kJ.kg^{-1}.k^{-1}$)	0.921
Thermal conductivity ($W.m^{-1}.k^{-1}$)	0.198

The amount of water vapor an adsorbent (silica gel) can adsorb at a temperature (T) and pressure (P) is depicted by the isotherm equation and one such isotherms available is the Dubinin–Astakhov or D-A equation. It estimates the uptake of the water vapor by the adsorbent in terms of *T* and *P* and is given as,

$$q = q_0 \exp\left[-\left(\frac{RT}{E} \ln\left(\frac{P}{P_0} \right) \right)^n \right] \qquad 6.1$$

where q_0 is the maximum adsorbed amount, E is the characteristic energy and n is the experimentally determined non-integer index, R is the universal gas constant, and

the P_0 is the equilibrium pressure. The transient adsorption rate of the adsorbent (silica gel) can be adequately is predicted using linear driving force adsorption kinetics Equation:

$$\frac{dq}{dt} = \frac{15 D_{s0} \exp\left(\frac{-E_a}{RT}\right)}{R_p^{\,2}} \left(q^* - q\right) \qquad 6.2$$

where D_{so} is the kinetic constant for the silica gel water system, E_a is the activation energy, R_p is the particle radius and q denotes the instantaneous uptake. The values of all the coefficients and the parameters are given Table 6.2.

Table 6.2 Values of the parameters used in the simulation program

Parameter	**Value**	**Unit**
q_0	0.592	kg/kg of silica gel
E	3.105	kJ/mole
n	1.1	-
D_{so}	2.54×10^{-4}	m^2/s
E_a (kJ/kg)	4.2×10^{-4}	kJ/kg
R_p	0.4	mm
Hot water inlet temperature	65-85	°C
Cooling water inlet temperature	30	°C
Mass of silica gel per bed, M_{sg}	36	kg
Adsorber/desorber bed heat transfer area	41.7	m^2
Tube length	0.576	m

$M_{HX}c_{p,HX}$	284.6	kJ/K
U_{ads}	250	W/m^{2}K
U_{des}	240	W/m^{2}K
Integrated evaporator-condenser		
Number of tubes (stainless steel)	60	-
$A_{\text{evaporator}}$	7.34	m^2
$A_{\text{condenser}}$	4.28	m^2
c_p	500	J/kgK
k	16.2	W/mK
Operation conditions		
t_{cycle}	300	s
$t_{swtiching}$	20	s

In a typical adsorbent bed design, the adsorbent (silica gel) is packed around the round fin-tubes heat exchanger. For an optimal fins size and fin gap, the temperature of the adsorbent, adsorbate and the heat exchanging materials are approximated to be a lumped value for each of the components. Thus, the numerical model employs a lumped parameter approach. The mass balance of the cycle is given by,

$$\frac{dM_{s,evap}}{dt} = \dot{m}_{sw,in} - \frac{dM_{d,cond}}{dt} \qquad 6.3$$

where $M_{s,evap}$ is the amount of sea water in the evaporator, $\dot{m}_{sw,in}$ is the rate of feed sea water and $M_{d,cond}$ is the mass of potable water extracted from the condenser.

Writing the energy balance for the adsorber or desorber beds during their communication with the evaporator and condenser, it can be written as:

$$\left(M_{sg}c_{p,sg} + M_{HX}c_{p,HX} + M_{abe}c_{p,a}\right)\frac{dT_{ads/des}}{dt} = \pm Q_{st}\left(T_{ads/des}, P_{evap/cond}\right) \times M_{sg}\frac{dq_{ads/des}}{dt} \pm \dot{m}_{cw/hw}\, c_{p,cw/hw}\left(T_{ads/des}\right)\left(T_{cw/hw,in} - T_{cw/hw,out}\right) \quad 6.4$$

In addition, the heat losses from the surface of the adsorber and desorber chambers to the surrounding are assumed to be negligible. The first three terms of the left hand side of the above Equation represent the thermal masses of the silica gel, heat exchanger material and adsorbed phase and Q_{st} is isosteric heat of adsorption. A more accurate description of Q_{st} is modelled as follow,

$$Q_{st} = h_{fg} + E\left\{-\ln\left(\frac{q}{q_m}\right)\right\}^{1/n} + Tv_g\left(\frac{\partial P}{\partial T}\right)_g \quad 6.5$$

where v_g is the specific volume of the gaseous phase, h_{fg} is the latent heat. The specific heat capacity of the adsorbed phase is calculated using

$$C_{p,a} = C_{p,g} + \left\{\frac{1}{T} - \frac{1}{v_g}\left(\frac{\partial v_g}{\partial T}\right)_P\right\}Q_{st} - \left.\frac{\partial Q_{st}}{\partial T}\right|_P \quad 6.6$$

where $C_{p,g}$ and v_g are the specific heat capacity and specific volume of the gaseous phase of the adsorbate. The energy balances for the evaporator and condenser sides of the integrated evaporator are:

$$\left[\left(mc_p\right)_{ss}+\left(mc_p\right)_{HX}+\left(mc_p\right)_{we}\right]\frac{dT_{evap}}{dt}=-\frac{dq}{dt}M_{sg}Q_{st}\left(T_{ads},P_{evap}\right)+U\,A(T_{cond}-T_{evap}) \quad 6.7$$

$$\left[\left(mc_p\right)_{ss}+\left(mc_p\right)_{HX}+\left(mc_p\right)_{wc}\right]\frac{dT_{cond}}{dt}=\frac{dq}{dt}M_{sg}Q_{st}\left(T_{des},P_{cond}\right)-U\,A\,(T_{cond}-T_{evap}) \quad 6.8$$

The integrated evaporator-condenser is fabricated using stainless steel materials to mitigate any corrosion by sea water

For the tube walls of the evaporator-condenser, a similar energy balance gives;

$$\left(mc_p\right)_{ss}\frac{dT_{w2}}{dt}=h_{cond}\,A_{cond}\left(T_{cond}-T_{w2}\right)-\frac{2\pi kL}{\ln\frac{r_1}{r_2}}\left(T_{w2}-T_{w1}\right) \quad 6.9$$

$$\left(mc_p\right)_{ss}\frac{dT_{w1}}{dt}=h_{evap}\,A_{evap}\left(T_{w1}-T_{evap}\right)+\frac{2\pi kL}{\ln\frac{r_1}{r_2}}\left(T_{w2}-T_{w1}\right) \quad 6.10$$

where h_{cond} and h_{cvap} are the heat transfer coefficients of the condensation and the evaporation of the evaporator-condenser device. T_{w1} is the temperature of the evaporator tube wall and T_{w2} is the temperature of the condenser tube wall, k is the thermal conductivity of the tube material and L is the length of the tubes.

The overall heat transfer coefficient of the evaporator-condenser unit is predicted as:

$$U = \frac{1}{\frac{1}{h_{cond}} + \frac{r_2 \ln \frac{r_1}{r_2}}{k} + \frac{r_2}{r_1}\frac{1}{h_{evap}}} \qquad 6.11$$

where the heat transfer coefficient of the boiling of the saline solution is predicted using the modified Rohsenow correlation for sub-atmospheric pressures [107]:

$$T_w - T = \left(\frac{C_{sf} h_{fg} \Pr_l^s}{C_{pf}}\right)\left[\frac{q''_{load}}{\mu_l h_{fg}}\sqrt{\frac{\sigma}{g(\rho_l - \rho_g)}}\right]^n \times \left(\frac{P}{P_{atm}}\right)^m \left(\frac{A_{wetted}}{A_{base}}\right)^\alpha \qquad 6.12$$

Nusselt film correlation is applied to calculate the heat transfer coefficient for condensation of the water vapor inside the condenser and it is given as:

$$h = F\left[\frac{\rho_l g k^3 (\rho_l - \rho_v)[h_{fg} + \frac{3}{8}C_{pl}(T - T_w)]}{D\mu(T - T_w)}\right]^{0.25} \qquad 6.13$$

For the desorption process, the energy to desorb water vapor from the silica gels, (Q_{des}), can be calculated by using the coolant temperatures of the heat source supplied to the reactors, and this is given by

$$Q_{des} = \dot{m}_{hw}\, c_{p,hw}\left(T_{hw,in} - T_{hw,out}\right) \qquad 6.14$$

where $\dot{m}_{hw}$ indicates the mass flow rate and $c_{p,hw}$ defines the specific heat capacity of heating fluid. Concomitantly, the energy rejected to the cooling water during the adsorption process is estimated by the inlet and outlet temperatures of cooling fluid supplied to the other reactor and this is written as

$$Q_{ads} = \dot{m}_{cw}\, c_{p,cw} \left(T_{cw,out} - T_{cw,in}\right) \qquad 6.15$$

where $\dot{m}_{cw}$ and $c_{p,cw}$ indicate the mass flow rate and the specific heat capacity of cooling fluid. At the same time, the heat of evaporation $\left(Q_{evap}\right)$, and the condensation energy $\left(Q_{cond}\right)$ rejected at the condenser are given by

$$Q_{evap} = h_{evap}\, A_{evap} \left(T_{w1} - T_{evap}\right) \qquad 6.16$$

$$Q_{cond} = h_{cond}\, A_{cond} \left(T_{cond} - T_{w2}\right) \qquad 6.17$$

where h_{evap} and h_{cond} are the heat transfer coefficients of the evaporation and boiling processes, A_{evap} is the total heat transfer area of the evaporator side and A_{cond} is the condenser side surface area in the evaporator-condenser device. The performance of the AD cycle is given by specific daily water production (SDWP) and performance ratio (PR), defined here as the ratio of useful effects to the energy input to get the useful effects, i.e., as follows:

$$SDWP = \int_0^{t_{cycle}} \frac{Q_{cond}\,\tau}{h_{fg}(T_{cond})M_{sg}}\,dt \qquad 6.18$$

$$PR = \int_0^{t_{cycle}} \frac{\dot{m}_{water} h_{fg}(T_{cond})\tau}{Q_{des}}\,dt \qquad 6.19$$

These set of energy and mass balance equations are solved by the **Adams-Moulton's** method in the DIVPAG subroutine of the IMSL Fortran math library subroutines. A double precision accuracy was applied and the tolerance is set to $1x10^{-12}$. The code runs on the platform of FORTRAN power station that is installed in a PC. As the AD cycle is operated in a batch manner, the connection or pointers for linking one sub-routine to another has to be carefully directed so that the correct boundary conditions are maintained during the computation. The cyclic steady state condition can be achieved in 4 to 5 cycles after the commencement of computation.

6.1.2. Results and Discussion

This section describes the predictions from numerical analysis of the advanced AD cycle based on the model discussed in the previous section. The analyses of the cycle under various operation modes such as different cycle times, hot and cooling water temperatures, different hot and cooling water flow rates, etc will be discussed.

Figure 6.2 shows the temperature-time history of the adsorber, desorber, evaporator and condenser of the advanced AD cycle at the cyclic-steady-state conditions. The horizontal axis represents the time in seconds and the vertical axis gives the temperature distributions. Owing to the integral evaporator-condenser design, it can be seen that the vapor pressurize has been increased during the

adsorption process. This increase is caused by the increase in the evaporator chamber temperatures which varies from 35°C to 40°C. The higher adsorption pressure enhances the adsorption capacity of the adsorbent.

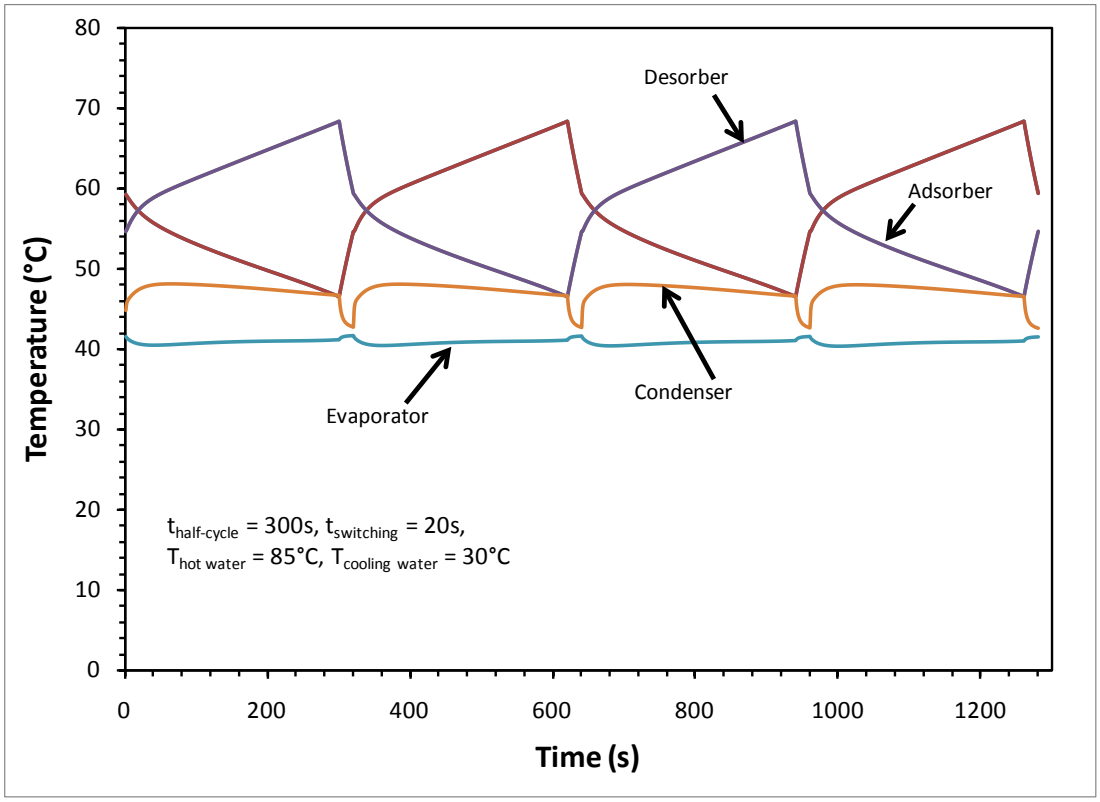

Figure 6.2 Predicted Temperature-Time histories of the adsorber, desorber, evaporator and condenser of the advanced AD cycle.

The predicted water production rate of the advanced AD cycle in terms of the litres per minute is given in Figure 6.3 where the equivalent specific daily water production (SDWP) of the cycle is about 26m^3 per tonne of silica gel per day. It is almost three times higher than the yield from a conventional AD cycle, as seen in Chapter 5. The high SDWP in the advanced AD cycle is attributed to two factors, namely, (i) an improvement in the adsorption capacity of the silica gel, up to 40% of the dry mass, owing to the pressurization effect during the adsorption process and (ii) a lowering of the effective condensation temperature in the condenser due to lesser

resistance in heat transfer and this tends to desorb more vapor out of the desorber during the desorption process.

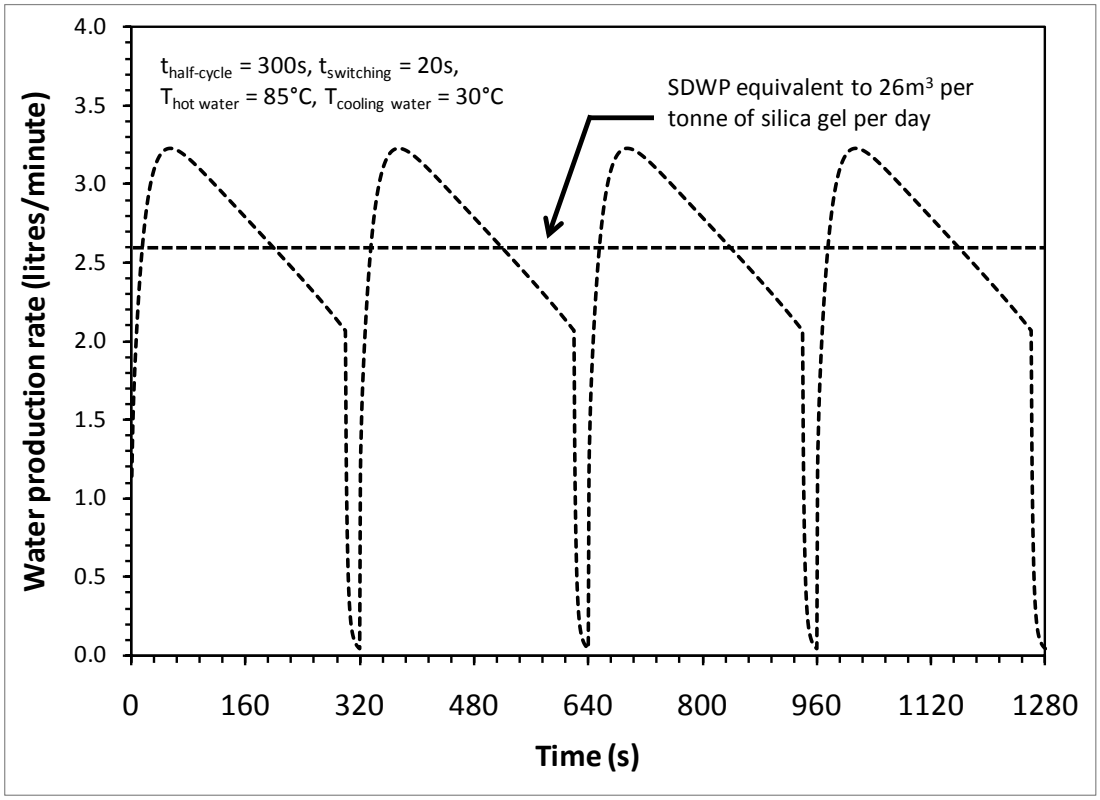

Figure 6.3 SDWP of the advanced AD cycle compared with conventional AD cycle at normalized cycle time

The performance of the evaporator-condenser device is also analysed using the overall heat transfer coefficient. The heat transfer coefficient of the evaporator-condenser unit is evaluated using Modified Rohsenow correlation for sub-atmospheric conditions [107] for evaporation and Nusselt film correlation for condensation. The thermal resistance imposed by the stainless steel tubes is also accounted for. Figure 6.4 gives the equivalent heat transfer network of the integrated condenser-evaporator unit while the overall heat transfer coefficient (U) of the evaporator-condenser device is shown in Figure 6.5.

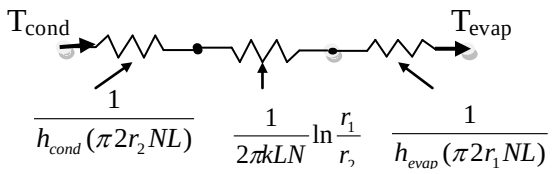

Figure 6.4 The equivalent heat transfer network of the integrated condenser-evaporator unit

The predicted data showed that the *U* value is higher at the beginning of every cycle and gradually lower with the cycle time. This is because the uptake and desorption amount by the silica gel is higher at the beginning of the cycle operation resulting rapid boiling and condensation. Thus, the *U* value is higher at that period. The uptake amount becomes lesser as the silica gel becomes situated as well as the desorption rate becomes slower as the cycle operation continues. However, during switching period, the *U* value drops to the value less than 500W/m^{2}K since. This is because there is no adsorption and desorption phenomena in this period and the resulted small value of *U* is due to the exchange of heat between the thermal mass of the evaporator and the condenser. The average overall heat transfer coefficient ($U_{overall}$) is found to be about 2300W/m^{2}K which is quite a good value across the vapour condensing in the condenser to the vapour leaving the saline solution falling over the surface of tubes of evaporator, as shown below in Figure 6.5.

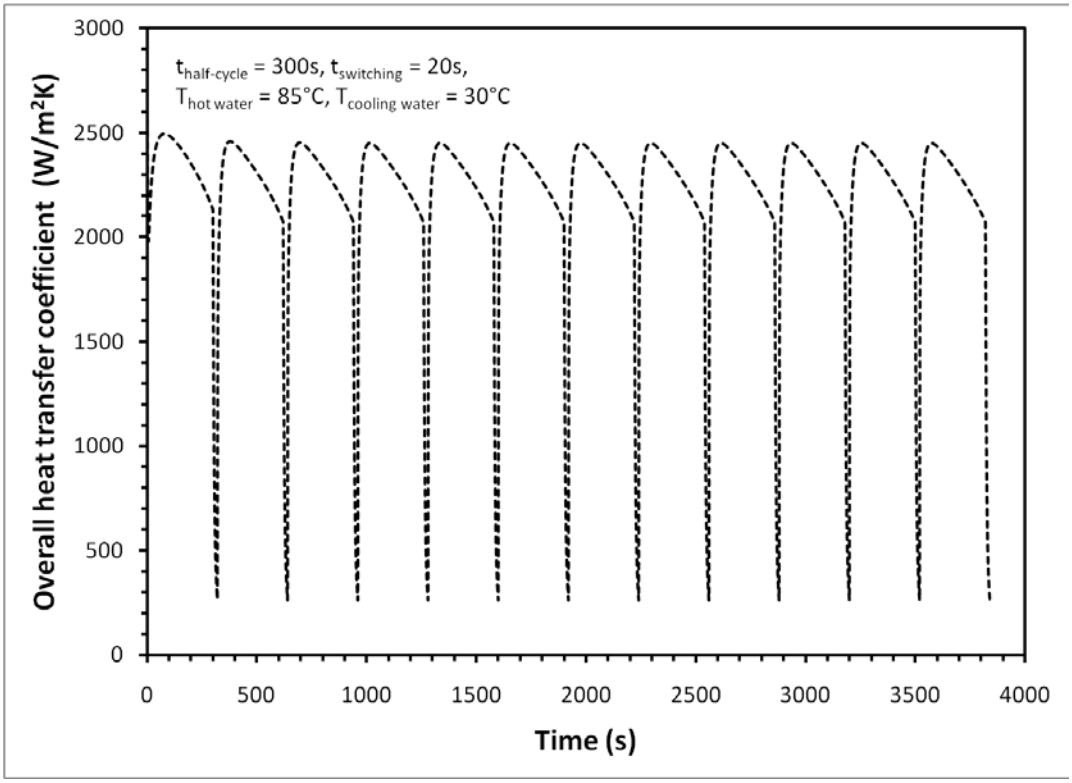

Figure 6.5 Overall heat transfer coefficient of the evaporator-condenser device

A parametric analysis on the advanced AD cycle has been conducted to study the performance of the cycle at various operating conditions such as different cycle times, different hot and cooling water inlet temperatures to the adsorber beds. The effect of the operation cycle time on the specific daily water production (SDWP) of the cycle at a fixed hot water temperature (85°C) is presented in Figure 6.6. It is noted that the optimal half-cycle time for the advanced AD cycle is 300s, and this is shorter by 50% when compared to the conventional AD cycle at the same heat source temperature. The shorter cycle time can lead to higher water production yield, as seen below.

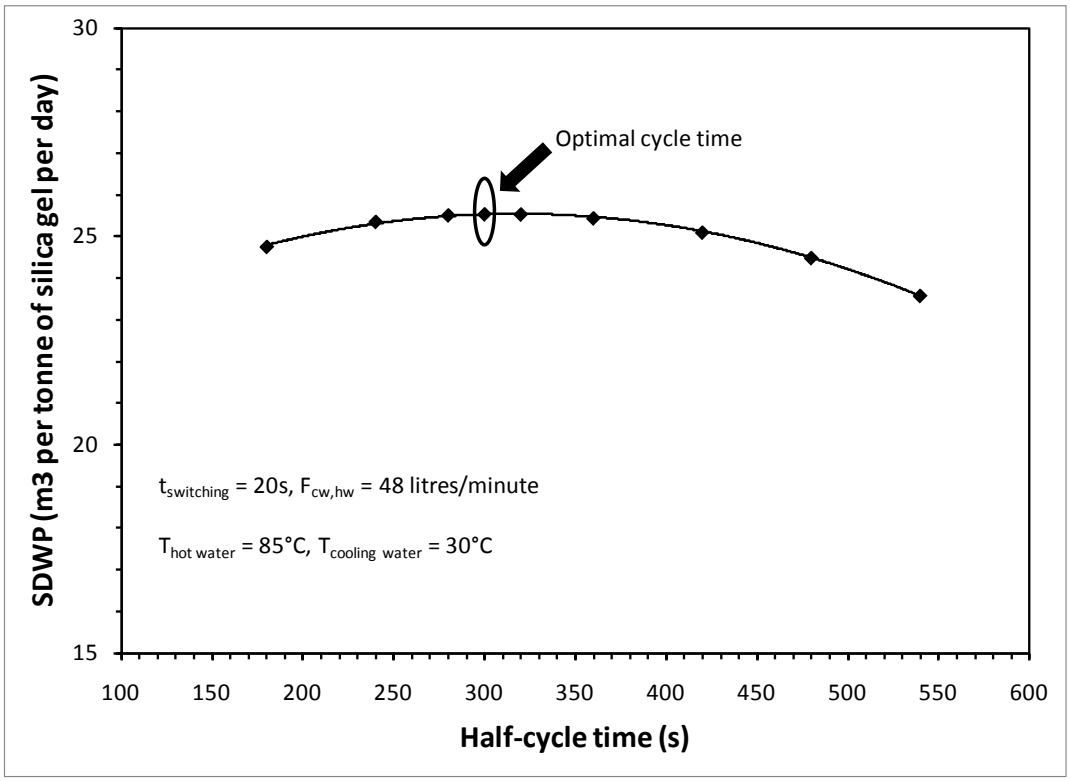

Figure 6.6 The optimal cycle time for SDWP of the advanced AD cycle

Figure 6.7 represents the specific daily water production (SDWP) and overall heat transfer coefficient (*U*) of the advanced AD cycle for assorted regeneration temperatures of 50°C to 85°C. The results show that the water production rate of the advanced cycle linearly varies with the hot water temperature. This is due to the better regeneration process for higher hot water temperatures. The results also show that the overall heat transfer coefficient increases with the increase in the hot water temperature.

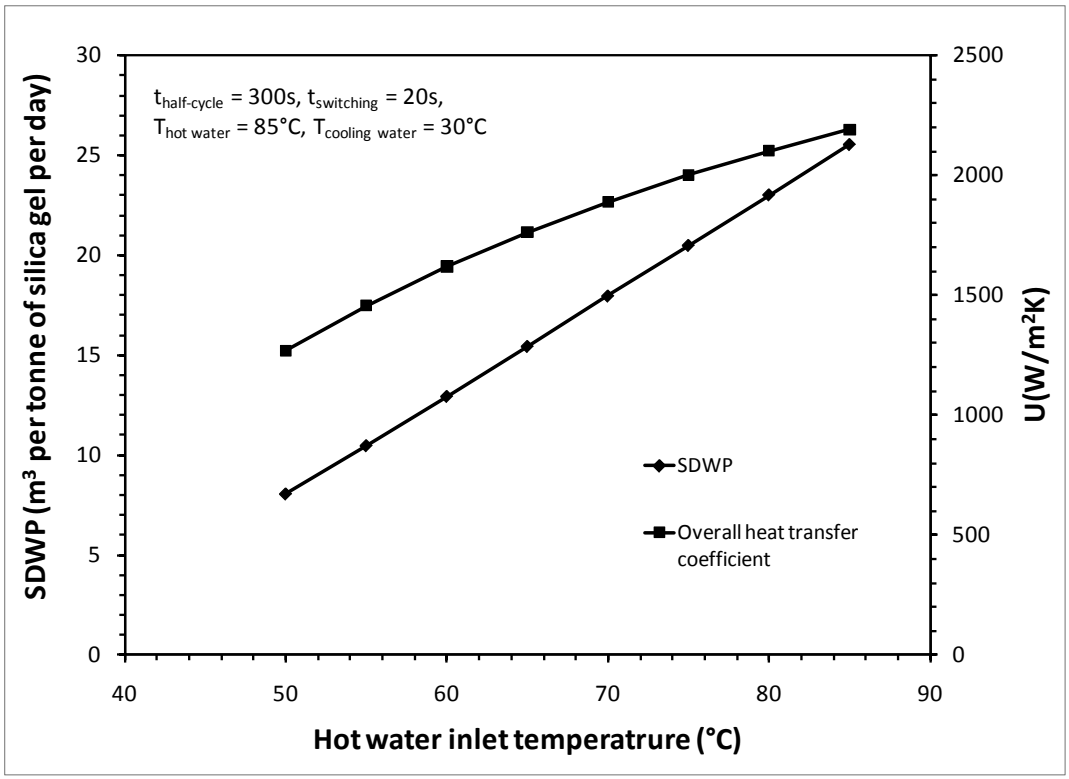

Figure 6.7 The predicted SDWPs and overall heat transfer coefficients of the advanced AD cycle at assorted hot water inlet temperatures

Another significant advantage of the advanced cycle is that it can be operated as low as 50°C hot water temperature that a conventional cycle is unable to do so. This temperature of activation is easily available from the solar thermal sources and the specific daily water production (SDWP) is found to be about 8.1 m^3per day. This production rate is comparable with that of the conventional cycle even at this low heat source temperature.

The effect of the cooling water temperature to the adsorber on the performance of the advanced AD cycle is also investigated. The temperature range is between 25°C to 35°C and this is a practical temperature range for the cooling water. The effect of the cooling water temperature on the cycle is investigated at two sets of hot water inlet temperatures i.e., 85°C and 80°C. The performance results are

presented in Figure 6.8 in which the results show that the cycle performs more efficiently at lower cooling water temperature giving higher SDWP. As the cooling water temperature increases, the SDWP of the cycle becomes lower. This phenomenon can be attributed to the isotherm behaviour of the silica gel: - the higher saturation temperature (hence pressure in condenser) retards the desorption of water vapor when the desorber beds undergoes heating.

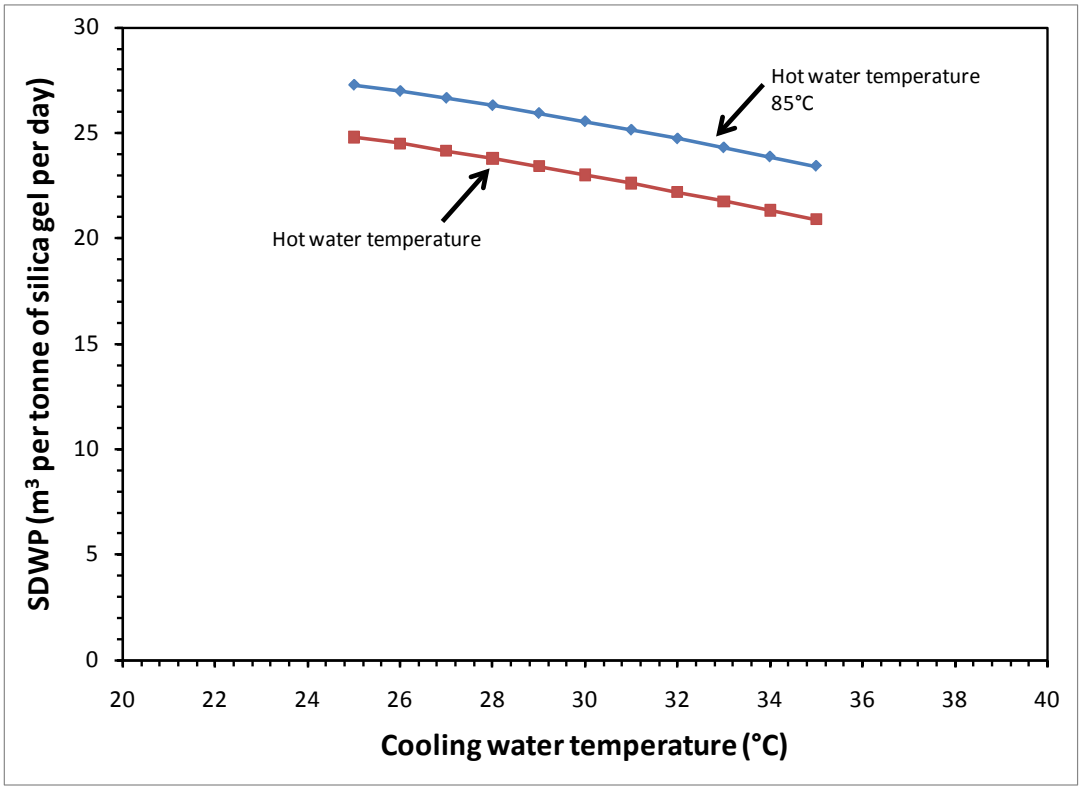

Figure 6.8 The predicted potable water production of the advanced AD cycle for different cooling water inlet temperatures

In summary, it is found that the advanced AD cycle has several distinctive advantages: Firstly, its SDWP rate is three times as high as that of the conventional AD cycle. Secondly, the advanced cycle is found operational even at a hot water

temperature as low as 50°C and yet produces 8.1 m^3 per tonne of silica gel per day. All these improvements can be achieved with only one heat source input.

6.2. The AD cycle with a coolant circuit between the evaporator and condenser

From the heat transfer point of view, the AD cycle retro-fitted with a coolant flowing circuit between the condenser and evaporator is inferior as compared to the cycle described in earlier section, i.e., having an integrated evaporator-condenser unit. Nevertheless, the coolant flowing through the condenser to evaporator has the similar heat recovery but it incurs higher heat transfer resistances due to flow resistances, etc. The key merits of having the retrofitted coolant circuit are i) the simplicity in retro-fitting the additional coolant circuit outside the vacuum environment and ii) the ease to switch the AD cycle from a single mode to a dual-mode operation (cooling cum desalting) by simply closing the coolant flow. A numerical simulation is presented in this section and the predictions can be compared with the experimental tests.

6.2.1. Description of the evaporator/condenser heat recovery circuit

In this arrangement, there is no change to the heat exchanger units of the conventional AD cycle except that the coolant flowing in the condenser to cooling tower is now diverted to the evaporator. Condensation heat is now recovered and dumped into the evaporator by a simple run-around coolant between them. The schematic diagram of the retro-fitted AD cycle with the said internal heat recovery is shown in Figure 6.9. The coolant lines denoted by red color indicates the warmer fluids after receiving the condensation heat whilst the blue lines indicate the cooler

coolant after heat is rejected into the evaporative process. The evaporative and condensation processes in the evaporator and condenser would maintain their saturation temperatures at an equilibrium level in accordance to the rate of heat transfers in these exchangers during the batch operation of adsorbers and desorbers.

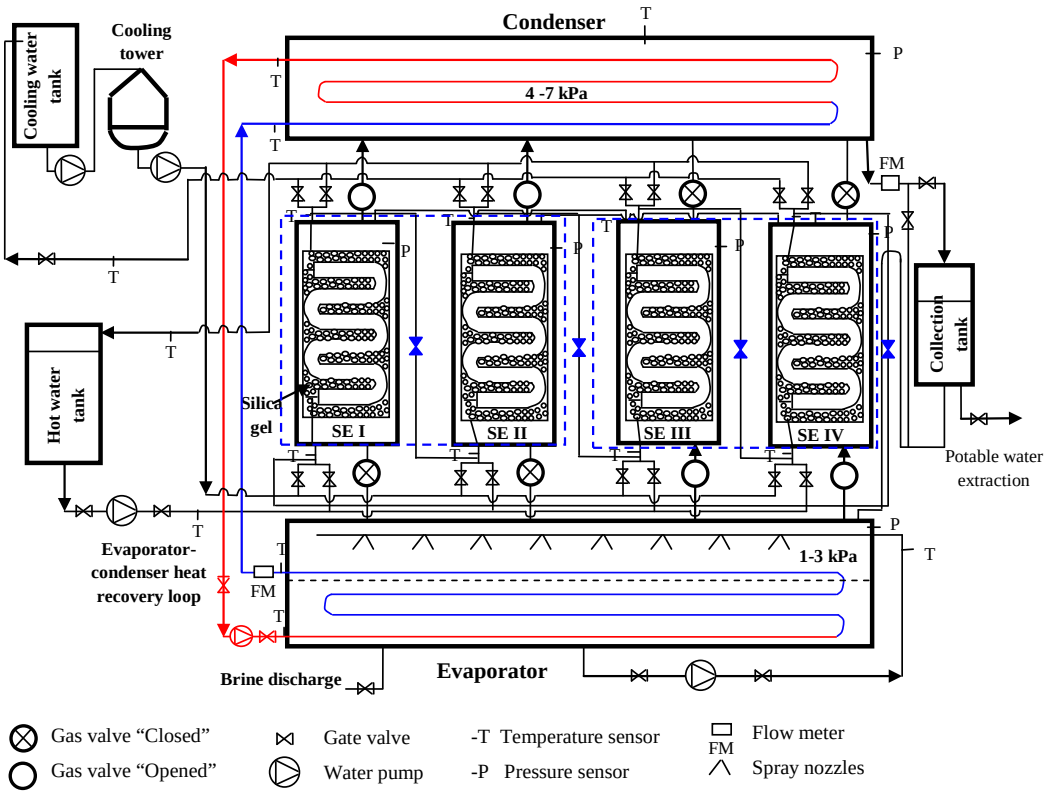

Figure 6.9 The schematic diagram of the advanced AD cycle with the internal heat recovery with an evaporator-condenser water circulating circuit.

6.2.2. Mathematical Modeling

The same mathematical model developed in the previous Chapters can be applied to this advanced AD cycle except that an additional coolant is flowing in between the condenser and evaporator and they will not be repeated here. The

boundary conditions of evaporator and condenser are now intrinsically linked during the computation.

6.2.3. Simulation result and Discussion

The transient temperature profiles of the major components such as the adsorber, the desorber, the evaporator and the condenser of the proposed AD cycle are shown in Figure 6.10. In this analysis, the hot water temperature at inlet is maintained at 85°C while the cooling water inlet temperature is kept at 30°C. The pressurization effect on the adsorption process can be seen from the higher equilibrium evaporator temperature of 30°C, and this is achieved solely by the recovered condensation energy. Thus, the amount of vapor uptake by the silica gel is expected to increase and hence, the water production capacity should improve also.

Figure 6.11 gives the transient water production rate by the advanced AD cycle with the evaporator-condenser heat recovery circuit. The equivalent specific daily water production (SDWP) of the cycle is about 13.5 m^3 of potable water per tonne of silica gel per day. This production rate is inferior as compared to that of the integrated condenser-evaporator design but it is about two times that of a conventional AD cycle. This is because of the additional energy losses incurred from the multiple heat transfer processes through a medium (water) involved in the evaporator-condenser circuit design.

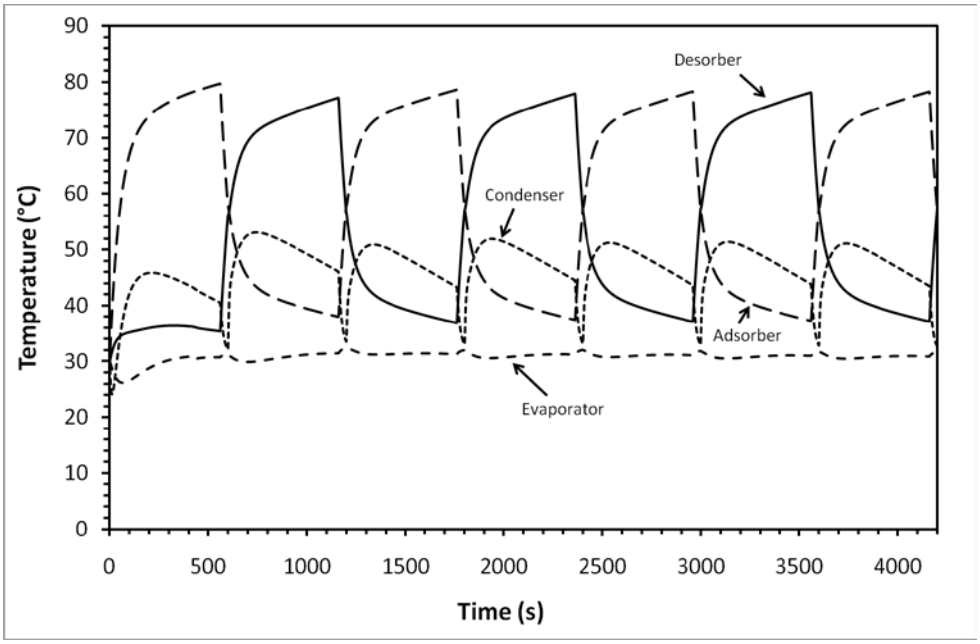

Figure 6.10 Temporal temperatures of the advanced AD chiller with the evaporator-condenser heat recovery circuit.

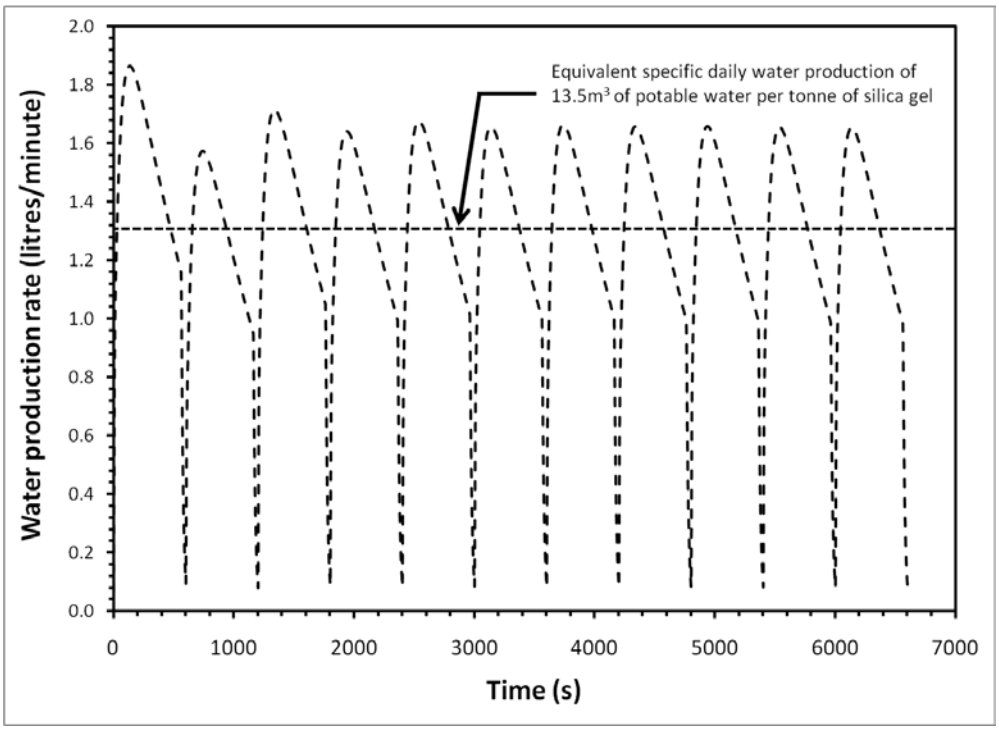

Figure 6.11 Transient water production rate of the advanced AD cycle with evaporator-condenser heat recovery circuit.

6.2.4. Experiments

For verification of any improvement in the heat recovery cycles, the existing prototype AD plant is retrofitted with a coolant circuit in between the condenser and the evaporator. Figure 6.12 gives the pictorial view of the retro-fitted cycle showing the installation of the heat recovery coolant loop between the condenser and the evaporator. Extensive experiments have been conducted using different hot water inlet temperatures ranging from 50°C to 70°C and different hot and cooling water flow rates (50LPM to 125LPM) to investigate the performance of the cycle.

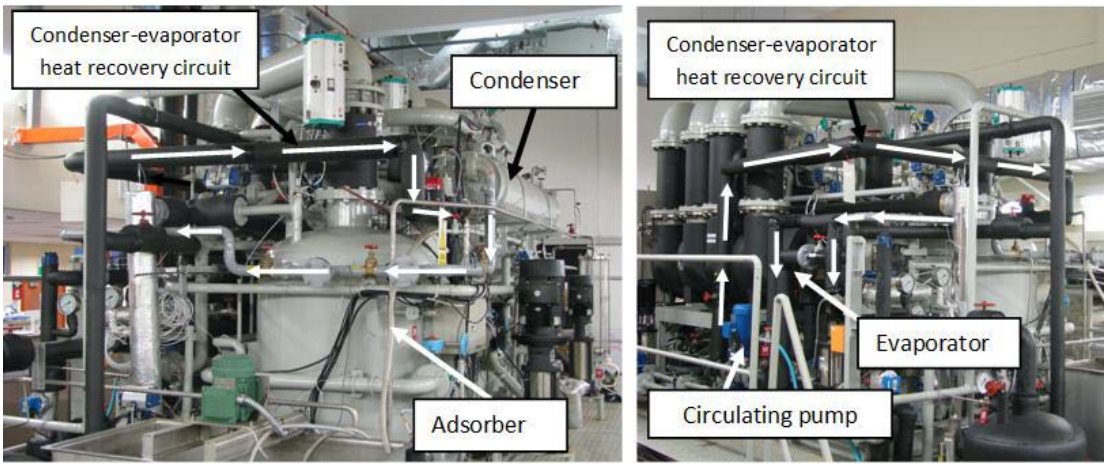

Figure 6.12 The pictorial view of the advanced AD cycle showing the heat recovery between the condenser and the evaporator

The experimentally-measured transient temperature profile of the major components of the advanced AD cycle that incorporates the heat recovery scheme between the condenser and the evaporator of the cycle is shown in Figure 6.13. In this experiment, the hot water inlet temperature was maintained at 55°C and the half-cycle time was 600s with the switching time 40s. The inlet and outlet water temperature profiles of the heating and cooling fluids are shown in the Figure 6.14. It is noted that the fluctuations of the hot and cooling waters occurs during the switching period and

this is because the pre-heating of the adsorber and the pre-cooling of the desorber reactors are performed during the switching period.

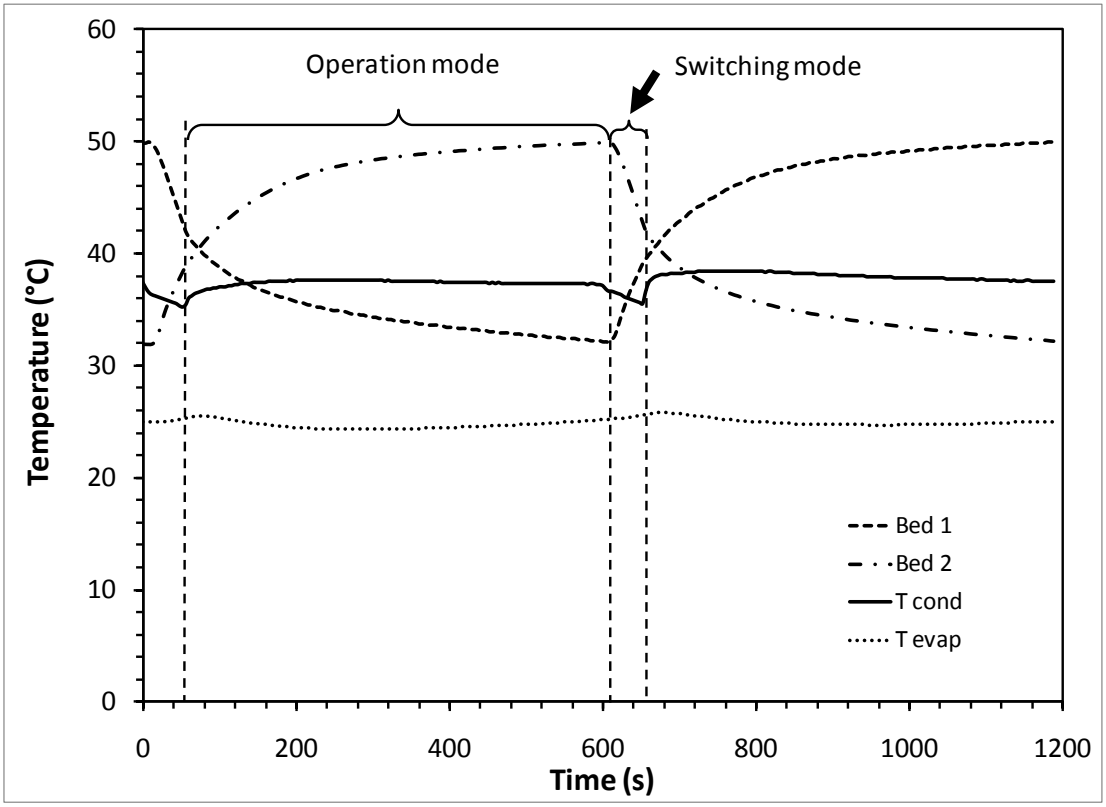

Figure 6.13 The experimentally-measured temperature profiles of the major components of the advanced AD cycle

In the advanced AD cycle with the evaporator-condenser heat recovery circuit, the outlet water from the evaporator is channeled to the condenser and vice versa. The evaporator outlet water is properly insulated to prevent heat leak as much as possible and it can be seen in Figure 6.14 that the temperature differences between the evaporator outlet and the condenser inlet, and that between the condenser outlet and the evaporator inlet are negligibly small. This small temperature changes along the circuit is resulted from the good thermal insulation of the pipes involved in the heat recovery circuit between the condenser and the evaporator.

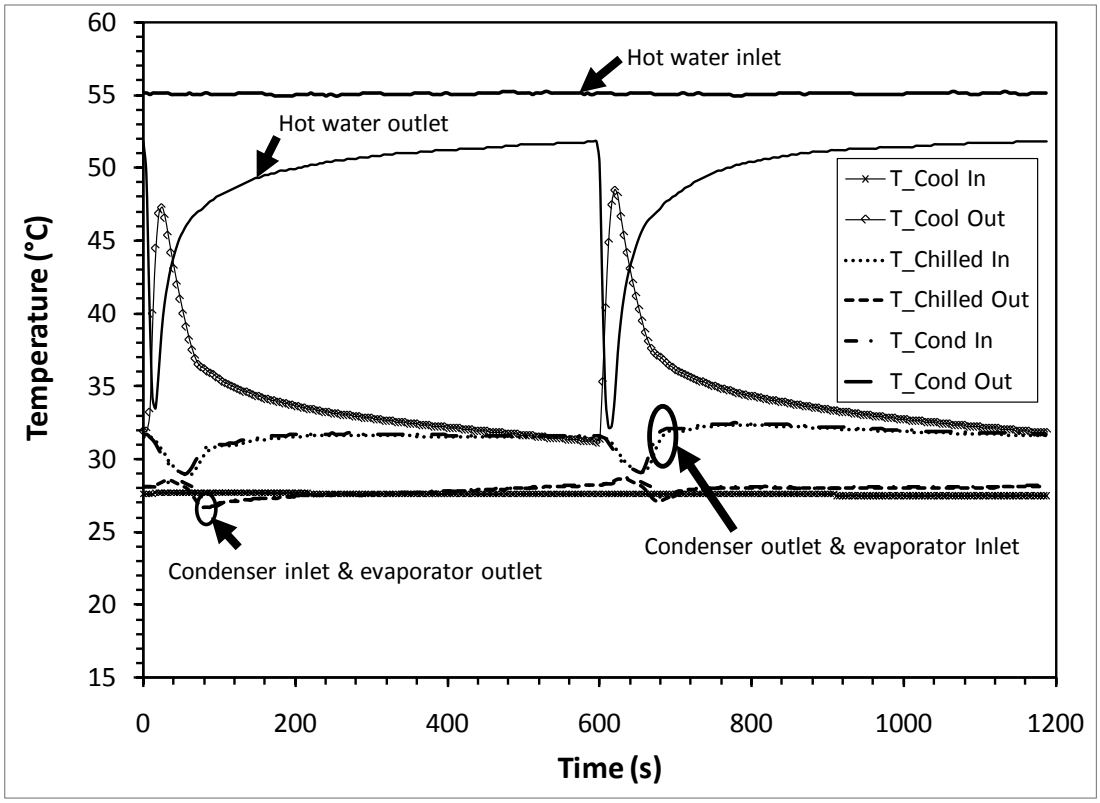

Figure 6.14 The temperature profiles of the inlet and outlet of the heat transfer fluids measured experimentally.

6.2.5. Validation of the simulation and experimental results

Experimental data from the prototype advanced AD plant are used for validation of the mathematical model. The comparison is performed on a 2-bed AD cycle operating over a half-cycle period. Figure 6.15 shows the comparison between the simulated and the experimentally-measured temperatures of the major components of the adsorption cooling cum desalination cycle.

In this analysis, the hot water inlet temperature to the desorber was maintained at 70°C while the half-cycle and the switching times are kept 600s with 40s, respectively. It is noted that the experimental temperature measurements are subjects to the time constant of the sensors. The results showed that the present

formulation of the advanced AD cycle gives reasonable results as validated by the experimental data.

The temperature profiles of the simulation and the experiments are found to be in agreement within the experimental error except that of the condenser. The condenser temperature measured in the experiments seems to be higher than from numerical simulation during the switching periods. This could be due to the location of the condenser temperature sensor. As the sensor is placed near the desorber vapour pipes, it may be influenced by the high temperature of the condenser shell as well as the vapor pipes and fail to capture the temperature drop by the cold front from the evaporator at the beginning of the cycle operation.

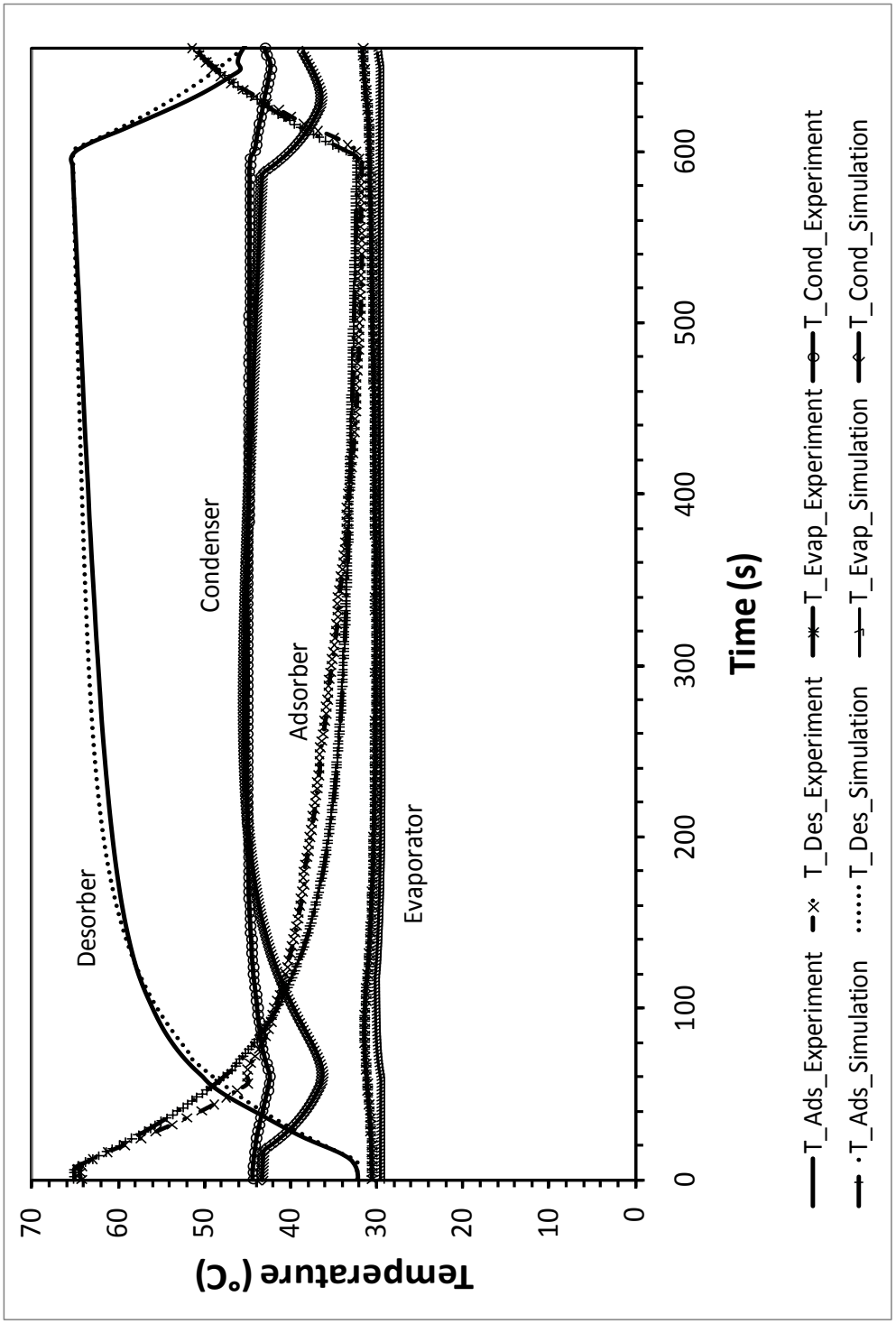

Figure 6.15 Temperature profiles of the major components of a 2-bed advanced AD cycle comparing the experimentally-measured and simulated values

A parametric study of the advanced AD cycle has been conducted to investigate the performance of the cycle under various hot water inlet temperatures selectively between 50°C and 80°C which reflects the typical temperatures that one could derived from a solar energy collectors or the waste heat sources. Figure 6.16 gives the specific daily water production (SDWP) and the performance ratio (PR) of the advanced AD cycle while operating at different hot water inlet temperatures. Both the simulation and experimental results are presented and the results show that the SDWP linearly varies with the hot water inlet temperature whilst the SDWP is 9.24 at 70°C hot water inlet temperature.

The improvement of the SDWP with the increase in the hot water temperature is attributed to the better desorption-condensation process at higher desorbing temperatures resulting in the better evaporation-adsorption process and thus giving higher SDWP. It is remarkable that the retro-fitted advanced AD cycle is able to operate at a 50^{o} C hot water inlet temperature, - a temperature range usually beyond the capability of a conventional AD cycle. At this low inlet hot water temperature, the produced SDWP is about 5.2 m^3 of potable water per tonne of silica gel per day. On the other hand, at the rated 85°C hot water inlet temperature, the SDWP of the advanced AD cycle is found to be 13.5 m^3 which is almost 90% higher than that of the conventional AD cycle.

The performance ratio - defined here as the ratio of the useful effects to the heat input, of the advanced cycle is found to remain relatively constant at 0.73 to 0.75 for all hot water inlet temperatures. This is a characteristic of the internal heat recovery.

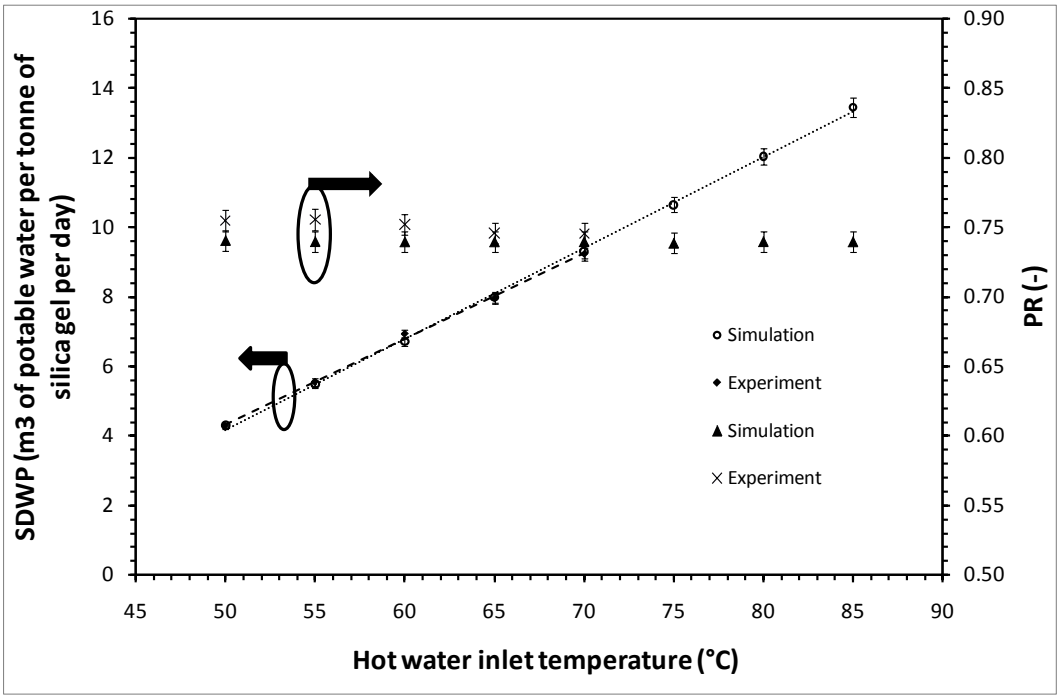

Figure 6.16 The SDWP and PR of the advanced AD cycle with assorted hot water inlet temperatures ranging from 50°C to 70°C.

Figure 6.17 gives the SDWP of the advanced AD cycle for assorted cooling water flow rates at specific hot water flow rate and fixed temperature of 70°C. The results showed that the water production rate significantly increased if the cooling water flow rate is changed from 50litres/minute to 100litres/minute. This is due to the improvement in the heat transfer coefficient at higher flow rates. It is also noted that the increase in the SDWP becomes less significant at flow rates higher than 100litres/minute due to finite amount of adsorption and desorption capacities of the adsorbent.

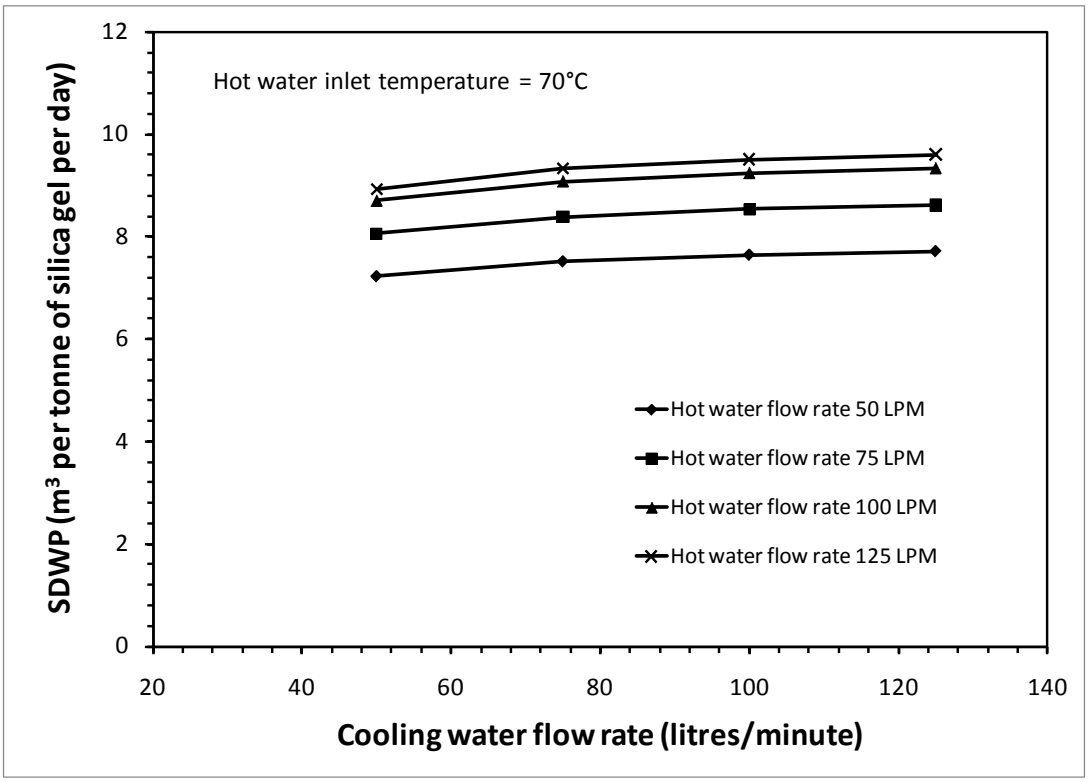

Figure 6.17 Specific daily water production of the advanced AD cycle for assorted cooling water flow rates.

The effect of the hot water flow rate on the performance of the advanced AD cycle is presented in Figure 6.18. These results show that the flow rate could increase the SDWP by as much as 20% as the flow rates increases but this effect reduces when the flow rate is higher than 100 l/min.

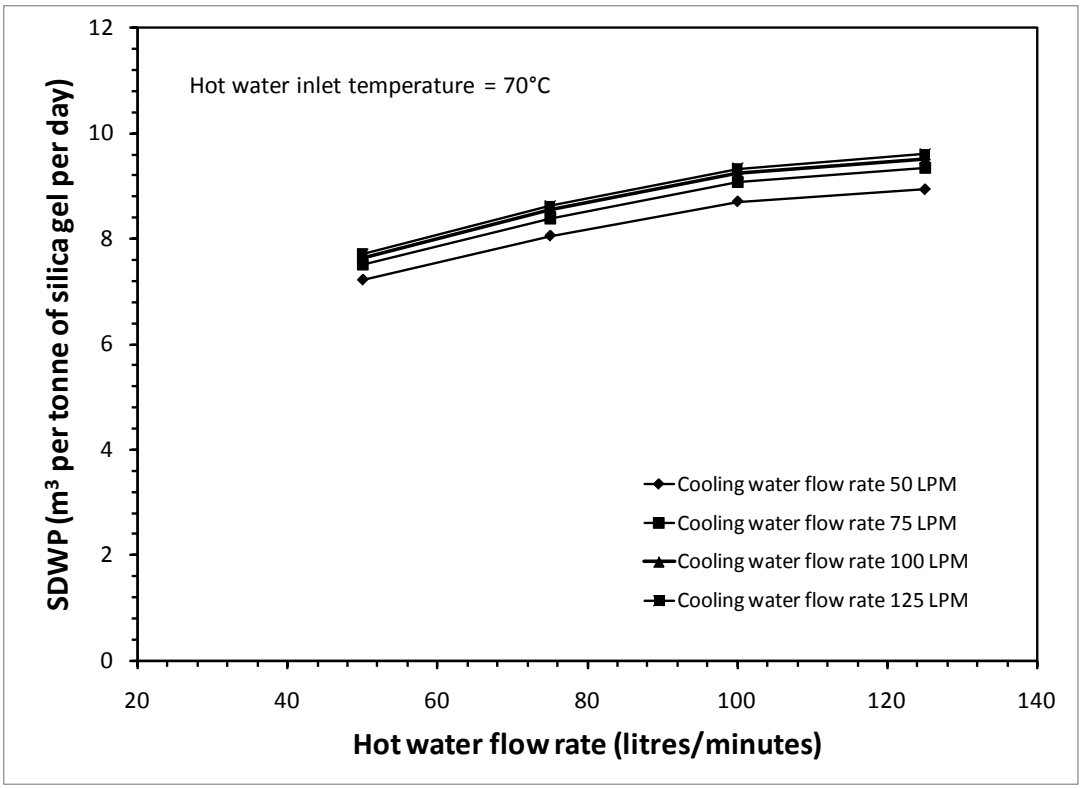

Figure 6.18 Specific daily water production of the advanced AD cycle for assorted hot water flow rates.

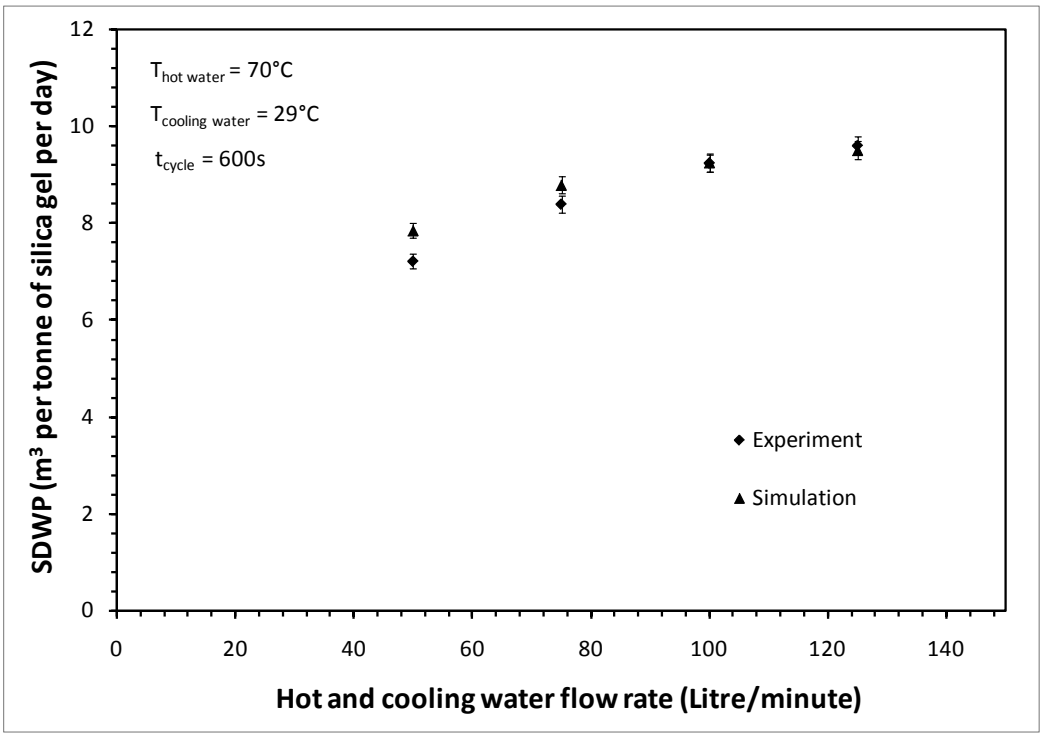

Figure 6.19 Performance of the advanced AD cycle using different flow rates of heating and cooling fluids at constant source temperatures.

The performance of the advanced AD cycle under different flow rates of the heating and cooling fluids is presented in Figure 6.19. It is found that the SDWP of the cycle increases with the increase in the flow rate while the temperature of heat source and cooling temperatures are held at 70°C and 29°C, respectively.

The effect of the cooling water inlet temperature on the performance of the advanced AD cycle is shown in Figure 6.20. The SDWP of the cycle for two sets of hot water inlet temperatures i.e., 70°C and 50°C is presented while varying the temperature of the coolant from 26°C to 32°C. Higher water production rate is achieved at lower coolant temperatures while the production rate decreases as increased in the coolant temperature.

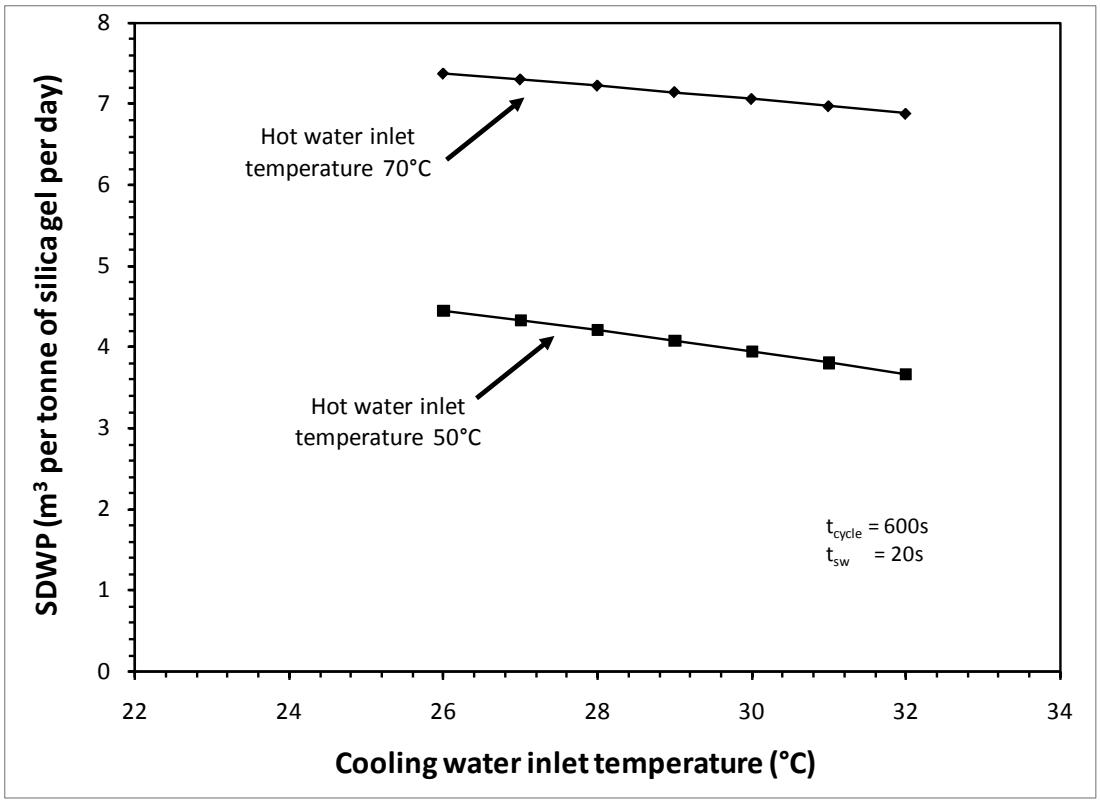

Figure 6.20 Specific daily water production of the advanced AD cycle at different cooling water inlet temperatures.

As discussed in Chapter 4, the cycle time at which the AD cycle gives the optimal potable water production varies with the available hot water inlet temperatures. The optimal cycles time for the advanced AD cycle have been experimentally evaluated for two different temperature levels of hot water and are shown in Figure 6.21. The results show that the optimal cycle times exist at the half-cycle time 570s and 600s for 70°C and 65°C, respectively whilst the corresponding SDWPs are 9.39 and 8.3. The optimal cycle time for the advanced AD cycle is shorter than that of the conventional AD cycle that has been reported.

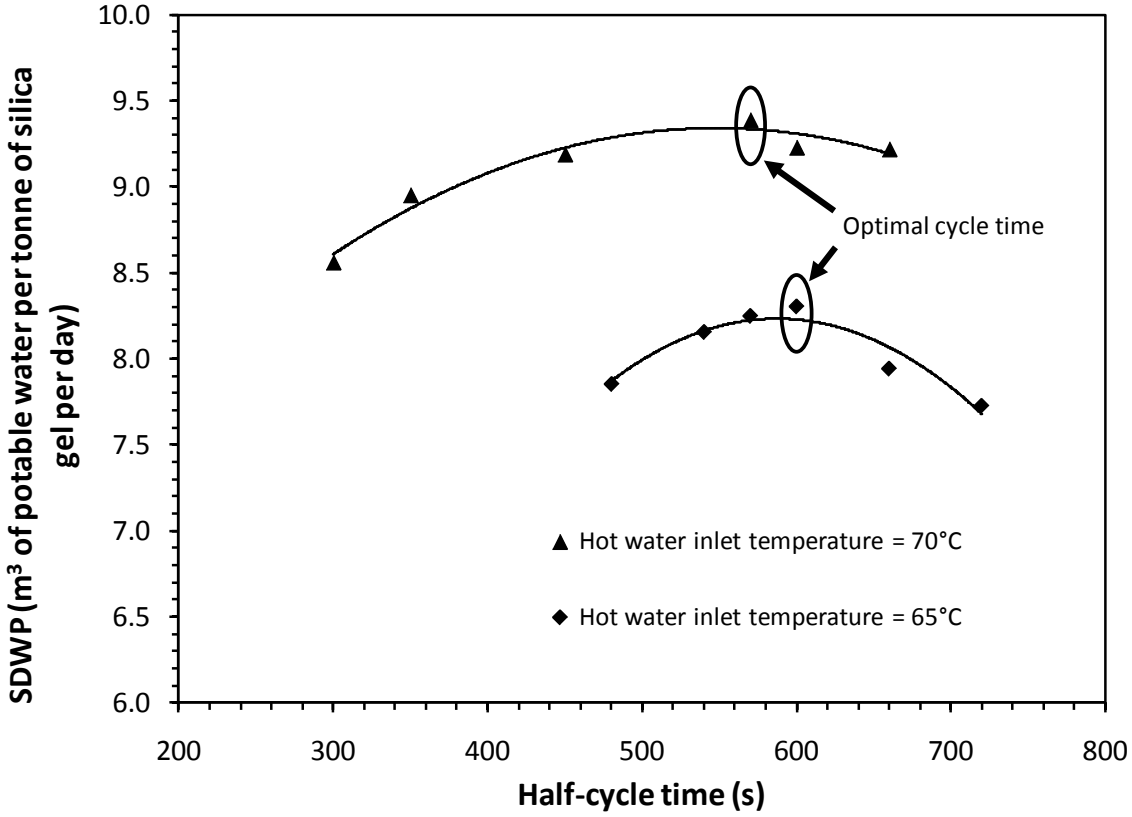

Figure 6.21 The performance of the advanced AD cycle showing the optimal cycle times at hot water inlet temperatures 70°C and 65°C.

This is because the evaporation-adsorption and desorption-condensation processes in the advanced AD cycle become much faster due to the pressurization of

the adsorption and the lower in the condensation temperature resulted from the heat recovery process between the condenser and the evaporator. The pressurization of the adsorption process is achieved since the relatively higher temperature water from the condenser is utilized for the evaporation. On the other hand, the temperature of the outlet water from the evaporator that is channeled to the condenser is around 25°C to 27°C and this cold front lower condensing temperature imparts the better desorption process. These effects are more significant at the beginning of the operation mode after switching process since the adsorption and desorption rates at maximum at that period.

Finally, the comparison on the water production rates of the AD cycles is given in Figure 6.22 where the horizontal axis shows the normalized half-cycle time and the vertical axis gives the water production rate.

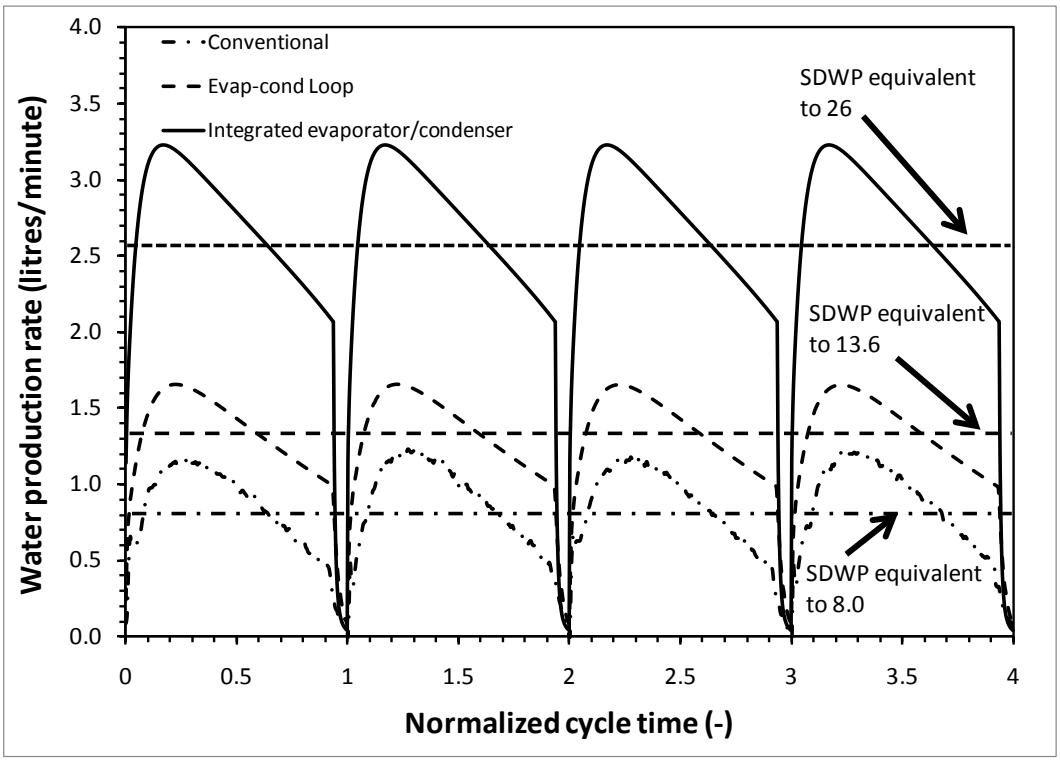

Figure 6.22 Comparison on the water production rates of different AD cycles

6.3. Summary of Chapter 6

The innovative advanced adsorption desalination (AD) cycle has been successfully developed and modeled. It achieves a quantum improvement in the specific daily water production rates and potentially, it could increase by three times of the conventional cycle. This is achieved by the use of internal heat recovery of the processes in the cycle, namely i) the design of an integrated evaporator-condenser design that fully recovers the evaporation and condensation energy that reduces heat transfer resistances substantially, and ii) the improvements in both adsorption and desorption off-take or uptake due to favorable pressures of evaporator and condenser, respectively. In addition, the advanced AD cycle saves much of the parasitic pumping power of the condenser and evaporator circuits without compromising the salient features of the conventional AD cycle. An important outcome from the tests conducted on the retro-fitted AD cycle is that it has proven its ability to operate safely at a temperature heat source at only 50°C – a level not matched, hitherto, by any other heat activated equipment. With these advantages, the specific unit cost for desalination of the advanced AD cycle is deemed to be the lowest and this topic will be discussed together with the chapter on the life-cycle analysis of the AD plant.

Chapter 7 Life-Cycle Analysis of Adsorption Desalination

Introduction

Unit water production cost is a major factor for the feasibility of installing a desalination system and it has significant influence on the system selection. It is by far the most equitable method for comparing the merits of an adsorption desalination (AD) plant versus the commercially available methods, such as the multi-stage-flash (MSF), the multi-effect-distillation (MED) and the reverse osmosis (RO). A life-cycle analysis is adopted as a platform for the evaluation of unit production cost of potable water from desalination. In this chapter, the published data from two RO plants of the same production capacity have been selected for comparison. The following section gives an overview of the factors affecting the desalination costs.

7.1. Factors affecting the cost of desalination

The factors employed for selection of a desalination technology are generic to most desalination plants but some of these factors are more dependent on factors of site. A list of the general factors contributing to the unit cost calculation of desalination plants are listed in Table 7.1. The less apparent or indirect factors such as the plant load factor, availability of skilled labors, storage and distribution of fresh water and plant capacity and location, could affect also the unit cost although to a lesser extent. For these indirect factors, a simple cost estimation methodology has been applied and the following section describes the quantum of these parameters in details.

Table 7.1 Factors to be considered in the estimation of desalting cost

No.	Cost factor	Description
1.	Performance ratio	The ratio of the fresh water output to the energy input to the desalination cycle or alternatively, it is the ratio of the condensing energy to the heat input.
2.	Plant life	This affects the capital costs of the plant through amortization period.
3.	Plant costs	The most important factor for the decision of the desalination technology and this cost may vary with the size and the capacity of the plant.
4.	Interest rates	It has influence on the capital cost and the total investment for the plant.
5.	Inflation rates	It has considerable effect on the unit production cost.
6.	Site costs	This relates to the land cost which varies with the location and the foot-print area of the plant.
7.	Seawater intake and brine discharge	This cost plays important role for the desalination process since the desalination plant should have easy access to the sea for the seawater intake as well as to discharge the brine. The short distance to the sea may reduce this cost.
8.	Feed water quality	The feed water quality is the direct function of the desalination cost for most of the desalination processes, especially membrane type desalination processes. The quality of the feed water decides the type of pretreatment and thus it also influences the pretreatment cost.
9.	Output water	The quality of the desalted water may be a deciding factor

	quality	for the membrane desalination process where the membrane life and the membrane replacement costs vary with the output water quality. However, thermally activated desalination process gives high quality water with TDS less than 15ppm (parts per million) and the output water quality may not be controllable parameters for such systems.
10.	Energy sources	All desalination process needs energy to separate the salts from the sea water. Types of energy source as well as the quality of the energy source contribute to the selection of the desalination technology. Renewable energy nowadays becomes a possible energy source for some desalination technologies where the adsorption desalination (AD) process is one of such systems that utilizes low temperature hot water from waste heat or solar energy.
11.	Pretreatment cost	Pretreatment is a necessary step in desalination processes in order to prevent or reduce the performance degradation of the separation unit such as the evaporators of the heat driven systems and the membranes of the pressure activated desalination systems.
12.	Chemical Costs	It has significant contribution to the desalination cost through operation cost and may vary with the type of the feed water

7.2. Cost estimation

This section gives the general description of the cost model in evaluating a desalination plant. The total cost of a desalination plant comprises the capital, the operational and the replacement costs of key components such as heat exchangers, membrane, etc. Depending on the plant type and the water production capacity, the plant life would affect the annualized capital cost via the amortization period (n) and the interest rate (i) through a capital recovery factor (CRF), i.e., the product between the initial investment and the CRF. The operational cost comprises the contributions from fuel and electricity rates, maintenance and replacement, pumping requirements, chemical treatment of feed and output water. In reality, all operational costs can be subjected to the inflation effect or rates (j), arising from the cost of primary fuel, electricity price fluctuations, etc. Such increases over a period of time into the future could be incorporated by using an inflation weighted factor, defined here as: $IWF = \frac{CRF(i,n)}{CRF(i',n)}$.

Based on the above-mentioned key variables, a life-cycle approach is given by the sum of the annualized capital and operational costs, i.e.,

$$C\left(\$/m^3\right) = \left(\sum_{k=1}^{m} C_{Capital}\left(CRF\ (i,n)\right)_k\right) + \left(\sum_{l=1}^{p} C_{operational}\left(\frac{CFR\ (i,n)}{CRF\ (i',n)}\right)_l\right) \qquad 7.1$$

where C is the unit cost of desalination on a volumetric basis, m is the number of items of capital investment, p is the number of items related to operational cost. These include factors such as direct capital cost, electricity cost, maintenance cost,

manpower cost, chemical cost, cost related to interest, pretreatment cost, membrane initial cost and membrane replacement cost, where the latter could be significant if the fouling level is high. The detailed description of the major costs involved in a typical desalination systems are given as follows.

a) Capital cost $\left(C_{capital}\right)$

Based on the total volume of water production over the life-cycle, the calculation of the capital cost per unit production of a desalination plant over the plant life is given as;

$$C_{capital} = \frac{D_{capital}\,\alpha}{V_L} \qquad 7.2$$

where V_L is the total volume of potable water produced by the plant per annum, $D_{capital}$ is the direct capital cost and α is the amortization factor. In general, direct capital cost relates to the cost for the equipment used in desalting. In an adsorption desalination (AD) plant, the direct capital cost includes the cost of adsorbent, heat exchangers for the adsorber, the desorber, the evaporator and the condenser, and the cost for the construction of the pretreatment and storage systems such as de-aeration and water storage tanks. Moreover, the cost of the pumps, water and vapor valves are also included in the capital cost estimation. The amortization factor or the capital recovery factor is calculated as;

$$\alpha = \frac{i(i+1)^n}{(i+1)^n - 1} \qquad 7.3$$

where, n is the plant life and i is interest rate.

b) Electricity cost $\left(C_{electrical}\right)$

In desalination processes, the parasitic pumping costs are the major contribution and they can be estimated as follows;

$$W_{pumps}\left(kW\right)=\sum_{j}\frac{\Delta P_{j}\left(kPa\right)\times V_{pump,j}\left(m^{3}/s\right)}{\eta_{j}} \qquad 7.4$$

where V_{pump} is the volumetric flow rate and η is the pump efficiency. The hourly electricity cost of pumps is given as;

$$E_{pump}\left(\$/h\right)=W_{pumps}\left(kW\right)\times Electricity\ rate\left(\$/kWh\right) \qquad 7.5$$

On a unit volumetric contribution basis, the electricity cost is calculated using the following Equation;

$$C_{electrical}=\frac{E_{pumps}\times yearly\ operating\ hour}{V_{L}} \qquad 7.6$$

c) Maintenance Cost $\left(C_{maintenance}\right)$

The maintenance cost of desalination process is usually given by the percentage of the direct capital cost of the plant. It is given as

$$M\left(\$/yr\right)=D_{capital}\times\beta\times\alpha \qquad 7.7$$

where β is the percentage of direct capital cost for plant maintenance and M is the maintenance cost per year. Therefore, the unit maintenance cost is calculated as;

$$C_{maintenance} = \frac{M}{V_L} \qquad 7.8$$

As one of the key advantages of an AD plant is the lack of moving parts, it has low maintenance cost as compared to other desalination methods. Also, the evaporation of saline water takes place at low temperature (less than 35^{o}C) and hence, fouling is significantly mitigated in the evaporating unit. The level of maintenance relating to the corrosion and scaling problems is significantly reduced. Hence, it is practical to assume that the maintenance cost of the AD plant is at 0.01% of direct capital cost of the AD plant.

d) Chemical Cost $(C_{chemical})$

The sea water feed to the evaporator needs to be treated with chemicals to prevent scaling and fouling to the separation units of the desalination processes. The unit chemical cost, $C_{chemical}$, of RO plants reported, hitherto, generally have their values between 0.025 \$/m^3 and 0.035 \$/m^3 [108, 109]. However, almost no chemical is required to treat the sea water in the AD process due to its low temperature and robust evaporative process. Thus, chemical cost, $C_{chemical}$, contribution is assumed to be negligible in the AD plant.

e) Pretreatment cost $(C_{pretreatment})$

The pretreatment cost is costs related to the equipments and materials for pre-treating the sea water feed. The pretreatment cost is substantial to the membrane desalination process and heat activated process such as multi-stage flash (MSF) distillation where the evaporation temperature is high. One of the advantages of the AD cycle is that the pretreatment cost is low as only the de-aeration process involves in the pretreatment of seawater feed of an AD plant.

f) Manpower cost $\left(C_{mempower}\right)$

This is the cost contribution arising from the payment of remunerations of personnel working in a desalination plant. The amount manpower cost depends on the capacity, the simplicity and the reliability of the desalination method. Owing to the simplicity of an AD plant, the manpower cost is usually low because the operation of the AD cycle is fully automated.

g) Membrane and membrane replacement cost $\left(C_{membrane}\right)$, $\left(C_{membrane\ replacement}\right)$

These are costs involved in the membrane desalination processes and are calculated as follows;

$$C_{membrane} = \frac{P_{membrane}}{V_L} \times \frac{i(i+1)^y}{(i+1)^y - 1} \times \frac{n}{y} \qquad 7.9$$

$$C_{membrane\ replacement} = \frac{S}{V_L \times y} \qquad 7.10$$

where $P_{membrane}$ is the cost of membrane purchase, y is membrane life and S is cost for the replacement of the membrane that includes the installation of membrane.

7.2.1. Unit production cost of the AD cycle

This section discusses the computation of unit production cost of the AD cycle. Using the basic cost data of the existing prototype AD plant, the methodology is extended to AD plants of larger production capacity.

The energy cost of AD plant includes the contributions of thermal energy and the electrical energy. The commercially available thermally-activated desalination processes such as the multi-stage effect (MSF) and the multi-effect distillation (MED) consume both the thermal and electrical energy to perform the desalting process. The thermal energy consumption of these systems is high because the evaporation condition of sea water occurs at higher temperatures, typically up to 180°C. On the other hand, desalination processes such as vapor compression (VC), Reverse Osmosis (RO) processes consume much electrical energy to generate high pressure saline feed to the membranes via the high pressure pumps, typically up to 6 to 8 MPa. From literature, the energy input to different types of desalination methods are collated as in Table 7.2.

On the other hand, the AD cycle utilizes only low temperature heat sources, typically less than 85^{o}C, to produce potable water through the sorption processes. Being at low temperature, the heat source is deemed to be free because if it is unused, it would have been purged into the ambient. Such low temperature heat sources are available in abundance from either the industrial waste heat or the solar thermal energy source. To operate the AD cycle, however, a small amount of electrical energy is needed to operate the water pumps (hot water, cooling water, chilled water and condenser water) so as to provide the necessary circulation of fluids in and out of the

batch-operated cycle. The pumping occurs only at low pressures because they are used mainly to overcome the frictional and minor losses in the flow circuits. The electrical energy consumption of the advanced AD cycle is computed to be about 1.38kWh/m^3 whilst the conventional AD cycle consumes about 4.92kWh/m^3. This low value of the advanced cycle is about twice that of the thermodynamic limit of 0.78 kWh/m^3 which forms the theoretical limit for a desalination process. The detailed calculations of the pumping power required for the AD system is given the Appendix H.

Table 7.2 A comparison of the energy cost of different desalination methods

Method of Desalination	**Thermal energy consumed kWh/m^3 (A)**	**Electric energy kWh/m^3 consumed**	**Energy cost of water US$ per m^3= $\left[5*(A*3.6)/(1055\times\eta_b)+B*0.133\right]$**
Multi-stage Flash (MSF)	19.4	5.2	1.11
Multi-effect Distillation (MED)	16.4	3.8	0.86
Vapor compression (VC)	-	11.1	1.48
Reverse Osmosis (RO) – single	-	8.2	1.09
Reverse Osmosis (RO) – double	-	9.0	1.20
Advanced AD (High grade water)	Free energy from waste heat	**1.38**	**0.18**

(All data is extracted from Seawater Desalination in California, California coastal commission Chapter 1-: Energy Use section, http://www.coastal.ca.gov/index.html. The conversion units of 1 AF = 1345 m^3, 1 million BTU (1.055 GJ) of Natural gas costs US$5 (adopted from Singapore's natural gas prices quoted in 2005) and the electricity rate US$0.13/kWh. The efficiency of boiler, η_b, is 80 % [120].)

Using a life-cycle cost approach, the unit cost of the AD cycle was evaluated based on the performance data of the pilot AD plant. A summary of the parameters used in the calculation of the unit production cost is tabulate din Table 7.3. Owing to

the low maintenance of the AD plant, the maintenance cost factor (β) of the AD plant is assumed to be 4.63% of direct capital cost. The feed seawater is pre-treated only with micro air bubbles in the prototype plant to remove the suspended solids by flocculation and almost no chemicals are used, and thus, reduces the pre-treatment cost significantly to only 0.35% of the direct capital cost. The manpower cost consists of the salary of operators in the plant and it is dependent on the locality of the plant and based on survey, it is taken to be at 8.11% of the direct capital cost. As the thermal energy input to the AD plant is deemed free, there is no cost for the consumption of waste heat. However, there is a cost assigned to the equipment used for the thermal energy extraction such as heat exchangers and these costs have been included. For fair comparison with the RO plants, the electricity cost ($/kWh) is selected to be the same rate. The detailed calculation of the cost estimation of the AD cycle is presented in appendix I.

Table 7.3 Key parameters used in the unit cost estimation the AD cycle

Plant Life (years)	30
Interest rate (%)	5
Electricity rate (US$/kWh)	0.133
$(SDWP)_{advanced\ cycle}$	25
$(SDWP)_{conventional\ cycle}$	8

Figure 7.1 shows the unit potable water production cost of the different capacities of conventional and advanced AD plant. It is noted that the asymptotic unit production cost of the advanced AD process is about $\$0.457/m^3$ while that of the conventional cycle is about 4 times higher at $\$1.91/m^3$. The lower unit cost of the advanced AD cycle is attributed to the improvements in the cycle:

i) **Design improvement-** a better heat transfer coefficient of the condenser/evaporator device as well as the savings in the construction cost for the construction cost In addition, there is a elimination of the chilled water and condenser water circuits and the associated pumps.

ii) **Reduction in Pumping Power-** With the redundant water pumps (chilled water and condenser water pumps) in the advance design, there is savings in the pumping cost.

iii) **Improvement in the Water production rate -T**he specific daily water production (SDWP) of the Advanced AD cycle increased by three times owing to better overall heat transfer coefficient of the condenser-evaporator integrated design and this reduces the unit cost significantly.

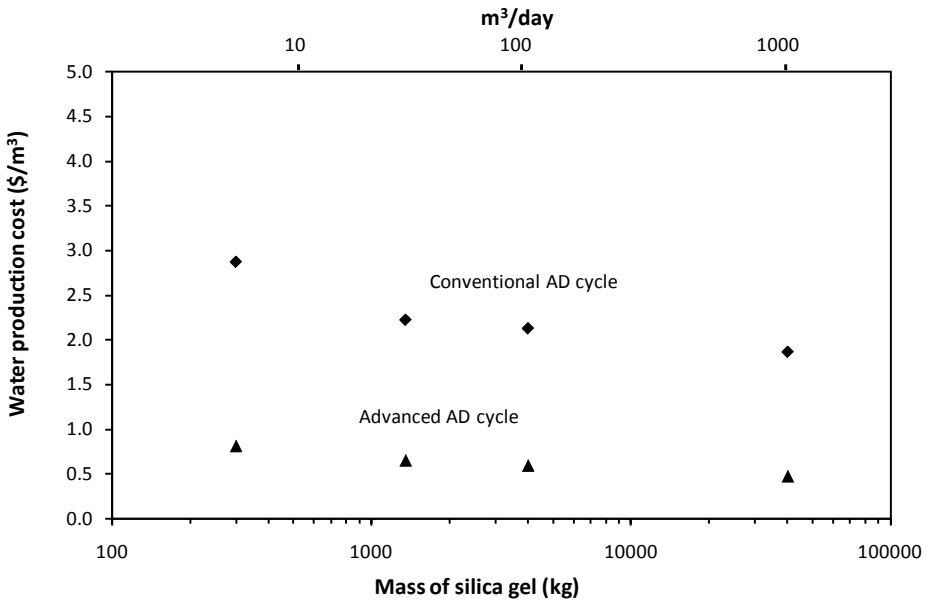

Figure 7.1 Life cycle cost of the conventional and advanced AD cycles

The lowest unit production cost of a AD plant is the capital and operation costs which sums to \$0.457/m^3, as shown in Figure 7.2. The operation cost reduces asymptotically with respect to the output capacity whilst the capital cost decreases more rapidly due to the up-scaling of the plants. At 1000 m^3/day, the relative

contributions from the capital and operation are roughly equal but at lower capacities, the capital cost contribution increases with decreasing water production per day.

For a better understanding of the cost, a sensitivity analysis on the unit production cost by the AD plant with 1000 m^3/day has been conducted for two factors. In the first scenario, the changes in the annual interest rate of capital cost have been evaluated about a nominal rate of 5%. A one percent change below and above the nominal rate has a 6.3% to 6.6 % change on the unit cost. The second analysis pertains to the uncertainty contributed by the electricity rates used in the unit cost computation. A reduction of 3 cents in the electricity rate could have about 9% reduction in the unit cost whilst an increase of similar amount has a positive increase of unit cost by 7.2 % over the nominal case. Table 7.4 summarizes the results of the sensitivity analyses.

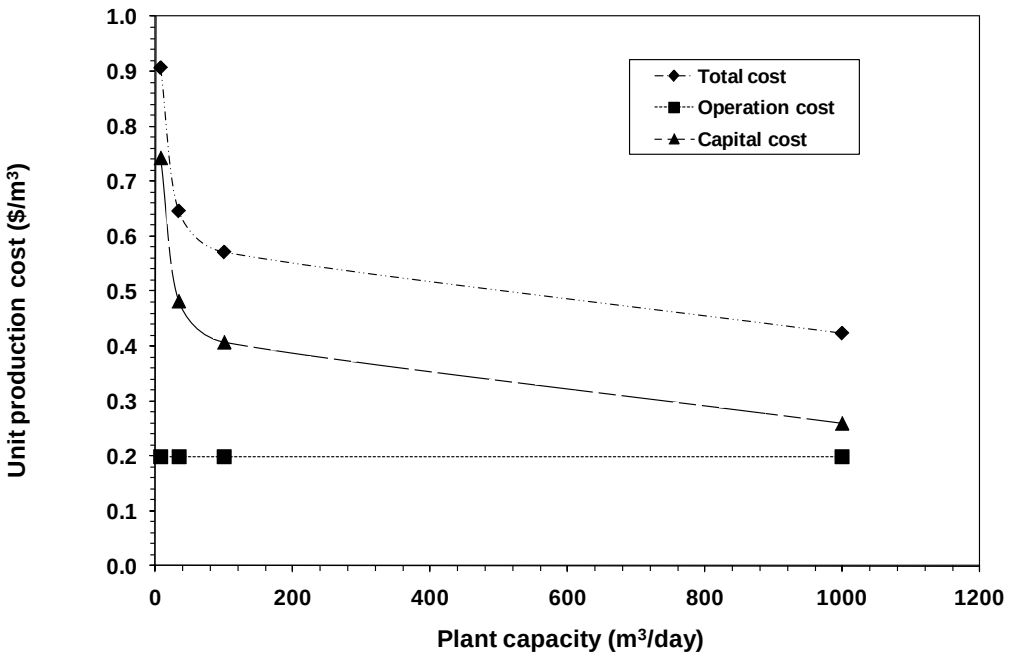

Figure 7.2 Potable water production cost by AD cycle with different plant capacities

Table 7.4 Sensitivity analysis on the unit production cost of water by the AD plant with changes in the interest rate and the electricity rate.

Interest rate (%)	% change in unit production cost	Electricity rate (US$/kWh)	% change in unit production cost
4.0	-6.3	0.100	-9.0
4.5	-3.2	0.120	-3.6
5.0	0.0	0.133	0.0
5.5	3.3	0.147	3.6
6.0	6.6	0.160	7.2

7.2.2. The unit production cost comparison between the AD and RO plants

For a fair comparison with the desalination methods, the electricity rate is kept the same for the study. Amongst the available desalination systems such as multi-stage flash (MSF) distillation, multi-effect (ME) distillation and reverse osmosis (RO), the RO gives the lowest unit production cost. By adopting the parameters of RO plants and designing the AD cycle to the same production capacity of 1000 m^3/day, the common parameters are (i) the plant life is 30 years and (ii) the nominal interest rate is 5%. Here, the inflation rate effect is omitted to give a lower bound value for the unit production costs and Table 7.5 summarizes these parameters used. The electricity rate (in US$) is adjusted with the published rates by the utility companies in Singapore of the past decade. Table 7.6 shows the results of the calculations with contributions from the items such as the capital, operational, maintenance, personnel, etc.

Table 7.5 Cost parameters of the AD plant and the reference RO plant with adjusted electricity rate and the interest rate.

	AD plant	Reference RO plant_1	Reference RO plant_2
Water production capacity (m^3/day)	1000	1000	1000
Plant life, *n* (years)	30	30	30
Interest rate, *i* (%)	5	5	5
Electricity rate (US$/kWh)	0.133	0.133	0.133

From Table 7.6, the unit cost of RO plant is found to be twice that of the AD's unit cost at \$0.944 per m^3. The higher cost contributions of RO are from the operational costs such as the electricity cost, chemical, maintenance and the membrane costs. Most reports of RO plants in the literature omitted or usually left vague the membrane replacement cost. The replacement period of membrane is known to vary from 1 to 5 years, depending on the quality of water feeding through. In the 2nd referenced RO plant [109], it was reported that an item known as "C_{others} "the costs attributed to factors not discussed here". This is likely the replacement cost of the membranes which amounts to about \$0.228/m^3. This factor is depicted as "others" In the last row of Table 7.6, and it contributes up to 20% of the unit production cost of water.

Table 7.6 Contributions to the total costs for AD and RO plants at 1000- m^3/day

Unit cost factors	AD plant			RO plant_1 [108]			RO plant_2 [109]		
	(\$/m^3)	(% of total)		(\$/m3)	(% of total)		(\$/m3)	(% of total)	
$C_{capital}$	0.259	56.7		0.215	22.8		0.127	15.9	
$C_{electrical}$	0.164	35.9	43.3	0.260	27.5	77.2	0.260	32.6	84.1
$C_{menpower}$	0.021	4.6		0.050	5.3		0.021	2.6	
$C_{pretreatment}$	0.001	0.2		0.035	3.7		0.0035	0.4	
$C_{chemical}$	-	-		0.035	3.7		0.1	12.5	

$C_{maintenance}$	0.012	2.6		0.061	6.5		0.039	4.9	
$C_{membrane}$	-	-		0.060	6.4		0.02	2.5	
C_{others}	-	-		0.228	24.1		0.228	28.6	
Total Cost = $\sum_i C(\$/m^3)$	0.457	100		0.944	100		0.799	100	

(Here, the parameters $C_{pretreatment}$, $C_{chemical}$, $C_{membrane}$ and C_{others} are the pre-treatment cost, chemical cost, membrane replacement cost and cost per unit volume of the potable water, respectively.)

Using the cost data available in the literature, figure 7.3 compares the unit potable water production costs by conventional desalination methods such as MSF, MED, membrane distillation (MD) [105], BWRO and SWRO, compared with the AD cycles. Despite the higher capital cost, the AD cycle still offer the lowest production costs for the sea water desalination process for the following reasons: Firstly, the AD cycle is operated by waste or renewable heat which is available free and the parasitic electricity consumption in the plant is deemed the lowest. Secondly, the AD plant has almost no major moving parts and as the desalting is occurring at low temperatures. The maintenance cost is reduced to the lowest possible level a plant could have (only the maintenance of water pumps). Most importantly, the AD cycle requires no chemicals for cleaning at the pre-treatment of seawater and post treatment of fresh water. With such key advantages and robust cycle, the AD plant is believed to be the most efficient desalination process known hitherto.

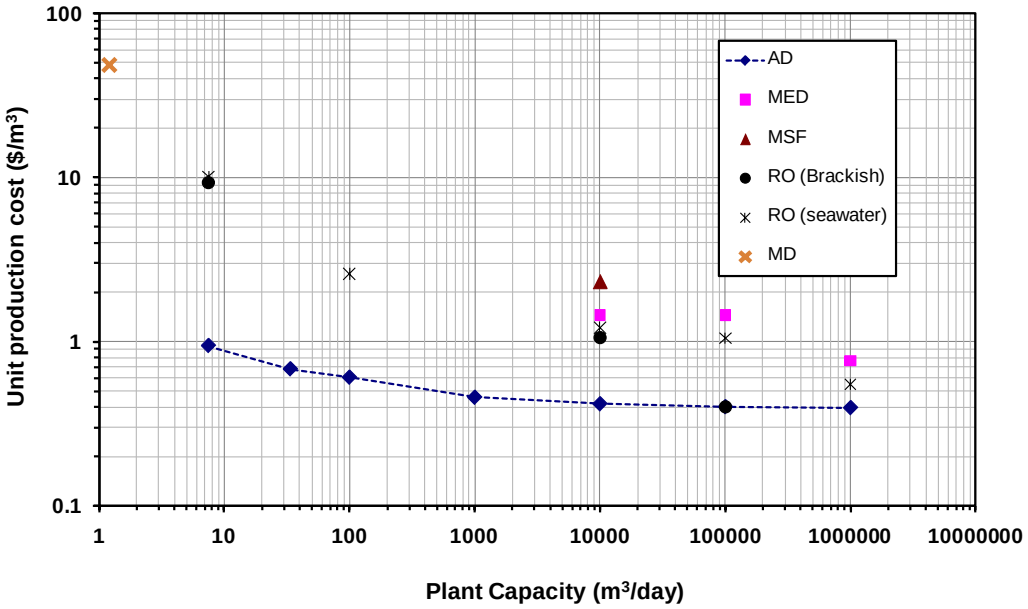

Figure 7.3 Comparison of unit production costs by different desalination methods and plant capacities.

7.3. CO_2 Emission Savings

The CO_2 emission study is made with a direct comparison to the existing desalination methods when both the thermal and electricity are consumed. If the AD cycle is utilized for fresh water production, some CO_2 emission can be avoided because the AD cycle consumes only low temperature heat source and hence, reduces global warming directly. The environmental friendly aspect of the AD plant is demonstrated by comparing the amount of CO_2 emission.

Assuming an emission rate of CO_2 at 64.2 tonnes per TJ for the natural gas (used as a primary fuel) [110] and from the thermal and electricity consumption rates of Table 7.2, the corresponding CO_2 emission of the desalination processes of MSF, MED and RO plants can be computed and the detailed calculations of CO_2 emission is

outlined in Appendix J. The baseline emission for thermal, electricity consumption of the conventional desalination methods are compared to the emission obtained by the AD plant, as shown in Table 7.7 whilst the last column indicates the CO_2 savings.

Table 7.7 CO_2 emissions of the conventional and AD desalination methods for a water production capacity of 1000m^3/day.

Method of desalination	$TB_{th,y}$(tCO_2/yr) (Thermal)	$EB_{elec,y}$(tCO_2/yr) (Electricity)	BE_y(tCO_2/yr) (combined)	Savings if the AD cycle were used for production here ER_y(tCO_2/yr)
MSF	1637	875	2512	= 2512-207 = 2305
MED	1383	640	2023	=2023-207 =1816
RO	0	1380	1380	=1380-207 =1173
AD	0	207	207	(reference datum)

(In this table, $TB_{th,y}$ is the annual CO_2 emission from the burning of natural gas, $EB_{elec,y}$ is the emission from the generation of electricity consumed, BE_y is the baseline annual CO_2 emission and ER_y is the annual CO_2 emission reduction by the AD plant for the same amount of desalting)

7.4. Summary of Chapter 7

The thermo-economic viability of the adsorption desalination (AD) process has been presented using a life-cycle approach. The specific energy cost of AD plant is found to be 1.38 kWh/m^3 which is twice that of the thermodynamic limit: – The lowest energy usage ever reported for a desalination method. At 1000 m^3/day or higher, the total life-cycle cost asymptotic to a unit production cost of \$0.457/m^3 as compared to \$0.944/m^3 of an equivalent RO plant. With low specific energy consumption and simplicity in the operation, the AD cycle is distinctly a superior

method for desalination when a low temperature waste heat source is available. In addition, it could produce both the high-grade water (tds < 10 ppm) and cooling (as discussed previously) with almost no chemicals usage for the pre and post-treatment of seawater. Owing to waste heat recovery, the AD cycle emits significantly lesser CO_2:- When compared to a RO plant of the same water production capacity, a savings of at least 1172 tonnes of CO_2/year or 3.2 kg of CO_2 per m^3 of water can be realized with the AD cycle. Hence, the AD cycle is an excellent and practical solution for quenching the global thirst by desalination.

Chapter 8 Conclusion

The theory and experiments on the low temperature heat source-driven (waste heat or solar) Adsorption Desalination (AD) cycles have been extensively explored in this thesis. The thermodynamic framework for the adsorbent-adsorbate system, for desalination, silica gel and water pair, has been developed. The extensive thermodynamic properties such as the internal energy, the enthalpy, and the entropy of this working pair are described in terms of the temperature (T), pressure (P) and the adsorption amount or uptake (q) where the effect of the isosteric heat and the specific heat are taken into account. These thermodynamic properties could be useful in the modeling of the adsorption desalination process.

The physical and adsorption characteristics of the silica gel-water used as the adsorbent-adsorbate pair in the adsorption desalination process, have been investigated. The AutoSorp-1 and HydroSorp analyzers were used to evaluate the isotherm and kinetic characteristics of different types of silica gels. It was found that type RD-MYCOM silica gel has superior performance other type of silica gel in terms of surface area and water uptake capacity. It should be noted that only Type RD silica gel was selected due to the fact that it is the only type which is available for commercial use. Therefore, it is recommended to extend the development and testing of the adsorption characteristics of other adsorbents which may have better adsorption characteristic.

The mathematical modeling of the conventional two-bed and four-bed adsorption desalination plant was developed in Chapter 4. A prototype AD plant was

designed, constructed and the performance tests were conducted extensively such as different hot water inlet temperatures, different cycle times and different evaporation temperatures of the sea water. It was found that the predicted results of both two-bed and four-bed mode AD plants were within ±5% of the experimental results. The results also showed that two-bed mode AD process was capable of producing specific daily water production (SDWP) of 7.8 m^3 of potable water per tonne of silica gel per day while the SDWP of 10 was achieved by four-bed mode AD plant coupled with all the heat and mass recovery schemes such as i) water recirculation process, ii) water valve delay, iii) gas valve delay and iv) pressure equalization process. The lump parameter model was adapted since the current objective was to evaluate the performance of the AD plant and, being in mind, the operation process of the AD plant such as heat and mass recovery schemes are rather complicated. The distributive modeling of the AD plant should be extended in order to evaluate the adsorption phenomena inside the adsorbent.

The operation strategies of the AD plant for both two-bed and four-bed mode operations were developed for the first time. The optimal cycle time for a specific hot water inlet temperature ranging from 60^{o}C to 85^{o}C for both two-bed and four-bed operation modes were experimentally evaluated. The experimental results showed that the operation cycle time for the optimal performance of the AD plant varies with the regeneration temperature of the plant. A longer cycle time is required for lower heat source temperatures in order to completely regenerate subsequently giving the higher water production rate. This work may be applied as a general operation guideline in the adsorption desalination industry where the available heat source temperature may not be at a constant temperature.

Recovery ratio of the AD plant defined as the ratio of potable water extraction to the feed sea water input which is an important factor for the selection of the desalination technology was investigated for the first time. Through extensive experiments on the AD plant, the recovery ratio of the AD plant was found to be 70% without compromising the performance of the plant. This significantly high recovery ratio is attributed to i) the low evaporation temperature of the sea water and ii) the fact that the evaporation is governed by the uptake of the silica gel.

The numerical simulation and the experimental investigation of the dual effect (cooling and desalination) adsorption desalination cycle have been reported in Chapter 5. The AD plant was capable of producing SDWP 4 m^3 of potable water and the cooling capacity 5 Rton while the chilled water temperature was 12.5^oC which is suitable for refrigeration purpose. On the other hand, the plant was able to produce SDWP 10 and the cooling capacity 25 Rton if the chilled water temperature was about 20^oC which might be used for machine cooling. This improvement in SDWP and the cooling capacity was obtained due to the increase in the evaporating temperature.

The temperature-entropy (T-s) diagram of the AD cycles (both simulation and experimental results) where the paths of the processes in the cycle have been accurately traced and the energy transactions as well as the amount of adsorbate (vapor) of each process can be computed.

An advanced novel adsorption desalination process where the heat of condensation is recovered for the evaporation of the sea water was developed. The

heat recovery was achieved by using an integrated evaporator-condenser device or a heat recovery loop between the evaporator and the condenser. The computer simulation results showed that the advanced AD cycle coupled with the integrated evaporator-condenser device was capable of producing the specific daily water production (SDWP) of 25 m^3 at hot water temperature 85^oC. With this developed AD cycle, the specific electricity consumption of producing potable water was less than the benchmarked value of 1.5 kWh/m^3. This significant improvement in the performance of the AD plant was attributed to two factors. The first factor was the increment in the potable water production rate per cycle (threefold compared to conventional AD cycle) with the same heat input. This high production rate was obtained due to the improvement on the uptake of the silica gel which was achieved by the higher pressure adsorption environment in the advanced cycle. The second contributing factor was the saving of pumping power in the advanced AD cycle where two water pumps i.e., the chilled water pump and the condenser water pump were eliminated with the introduction of the integrated evaporator-condenser device. The experimental investigation of the advanced AD cycle with an integrated evaporator-condenser device is beyond the scope of this thesis since the construction of the experimental setup coupled with the construction of evaporator-condenser device is very complicated and remains as a future research area to explore.

A heat recovery water circuit between the evaporator and the condenser which shares the same principle with the Advanced AD cycle of recovering the condensation heat to the evaporation was instead introduced to the existing adsorption desalination experimental setup. The experimental and simulation results confirmed that the water production rate of the AD plant increased up to 90% with the introduction of the heat

recovery circuit. It is noted that the advanced AD cycle with the integrated evaporator-condenser device gives better performance compared to the AD cycle with condenser-evaporator heat recovery circuit. However, the latter system has advantages such as simplicity in fabrication as well as the flexibility to easily switch the cycle between a dual-effect (cooling and desalination) cycle and a single effect cycle optimized for potable water. An important outcome from the tests conducted on the retro-fitted AD cycle is that it has proven its ability to operate safely at a temperature heat source at only 50°C – a level not matched, hitherto, by any other heat activated equipment.

The economic analysis of the AD process was discussed in Chapter 7. The analysis was explored on different sizes of the AD plant and the comparison between the AD plant and Reverse Osmosis was also presented. The results showed that the unit potable water production cost of the AD plant was lower than that of RO plant for larger scale with the implementation of the concrete bed design). In this thesis, the life-cycle cost of the AD plant was estimated by the numerical analysis and unit production cost over a life cycle of 30 year is found to be $\$0.457/m^3$. Not only the AD plants are cost-effective, it produces water of high grade quality and almost no chemical is used at the pre and post-treatment stages of sea or brackish water. The AD processes emit lesser CO_2 by comparison to a RO plant of the same production capacity:- a reduction of at least 1172 tonnes of CO_2/year or a savings of 3 kg of CO_2 per m^3 of water. Hence, the AD cycle is a promising and practical solution for quenching the global thirst by desalination as well as an excellent method of reducing the global warming.

References

1. O.K. Buros in The ABC's of Desalting, second edition, produced by saline water conversion council for the International Desalination Association, (2000).
2. Ng, K. C., Wang, X.L, Gao, L. Z., Chakraborty, A., Saha, B. B. and Koyama, S., " Apparatus and method for desalination, SG Patent application number 200503029-1 (2005) and WO Patent no. 121414A1 (2006).
3. IDA, IDA worldwide desalting inventory 2002 in International Desalination Association, (2002).
4. I.A. Shiklomanov in Water in Crisis: A Guide to the World's Fresh Water Resources, P.H. Gleick, ed. Oxford University Press, New York, (1993).
5. James E. Miller, Review of Water Resources and Desalination Technologies, (2003).
6. World Health Organization, Guidelines for drinking-water quality, volume 1 recommendation, pp 218, (2008).
7. http://atlas.nrcan.gc.ca/site/english/maps/freshwater/1
8. http://www.data360.org/dsg.aspx?Data_Set_Group_Id=757
9. H.T. El-Dessouky, H.M. Ettouney, Fundamentals of salt water desalination, Elsevier, Amsterdam, the Netherlands, (2002).
10. H.H.G. Savenije in Water Scarcity Indicators; the deception of the numbers, Phys. Chem. Earth (B), Vol. 25, No. 3, pp. 199-204, (2000).
11. Brown Lester R., (ed). in State of the World 1995. Earthscan Publications Ltd., London, UK, (1995).

12. Falkenmark, M. and J. Lundqvist in Towards water security: political determination and human adaptation crucial. Natural Resources Forum, Vol. 21, No. 1, pp. 37-51, (1998).

13. A thirsty world, UNESCO courier, pp 21, September, (2001).

14. http://www.worldwater.org/data.html

15. http://water.org/learn-about-the-water-crisis/facts/

16. Semih Otles and Serkan Otles, Desalination techniques, in Electronic journal of Environmental, Aricultural and Food Chemistry, 4 (4), [963-969], (2004).

17. The 2nd United Nations World Water Development Report, 'Water, a shared responsibility', (2008).

18. http://www.unesco.org/water/wwap/wwdr/index.shtml

19. Human development report, United Nations development programme, pp 6, 7, 35, (2006).

20. Nidal Hadadin, Maher Qaqish, Emad Akawwi, Ahmed Bdour, in Water shortage in Jordan-Sustainable solutions, Desalination 250 (2010) 197-202, (2009).

21. Stephan Lonergan and Barb Kavanagh, Climate change, water resources and security in the Middle Easte in Global Environmental Change, September, (1991).

22. Franz Trieb, Hans Müller-Steinhagen, Concentrating solar power for seawater desalination in the Middle East in Desalination, 220 165–183, (2008).

23. Roshdy A. Abdelrassoul, Potential for economic solar desalination in the Middle East in Renewable Energy, Vol. 14, Nos. 1-4, pp. 345-349, (1998).

24. Abou Rayan, M. Prospects of solar desalination in Second International Water Technology Conference, IWTC'97, Alexandria, Egypt, 28 - 31 March, 339 – 354, (1997).

25. Ralph Sanders, Water desalting and the Middle Easte peace process in Technology in Society 31, 94–99, (2009).

26. S.L. Postel, G.C. Daily, P.R. Ehrlich, Science 271, 785, (1996).

27. Ulrich Ebensperger, Phyllis Isley, Review of the current state of desalination, Water Policy Working Paper 008-(2005).

28. GWI DesalData/IDA, 21st GWI/International Desalination Association Worldwide Desalting Plant Inventory, Desalination in 2008, Global Market snapshot, (2008).

29. Tamim Younos, Kimberly E. Tulou, Overview of Desalination Techniques, Journal of contemporary water research and education, (132), pp 3-10, (2005).

30. Desalination and water purification technology roadmap report, U.S. Department of energy, (2003).

31. Raphael Semiat in Desalination: Present and Future, Water International, Vol. 25, No. 1, pp. 54.65, March (2000).

32. Silver R.S., British Patent Application No. 829820, September, (1957).

33. Wangnick/GWI. 2004 Worldwide desalting plants inventory. Global Water Intelligence, (2005).

34. K.S. Spiegler and Y.M. El-Sayed, A Desalination Primer, Balaban Desalination Publications, Santa Maria Imbaro, Italy (1994).

35. M.A. Darwish, N.M. Al-Najem in Energy consumption by multi-stage flash and reverse osmosis desalters, Applied Thermal Engineering, 20 399 (2000).

36. P. Fiorinia, E. Sciubbaa, C. Sommarivab, A new formulation for the non-equilibrium allowance in MSF processes, Desalination 136 177–188, (2001).

37. Narmine H. Aly, Adel K. El-Fiqi, Thermal performance of seawater desalination systems, Desalination, Vol. 158 pp. 127-142 (2003).

38. M. A1-Shammiri, M. Safar, Multi-effect distillation plants: state of the art, Desalination, Vol. 126 pp. 45-59, (1999).

39. Hafizur Rahman, M.N.A. Hawlader, A. Malek, An experiment with a single-effect submerged vertical tube evaporator in multi-effect desalination, Desalination, Vol. 156 pp. 91-100 (2003).

40. H.T. El-Dessouky, H.M. Ettouney, Multiple-effect evaporation desalination systems: thermal analysis, Desalination Vol. 125 pp. 259–276 (1999).

41. Hisham T. El-Dessouky, Hisham M. Ettouneya, Faisal Mandani, Performance of parallel feed multiple effect evaporation system for seawater desalination, Applied Thermal Engineering, Vol 20 pp. 1679-1706, (2000).

42. Ali M. E1-Nashar, Amer A. Qamhiyeh, Simulation of the steady-state operation of a multi-effect stack seawater distillation plant, desalination, Vol. 101 pp. 231-243, (1995).

43. Bart Van der Bruggen, Carlo Vandecasteele, Distillation vs. membrane filtration: overview of process evolutions in seawater desalination, Desalination Vol. 143 pp. 207-218 (2002).

44. Hisham T. E1-Dessouky, Hisham M. Ettouney, Plastic/compact heat exchangers for single-effect desalination systems, Desalination Vol. 122 pp. 271-289 (1999).

45. HishamT.El-Dessouky, HishamM.Ettouney, YousefAl-Roumi, Multi-stage flash desalination: present and future outlook, Chemical Engineering Journal Vol. 73 pp. 173-190 (1999).

46. Mohammad Abdul-Kareem Al-Sofi, Fouling phenomena in multi stage flash (MSF) distillers, Desalination Vol. 126 pp. 61-76 (1999).

47. M.A. Darwish, Thermal Analysis of Vapor Compression Desalination System, Desalination, Vol. 69 pp. 275-295 (1988).

48. Hisham Ettouney, Design of single-effect mechanical vapor compression, Desalination Vol. 190 pp. 1–15 (2006).

49. D.E. Weiss, The role of ion-exchange desalination in municipal water supplies, Desalination, 1, 107-128, 1966.

50. Marian Turek, Cost effective electrodialytic seawater desalination, Desalination Vol. 153 pp. 371-376 (2002).

51. José M. Veza, Baltasar Peňate,, Fernando Castellano, Electrodialysis desalination designed for off-grid wind energy, Desalination, Vol. 160 pp. 211-221 (2004).

52. M.N.A. Hawlader, J.C. Ho, Chua Kok Teng, Desalination of seawater: an experiment with RO membranes, Desalination Vol. 132 pp. 275-280 (2000).

53. Yosef Dreizin, Ashkelon seawater desalination project - off-taker's self costs, supplied water costs, total costs and benefits, Desalination Vol. 190 pp, 104–116 (2006).

54. M. A1-Shammiri and M. A1-Dawas, Maximum recovery from seawater reverse osmosis plantsin Kuwait, Desalination Vol. 110 pp. 37-48 (1997).

55. Lauren F. Greenlee, Desmond F. Lawler, Benny D. Freeman, Benoit Marrot, Philippe Moulin, Reverse osmosis desalination: Water sources, technology, and today's challenges, Water Research, Vol 43 pp. 2317–2348 (2009).

56. C.E. Harland, Ion Exchange: Theory and Practice, 2nd Edition, The Royal Society of Chemistry, Cambridge, UK (1994).

57. B.A. Bolto, K.H. Eppinger, M.B. Jackson, R.V. Siudak, An ion-exchange process with thermal regeneration XVI oxygem-resistant polyamine resins, Desalination, Vol 42 pp. 11 (1982).

58. L. Lazare, The puraq seawater desalination process,Desalination Vol 42 pp. 11 (1982).

59. J. Phattaranawik, R. Jiraratananon, A.G. Fane, Heat transport and membrane distillation coefficients in direct contact membrane distillation, Journal of Membrane Science, Vol 212 pp. 177–193 (2003).

60. Paz Godino, Luis Peña, Juan I. Mengual, Membrane distillation: theory and experiments, Journal of Membrane Science Vol. 121 pp. 83-93 (1996).

61. J.I. Mengual, M. Khayet, M.P. Godino, Heat and mass transfer in vacuum membrane distillation, International Journal of Heat and Mass Transfer Vol. 47, pp. 865-875, (2004).

62. K.S. Spiegler and Y. M. El-Sayed, The energetics of desalination processes, Desalination, 134 (2001) 109-128.

63. Raphael Semiat, Energy issues in desalination processes, Environmental Science & Technology, Vol. 42, No. 22, (2008).

64. E. Tzen, R. Morris, Renewable energy sources for desalination, Solar Energy, Vol. 75 pp. 375–379 (2003).

65. D. Hoffman, The application of solar energy for large-scale seawater desalination, Desalination, Vol. 89 pp. 115–184 (1992).

66. Garcia-Rodriguez L, Gomez-Camacho C. Perspectives of solar desalination, Desalination, Vol. 136 pp. 213–8 (2001).

67. Joachim Koschikowski, Marcel Wieghaus, Matthias Rommel, Solar thermal-driven desalination plants based on membrane distillation, Desalination Vol. 156 pp. 295-304, (2003).

68. T.V. Arjunan, H.S¸ Aybar, N. Nedunchezhian, Status of solar desalination in India, Renewable and Sustainable Energy Reviews Vol. 13 pp. 2408–2418 (2009).

69. M.N.A. Hawlader, Prasanta K. Dey, Sufyan Diab, Chan Ying Chung, Solar assisted heat pump desalination system, Desalination Vol. 168 pp. 49-54 (2004).

70. Ioannis C. Karagiannis, Petros G. Soldatos, Water desalination cost literature: review and assessment, Desalination Vol. 223 pp. 448–456 (2008).

71. Mohamed A. Eltawil, Zhao Zhengming, Liqiang Yuan, A review of renewable energy technologies integrated with desalination systems, Renewable and Sustainable Energy Reviews Vol. 13 pp. 2245–2262 (2009).

72. J.E. Blank, G.F. Tusel, S. Nisan, The real cost of desalted water and how to reduce it further, Desalination Vol. 205 pp. 298–311 (2007).

73. Chi Tien, Adsorption calculation and modeling, Butterworh-Heinemann series in chemical engineering, Boston, 1994.

74. F. Rouquerol, J. Rouquerol and K. Sing, Adsorption by powers & porous solids, principles, methodology and applications, Boston, 1999.

75. A. Dąbrowski, Adsorption - from theory to practice, Advances in Colloid and Interface Science Vol. 93 pp. 135-224 (2001).

76. E.C. Boelman, B.B. Saha, T. Kashiwagi, Experimental investigation of a silica gel–water adsorption refrigeration cycle – the influence of operating conditions on cooling output and COP, ASHRAE Trans. Res. 101 (2) 358–366 (1995).

77. E.C. Boelman, B.B. Saha, T. Kashiwagi, Parametric study of a silica gel–water adsorption refrigeration cycle – the influence of thermal capacitance and heat exchanger UA-values on cooling capacity, power density and COP, ASHRAE Trans. 103 (1) 139–148 (1997).

78. K. C. Ng, H.T. Chua, C.Y. Chung, C.H. Loke, T. Kashiwagi, A. Akisawa, B.B. Saha, Experimental investigation of the silica gel-water adsorption isotherm characteristics, Applied Thermal Engineering, 21, 1631-1642 (2001).

79. K.C. Ng, H.T. Chua, X.L. Wang, T. Kashiwagi, B.B. Saha, Prototype testing of a novel four-bed regenerative silica gel–water adsorption chiller, International conference of refrigeration, Washington DC, (2003).

80. Saha BB, Kashiwagi T. Experimental investigation of an advanced adsorption refrigeration cycle. ASHRAE Trans, 103(2):50–58 (1997).

81. D.C. Wang, Y.H. Li, D. Li, Y.Z. Xia, J.P. Zhang, A review on adsorption refrigeration technology and adsorption deterioration in physical adsorption systems, Renewable and Sustainable Energy Reviews Vol. 14 pp. 344–353 (2010).

82. Suzuki, M. Adsorption Engineering Elsevier, Amsterdam, the Netherlands, (1990).

83. Critoph RE, Vogel R. Possible adsorption pairs for use in solar cooling, Ambient Energy Vol. 7 pp. 183–90 (1986).

84. Meunier F, Douss N. Performance of adsorption heat pumps. Active carbon–methanol and zeolite–water pairs, ASHRAE Transactions 2:267–74 (1990).

85. Wang RZ, Jia JP, Teng Y, Zhu YH, Wu JY, Study on a new solid adsorption refrigeration pair, active carbon fiber–methanol, ASME Journal of Solar Energy Engineering;119:214–8 (1997).

86. Restuccia G, Cacciola G., Performances of adsorption systems for ambient heating and air conditioning, International Journal of Refrigeration Vol. 22 pp. 18–26 (1999).

87. T.F. Qu, R.Z. Wang, W. Wang, Study on heat and mass recovery in adsorption refrigeration cycles, Applied Thermal Engineering Vol. 21 pp. 439–452 (2001).

88. R.Z. Wang, Performance improvement of adsorption cooling by heat and mass recovery operation, Int J Refrig 24 (7) 602–611 (2001).

89. K.C. Ng, Xiaolin Wang, Yee Sern Lim, Bidyut Baran Saha, Anutosh Chakarborty, Shigeru Koyama, Atsushi Akisawa, Takao Kashiwagi, International Journal of Heat and Mass Transfer 49 3343–3348 (2006).

90. KC Ng, JM Gordon, HT Chua, Anutosh Chakraborty, Electro-adsorption Chiller: A Miniaturized Cooling Cycle with Applications from Microelectronics to Conventional Air-conditioning, US patent no. 6434955, (2002).

91. Chua, H.T., Anutosh Chakraborty and Xiaolin Wang., An adsorption chiller driven by thermoelectricity, The Tenth International Refrigeration and Air Conditioning Conference at Purdue USA, July 12-15, (2004).

92. Chua, H.T.; Ng, K.C.; Malek, A; Kashiwagi, T.; Akisawa, A.; Saha, B.B. Multi-bed regenerative adsorption chiller - improving the utilization of waste heat and reducing the chilled water outlet temperature fluctuation. International Journal of refrigeration Vol. 24 pp. 124-136 (2001).

93. D.B. Broughton, Continuous desalination process, USPO 4,447,329, May 8, (1984).

94. D. Zejli, R. Benchrifa, A. Bennouna, O.K. Bouhelal, A solar adsorption desalination device: first simulation results, Desalination Vol. 168 pp. 127-135 (2004).

95. S. Al-kharabsheh, D.Y. Goswami, Theoretical analysis of a water desalination system using low grade solar heat, Journal of solar energy engineering transactions of the ASME Vol. 126 pp. 774–780 (2004).

96. X. Wang, K.C. Ng, Experimental investigation of an adsorption desalination plant using low-temperature waste heat, Applied Thermal Engineering, 25 2780–2789 (2005).

97. Sverdrup et al. The Oceans, Prentice-Hall, New York, (1946).

98. Chua, H. T., K. C. Ng, A. Malek and N. M. Oo, General thermodynamic framework for understanding temperature-entropy diagram of batchwise operating thermodynamic cooling cycles, Journal of Applied Physics, Vol. 89, No. 9, pp. 5151-5158, (2001).

99. Ng, Kim Choon, Saha, Bidyut Baran, Chakraborty, Anutosh and Koyama, Shigeru, Adsorption Desalination Quenches Global Thirst, Heat Transfer Engineering, 29: 10, 845 - 848, (2008).

100. Anutosh Chakraborty, Bidyut Baran Saha, Kim Choon Ng, Shigeru Koyama, and Kandadai Srinivasan, Theoretical Insight of Physical Adsorption for a

Single-Component Adsorbent + Adsorbate System: I. Thermodynamic Property Surfaces, Langmuir, 25, 2204-2211, (2009).

101. Anutosh Chakraborty, Bidyut Baran Saha, Kim Choon Ng, Shigeru Koyama, and Kandadai Srinivasan, Theoretical Insight of Physical Adsorption for a Single Component Adsorbent + Adsorbate System: II. The Henry Region, Langmuir, 25(13), 7359–7367, (2009).

102. Ruthven, D.M. Principles of adsorption and adsorption processes, John Wiley & Sons, New York, USA, (1984).

103. Chihara, K.; Suzuki, M. Air drying by pressure swing adsorption. Journal of Chemical Engineering, Japan, 16, 293-298, (1983).

104. http://www.solcomhouse.com/solarpower.htm

105. Solar powered desalination: An autonomous water supply?, Desalination (a Filtration+Separation publication) Vol. 3 issue 2.

106. NG Kim Choon, Kyaw THU, Yanagi HIDEHARU, Bidyut Baran SAHA, Anutosh CHAKRABORTY, Tawfiq Y AL-GHASHAM, Apparatus and Method for Improved Desalination, PCT/SG2009/ 000223.

107. Ng Kim Choon, Anutosh Chakraborty, Sai Maung Aye, Wang Xiaolin, New pool boiling data for water with copper-foam metal at sub-atmospheric pressures: Experiments and correlation, Applied Thermal Engineering, Applied Thermal Engineering Vol. 26 pp. 1286–1290 (2006).

108. U. Atikol, Hikmet S. Aybar, Estimation of water production cost in the feasibility analysis of RO systems, Desalination Vol. 184 pp. 253–258 (2005).

109. G. Fiorenza, V.K. Sharma and G. Braccio, Techno-economic evaluation of a solar powered water desalination plan. Energy Conversion and Management, Vol. 44 pp. 2217–2240 (2003).

110. http://www.naturalgas.org/environment/naturalgas.asp. Date of accessed: 25th November 2005.

111. IPCC Guidelines for National Greenhouse Gas Inventories, 2006, volume 2, Energy.

112. UNFCCC/CCNUCC, "Tool to calculate the emission factor for an electricity system Information on emission factor"

113. Information on Emission factors, Singapore National Environmental Agency, (2009).

114. Wang, X., Anutosh, C. and Ng, K.C., How heat & mass recovery strategies impact the performance of adsorption desalination plant: theory and experiments, Heat Transfer Engineering, (2006).

115. Amy Tan Aan Mee, Experimental Investigation of Adsorption Desalination Plant, Bachelor thesis, National University of Singapore, Singapore, (2008).

116. KHURRAM MAQSOOD, Experimental Investigation of Adsorption Desalination Plant, Bachelor thesis, National University of Singapore, Singapore, (2007).

117. Foo Yong Zhao,Colin, Experimental Testing of an Adsorption Desalination Plant, Bachelor thesis, National University of Singapore, Singapore, (2007).

118. Tong Wey Shyang, Experimental testing of an adsorption desalination plant, Bachelor thesis, National University of Singapore, (2006).

119. Sircar.S, Hufton,J.R, Why does the linear driving force model for adsorption kinetics work? Adsorption 6, 137-147 (2000).

120. Seawater Desalination in California, California coastal commission Chapter 1: Energy Use section, http://www.coastal.ca.gov/index.html - date of access is 15/01/2007.

121. Groot, S.R. De and P. Mazur. Non-equilibrium Thermodynamics. pp. 11-42, Amsterdam: North-Holland Pub co. (1962).

Appendix A: Minimum energy requirement for desalting by Gibbs free energy approach

A typical desalting process is illustrated in Figure A.1 where the feed sea water has the concentration, X_s and the rejected brine has concentration, X_b which is greater than X_s with the production of salt free potable water.

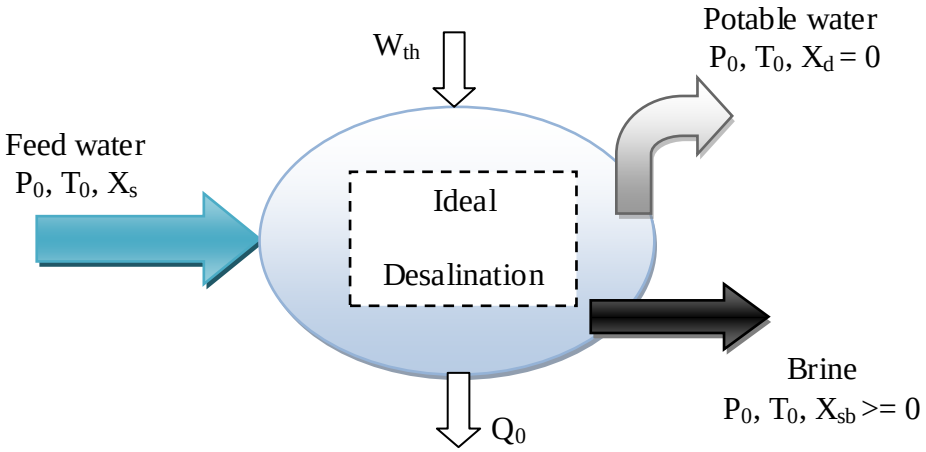

Figure A.1 A typical desalination process

A simple expression for the free energy of separation per unit amount of potable water can be written assuming that the solution is dilute, the recovery approaches to zero and the product water is salt free as

$$(dG)_{P_0,T_0} = \sum_i \mu_i dM_i = \left(\mu_w^0 dM_d\right)_{distillate\ stream} + \left(\mu_w dM_b + \sum_s \mu_s dM_s\right)_{brine\ stream} \quad \text{A.1}$$

where G is Gibbs free energy, μ_i is the chemical potential of species i and M_i is the mass of species i. μ_w^0 represents the pure water, M_d is the mass of distillate, μ_w is the water in the brine whereas μ_s refers to the salt species. It is assumed that the product

is salt free and thus, from mass balance $dM_d = -dM_b$ and dM_s=0 and hence Equation 3.1 becomes,

$$(dG)_{P_0,T_0} = (\mu_w^0 - \mu_w)\, dM_d \qquad \text{A.2}$$

For dilute solution, $(\mu_w^0 - \mu_w) = -RT_0 \ln(X_w)$ and for large amount of X_w, $-\ln(X_w) = X_s$ where X_s is the mole fraction of the total salts in the feed and X_w is the mole fraction of water. Thus, the theoretical minimum work per unit product for a small recovery approaching zero can be written as

$$W_{th0} = \left(\frac{\partial G}{\partial M_w}\right)_{P_0,T_0} = R\, T_0\ X_s \qquad \text{A.3}$$

For the ionic composition, the factor, φ is introduced into Equation A.3 and then the theoretical minimum work for desalination is given by

$$W_{th0} = \left(\frac{\partial G}{\partial M_w}\right)_{P_0,T_0} = \varphi\, R\, T_0\ X_s \qquad \text{A.4}$$

Using Equation A.4, the theoretical minimum work for the separation for desalination process for different initial salt concentrations at constant solution temperature of 27℃ is given in Figure A.2. The theoretical minimum free energy for desalination process linearly varies with the initial salt concentration whilst the minimum free energy at salinity 35.4 g/kg of water is about 0.86kWh/m^3.

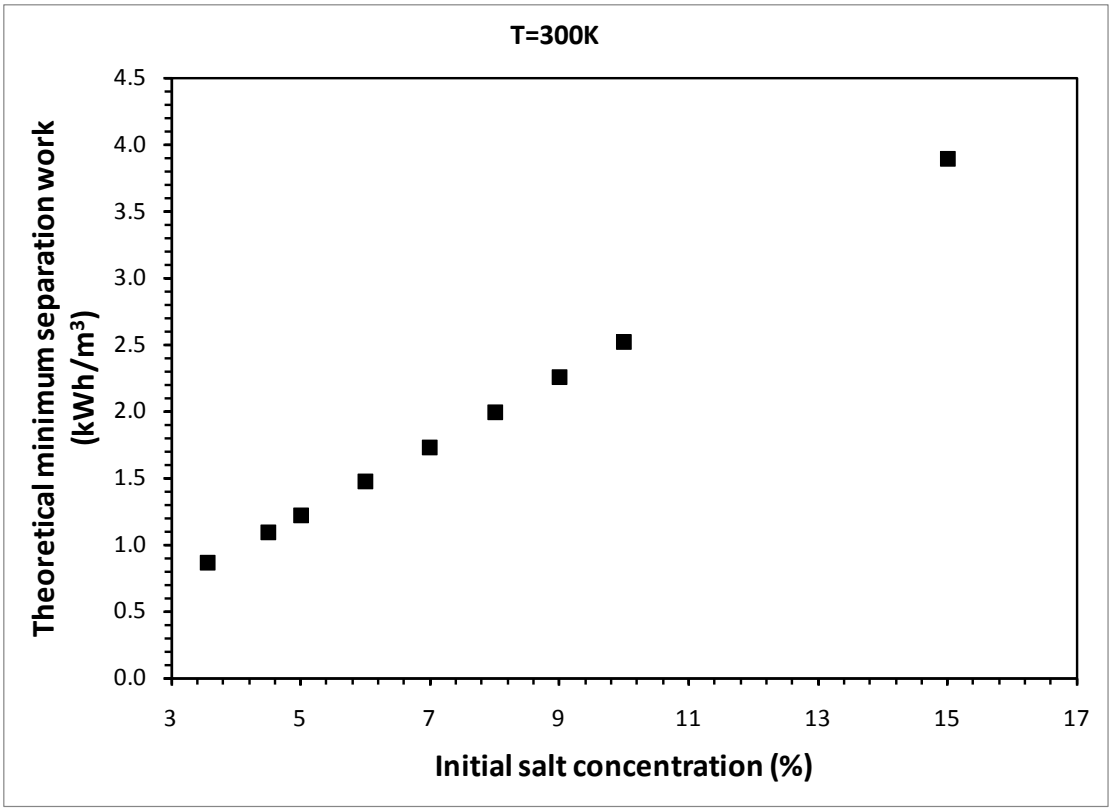

Figure A.2 Theoretical minimum separation work for desalination with initial salt concentration

For the finite recovery amount of potable water from the feed sea water, Equation A.4 is integrated from the feed concentration, X_s, to the brine concentration, X_b, as;

$$W_{thR} = \frac{1}{M_d} \int_{X_s}^{X_b} R\, T_0\, X\, dM_d \qquad \text{A.5}$$

For any X and M between X_s, M_f and X_b, M_b, the differential increase in the salt content of M for pure water is $M\,X = (M - dM_w)(X + dX)$ and i.e., $M\,dX = (X + dX)dM_w$. However, $dX\,dM_w$ is negligible and thus $M\,dX = X\,dM_w$ and furthermore, $M\,X = M_f\,X_s$ and Equation A.5 becomes

$$W_{thR} = \frac{M_f}{M_d} R T_0 X_s \ln \frac{X_b}{X_s} \qquad \text{A.6}$$

However $\frac{M_d}{M_f}$ is the recovery ratio, using salt and mass balance, $\frac{M_f}{M_d} = \frac{X_b}{X_b - X_s}$ and finally the theoretical free energy for finite recovery becomes,

$$W_{thR} = R T_0 \frac{X_s X_b}{X_b - X_s} \ln \frac{X_b}{X_s} \qquad \text{A.7}$$

Using Equation A.7, the free energy for different recovery ratios by the desalination process is presented in Figure A.3 where the recovery of the potable water from the sea water with different initial salt concentrations such as 4.5%, 3.5% and 0.5% at constant temperature 27°C. It is noted that for brackish water desalination, the theoretical free energy required is less than 0.4kWh/m^3.

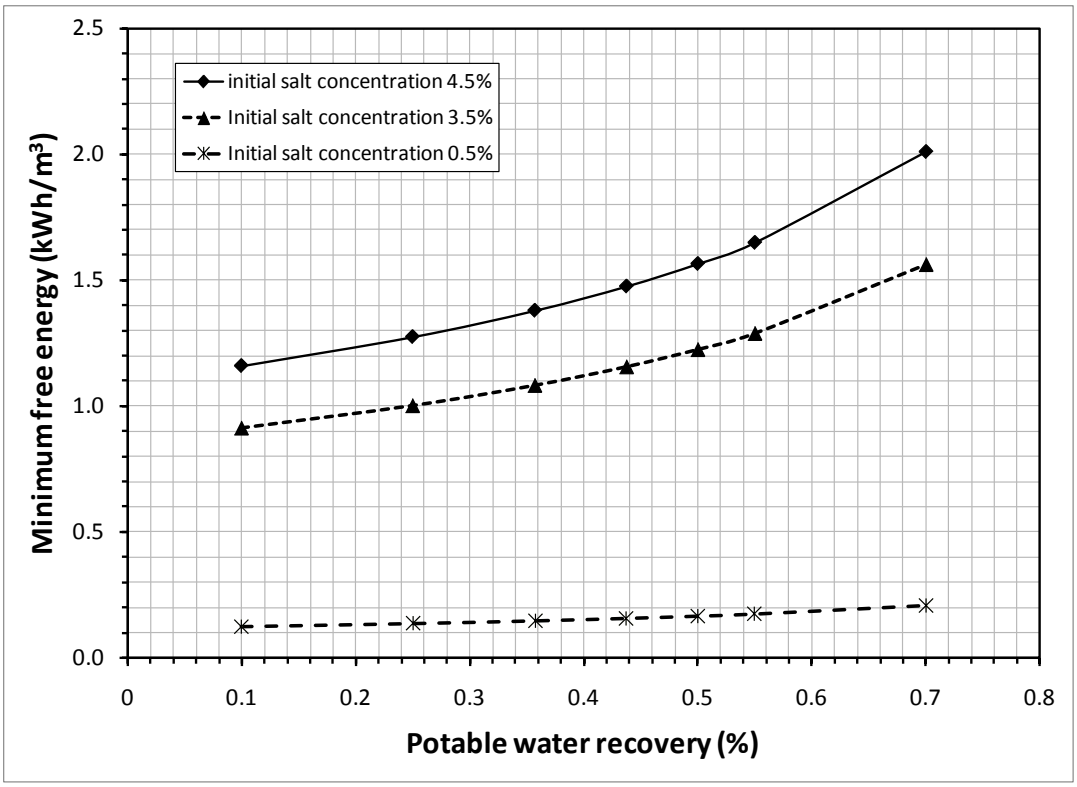

Figure A.3 Theoretical free energy of desalting for the potable water recoveries of solution with different initial salt concentration

Appendix B: Minimum energy requirement for desalting by Work done approach

Figure B.1 shows a typical desalting process where the osmosis pressure applied to prevent the diffusion of the water through the membrane that allows only water to pass through to the salt water.

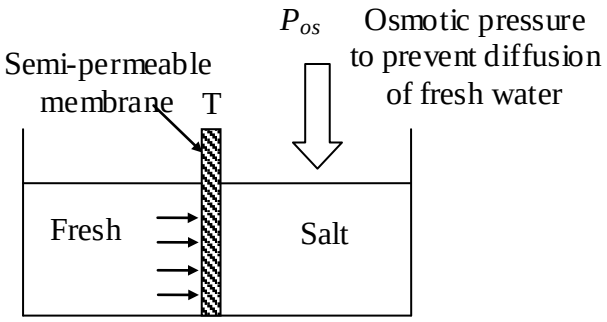

Figure B.1 Description of the separation of pure water from salt solution using membrane

The chemical potential of water in solution is given by

$$\mu = \mu_0 + P\bar{v} + RT\ln a \qquad \text{B.1}$$

where μ_0 is the chemical potential of pure water at 1 atm pressure, P is the pressure in access of the 1 atm acting on the solution, $\bar{v}$ is the molar volume of water, R is the gas constant, T is solution temperature, and a is the activity of the water in the solution where a decreases with the increase in salt concentration. At the membrane

interface, the water on both side of the membrane is in equilibrium and thus their chemical potentials are also the same:

$$\mu_0 = \mu_0 + P_{os}\,\bar{v} + RT\ln a \qquad \text{B.2}$$

$$P_{os} = -\frac{RT}{\bar{v}}\ln a \qquad \text{B.3}$$

Certain amount of pressure which is higher than the osmotic pressure is required to separate water from the salt solution. For the infinitesimal compression step to produce the fresh water volume of dv, the work done dW is given as

$$dW = P_{os}\,dv \qquad \text{B.4}$$

For the initial and final volumes of the salt solution v_1 and v_2, the total work per litre of fresh water produced is

$$W = \frac{1}{v_1 - v_2}\int_{v_1}^{v_2} P_{os}\,dv = \frac{-RT}{(v_1 - v_2)\bar{v}}\int_{v_1}^{v_2}\ln a\,dv \qquad \text{B.5}$$

The activity is defined as $a \equiv \frac{P}{P_0}$ where P_0 and P are the equilibrium water vapor pressures above pure water and the solution. The vapor pressure of the sea water is given by $P = P_0(1 - AS)$ [Sverdrup et al.] where A=0.000537 and S is the salinity and hence Equation B.5 becomes

$$W_{thR} = \frac{-RT}{(v_1 - v_2)\bar{v}} \int_{v_1}^{v_2} \ln(1 - AS)dv = \frac{ART}{(v_1 - v_2)\bar{v}} \int_{v_1}^{v_2} S\, dv \qquad \text{B.6}$$

since $A\,S$ is small compared to 1 and there is no salt passes through the membrane in the process, $S\,v = S_1\,v_1$ and thus

$$W_{thR} = \frac{ART}{\bar{v}} \frac{v_1}{(v_1 - v_2)} \ln \frac{v_2}{v_1} \qquad \text{B.7}$$

For a very small recovery, i.e., the recovery approaches to zero, the minimum free energy required for desalting at T=298K, S=34.3% is

$$W_{th0} = \frac{ARTS}{\bar{v}} = 0.706 kWh/m^3, \quad (v_1 - v_2) \to 0 \qquad \text{B.8}$$

For finite amount of recovery from v_1 to v_2, the free energy required for the separation is estimated using Equation B.6 and results are presented in Figure B.2 where the required free energy by Gibbs approach with different values of φ are also compared. The value of the ionic composition, φ, is between 1 and 2 [62] and it is found that at φ=1.6, the free energy for desalting process by Gibbs approach agrees with that by work done approach.

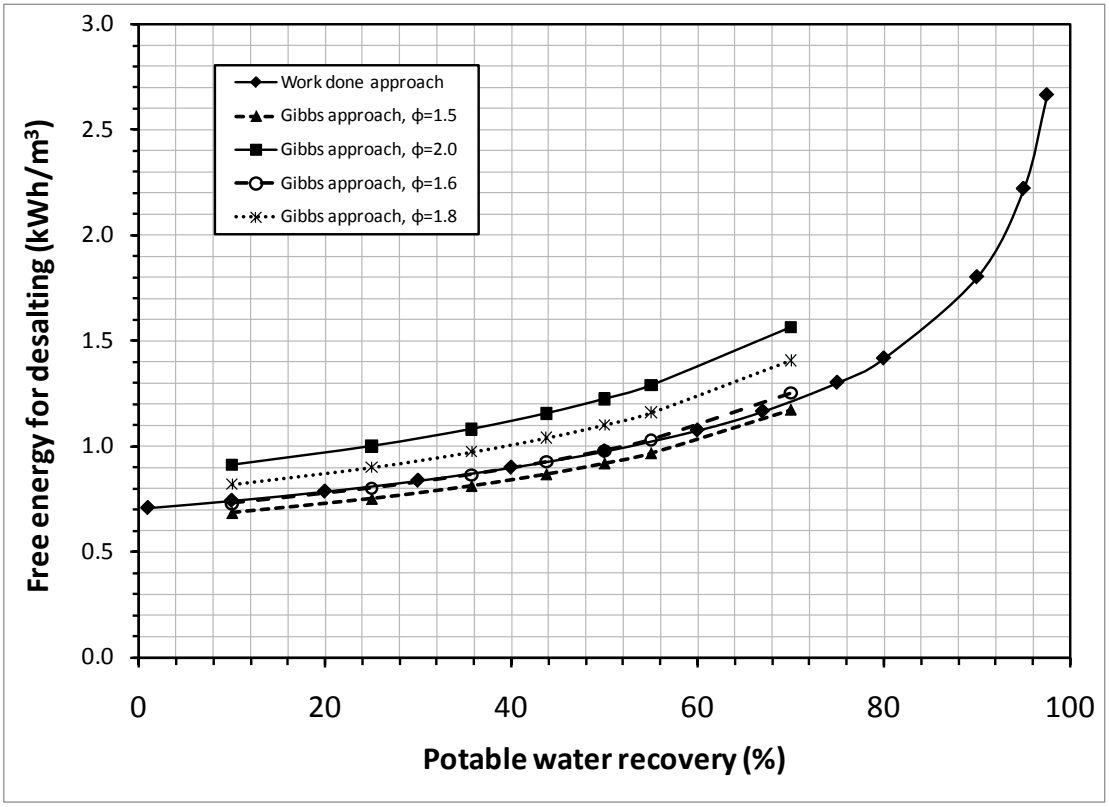

Figure B.2 Free energy for desalting for different recoveries in comparison between Gibbs and work done approach

Appendix C: Derivation of mass, energy and entropy balances

I Conservation of mass

Equation 3.16 is applied for the fixed control volume with the total mass in the system, the conservation of mass states that rate of change of mass of a system is zero [121]. Using Reynolds' transport Theorem where $\alpha = 1$,

$$\frac{D}{Dt}\left(\int_{Volume} \rho dV\right) = \frac{\partial}{\partial t}\left(\int_{CV} \rho \, dV\right) + \int_{CS} \left(\rho \vec{v} . d\vec{A}\right) = 0 \qquad \text{C.1}$$

Since the control volume is fixed with respects to a coordinate system attached it, the limits of integration are also fixed and hence

$$\int_{CV} \frac{\partial \rho}{\partial t} dV + \int_{CS} \left(\rho \vec{v} . d\vec{A}\right) = 0 \qquad \text{C.2}$$

Applying Gauss divergence Theorem, the surface integral is converted to volume integral and obtains as

$$\int_{CV} \frac{\partial \rho}{\partial t} dV + \int_{CV} \nabla . (\rho \vec{v}) dV = 0 \qquad \text{C.3}$$

$$\int_{CV} \left(\frac{\partial \rho}{\partial t} + \nabla . (\rho \vec{v})\right) dV = 0 \qquad \text{C.4}$$

Setting the integrand to zero, the conservation of mass becomes

$$\frac{\partial \rho}{\partial t} + \nabla.(\rho \vec{v}) = 0 \qquad \text{C.5}$$

where ρ is the total density which is $\rho = \sum_{k=1}^{n} \rho_k$ and v is the barycentric velocity, $v = \sum_{k=1}^{n} \frac{\rho k v k}{\rho}$.

II Conservation of momentum:

The conservation of momentum states that

$$F_{total} = \sum (External\ \ forces\ acting\ on\ the\ \ fluid\ \ system)$$

The Equation of motion of a system is given by,

$$\rho \frac{dv_\alpha}{dt} = -\sum_{\beta=1}^{3} \frac{\partial}{\partial x_\beta} P_{\beta\alpha} + \sum_{k=1}^{3} \rho_k F_{k\alpha}, \qquad (\alpha = 1,2,3) \qquad \text{C.6}$$

where $v_\alpha\ (\alpha = 1,2,3)$ is a Cartesian component of v, and where $x_\alpha\ (\alpha = 1,2,3)$ are the Cartesian coordinates. The derivative $\frac{dv_\alpha}{dt}$ is a component of the acceleration of the centre of gravity motion. The quantity, $P_{\beta\alpha}\ (\beta, \alpha = 1,2,3)$, is the Cartesian component of the stress (or Pressure) tensor P of the medium and it is assumed that pressure

tensor ***P*** is symmetric i.e., $P_{\beta\alpha} = P_{\alpha\beta}$ and $F_{k\alpha}\left(k, \alpha = 1,2,3\right)$ is the Cartesian component of the force per unit mass $\mathbf{F}_k$ exerted on the chemical component k. The tensor notation of the Equation C.6 can be written as

$$\frac{d\rho\vec{v}}{dt} = -\nabla.P + \sum_k \rho_k \mathbf{F}_k \qquad \text{C.7}$$

From a microscopic point of view, the pressure tensor resulted from the short-range interactions between the particles of the system and $\boldsymbol{F}_k$ is resulted from the external forces and long-range interactions in the system. By constraining into the conservatives forces derived from the potential ψ_k not a function of time, one has $F_k = -\nabla.\psi_k$ and $\frac{\partial \psi_k}{\partial t} = 0$.

Using Reynolds transport Theorem and Gauss divergence Theorem, the conservation of momentum where $\alpha = \vec{v}$ can be written as

$$\frac{d\left(\rho\vec{v}\right)}{dt} = \frac{\partial\left(\rho\vec{v}\right)}{\partial t} + \nabla.\left(\rho\vec{v}\vec{v}\right) \qquad \text{C.8}$$

From Equation C.7 and C.8, the conservation of momentum Equation is obtained as

$$\frac{\partial\left(\rho\vec{v}\right)}{\partial t} + \nabla.\left(\rho\vec{v}\vec{v}\right) = -\nabla.P + \sum_k \rho_k F_k \qquad \text{C.9}$$

Thus, the balance Equation of the momentum density becomes

$$\frac{\partial(\rho\vec{v})}{\partial t} = -\nabla.(\rho\vec{v}\vec{v} + P) + \sum_k \rho_k F_k \qquad \text{C.10}$$

Here $\rho\vec{v}$ is momentum density, $\rho\vec{v}\vec{v} + P$ is momentum flow where $\rho\vec{v}\vec{v}$ is the convective part and $\sum_k \rho_k F_k$ is the source of momentum and $\vec{v}\vec{v}$ is an ordered (dyadic) product.

Hence the kinetic energy balance of the centre of gravity motion by multiplying with the v_a of the barycentric velocity and summing over α as

$$\frac{\partial\left(\frac{1}{2}\rho\vec{v}^2\right)}{\partial t} = -\nabla.\left(\frac{1}{2}\rho\vec{v}^2\vec{v} + P.\vec{v}\right) + \mathbf{P}:\nabla.\vec{v} + \sum_k \rho_k F_k.\vec{v} \qquad \text{C.11}$$

Noting that

$$\Rightarrow \left[\nabla\cdot(\rho\vec{v}\vec{v})\right]\cdot\vec{v} = \left(\sum_{i=1}^{3}\frac{\partial}{\partial x_i}\rho v_i v_j\right)v_j \quad i, j = 1,\cdots,n$$
$$= \sum_{i=1}^{n}\frac{\partial}{\partial x_i}\frac{1}{2}\rho v_i v_j^2$$
$$= \nabla\cdot\left(\frac{1}{2}\rho\vec{v}^2\vec{v}\right)$$

and

$$\Rightarrow -\nabla\cdot\left(P\cdot\vec{v}\right)+\mathbf{P}:\nabla.\vec{v}=-\sum_{i=1}^{n}\frac{\partial}{\partial x_i}\left(\sum_{j=1}^{n}P_{ij}v_j\right)+\sum_{i=1}^{n}\sum_{j=1}^{n}P_{ij}\frac{\partial}{\partial x_i}v_j \quad i,j=1,2,3,\cdots,n$$

$$=-\sum_{i=1}^{n}\sum_{j=1}^{n}\left(v_j\frac{\partial}{\partial x_i}P_{ij}+P_{ij}\frac{\partial}{\partial x_i}v_j\right)+\sum_{i=1}^{n}\sum_{j=1}^{n}P_{ij}\frac{\partial}{\partial x_i}v_j$$

$$=-\sum_{j=1}^{n}v_j\sum_{i=1}^{n}\left(\frac{\partial}{\partial x_i}P_{ij}\right)$$

$$=-\left(\nabla\cdot P\right)\cdot\vec{v}$$

Similarly, the Equation for the rate of change of the potential energy density, $\rho\psi=\sum_k\rho_k\psi_k$, can be derived as

$$\frac{\partial\left(\rho\psi\right)}{\partial t}=-\nabla.\left(\rho\psi\vec{v}+\sum_{k=1}^{n}\psi_k J_k\right)-\sum_{k=1}^{n}\rho_k F_k.\vec{v}-\sum_{k=1}^{n}J_k F_k+\sum_{k=1}^{n}\sum_{j=1}^{r}\psi_k\nu_{kj}J_j \qquad \text{C.12}$$

The last term of the above Equation vanishes since the potential energy in the chemical is conserved i.e., $\sum_{k=1}^{n}\psi_k\mathbf{v}_{kj}=0 \quad \left(j=1,\cdots,r\right)$ and thus

$$\frac{\partial\left(\rho\psi\right)}{\partial t}=-\nabla\left(\rho\psi\vec{v}+\sum_{k=1}^{n}\psi_k J_k\right)-\sum_{k=1}^{n}\rho_k F_k.\vec{v}-\sum_{k=1}^{n}J_k F_k \qquad \text{C.13}$$

By summing Equations for the rate of change of kinetic and potential energies, one gets

$$\Rightarrow \frac{\partial\left(\frac{1}{2}\rho v^2\right)}{\partial t}+\frac{\partial(\rho\psi)}{\partial t}=-\nabla.\left(\frac{1}{2}\rho\vec{v}^2\vec{v}+P.\vec{v}\right)+P:\nabla.\vec{v}+\sum_k\rho_k F_k.\vec{v}$$
$$-\nabla.\left(\rho\psi\vec{v}+\sum_{k=1}^{n}\psi_k J_k\right)-\sum_{k=1}^{n}\rho_k F_k.\vec{v}-\sum_{k=1}^{n}J_k F_k$$

$$\frac{\partial\rho\left(\frac{1}{2}\vec{v}^2+\psi\right)}{\partial t}=-\nabla.\left(\frac{1}{2}\rho\vec{v}^2\vec{v}+P.\vec{v}+\rho\psi\vec{v}+\sum_{k=1}^{n}\psi_k J_k\right)+\mathbf{P}:\nabla.\vec{v}-\sum_{k=1}^{n}J_k F_k$$

C.14

where $\sum_{k=1}^{n}J_k F_k$ = the source term and thus the sum of the kinetic and potential energy is not conserved.

III Conservation of energy

According to the principle of conservation of energy, the total energy content within an arbitrary volume V of the system can only change due to the energy flows through the boundary and can be expressed as

$$\frac{d}{dt}\int_{CV}\rho e dV=\int_{CV}\frac{\partial(\rho e)}{\partial t}dV=-\int_{CS}\mathbf{J}_e dA \qquad \text{C.15}$$

Here $\mathbf{J}_e$ is the total energy flux which is $\mathbf{J}_e=\rho e\vec{v}+P.\vec{v}+\sum_{k=1}^{n}\psi_k J_k+\mathbf{J}_q$ and $e=\left(\frac{1}{2}\rho\vec{v}^2+\psi+u\right)$, u is the internal energy. From the microscopic point of view, it represents the energy due to the short-range molecular interactions and of thermal

agitation. In the total energy flux, $\rho e \vec{v}$ is the convective term, $P.\vec{v}$ is the energy flux due to the mechanical worked applied to the system, $\sum_{k=1}^{n} \psi_k J_k$ is the potential energy flux due to the diffusion of the various components in the field of force, and $\mathbf{J}_q$ is the heat flow.

Using Reynolds Transport Theorem and Gauss Divergence Theorem, the conservation of energy can be written as

$$\frac{\partial(\rho e)}{\partial t} = -\nabla.\mathbf{J}_e \qquad \text{C.16}$$

$$\frac{\partial \rho\left(\frac{1}{2}\vec{v}^2 + \psi + u\right)}{\partial t} = -\nabla.\left(\rho e \vec{v} + P.\vec{v} + \sum_{k=1}^{n} \psi_k J_k + \mathbf{J}_q\right) \qquad \text{C.17}$$

The left hand side of Equation C.17 can be split into the sum of potential and kinetic terms, and the internal energy as

$$\frac{\partial \rho\left(\frac{1}{2}\vec{v}^2 + \psi\right)}{\partial t} + \frac{\partial(\rho u)}{\partial t} = -\nabla.\left(\rho e \vec{v} + P.\vec{v} + \sum_{k=1}^{n} \psi_k J_k + \mathbf{J}_q\right) \qquad \text{C.18}$$

$$\Rightarrow \frac{\partial(\rho u)}{\partial t} = -\nabla.\left(\rho e \vec{v} + P.\vec{v} + \sum_{k=1}^{n} \psi_k J_k + \mathbf{J}_q\right) - \frac{\partial \rho\left(\frac{1}{2}\vec{v}^2 + \psi\right)}{\partial t} \qquad \text{C.19}$$

By substituting the last term of the above Equation with Equation C.14, one has

$$\frac{\partial(\rho u)}{\partial t} = -\nabla.\left(\rho\left\{\frac{1}{2}\vec{v}^2 + \psi + u\right\}\vec{v}\right) - \nabla.\left(P.\vec{v} + \sum_{k=1}^{n}\psi_k J_k + \mathbf{J}_q\right)$$
$$+\nabla.\left(\frac{1}{2}\rho\vec{v}^2\vec{v} + P.\vec{v} + \rho\psi\vec{v} + \sum_{k=1}^{n}\psi_k J_k\right) - \mathbf{P}:\nabla.\vec{v} + \sum_{k=1}^{n} J_k F_k$$

$$\Rightarrow \frac{\partial(\rho u)}{\partial t} = -\nabla.\left(\frac{1}{2}\rho\vec{v}^2\vec{v} + \rho\psi\vec{v} + \rho u\vec{v} + P.\vec{v} + \sum_{k=1}^{n}\psi_k J_k + \mathbf{J}_q - \frac{1}{2}\rho\vec{v}^2\vec{v} - P.\vec{v} - \rho\psi\vec{v} - \sum_{k=1}^{n}\psi_k J_k\right)$$
$$-\mathbf{P}:\nabla.\vec{v} + \sum_{k=1}^{n} J_k F_k$$

$$\frac{\partial(\rho u)}{\partial t} = -\nabla.\left(\rho u\vec{v} + \mathbf{J}_q\right) - \mathbf{P}:\nabla.\vec{v} + \sum_{k=1}^{n} J_k F_k \qquad \text{C.20}$$

Here $\rho u\vec{v} + \mathbf{J}_q$ is the energy flow due to convection and thermal energy transfer that gives rise to an internal energy change, while $-\mathbf{P}:\nabla.\vec{v} + \sum_{k=1}^{n} J_k F_k$ is an internal energy source term. Equation C.20 can be further simplified as

$$\rho\frac{du}{dt} - \nabla\cdot\left(\rho u\vec{v}\right) = -\nabla\cdot\left(\rho u\vec{v} + \mathbf{J}_q\right) - \mathbf{P}:\nabla.\vec{v} + \sum_{k=1}^{n} J_k F_k \qquad \text{C.21}$$

The third term of the Equation 3.37 can be split into a scalar hydrostatic part *p* and a tensor Π as $\mathbf{P} = pU + \Pi$ where U is the unit matrix and thus Equation C.21 becomes

$$\rho\frac{du}{dt} = -\nabla\cdot\mathbf{J}_q - p\nabla\cdot\vec{v} - \Pi:\nabla.\vec{v} + \sum_{k=1}^{n} J_k F_k \qquad \text{C.22}$$

It is noted that $\rho\frac{dq}{dt} = -\nabla.\mathbf{J}_q$ and $\rho\frac{d\nu}{dt} = \nabla\cdot\vec{\nu}$ and hence the energy balance Equation becomes

$$\frac{du}{dt} = \frac{dq}{dt} - p\frac{d\nu}{dt} - \nu\Pi:\nabla.\vec{\nu} + \nu\sum_{k=1}^{n} J_k F_k \qquad \text{C.23}$$

The first term of the Equation C.23 represents the heat flux, the second and third term stand for the mechanical work and the last term states the conservative forces such as electro-magnetic forces.

IV Entropy Balance

For any macroscopic thermodynamic system, the variation of the state function entropy, dS may be written as $dS = d_eS + d_iS$ where d_eS is the entropy contributed by the surroundings and d_iS is the entropy produced inside the system. By the second law of thermodynamics, the entropy generation inside the system $d_eS \geq 0$. Using the Reynolds Transport Theorem again, the entropy functions can be written as

$$S = \int_{CV} \rho s dV \qquad \text{C.24}$$

$$\frac{d_eS}{dt} = -\int_{CS} \mathbf{J}_{s,tot} d\vec{A} \qquad \text{C.25}$$

$$\frac{d_iS}{dt} = -\int_{CV} \sigma dV \qquad \text{C.26}$$

where $\mathbf{J}_{s,tot}$ is the total entropy flow per unit area and unit time and σ is the total entropy generation inside the unit control volume per unit time. Applying Gauss Theorem,

$$\int_{CV}\left(\frac{\partial \rho s}{\partial t}+\nabla.\mathbf{J}_{s,tot}-\sigma\right)dV=0 \qquad \text{C.27}$$

$$\frac{\partial \rho s}{\partial t}=-\nabla.\mathbf{J}_{s,tot}+\sigma \qquad \textit{where } \sigma \geq 0 \qquad \text{C.28}$$

Equations C.27 and C.28 are the local mathematical forms of the second law of thermodynamics. Equation C.28 can be also written as

$$\frac{\partial \rho s}{\partial t}+\nabla \rho s\vec{v}=-\nabla.\left(\mathbf{J}_{s,tot}-\rho s\vec{v}\right)+\sigma \qquad \text{C.29}$$

$$\rho\frac{ds}{dt}=-\nabla.\left(\mathbf{J}_{s}\right)+\sigma \qquad \text{C.30}$$

where $\mathbf{J}_s=\mathbf{J}_{s,tot}-\rho s v$ is the entropy flux. The entropy per unit mass is a function of the internal energy u, the specific volume v, and the mass fractions c_k which is $c_k=\frac{\rho_k}{\rho},\left(\sum_{k=1}^{n}c_k=1\right)$. Applying Gibbs relation, the total differential of the entropy at equilibrium is written as

$$Tds = du + pdv - \sum_{k=1}^{n} \mu_k dc_k \qquad \text{C.31}$$

Here p is the equilibrium pressure and μ_k is the chemical or thermodynamic potential of component *k*. It is assumed that a state of local equilibrium exists within small mass elements even though the total system is not in equilibrium and Equation C.31 now can be written as

$$T\frac{ds}{dt} = \frac{du}{dt} + p\frac{dv}{dt} - \sum_{k=1}^{n} \mu_k \frac{dc_k}{dt} \qquad \text{C.32}$$

Inserting $\frac{du}{dt}$ and $p\frac{dv}{dt}$ from Equation C.23

$$\rho\frac{ds}{dt} = -\frac{\nabla \cdot \mathbf{J}_q}{T} - \frac{1}{T}\Pi : \nabla.\vec{v} + \frac{1}{T}\sum_{k=1}^{n} J_k F_k + \frac{1}{T}\sum_{k=1}^{n} \mu_k \nabla.\mathbf{J}_k - \frac{1}{T}\sum_{j=1}^{r} A_j J_j \qquad \text{C.24}$$

where A_j is the chemical affinities of the reactions *j* and is defined by $Aj = \sum_{k=1}^{n} \nu_{kj}\mu_{kj}$.

Finally, the entropy balance Equation can be arranged as

$$\begin{aligned} \rho\frac{ds}{dt} = &-\nabla.\left(\frac{\mathbf{J}_q - \sum_{k=1}^{n}\mu_k \mathbf{J}_k}{T}\right) - \frac{1}{T^2}\mathbf{J}_q.\nabla T \\ &-\frac{1}{T}\Pi : \nabla.\vec{v} - \frac{1}{T}\sum_{k=1}^{n} J_k.\left(T\nabla\frac{\mu_k}{T} - F_k\right) - \frac{1}{T}\sum_{j=1}^{r} A_j J_j \end{aligned} \qquad \text{C.25}$$

Comparing with the Equation C.30, the entropy flux and the entropy generation now become

$$\mathbf{J}_s = \frac{1}{T}\left(\mathbf{J}_q - \sum_{k=1}^{n} \mu_k \mathbf{J}_k\right) \qquad \text{C.26}$$

$$\sigma = -\frac{1}{T^2}\mathbf{J}_q.\nabla T - \frac{1}{T}\Pi : \nabla.\vec{v} - \frac{1}{T}\sum_{k=1}^{n} J_k.\left(T\nabla.\frac{\mu_k}{T} - F_k\right) - \frac{1}{T}\sum_{j=1}^{r} A_j J_j \qquad \text{C.27}$$

Appendix D: Specific heat capacity of the adsorbed phase

The specific heat capacity of the adsorbed phase is defined as the temperature derivatives of the differential adsorbed phase enthalpy at constant surface coverage, x, i.e., $C_{p,a} = \left(\frac{\partial h_a}{\partial T}\right)_x$. Now we use a useful mathematical tool named the functional determinants or Jacobians for the calculation of $\left(\frac{\partial h_a}{\partial T}\right)_x$, where h_a and x for T are the determinants.

$$\left(\frac{\partial h_a}{\partial T}\right)_x = \begin{vmatrix} \left(\frac{\partial h_a}{\partial T}\right)_x & \left(\frac{\partial h_a}{\partial T}\right)_T \\ 0 & 1 \end{vmatrix} = \begin{vmatrix} \left(\frac{\partial h_a}{\partial T}\right)_x & \left(\frac{\partial h_a}{\partial T}\right)_T \\ \left(\frac{\partial x}{\partial T}\right)_x & \left(\frac{\partial x}{\partial x}\right)_T \end{vmatrix} = \frac{\partial(h_a, x)}{\partial(T, x)} = \frac{\partial(h_a, x)}{\partial(T, P)} \Big/ \frac{\partial(T, x)}{\partial(T, P)} \quad \text{D.1}$$

Hence the Jacobians of h_a and x for the two variables P and T are the determinants, i.e.,

$$\frac{\partial(h_a, x)}{\partial(T, P)} = \begin{vmatrix} \left(\frac{\partial h_a}{\partial T}\right)_P & \left(\frac{\partial h_a}{\partial P}\right)_T \\ \left(\frac{\partial x}{\partial T}\right)_P & \left(\frac{\partial x}{\partial P}\right)_T \end{vmatrix} = \left(\frac{\partial h_a}{\partial T}\right)_P \left(\frac{\partial x}{\partial P}\right)_T - \left(\frac{\partial h_a}{\partial P}\right)_T \left(\frac{\partial x}{\partial T}\right)_P \quad \text{D.2}$$

And $$\frac{\partial(T, x)}{\partial(T, P)} = \begin{vmatrix} 1 & 0 \\ \left(\frac{\partial x}{\partial T}\right)_P & \left(\frac{\partial x}{\partial P}\right)_T \end{vmatrix} = \left(\frac{\partial x}{\partial P}\right)_T \quad \text{D.3}$$

By substituting,

$$\left(\frac{\partial h_a}{\partial T}\right)_x = \frac{\left(\frac{\partial h_a}{\partial T}\right)_P \left(\frac{\partial x}{\partial P}\right)_T - \left(\frac{\partial h_a}{\partial P}\right)_T \left(\frac{\partial x}{\partial T}\right)}{\left(\frac{\partial x}{\partial P}\right)_T} = \left(\frac{\partial h_a}{\partial T}\right)_P - \left(\frac{\partial h_a}{\partial P}\right)_T \left(\frac{\partial x}{\partial T}\right) \Big/ \left(\frac{\partial x}{\partial P}\right)_T \quad \text{D.4}$$

The thermodynamics quantity uptake x is a function of two variables P and T or $x = x(P,T)$, it is justified in considering P as a function of T and q or $P = P(T,x)$ and T as a function of P and q or $T = T(P,x)$. Therefore, the following relations uniquely relate all possible derivatives of these three functions.

$$\left(\frac{\partial x}{\partial P}\right)_T \left(\frac{\partial P}{\partial T}\right)_x \left(\frac{\partial T}{\partial x}\right)_P = -1 \Rightarrow \left(\frac{\partial P}{\partial T}\right)_x = -\left(\frac{\partial x}{\partial T}\right)_P \Big/ \left(\frac{\partial x}{\partial P}\right)_T \quad \text{D.5}$$

Being properties of a thermodynamics system, the exact behavior of $C_{p,a}$ could be obtained by substituting,

$$C_{p,a} = \left(\frac{\partial h_a}{\partial T}\right)_x = \left(\frac{\partial h_a}{\partial T}\right)_P + \left(\frac{\partial h_a}{\partial P}\right)_T \left(\frac{\partial P}{\partial T}\right)_x \quad \text{D.6}$$

The Gibbs law and the Maxwell relations are invoked to transformed the enthalpy changes with respect to pressure at constant temperature and uptake can be written as,

$$\left(\frac{\partial h_a}{\partial P}\right)_T = -T\left(\frac{\partial v_a}{\partial T}\right)_P + v_a + P\left(\frac{\partial v_a}{\partial P}\right)_T \quad \text{D.7}$$

where the first term indicates thermal expansion of the adsorbed phase and the last term defines the isothermal compressibility of the adsorbed phase on the adsorbents. Here v_a is the specific volume of the adsorbed phase. For simplicity,

$$\left(\frac{\partial h_a}{\partial P}\right)_T \approx -T\left(\frac{\partial v_g}{\partial T}\right)_P + v_g + P\left(\frac{\partial v_g}{\partial P}\right)_T \qquad \text{D.8}$$

Substituting these transformations into Equation D.6, C_p of the adsorbed phase is now expressed in terms of the measurable variables, i.e.,

$$\begin{aligned} C_{p,a} &= C_{p,g} + \left[-T\left(\frac{\partial v_g}{\partial T}\right)_P + v_g + P\left(\frac{\partial v_g}{\partial P}\right)_T\right]\left(\frac{\partial P}{\partial T}\right)_x \\ &= C_{p,g} + \left\{-T\left(\frac{\partial v_g}{\partial T}\right)_P + v_g\right\}\left(\frac{\partial P}{\partial T}\right)_x + P\left(\frac{\partial v_g}{\partial P}\right)_T\left(\frac{\partial P}{\partial T}\right)_x \end{aligned} \qquad \text{D.9}$$

The partial gradient $\left(\frac{\partial P}{\partial T}\right)_x$ could be extracted from the adsorption isotherm. Invoking Clausius-Clapeyron equation, the mentioned partial gradient can be replaced by measureable heat of adsorption, $\left(\frac{\partial P}{\partial T}\right)_x = P\left(\frac{\partial \ln P}{\partial T}\right) = \frac{Q_{st}}{Tv_g}$, where Q_{st} is the isosteric heat of adsorption. The third term on the right hand side of Equation D.9 approximately approaches to $P\left(\frac{\partial v_g}{\partial P}\right)_T\left(\frac{\partial P}{\partial T}\right)_x = -\left.\frac{\partial Q_{st}}{\partial T}\right|_P$

Now Equation D.9 can be written as

Appendix D: Derivation specific capacity of the adsorbed phase

$$C_{p,a} = C_{p,g} + \left\{ -T\left(\frac{\partial v_g}{\partial T}\right)_P + v_g \right\} \frac{Q_{st}}{T v_g} - \left.\frac{\partial Q_{st}}{\partial T}\right|_P$$

$$= C_{p,g} + \left\{ \frac{1}{T} - \frac{1}{v_g}\left(\frac{\partial v_g}{\partial T}\right)_P \right\} Q_{st} - \left.\frac{\partial Q_{st}}{\partial T}\right|_P \qquad \text{D.10}$$

Appendix E: Detailed description of AutoSorp-1 analyser

Figure E-1 gives the pictorial view of the AutoSorp 1 analyzer which can perform the characteristic analysis of adsorbent using non-corrosive adsorbate gases.

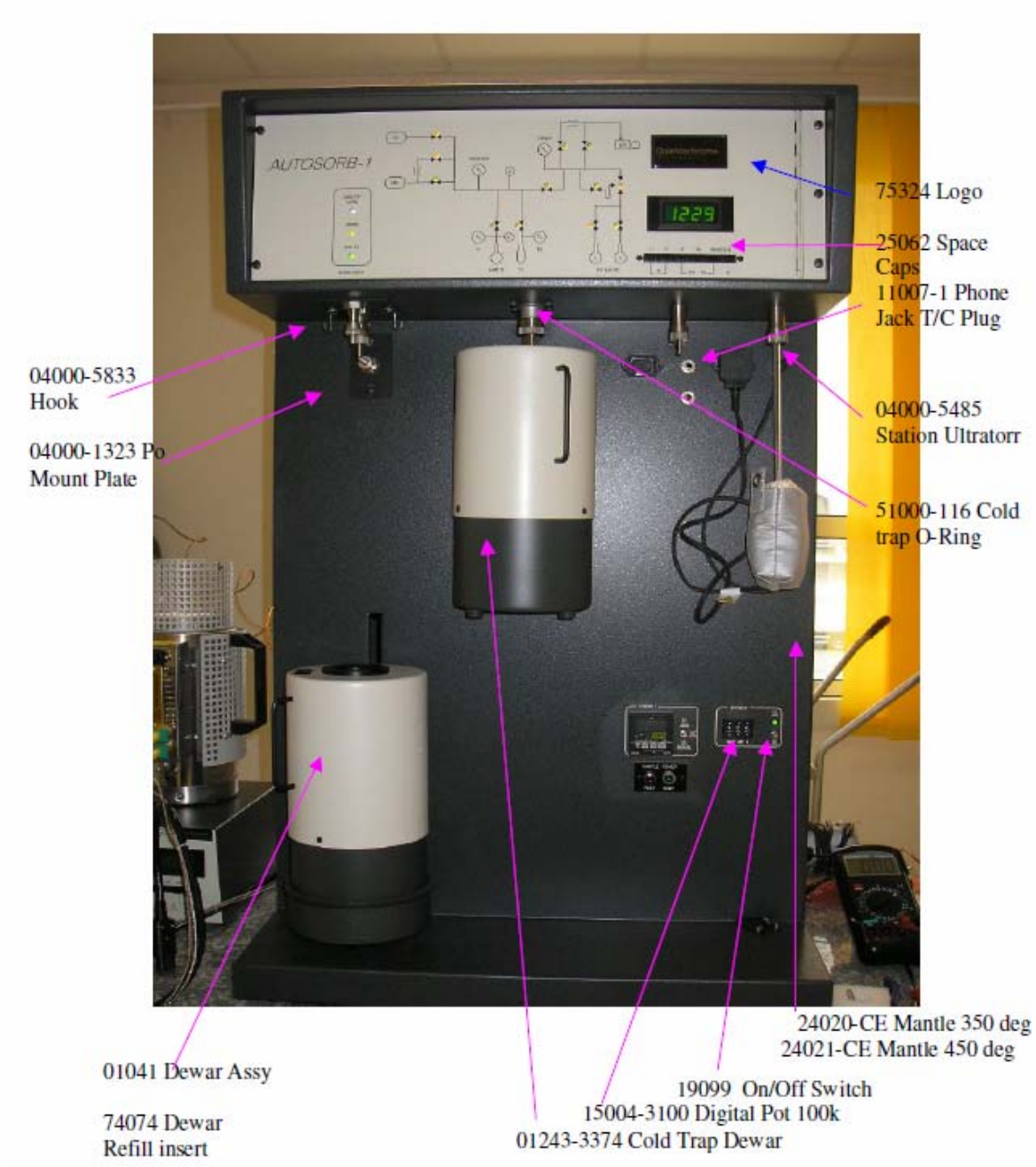

Figure E-1 Pictorial view of the AiutoSorp 1 analyzer

The AUTOSORB-1 operates by measuring the quantity of gas adsorbed onto or desorbed from a solid surface at some equilibrium vapor pressure by the static volumetric method. The data are obtained by admitting or removing a known quantity of adsorbate gas into or out of a sample cell containing the solid adsorbent maintained at a constant temperature below the critical temperature of the adsorbate. As adsorption or desorption occurs the pressure in the sample cell changes until equilibrium is established. The quantity of gas adsorbed or desorbed at the equilibrium pressure is the difference between the amount of gas admitted or removed and the amount required to fill the space around the adsorbent (void space).

The AUTOSORB-1 has the capability of measuring adsorbed or desorbed volumes of nitrogen at relative pressures in the range 0.001 to slightly under 1.0. When the krypton and micropore options are added, the lower limit is extended to 1x10-6 and data points can be requested at 1x10-7. This volume-pressure data can be reduced by the AUTOSORB-1 software into BET surface area (single and/or multipoint), Langmuir surface area, adsorption and/or desorption isotherms, pore size and surface area distributions, micropore volume and surface area using an extensive set of built-in data reduction procedures.The Quantachrome AUTOSORB Software interfaces the AUTOSORB to a computer for data acquisition, reduction and archiving.

Appendix F: Detailed description of HydroSorb-1000 analyser

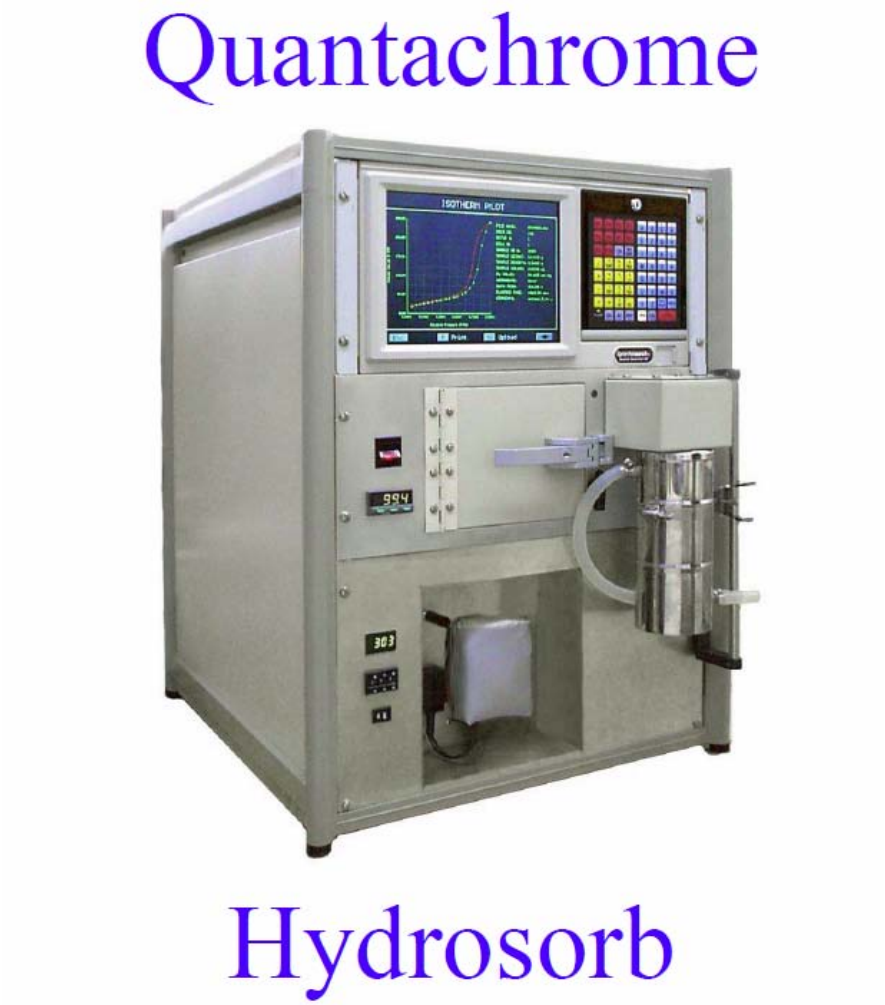

Figure F-1 Pictorial view of Hydrosorb-1000 analyser

The Hydrosorb 1000 is offers fully automated, rapid measurement of adsorption and desorption water isotherms including BET surface area calculations and heats of adsorption. The analysis temperature ranges from 12deg to 47degC of adsorbate. Accurate water vapor dosing is made possible by using a unique, heated (100° C) manifold design. HydroWin PC software provides convenient set-up of analysis parameters, data reduction and reporting.

Appendix G: Properties of sea water

a. Vapor pressure of sea water

$$P_{sea} = P_{sat}(T) \times \left(1 - 5.37 \times 10^{-4} \times S\right)$$

where P_{sea} is the vapour pressure of sea water, *Psat* is the saturation pressure of pure water and S is the salinity in ppm.

b. Boling point elevation

$$BPE = (A + B \times S) \times S$$

$$A = \left(6.71 + 6.43 \times 10^{-2} \times \mathrm{T} + 9.74 \times 10^{-5} \times \mathrm{T}^2\right) \times 10^{-3}$$

$$B = 2.38 + 9.59 \times 10^{-3} \times \mathrm{T} + 9.42 \times 10^{-5} \times \mathrm{T}^2) \times 10^{-5}$$

where BPE is the boiling point elevation which is a function of sea water temperature and salinity.

c. Specific heat capacity

$$c_{p,sea} = 2.38846 \times 10^{-4} \times (\mathrm{A1} + \mathrm{A2} \times \mathrm{T} + \mathrm{A3} \times \mathrm{T}^2 + \mathrm{A4} \times \mathrm{T}^3)$$

$$\mathrm{A1} = 4.2068 \times 10^{3} - 6.6197 \times \mathrm{S} + 1.2288 \times 10^{-2} \times \mathrm{S}^2$$

$$\mathrm{A2} = -1.1262 + 5.4718 \times 10^{-2} \times \mathrm{S} - 2.2719 \times 10^{-4} \times \mathrm{S}^2$$

$$\mathrm{A3} = 1.2026 \times 10^{-2} - 5.3566 \times 10^{-4} \times \mathrm{S} + 1.8906 \times 10^{-6} \times \mathrm{S}^2$$

$$\mathrm{A4} = 6.8774 \times 10^{-7} + 1.5170 \times 10^{-6} \times \mathrm{S} - 4.4268 \times 10^{-9} \times \mathrm{S}^2$$

d. Specific enthalpy of sea water

$$h_{sea} = (H_0 + \mathrm{CPS} \times \mathrm{T}) \times 4186.8$$

$$H_0 = 2.3\mathrm{D} - 3 \times \mathrm{S} - 1.03 \times 10^{-4} \times \mathrm{S}^2$$

$$\mathrm{CPS} = 2.38846 \times 10^{-4} \times (\mathrm{A1} + \mathrm{A2} \times \mathrm{T} + \mathrm{A3} \times \mathrm{T}^2 + \mathrm{A4} \times \mathrm{T}^3)$$

$$\mathrm{A1} = 4.2068 \times 10^{3} - 6.6197 \times \mathrm{S} + 1.2288 \times 10^{-2} \times \mathrm{S}^2$$

$$\mathrm{A2} = -1.1262 + 5.4718 \times 10^{-2} \times \mathrm{S} - 2.2719 \times 10^{-4} \times \mathrm{S}^2$$

$$\mathrm{A3} = 1.2026 \times 10^{-2} - 5.3566 \times 10^{-4} \times \mathrm{S} + 1.8906 \times 10^{-6} \times \mathrm{S}^2$$

$$\mathrm{A4} = 6.8774 \times 10^{-7} + 1.5170 \times 10^{-6} \times \mathrm{S} - 4.4268 \times 10^{-9} \times \mathrm{S}^2$$

Appendix H: Experimental results on Bed cooling scheme

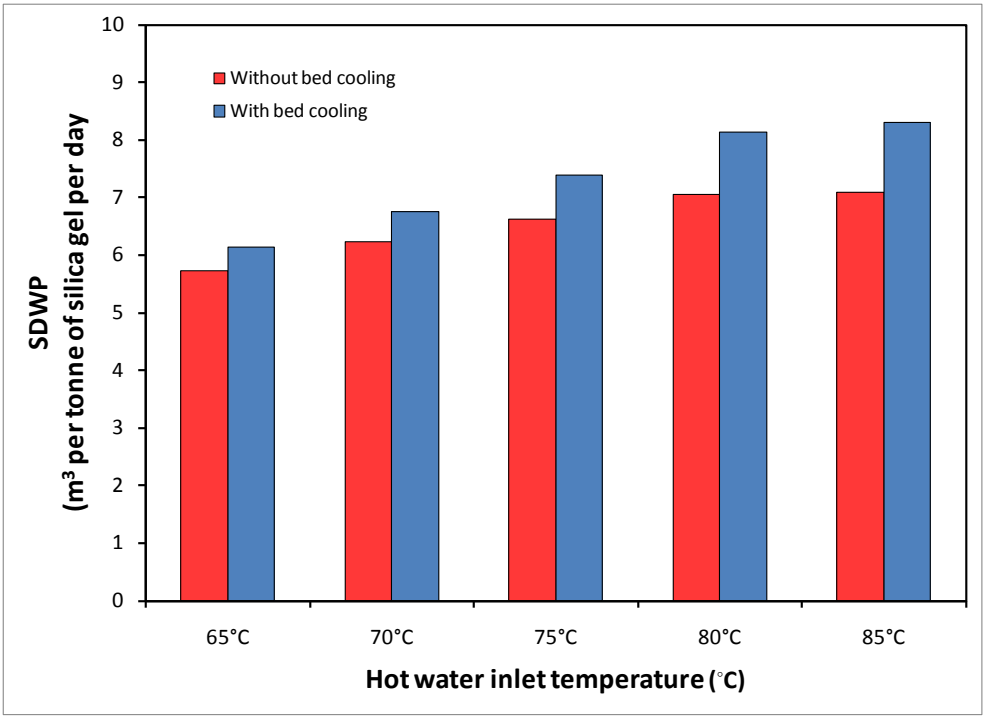

Figure H-1 Comparison on the SDWP of a two-bed AD cycle without and bed cooling at load water flow rate 50 LPM

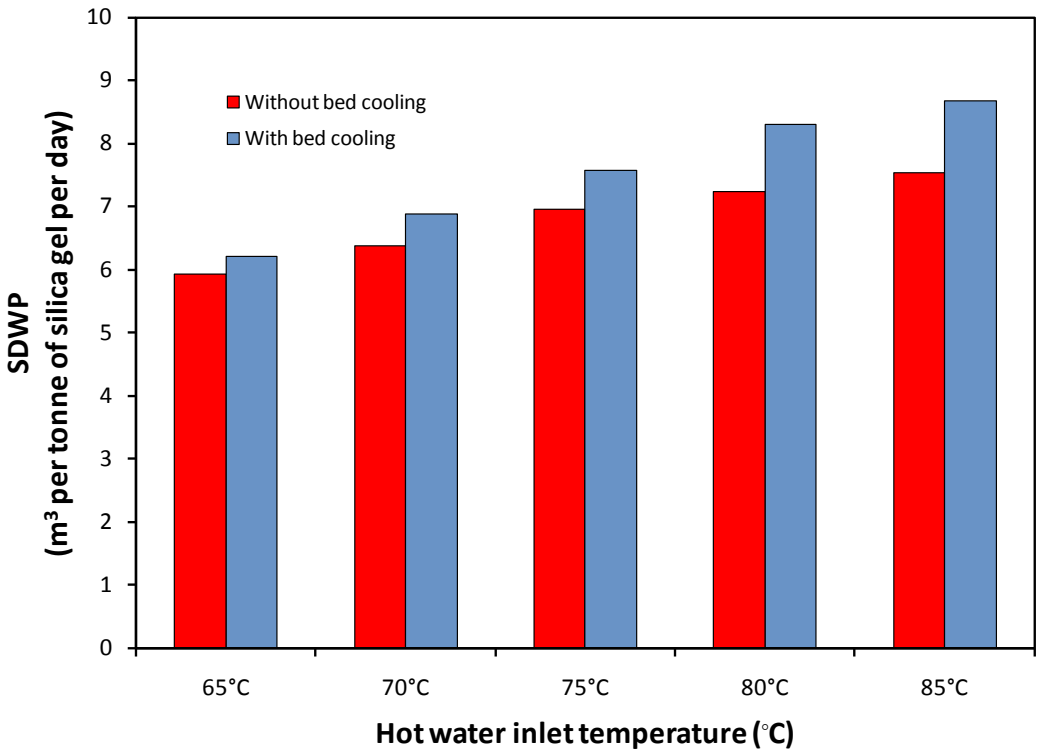

Figure H-2 Comparison on the SDWP of a two-bed AD cycle without and bed cooling at load water flow rate 75LPM

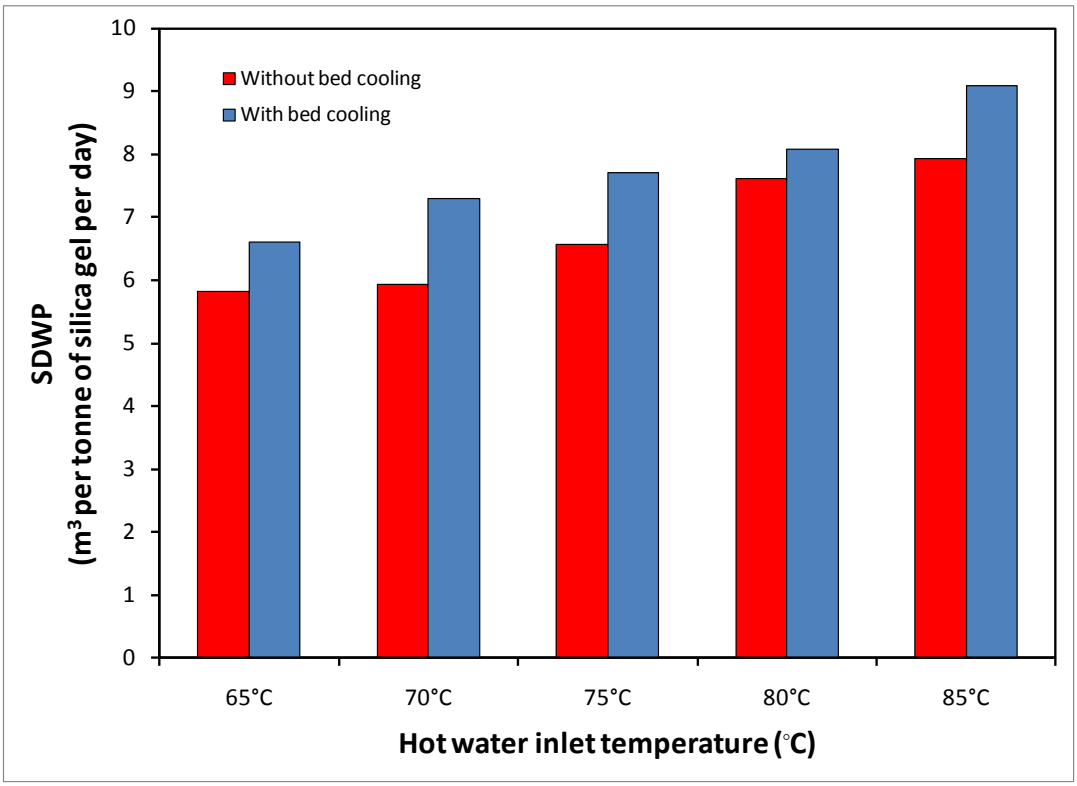

Figure H-3 Comparison on the SDWP of a four-bed AD cycle without and bed cooling at load water flow rate 50 LPM

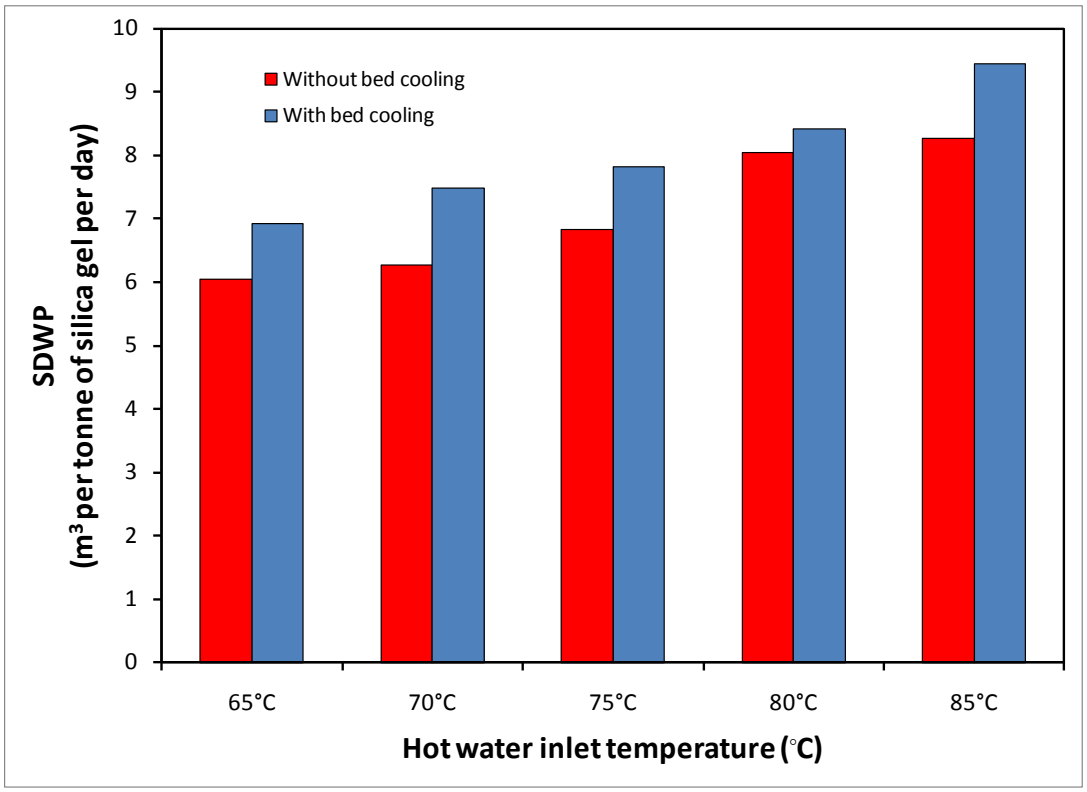

Figure H-4 Comparison on the SDWP of a four-bed AD cycle without and bed cooling at load water flow rate 75LPM

Appendix I: Pumping power required for the AD system

Specifications for the evaporator:

- Flow rate per distribution = 48/4 = 12 LPM
- Diameter of pipes, D = 0.0162m
- Pipe length = 1.994 x 13 = 25m
- Number of flanged regular 90^o elbows = 4
- Number of 180^o return bends = 0
- Temperature of water in pipes = 34^o
- Viscosity of water, μ = 0.00074 Pa.s
- Density of water = 1000 kg/m^3
- Relative Roughness of tube, ε = 0.000045

Calculations:

a. Pipe area = $\frac{\prod D^2}{4}$

$= \frac{\prod \times 0.0162^2}{4}$

$= 0.000206\ m^2$

b. Velocity of water flow, V = $\frac{FlowRate(LPM)}{1000 \times 60(s)} \div pipe\ area$

$= \frac{4}{1000 \times 60} \times \frac{1}{0.000206}$

=0.323 m/s

c. Reynold's Number = $\frac{\rho(kg/m^3) \times V(m/s) \times D(m)}{\mu(kg/s.m)}$

= 7080

d. Roughness Ratio = $\frac{\varepsilon}{D}$

= $\frac{0.000045}{0.0162}$

= 0.00278

e. Equivalent Length of minor losses

= (Number of regular 90^o elbows $\times$ 0.3) +

(Number of return bends $\times$ 2.2) + (Number of fully open gate valves $\times$ 0.15)

+

contraction loss + enlargement loss

f. To calculate the Moody friction factor,

$$f = \frac{1.325}{\left[\ln\left(\frac{e}{3.7D} + \frac{5.74}{\mathrm{Re}^{0.9}}\right)\right]^2}$$

$$= \frac{1.325}{\left[\ln\left(\frac{0.000045}{3.7\times 0.0162}+\frac{5.74}{7080^{0.9}}\right)\right]^2}$$

$$= 0.038$$

g. Head loss in pipes due to friction and minor losses

$$= (\frac{fL}{D}+\xi_{total\ minor})\times\frac{v^2}{2g}$$

$$= 0.14\text{m}$$

h. Elevation head loss in the hot water circuit, $\Delta Z = 0\text{m}$ (Close loop)

i. Pump Power = $\rho\times g\times H\times Q/\eta$ (Efficiency of pump is taken as 85%)

$$=\underline{\boldsymbol{1.3W}}$$

Total Pump Power Consumption

Total Pump Power Required

$= \text{Pump}_{\text{hot water pipe line}} + \text{Pump}_{\text{cooling water pipe line}} + \text{Pump}_{\text{condenser pipe line}} + \text{Pump}_{\text{chilled water pipe}} + \text{Pump}_{\text{hot bed}} + \text{Pump}_{\text{cold bed}} + \text{Pump}_{\text{evaporator}} + \text{Pump}_{\text{condenser}}$

$= 209\ \text{W}$

Power Consumption per unit volume of water produced

Sample Calculation:

Electrical power for pumping, E = **0.209** kW

Total running hour, T = **24** hr

Volume of product water per kilogram of silica-gel, A = 0.00635 m^3/min-kg (Conventional cycle)

t_{cycle} = 6.66 min

Numbers of cycles per day = 24*60/6.66 = 216.2

Mass of Silica-gel, M_{sg} = 144 kg

A= water production per cycle per kg of Si

$$= \frac{\dot{m} \quad Flowrate(m^3/\min)}{144(kg)}$$

=0.00635 m^3/min.kg

$$\text{Total power consumption} = \frac{E*T}{A*t_{cycle}*B*M_{sg}}$$

$$= \frac{0.209(kW)\times 24(h)}{0.00635(\frac{m^3}{\min.kg})\times 6.66(\min)\times 216.2\times 144(kg)}$$

= 3.8 kWh/m^3 (for conventional cycle)

For advanced AD cycle,

the total pumping power = $\text{Pump}_{\text{hot water pipe line}} + \text{Pump}_{\text{cooling}}$

$\text{Pump}_{\text{water pipe line}} + \text{Pump}_{\text{hot bed}} + \text{Pump}_{\text{cold bed}}$

= 178.3W

Total power consumption = 1.38kWh/m^3

Appendix J: Sample calculation of the 10Rton AD plant

Plant life = 30years

Interest rate =5%

Table J-1 Direct capital cost

No.	name of the equipment	Cost (S$/m^3)
1.	Adsorber bed including the adsorbent	22,509.00
2.	Water valves	800
3.	Evaporator-condenser unit	10700
4.	Condenser vapour valves	1084
5.	Pumps (Cooling water and hot water)	3000
6.	Total (US$-using exchange rate 1.5)	25395.33
	Total direct capital cost ($/m^3)	**0.743**

Table J-2 Operational cost

	Total Pump Power (Advanced cycle)- kWh/year	3377
1.	Electricity rate ($/kWh)	0.1333
2.	Water production rate (m^3/day)	7.5
3.	**Total electricity cost ($/m^3)**	**0.164**
4.	**Pre-treatment cost ($/m^3)**	**0.001**
5.	**Manpower cost ($/m^3)**	**0.021**
6.	**Maintenance cost ($/m^3)**	**0.012**

Life cycle cost of the 10Rton AD plant is thus the sum of all the capital and operational cost which is 0.941$/m^3.

Appendix K: Baseline calculation for the emission of CO_2

The baseline emissions of CO_2 by a desalination process can be estimated as the sum of CO_2 emissions from thermal energy and electrical energy utilization. For the thermally activated systems, the emission of CO_2 emanates from the energy consumed in evaporating the sea water as well as the electricity consumption for the moving the coolant or heat sources. On the other hand, the membrane desalination processes would consume electricity for pushing the saline solution and permeate. The following Equations provide the method of calculation for the baseline emission for a desalination process.

$$BE_y(tCO_2/yr) = TB_{th,y} + EB_{elec,y}$$

where BE_y is the baseline annual CO_2 emission, $EB_{elec,y}$ is the emission from the generation of electricity consumed and $TB_{th,y}$ is the annual CO_2 emission from the burning of natural gas for desalting. $TB_{th,y}$ can be calculated using the following Equation

$$TB_{th,y} = Q_{elec,y}(MJ/yr) \times EF_{gas}(tCO_2/MJ)$$

where $Q_{elec,y}(MJ/yr)$ is the annual thermal energy required for the desalination of typical amount of potable water and $EF_{gas}(tCO_2/MJ)$ is the emission factor for the burning of natural gas. The value of EF_{gas} is taken as 6.42×10^{-5} tCO_2/MJ [111].

The emission from the electricity consumed in desalination process, $EB_{elec,y}$, is calculated as

$$EB_{elec,y} = EG_y(MWh/yr) \times CEF_{elec}(tCO_2/MWh)$$

where EG_y is the amount of electricity generated by the power plant and CEF_{elec} is the CO_2 emission factor for the generation of the electricity and its value is taken as 0.4612 [112, 113].

The CO_2 emission reduction by AD process is given by;

$$ER_y(tCO_2/yr) = BE_y - ADE_y$$

Here, ER_y and ADE_y are the annual CO_2 emission reduction and the annual CO_2 emission by the AD plant. The following expressions are used to estimate the CO_2 emission by the AD plant.

$$ADE_y(tCO_2/yr) = EB_{elec,y}$$

and the units are similar at tones of CO_2/year.